MYOCARDIAL ENERGY METABOLISM IN CARDIOMYOPATHIES

by

Amanda Ashleigh Greenwell

A thesis submitted in partial fulfillment of the requirements for the degree of

Doctor of Philosophy

in

Pharmaceutical Sciences

Faculty of Pharmacy and Pharmaceutical Sciences
University of Alberta

Abstract

As the most metabolically demanding organ in the body, the heart must continually produce extraordinary amounts of energy to sustain constant contractile function. To accommodate for alterations in fuel source availability, the healthy mature heart is omnivorous and possesses the capacity to flexibly metabolize numerous fuel substrates including fatty acids, carbohydrates, ketone bodies and amino acids delivered to it through the coronary circulation. Accordingly, disturbances in this metabolic flexibility contribute to the development of numerous cardiovascular disorders, including various cardiomyopathies that often precede the development of heart failure. Although perturbation of myocardial energy metabolism represents a shared feature of cardiomyopathies with diverse origins and basic disease mechanisms, the specific metabolic profile and, thus, potential targets for therapeutic intervention are often unique to the particular cardiomyopathy type. Herein, we investigated the alterations in myocardial intermediary energy metabolism present in the cardiomyopathies associated with Barth syndrome and obesity/type 2 diabetes. Furthermore, we determined whether pharmacological optimization of cardiac substrate utilization, or modulation of the systemic nutrient environment to mitigate cardiovascular risk factors, represent viable targets for the treatment of cardiac dysfunction in Barth syndrome and obesity/type 2 diabetes.

Barth syndrome is a rare, X-linked disorder caused by mutations in the *TAFAZZIN* gene that results in impaired mitochondrial cardiolipin remodeling, mitochondrial dysfunction, and the infantile development of cardiomyopathy. Utilizing a mouse model of human Barth syndrome (TazKD mice; doxycycline-inducible short hairpin RNA-mediated *Tafazzin* knockdown), myocardial

glucose oxidation rates were demonstrated to be markedly reduced in the tafazzin-deficient isolated working heart. Notably, impaired myocardial glucose oxidation was associated with the development of adverse hypertrophic left ventricular remodeling in TazKD mice. To assess whether pharmacological enhancement of myocardial glucose oxidation could mitigate pathological cardiac remodeling in Barth syndrome, TazKD mice were treated with dichloroacetate (70 mM) added to the drinking water for four weeks. Despite decreasing inhibitory phosphorylation of cardiac pyruvate dehydrogenase, suggestive of increased glucose oxidation, dichloroacetate failed to improve cardiac hypertrophy in TazKD mice. Therefore, stimulation of myocardial glucose oxidation may not represent an effective strategy to mitigate cardiomyopathy development and progression in Barth syndrome.

In obese, prediabetic mice, transition to a ketogenic diet for eight weeks failed to induce significant body weight loss and improve obesity-induced impairments in glucose homeostasis. Furthermore, although maintenance on a ketogenic diet did not impair cardiac function, it increased cardiac lipid accumulation which may indicate the presence of pathological molecular alterations. In consideration of the present findings, caution should be exercised when considering a ketogenic diet as a non-pharmacological strategy to reduce cardiovascular risk factors in obesity and diabetes.

Myocardial ketone body oxidation was blunted in isolated working hearts from mice with experimental type 2 diabetes, however, this decreased reliance on ketone bodies as an energy substrate may not be detrimental for the myocardium given that further inhibition by treatment with pimozide neglected to impair cardiac function. Our results offer fundamental insight

regarding a potential adaptive role for decreased cardiac ketone body utilization in diabetic cardiomyopathy.

In summary, the studies presented herein support that although alterations of myocardial energy metabolism represent a common feature of cardiomyopathies, modulation of intermediary metabolic pathways may not always represent an effective therapeutic approach. Furthermore, the results of the present studies provide fundamental insight into the myocardial metabolic profile characteristic of Barth syndrome and diabetic cardiomyopathies, which may serve to guide the development of targeted therapies.

Preface

This thesis is an original work by Amanda Ashleigh Greenwell. Ethics approval for the following research was received from the University of Alberta Animal Use and Care Committee, under Animal Use Protocol #00001412 and #00002380.

Chapter 1 contains excerpts from the following publications:

Greenwell AA, Gopal K, and Ussher JR. Myocardial Energy Metabolism in Non-ischemic Cardiomyopathy. *Front Physiol* 11: 570421, 2020.

All authors listed have made a substantial, direct, and intellectual contribution to the work.

Greenwell AA, Tabatabaei Dakhili SA, and Ussher JR. Myocardial disturbances of intermediary metabolism in Barth syndrome. *Front Cardiovasc Med* 9: 981972, 2022.

All authors listed have made a substantial, direct, and intellectual contribution to the work.

Tabatabaei Dakhili SA*, Greenwell AA*, and Ussher JR. Pyruvate dehydrogenase complex and glucose oxidation as a therapeutic target in diabetic heart disease. *J Lipid Atheroscler* 12:e3, 2022. *Denotes equal contribution

All authors listed have made a substantial, direct, and intellectual contribution to the work.

Chapter 2 has been published: Greenwell AA, Gopal K, Altamimi TR, Saed CT, Wang F, Tabatabaei Dakhili SA, Ho KL, Zhang L, Eaton F, Kruger J, Al Batran R, Lopaschuk GD, Oudit GY, and Ussher JR. Barth syndrome-related cardiomyopathy is associated with a reduction in myocardial glucose oxidation. *Am J Physiol Heart Circ Physiol* 320: H2255-H2269, 2021.

A.A.G, K.G, and J.R.U conceived and designed the research plan. A.A.G organized all experiments, acquired and analyzed echocardiography images, completed molecular work (western blotting, real-time qPCR, PDH activity) and in vivo experiments (assessment of circulating insulin and glucose levels), completed all data analysis and drafted the

manuscript. K.G assisted with echocardiography. T.R.A performed the isolated working heart perfusions. F.W completed Masson's trichrome and wheat-germ agglutinin staining of heart tissue samples. K.L.H performed experiments to assess PDH acetylation. L.Z measured myocardial triacylglycerol and glycogen content, the incorporation of [9,10-^{3}H]palmitate into cardiac triacylglycerol pool, and the incorporation of glycogen of [U-^{14}C]glucose into the cardiac glycogen pool. J.K and F.E set up breeding pairs and managed plug testing, and F.E genotyped the mouse pups. C.T.S, and S.A.T.D assisted with western blotting and real-time qPCR experiments. R.A prepared samples for assessment of myocardial short-chain CoA content. A.A.G, G.D.L, G.Y.O, and J.R.U edited and revised the manuscript.

Chapter 3 has been published: Greenwell AA*, Tabatabaei Dakhili SA*, Gopal K, Saed CT, Chan JSF, Kazungu Mugabo N, Zhabyeyev P, Eaton F, Kruger J, Oudit GY, and Ussher JR. Stimulating myocardial pyruvate dehydrogenase activity fails to alleviate cardiac abnormalities in a mouse model of human Barth syndrome. *Front Cardiovasc Med* 23: 2659, 2022. *Denotes equal contribution

A.A.G, S.A.T.D, and J.R.U conceived and designed the research plan. A.A.G organized all experiments, acquired and analyzed echocardiography images, completed molecular work (western blotting, real-time qPCR, PDH activity) and in vivo experiments (management of treatment protocol, assessment of body composition, water intake and circulating glucose levels), completed all data analysis and drafted the manuscript. S.A.T.D assessed protein carbonylation and ATP content in myocardial tissue. K.G assisted with echocardiography. J.K and F.E set up breeding pairs and managed plug testing, and F.E genotyped the mouse pups. C.T.S, and S.A.T.D, J.S.F.C, and N.K.M assisted with western blotting and real-time qPCR experiments. P.Z assisted with mouse euthanasia and cardiac tissue extraction. A.A.G, G.Y.O, and J.R.U edited and revised the manuscript.

Chapter 4 has been published: Greenwell AA, Saed CT, Tabatabaei Dakhili SA, Ho KL, Gopal K, Chan JSF, Kaczmar OO, Dyer SA, Eaton F, Lopaschuk GD, Al Batran R, and Ussher JR. An

isoproteic cocoa butter-based ketogenic diet fails to improve glucose homeostasis and promote weight loss in obese mice. *Am J Physiol Endocrinol Metab* 323: E8-E20, 2022.

A.A.G, K.L.H, and J.R.U conceived and designed the research plan. A.A.G organized all experiments, acquired and analyzed echocardiography images, completed molecular work (western blotting, real-time qPCR) and in vivo experiments (management of treatment protocol, assessment of body composition, assessment of glucose homeostasis, insulin sensitivity and circulating insulin levels), completed all data analysis and drafted the manuscript. C.T.S, S.A.T.D, J.S.F.C, K.G, and R.A. assisted with molecular work and in vivo experiments. K.L.H assisted with echocardiography and in vivo experiments. J.S.F.C completed assessment of myocardial triacylglycerol content and assisted in the analysis of echocardiography images. O.O.K, and S.A.D assisted with data analysis. F.E assisted with management of mouse care. In vivo metabolic assessment was completed by Amy Barr at the Cardiovascular Research Centre Core Services. A.A.G, G.D.L, and J.R.U edited and revised the manuscript.

Chapter 5 is under preparation for publication: Greenwell AA, Tabatabaei Dakhili SA, Wagg CS, Saed CT, Chan JSF, Yang K, Gopal K, Eaton F, Lopaschuk GD, Ussher JR. Pharmacological inhibition of myocardial ketone body oxidation with pimozide improves diastolic function in a mouse model of type 2 diabetes.

A.A.G, S.A.T.D, and J.R.U conceived and designed the research plan. A.A.G organized all experiments, acquired and analyzed echocardiography images, completed molecular work (western blotting, real-time qPCR, SCOT activity assay) and in vivo experiments (management of treatment protocol, assessment of body composition and glucose homeostasis), completed all data analysis and drafted the manuscript. C.S.W performed isolated working heart perfusions. C.T.S, S.A.T.D, J.S.F.C, K.Y, and K.G assisted with molecular work and in vivo experiments. K.Y assessed insulin levels in mouse plasma. F.E assisted with management of mouse care. A.A.G, G.D.L, and J.R.U edited and revised the manuscript.

Acknowledgements

I would first like to thank my supervisor, Dr. John Ussher. If it was not for your unwavering confidence in my potential as a scientist and your invaluable mentorship, I would not be the researcher, critical thinker, or person that I am today. When I first started as a summer student in your lab, I would never have been able to imagine the incredible journey that I would go on over the next four and a half years. Thank you for showing me the opportunities, excitement and challenges that research can bring, and for helping me to discover my own love for research. You gave me an invaluable opportunity by taking me on as a summer student, then master's student, and finally as a PhD student, and I will always hold with me the lessons I learned from you as I continue to pursue my future endeavors. To my committee members, Dr. Gary Lopaschuk and Dr. Gopinath Sutendra, thank you for your support, guidance and for challenging me to become a better researcher. I am so incredibly grateful to have had the opportunity to learn from two expectational scientists over the years. I would also like to thank the Canadian Institutes of Health Research and the University of Alberta Women and Children's Health Research Institute for providing financial support.

To my lab mates, Dr. Seyed Amirhossein Tabatabaei Dakhili (yes, you are real doctor), Christina Saed, Jordan Chan and Kunyan (Martin) Yang, I would never have been able to finish this thesis without all of your contributions. Thank you for the being the most incredible lab family and for making the Ussher lab truly a second home for me. Thank you for the movie nights, late-night dinners and drinks, and for allowing me to blast Olivia Rodrigo's "Driver's License" in the lab. I have made memories here that will last a lifetime and I could never thank you all enough. To Farah Eaton, Dr. Keshav Gopal and Dr. Rami Al Batran, thank you for all your support and guidance throughout the years. Your insight, expertise and contributions were essential for the success of my projects and I learned so much from all of you that I will take with me as I move forward towards becoming a clinician-scientist.

Finally, I would like to thank my family, my Mom, Dad and little sister, Kaitlin. Thank you for always believing in me even at times when I didn't believe in myself. Thank you for being my source of inspiration and my biggest cheerleaders. Thank you for always diligently reading the

manuscripts I was so excited to show you even if you didn't know what they were about. You truly are the backbone to my success and I never would have made it to this stage of my career without your unconditional love, encouragement, and support along the way.

Table of Contents

List of Tables

List of Figures

List of Abbreviations

ACAT1	Acetoacetyl CoA thiolase
ACC	Acetyl CoA carboxylase
ADP	Adenosine diphosphate
ANOVA	Analysis of variance
ANT	Adenine nucleotide translocase
ATP	Adenosine triphosphate
AUC	Area under the curve
BCAA	Branched chain amino acid
BCAT	Branched chain amino-transferase
BCKA	Branched chain α-keto-acid
BCKDH	Branched chain α-keto acid dehydrogenase
BCKDK	Branched chain α-keto acid dehydrogenase kinase
BDH1	β-hydroxybutyrate dehydrogenase
BTHS	Barth syndrome
BW	Body weight
CD36	Cluster of differentiation 36
CL	Cardiolipin
CO	Cardiac output
CoA	Coenzyme A
CPT	Carnitine palmitoyl transferase
CT	Carnitine translocase
CVOT	Cardiovascular outcomes trial
DCA	Dichloroacetate
EF	Ejection fraction
ETC	Electron transport chain
FACS	Fatty acyl CoA synthetase
$FADH_2$	Reduced flavin adenine dinucleotide
FATP	Fatty acid transport protein
FoxO1	Forkhead box protein O1

FS	Fractional shortening
GLP-1R	Glucagon-like peptide 1 receptor
GLUT	Glucose transporter
GSK-3β	Glycogen synthase kinase-3β
HFD	High-fat diet
HFpEF	Heart failure with preserved ejection fraction
HFrEF	Heart failure with reduced ejection fraction
IMM	Inner mitochondrial membrane
IP	Intraperitoneal
IPGTT	Intraperitoneal glucose tolerance test
iPSC	Induced pluripotent stem cell
IR	Insulin receptor
ITT	Insulin tolerance test
KD	Ketogenic diet
L_4CL	Tetralinoleoyl cardiolipin
LC-MS/MS	Liquid Chromatography with tandem mass spectrometry
LCAD	Long-chain acyl CoA dehydrogenase
LCFA	Long-chain fatty acid
LCHAD	Long-chain hydroxyacyl-CoA dehydrogenase
LDH	Lactate dehydrogenase
LDL	Low-density lipoprotein
LFD	Low-fat diet
LIVCS	Branched chain amino acid:cation symporter family
LPL	Lipoprotein lipase
LV	Left ventricle
LVAW	Left ventricular anterior wall thickness
LVID	Left ventricular interior diameter
LVNC	Left ventricular non-compaction
LVPW	Left ventricular posterior wall thickness
MAS	Malate aspartate shuttle
MCAD	Medium-chain acyl-CoA dehydrogenase

MCD	Malonyl CoA decarboxylase
MCFA	Medium-chain fatty acid
MCT	Monocarboxylic acid transporter
MCU	Mitochondrial calcium uniporter
MDH	Malate dehydrogenase
MLCL	Monolysocariolipin
MPC	Mitochondrial pyruvate carrier
NADH	Reduced nicotinamide adenine dinucleotide
NMR	Nuclear magnetic resonance
OGTT	Oral glucose tolerance test
PCr	Phosphocreatine
PDH	Pyruvate dehydrogenase
PDHK	Pyruvate dehydrogenase kinase
PDHP	Pyruvate dehydrogenase phosphatase
PPAR	Peroxisome proliferator-activated receptor
PPC2	Protein phosphatase 2C
RER	Respiratory exchange ratio
ROS	Reactive oxygen species
SCOT	Succinyl CoA:3-ketoacid CoA transferase
SGLT2	Sodium-glucose cotransporter-2
SLC	Solute carrier
STZ	Streptozotocin
T1D	Type 1 diabetes mellitus
T2D	Type 2 diabetes mellitus
TAG	Triacylglycerol
TazKD	*Tafazzin* knockdown mice
TCA	Tricarboxylic acid cycle
TFP	Mitochondrial trifunctional protein
VC	Vehicle control
VLCAD	Very long-chain acyl CoA dehydrogenase
VLDL	Very-low density lipoprotein

WT	Wild type
α-KGDH	α-ketoglutarate dehydrogenase
βHAD	β-hydroxyacyl CoA dehydrogenase
βOHB	β-hydroxybutyrate

Chapter 1: Introduction

1.1 Introduction to Cardiomyopathies and Myocardial Intermediary Energy Metabolism

1.1.1 Clinical Characterization of Cardiomyopathies

Cardiomyopathies represent a broad spectrum of heart muscle diseases with complex and diverse etiologies (1). Failure of myocardial performance is a consequence of cardiomyopathy development and can be defined as mechanical dysfunction resulting from impaired myocardial contraction (systolic dysfunction) or relaxation (diastolic dysfunction), or electrical dysfunction which can predispose an individual to life-threatening arrhythmias. Since 1957 when the term was first introduced (2), the definition and classification of cardiomyopathies has evolved significantly (3). According to the most recent definition proposed by the American Heart Association in 2006:

> "*Cardiomyopathies are a heterogeneous group of diseases of the myocardium associated with mechanical and/or electrical dysfunction that usually (but not invariably) exhibit inappropriate ventricular hypertrophy or dilatation and are due to a variety of causes that frequently are genetic. Cardiomyopathies either are confined to the heart or are part of generalized systemic disorders, often leading to cardiovascular death or progressive heart-related disability (3)*."

The classification scheme presented by the American Heart Association identifies cardiomyopathies as belonging to one of two major groups (3). Cardiomyopathies that are most effectively classified as *primary* are solely or predominately confined to the heart muscle and can be further categorized as genetic, mixed (genetic and nongenetic origins) or acquired. *Secondary* cardiomyopathies represent myocardial complications that occur as a result of systemic disorders that affect multiple organs. However, distinct classification of cardiomyopathies is exceptionally complex as primary cardiomyopathies can also have extra-cardiac implications and secondary cardiomyopathies can chiefly affect the myocardium although result from systemic illness. Consequently, overlap between categories is an inevitable limitation of the proposed classification

scheme which has been a topic of debate in the literature (4, 5). As such, the European Society of Cardiology proposed an update to the present classification system in 2008 that grouped cardiomyopathies according to the specific morphological and functional phenotype (6). **Figure 1.1 and Table 1.1** outline and list the disease prevalence, respectively, of the four primary cardiomyopathy phenotypes: hypertrophic, dilated, arrhythmogenic and restrictive (6, 7). Non-invasive echocardiography is a cardiac imaging modality that can be effectively utilized both in humans and animal models to assess myocardial function and determine the cardiomyopathy phenotype. Representative echocardiography images and associated assessment parameters are detailed in **Figure 1.2**.

The studies presented herein investigate Barth syndrome cardiomyopathy, as well as the cardiomyopathy associated with obesity and diabetes mellitus. Perturbations in cardiac intermediary energy metabolism is postulated to be a key contributing mechanism to cardiomyopathy development in Barth syndrome and diabetes. As such, altered cardiac bioenergetics in cardiomyopathies was the primary topic of investigation for the studies enclosed within.

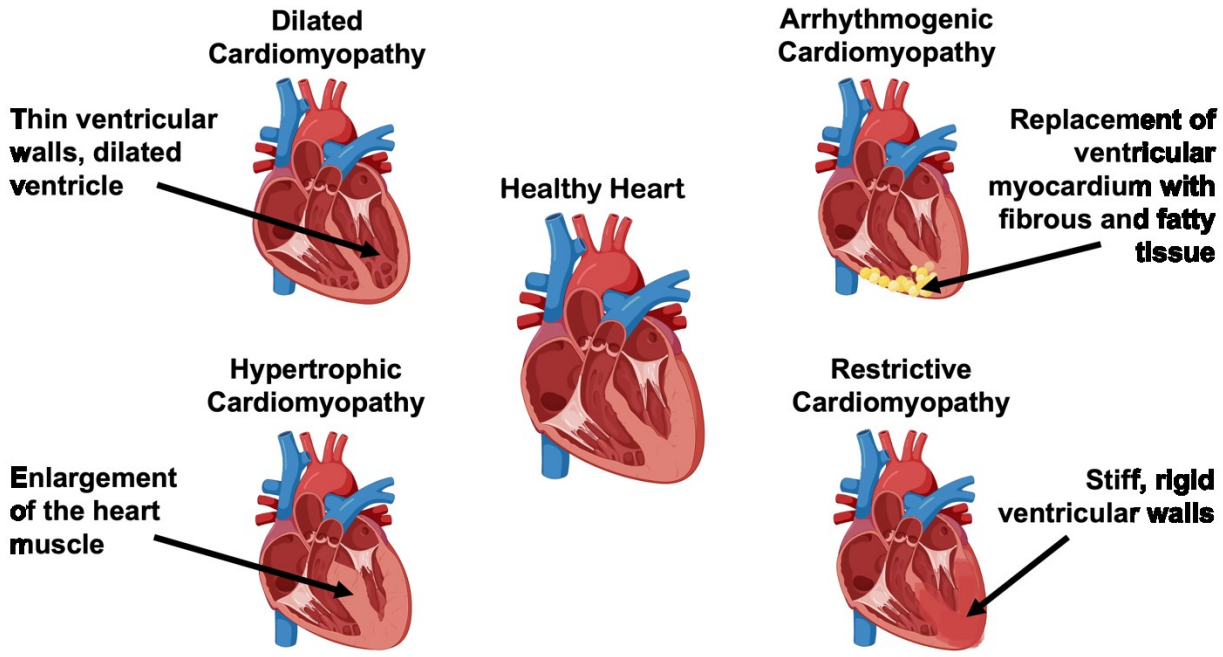

Figure 1.1. *Cardiomyopathy phenotypes*. Dilated cardiomyopathy is defined by dilatation of the left or both ventricles with normal or reduced ventricular wall thickness and is associated with ventricular systolic dysfunction (7). Hypertrophic cardiomyopathy is characterized by the presence of left ventricular cardiac myocyte hypertrophy and interstitial fibrosis leading to increased ventricular wall thickness and an impairment of ventricular diastolic function (8). Arrhythmogenic cardiomyopathy is histologically characterized by the extensive replacement of primarily right ventricular myocardium with fatty and fibrous tissue, predisposing individuals to ventricular arrythmias, impairment of ventricular systolic function and sudden cardiac death (9). Although the original characterization defined predominant right ventricular involvement, greater left ventricular involvement in arrhythmogenic cardiomyopathy has also been reported (10). Restrictive cardiomyopathy can affect either or both ventricles and results from increased myocardial wall stiffness with normal wall thickness leading to ventricular diastolic dysfunction and arrythmias (11). Created with BioRender.com.

Table 1.1. Prevalence of the primary cardiomyopathy phenotypes

Cardiomyopathy Phenotype	**Adults (19-64 years)**
Hypertrophic	1:200/500* (12, 13)
Dilated	1:250/500 (14)
Arrhythmogenic	1:1000/5000 (9, 15)
Restrictive	Uncommon (11)

Adapted from McKenna *et al.* (2017) (16). *Estimates include the prevalence of carriers of sarcomere protein gene mutations known to cause hypertrophic cardiomyopathy in the general population (13).

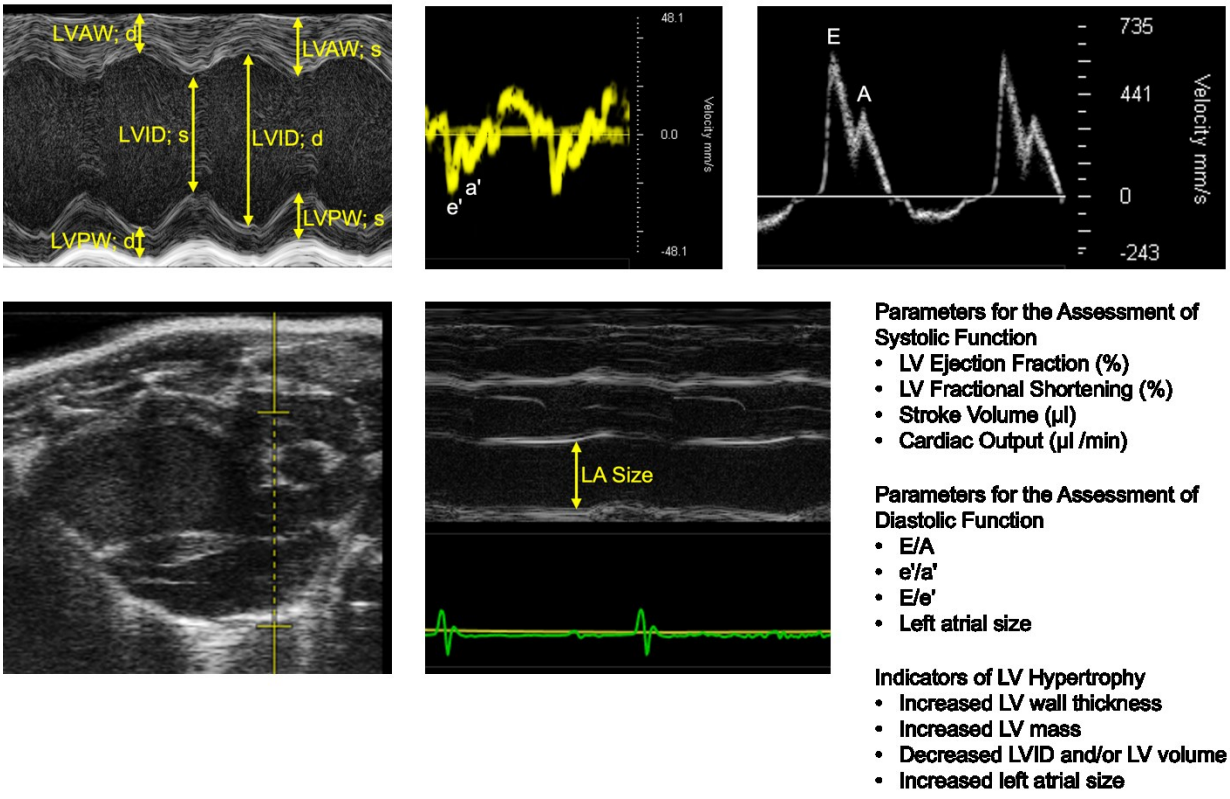

Figure 1.2. *Evaluation of cardiac structure and function utilizing echocardiography.* Upper panel from left to right: parasternal short axis view in M-mode, mitral annular velocity obtained by tissue Doppler imaging in the parasternal short axis view, mitral valve inflow obtained by pulsed wave Doppler imaging in the apical four chamber view. Lower panel from left to right: parasternal long axis view in B-mode with the position for the measurement of anteroposterior left atrial diameter indicated, parasternal long axis view in M-mode. LV, left ventricle; LVAW, left ventricular anterior wall; LVPW, left ventricular posterior wall; LVID, left ventricular internal diameter; s, systole; d, diastole; e', early diastolic mitral annular velocity; a', late diastolic mitral annular velocity; E, mitral peak early diastolic filling velocity; A, mitral peak late diastolic filling velocity; LA, left atrium. LA size is represented by maximal anteroposterior left atrial diameter.

1.1.2 Intermediary Energy Metabolism in the Healthy Heart

Relative to its size, the heart possesses a metabolic demand that far exceeds that of any other organ in the body (17, 18). However, despite the extraordinary energy requirements necessary to sustain constant contractile function, basal metabolic processes and ionic homeostasis, the heart has limited energy reserves and, therefore, must continually regenerate adenosine triphosphate (ATP) in order to maintain function. Although the heart relies preferentially on fatty acid metabolism to sustain a sufficient ATP supply, the heart acts omnivorously and demonstrates a unique capability to metabolize a variety of substrates in addition to fatty acids, such as carbohydrates (glucose and lactate), ketone bodies and amino acids (17, 18). This flexibility of substrate utilization allows the heart to accommodate alterations in substrate availability throughout various physiological states (e.g., nutrient ingestion, fasting). Of importance, this flexibility may deteriorate in response to pathological conditions where the heart must adjust its substrate preference to accommodate a perturbation in energy supply or demand, such as that seen in cardiomyopathies and subsequent heart failure (18-20).

The heart derives the majority (~95%) of its ATP production from the mitochondrial oxidation of fatty acids, carbohydrates, ketone bodies (e.g., acetoacetate, β-hydroxybutyrate (βOHB)), and amino acids, with the remainder being produced through aerobic glycolysis (17, 18). In the mature heart, fatty acids account for the majority of oxidative metabolism (50-70%), with the oxidation of glucose primarily accounting for the remainder. However, in response to nutrient ingestion, carbohydrates (glucose) can become the predominant fuel in the mature, metabolically flexible heart, due to the ensuing insulin response (17, 18). Although the heart is capable of metabolizing ketone bodies and amino acids, the majority of studies have demonstrated minimal contribution of these substrates to myocardial ATP production (17). Conversely, recent studies in isolated working mouse hearts have demonstrated that ketone bodies can become a major fuel source for the heart, particularly at circulating concentrations representative of prolonged fasting/starvation (21).

1.1.3 Fatty Acid Metabolism in the Healthy Heart

The heart's coronary circulation provides it with its fatty acid supply either as free fatty acids bound to albumin or following the release of fatty acids from the hydrolysis of triacylglycerol (TAG)-containing lipoproteins or chylomicrons, mediated predominantly by the actions of lipoprotein

lipase (18, 22). The majority of extracellular fatty acid uptake into the cardiac myocyte occurs through protein-mediated transport, which involves transporters such as cluster of differentiation 36 (CD36) and fatty acid transport proteins (FATP), whereas passive diffusion is thought to contribute to a smaller extent (18, 23, 24). Once present in the cytosol, fatty acids are rapidly activated for further metabolism via esterification to coenzyme A (acyl CoA) in an ATP-dependent manner by fatty acyl CoA synthetase.

Acyl CoAs have three primary metabolic fates in the heart, where they can be stored as TAG, utilized for the biosynthesis of membranes, and most importantly, due to the heart's enormous energy demand, transported into the mitochondria for subsequent β-oxidation (18). Because the mitochondrial membrane is impermeable to long chain acyl CoAs, mitochondrial fatty acid uptake and subsequent β-oxidation is dependent upon a carnitine shuttle comprised of three enzymes. An outer mitochondrial membrane-localized carnitine palmitoyl transferase 1 (CPT1) catalyzes the conversion of long chain acyl CoA into acylcarnitine for transport to the mitochondrial matrix by carnitine acyl translocase, following which the acyl CoA is regenerated via CPT2 present in the inner leaflet of the inner mitochondrial membrane (18). Of importance, this carnitine shuttle regulating mitochondrial fatty acid uptake and subsequent β-oxidation is highly sensitive to regulation via malonyl CoA, a potent endogenous inhibitor of CPT1. Malonyl CoA is the product of acetyl CoA carboxylation via acetyl CoA carboxylase (ACC), whereas it is degraded by malonyl CoA decarboxylase (MCD). Once inside the mitochondrial matrix, the CPT2 regenerated acyl CoA is finally subjected to repeated cycles of β-oxidation, a process involving four enzymes (acyl CoA dehydrogenase, enoyl CoA hydratase, 3-hydroxyacyl CoA dehydrogenase, and 3-ketoacyl CoA thiolase) that progressively shortens the acyl CoA via 2 carbons released as acetyl CoA with each cycle. Acetyl CoA subsequently enters the tricarboxylic acid (TCA) cycle where it joins with oxaloacetate to form citrate and undergo a series of redox reactions. The TCA cycle results in the formation of reducing equivalents (reduced flavin adenine dinucleotide/nicotinamide adenine dinucleotide) that donate their electrons to the complexes of the electron transport chain (ETC) for the generation of ATP during oxidative phosphorylation. The heart also contains endogenous TAG stores that can be used to support ATP production, with some studies suggesting that fatty acids taken up into the heart are first shuttled through the intracellular TAG pool prior to undergoing mitochondrial β-oxidation (25, 26).

1.1.4 Carbohydrate Metabolism in the Healthy Heart

Myocardial glucose metabolism for energy production involves three major steps: glucose uptake, glycolysis, and the mitochondrial oxidation of glycolytically-derived pyruvate, a process referred to as glucose oxidation. Glucose uptake into cardiac myocytes is facilitated by glucose transporters (GLUT), of which GLUT4 and GLUT1 are responsible for insulin-dependent and insulin-independent glucose uptake, respectively (27, 28). Glucose subsequently undergoes glycolysis in the cytosol, a metabolic pathway comprised of ten enzymes that result in the formation of minimal energy (2 ATP) and the three-carbon end-product, pyruvate. Glycolytically-derived pyruvate has two primary metabolic fates, where it can either be converted to lactate by lactate dehydrogenase or shuttled into the mitochondrial matrix by a monocarboxylic acid transporter (referred to as the mitochondrial pyruvate carrier (MPC)) for subsequent oxidation. In the healthy mature heart where oxygen is not limiting, the latter mechanism predominates and is regulated by the actions of the pyruvate dehydrogenase (PDH), the rate-limiting enzyme of glucose oxidation (29, 30).

The PDH complex is a multienzyme complex that decarboxylates pyruvate into acetyl CoA, which has the same fate as fatty acid oxidation-derived acetyl CoA and enters the TCA cycle to generate reducing equivalents for supporting oxidative phosphorylation in the ETC. The PDH complex is intricately regulated by numerous post-translational modifications, including phosphorylation-mediated inactivation via four PDH kinase (PDHK) isoforms, and dephosphorylation-mediated activation via two PDH phosphatase (PDHP) isoforms (29-31). Recent studies have also demonstrated that PDH activity and subsequent glucose oxidation can be stimulated via sirtuin 3-mediated deacetylation (32). As many mitochondrial dehydrogenases including PDH are sensitive to calcium-mediated stimulation (33), it has been demonstrated that mitochondrial calcium uptake mediated by the mitochondrial calcium uniporter (MCU) can positively regulate PDH activity (34).

The heart also contains endogenous glycogen stores from which glucose can be mobilized to support myocardial ATP production when needed. Another metabolic pathway of glucose includes the pentose phosphate pathway which plays a major role in the production of reduced nicotinamide adenine dinucleotide phosphate needed to generate the endogenous antioxidant, reduced glutathione (35). Although evidence suggests that perturbations in the pentose phosphate pathway

may be implicated in the pathology of heart failure (36), glucose flux through this pathway in the healthy mature heart is thought to be negligible (35, 37).

1.1.5 Ketone Body Metabolism in the Healthy Heart

βOHB and acetoacetate are the two primary ketone bodies that the heart utilizes to support energy production. While both can enter the cardiac myocyte via passive diffusion, at elevated concentrations it has also been suggested that ketone body uptake may involve monocarboxylic acid transporters (38, 39). βOHB is converted into acetoacetate via the actions of βOHB dehydrogenase (BDH1). Acetoacetate is subsequently activated for metabolism via esterification to CoA as acetoacetyl CoA, which is catalyzed via succinyl CoA:3-ketoacid CoA transferase (SCOT). Acetoacetyl CoA thiolase (ACAT1) then hydrolyzes acetoacetyl CoA into two molecules of acetyl CoA, which are subject to the same metabolic fate as either glucose or fatty acid oxidation-derived acetyl CoA, thereby entering the TCA cycle to generate reducing equivalents for supporting oxidative phosphorylation.

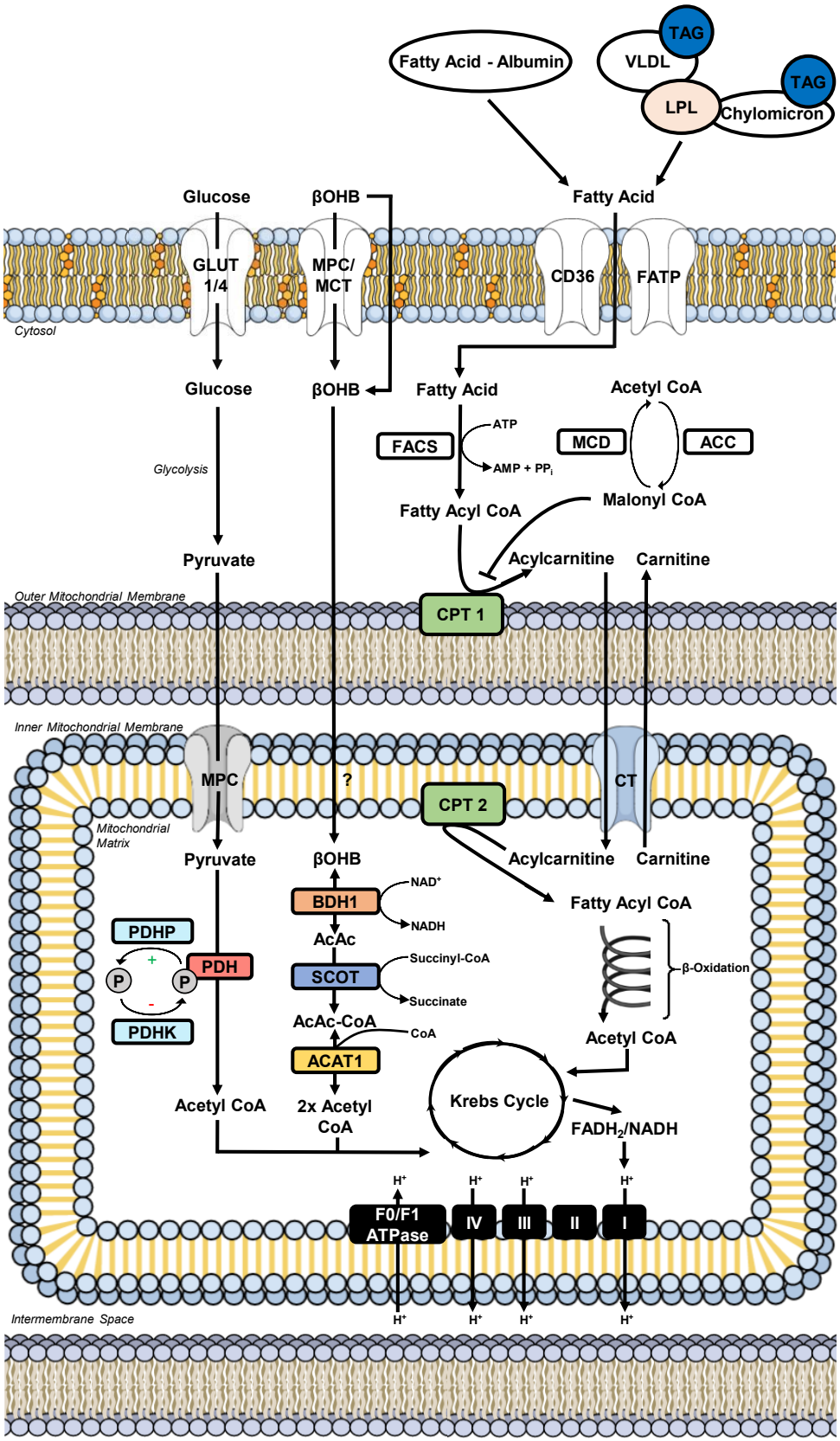
Fatty Acid - Albumin
TAG
VLDL
LPL
TAG
Chylomicron
Fatty Acid
Glucose
βOHB
GLUT 1/4
MPC/ MCT
CD36
FATP
Cytosol
Glucose
βOHB
Fatty Acid
Acetyl CoA
FACS
ATP
AMP + PPi
MCD
ACC
Glycolysis
Fatty Acyl CoA
Malonyl CoA
Pyruvate
Acylcarnitine
Carnitine
Outer Mitochondrial Membrane
CPT 1
Inner Mitochondrial Membrane
MPC
?
CPT 2
CT
Mitochondrial Matrix
Pyruvate
βOHB
Acylcarnitine
Carnitine
Fatty Acyl CoA
NAD+
BDH1
NADH
AcAc
PDHP
PDH
Succinyl-CoA
SCOT
Succinate
β-Oxidation
AcAc-CoA
CoA
ACAT1
Acetyl CoA
Acetyl CoA
2x Acetyl CoA
Krebs Cycle
FADH2/NADH
H+
F0/F1 ATPase
IV
III
II
I
Intermembrane Space

Figure 1.3. *Intermediary energy metabolism in the cardiac myocyte.* Illustration depicts intermediary metabolism of carbohydrates (glucose), fatty acids, and ketone bodies (βOHB) in the myocardium. Key nodes depicting the control of uptake into the cardiac myocyte, uptake into the mitochondria, and subsequent metabolism to acetyl CoA are highlighted. Acetyl CoA from the oxidation of carbohydrates, fatty acids, and ketone bodies is subsequently metabolized further in the TCA/Krebs cycle. This results in the formation of reducing equivalents (e.g., $FADH_2$/NADH) that donate their electrons to the complexes of the electron transport chain, driving oxidative phosphorylation and the ATP generation needed for sustaining contractile function. ACAT, acetoacetyl CoA thiolase; ACC, acetyl CoA carboxylase; BDH, β-hydroxybutyrate dehydrogenase; βOHB, β-hydroxybutyrate; CD36, cluster of differentiation 36; CPT, carnitine palmitoyl transferase; CT, carnitine translocase; FACS, fatty acyl CoA synthetase; $FADH_2$, reduced flavin adenine dinucleotide; FATP, fatty acid transport protein; GLUT, glucose transporter; LPL, lipoprotein lipase; MCD, malonyl CoA decarboxylase; MCT, monocarboxylic acid transporter; MPC, mitochondrial pyruvate carrier; NADH, reduced nicotinamide adenine dinucleotide; PDH, pyruvate dehydrogenase; PDHK, PDH kinase; PDHP, PDH phosphatase; SCOT, succinyl CoA:3-ketoacid CoA transferase; TAG, triacylglycerol; VLDL, very-low density lipoprotein. Published in Greenwell *et al*. 2020 (40).

1.1.6 Amino Acid Metabolism in the Healthy Heart

Amino acids, namely the branched chain amino acids (BCAAs; leucine, isoleucine, and valine) can also be utilized by the heart as a source of fuel (41). Once taken up into the cardiac myocyte by the branched chain amino acid:cation symporter family (LIVCS) and transported to the mitochondria, mitochondrial branched chain amino-transferase catalyzes the reversible transamination of BCAAs to their correspondent branched chain α-keto-acid (BCKA), including, α-ketoisocaproate (produced from leucine), α-keto-β-methylvalerate (produced from isoleucine), and α-ketovalerate (produced from valine) (42, 43). Oxidative decarboxylation of the BCKAs by mitochondrial branched chain α-keto acid dehydrogenase (BCKDH) then generates acetyl-CoA for the TCA cycle or succinyl CoA for anaplerosis (41). The activity of BCKDH is regulated by the phosphorylation state, whereby dephosphorylation mediated by mitochondrial protein phosphatase 2C activates BCKDH (44), and phosphorylation by mitochondrial branched-chain α-keto acid dehydrogenase kinase inhibits activity (45). While BCAA oxidation contributes

minimally to overall cardiac energy production, (~1-2%) (46, 47), BCAAs can act as critical modulators of signaling pathways in the heart (42).

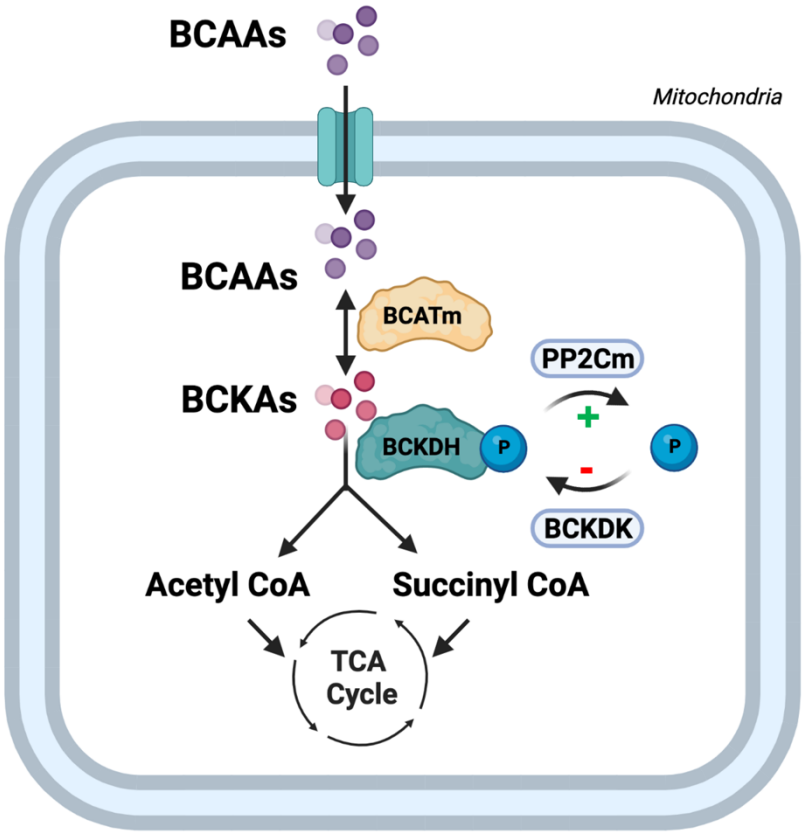

Figure 1.4. *Branched chain amino acid metabolism.* Illustration depicts branched chain amino acid (BCAA) metabolism in the cardiac myocyte. BCAAs are converted to to their correspondent branched chain α-keto-acid (BCKA) by mitochondrial branched chain amino-transferase (BCATm) and subsequently used by mitochondrial branched chain α-keto acid dehydrogenase (BCKDH) to generate acetyl CoA and succinyl CoA for the tricarboxylic acid (TCA) cycle. BCKDH is inhibited by phosphorylation mediated by mitochondrial branched chain α-keto acid dehydrogenase kinase (BCKDK) and activated by dephosphorylation mediated by mitochondrial protein phosphatase 2C (PP2Cm). P: phosphate group. Created with BioRender.com. Adapted from Karwi *et al*. 2022 (41).

1.1.7 Substrate Competition for Oxidative Metabolism

A significant contributor to the heart's robust metabolic flexibility to switch between fatty acids and glucose as major fuel sources during fasting and nutrient ingestion, respectively, involves substrate competition for oxidative metabolism. Joseph Shipp and colleagues were the first to demonstrate that increasing fatty acid availability to the heart leads to a marked inhibition of glucose oxidation (48). However, credit for the reciprocal relationship by which fatty acids and glucose compete for oxidative metabolism (glucose/fatty acid cycle) is attributed to the work of Philip Randle *et al*. (49), and is thus often referred to as the "Randle Cycle." A plethora of both animal and human studies have provided strong evidence to support substrate competition between fatty acids and glucose for oxidative metabolism in the heart (50-53). Conversely, recent evidence has suggested that increasing the heart's reliance on ketone bodies as an oxidative fuel source is not subject to the same reciprocal relationships that would be conjectured to lead to reduced glucose and fatty acid oxidation rates (21).

1.2 Disturbances of Myocardial Energy Metabolism in Barth Syndrome

1.2.1 Overview of Barth Syndrome-Related Cardiomyopathy

Cardiomyopathy is the most common clinical feature and primary driver of disease outcomes in Barth syndrome (BTHS; Online Mendelian Inheritance in Man [OMIM] 302060), a rare X-linked mitochondrial disorder first described by Dr. Peter Barth and colleagues in 1983 (54, 55). Despite the broad variability in clinical presentation, which can include features such as neutropenia, skeletal myopathy, exercise intolerance, 3-methylglutaconic aciduria, and pre-pubertal growth retardation, cardiomyopathy manifests in approximately 90% of males with BTHS (56-58). However, the severity and specific cardiomyopathy phenotype can vary both between individuals and throughout disease progression with no definite genotype-phenotype correlations having yet been identified (57, 59). Dilated cardiomyopathy is most common, however other forms including restrictive, hypertrophic, and hypertrophic-dilated cardiomyopathy have also been reported (55, 60, 61). Individuals with BTHS may also present with endocardial fibroelastosis and left ventricular non-compaction (LVNC) either alone or in conjunction with another cardiomyopathy phenotype (62, 63). An “undulating phenotype” referring to transition between cardiomyopathy forms has also been described in the context of LVNC (64, 65).

Barth syndrome is caused by pathogenic mutations in the *TAFAZZIN* gene, formerly notated as *TAZ,* on chromosome Xq28, which encodes for the tafazzin protein, a phospholipid transacylase responsible for cardiolipin (CL) remodeling (66). CL is a unique, dimeric, tetra-acyl phospholipid found almost exclusively in the inner mitochondrial membrane (IMM) with essential roles in the maintenance of mitochondrial morphology, and in fundamental mitochondrial functions including fission-fusion dynamics, mitophagy, apoptosis and energy metabolism (67-69). The tissue-specificity of the fatty acyl chain configuration of CL is functionally important with tetralinoleoyl-CL (L_4CL) being the predominant CL species in the mammalian heart (70, 71). Post-biosynthetic remodeling of nascent CL by deacylation to monolysocardiolipin (MLCL) and subsequent reacylation by acyltransferases including tafazzin is required to achieve mature CL compositions such as L_4CL (72). In BTHS, defective tafazzin-mediated CL remodeling results in a depletion of total CL and remodeled L_4CL, and an accumulation of the intermediate MLCL species (73, 74). As such, elevation of the MLCL/CL ratio in blood, lymphocytes, fibroblasts, and skeletal muscle represents a highly sensitive and selective diagnostic parameter for BTHS (75).

1.2.2 Impairment of Cardiac Energy Production in Barth Syndrome

Impaired cardiac energy production is a principal contributor to the development and progression of heart failure (19, 20), which appears to also be present in BTHS (76, 77). Indeed, the phosphocreatine to ATP ratio (PCr/ATP), an indicator of cardiac high-energy phosphate metabolism determined by ^{31}Phosphorus magnetic resonance spectroscopy, was reduced in young adults 18-36 years of age and children/adolescents with BTHS compared to healthy participants (78). Nonetheless, the molecular mechanisms linking tafazzin deficiency to perturbed myocardial energetics are presently not well-characterized. Although defective CL remodeling is associated with dysfunction of the inner mitochondrial membrane respiratory chain (72, 79), evidence that impairments in oxidative metabolism are substrate specific in BTHS may indicate a primary defect in upstream intermediary metabolism pathways (80-82). Accordingly, further investigation is needed to characterize the alterations in myocardial intermediary metabolism that accompany tafazzin deficiency in order to determine the potential of targeting these pathways as a therapeutic approach to mitigate the development of BTHS cardiomyopathy.

1.2.3 Mitochondrial Respiratory Abnormalities in Barth Syndrome

Notably, *TAFAZZIN* deficiency is associated with an impairment of mitochondrial respiratory capacity and ATP production, which to date, has largely been attributed to destabilization of the IMM ETC (83). There is evidence to suggest that the preferential incorporation of remodeled, structurally distinct CL species may enable the IMM of highly oxidative tissues to accommodate an enhanced surface density of oxidative phosphorylation proteins by mitigating the curvature stress associated with protein crowding (84, 85). Therefore, it can be postulated that impaired CL remodeling in BTHS may compromise the capacity of the inner membrane of cardiac mitochondria to concentrate oxidative phosphorylation proteins, thus limiting respiratory capacity. In line with this hypothesis, the relative abundances of all ETC complexes (complexes I-V) were reduced in cardiac mitochondria isolated from *Tafazzin* knockout mice at 5 months of age as measured by label-free quantitative proteomics (84). In addition, the combined spectral counts of proteins representing complexes I, III, IV and V (F_1F_0-ATP synthase) determined by LC-MS/MS analysis of the cardiac proteome were reduced in left ventricular tissue from individuals with BTHS compared to non-failing control heart samples, however, after normalization to the mitochondrial marker, citrate synthase, only a selective depletion in complex I was observed (86).

Furthermore, the abnormal CL profile in tafazzin-deficient mitochondria is associated with the destabilization of respiratory chain supercomplexes as demonstrated in lymphoblasts (87), fibroblasts (88), and induced pluripotent stem cells derived from individuals with BTHS (89), as well as in mouse models of BTHS (90, 91) and CL-deficient yeast (92). The organization of ETC components into supercomplexes is posited to enhance the efficiency of electron translocation and, thus, reduce reactive oxygen species (ROS) generation (93). Analysis of cardiac mitochondria isolated from 2-month-old cardiac myocyte-specific *Tafazzin* knockout mice prior to the appearance of cardiomyopathy revealed structural remodeling of the respiratory chain with a shift from high molecular weight supercomplexes containing complex I, dimeric complex III (III_2), and several copies of complex IV (also known as respirasomes) to lower molecular weight forms such as heterooligomers comprised of complexes I and III_2, as well individual complexes I, III and IV (91). This rearrangement of the respiratory chain was associated with increased mitochondrial ROS levels and reduced pyruvate, palmitate, and succinate/rotenone-supported state 3 (adenosine diphosphate (ADP)-stimulated) respiration rates and suggests that defective tafazzin-mediated CL

remodeling may impair the association of complex IV to supercomplexes, which has also been observed in lymphoblasts from BTHS patients (87). In addition, CL plays an integral role in the enzymatic activity of individual respiratory complexes which also feature specific CL binding sites (72, 94). In the BTHS heart, a reduction in the enzymatic activity of complex III in cardiac mitochondria isolated from *Tafazzin* knockdown (TazKD) mice 2 and 3-4 months of age was demonstrated (81, 83, 95), as well as a decrease in complex V (F_1F_0-ATP synthase) activity in TazKD mice and BTHS iPSC-derived cardiac myocytes (77, 81). The enzymatic activities of complexes I and IV were also reduced by 16 and 26%, respectively, in cardiac mitochondria from 4-6-month-old TazKD mice (82). Furthermore, a cardiac-specific impairment of succinate dehydrogenase (complex II) activity due to reduced protein levels was also observed in TazKD mice (95). Alternatively, protein levels and enzymatic activities of complexes I-IV were not altered in heart tissue and cardiac mitochondria, respectively, from 2-month-old cardiac myocyte-specific *Tafazzin* knockout mice (91).

Although the detrimental consequences of tafazzin deficiency on the structural integrity and optimal functioning of the ETC are well-defined, several studies have identified specific derangements in upstream intermediary energy metabolism pathways (80-82), thus highlighting the complexity of the metabolic phenotype and proposing that mechanisms beyond respiratory chain dysfunction may contribute to the cardiac energy deficit in BTHS cardiomyopathy. Indeed, although state 3 respiration rates supported by pyruvate and palmitoylcarnitine were impaired in cardiac mitochondria from TazKD mice 4-6 months of age, glutamate-supported rates were elevated and approximated rates supported by other substrates in wild-type (WT) mitochondria (82). Therefore, deficient tafazzin-mediated CL remodeling may not sufficiently limit oxidative phosphorylation-linked cardiac mitochondrial respiratory capacity, per se, but rather may selectively impair the oxidation of particular energy substrates as will be elucidated in the following sections.

1.2.4 Perturbation of Myocardial Fatty Acid Metabolism in Barth Syndrome

Several studies have provided evidence to support a link between tafazzin deficiency and impaired cardiac fatty acid metabolism in BTHS. Myocardial fatty acid extraction and uptake following positron emission tomography imaging with [1-^{11}C]palmitate were significantly reduced in young

adults with BTHS compared to healthy, age-matched controls, though myocardial fatty acid oxidation remained similar (76). Furthermore, cardiac mitochondria isolated from TazKD mice at 2 months or 4-6 months of age, and from 2-month-old mice with a cardiac-specific *Tafazzin* deficiency demonstrated a significant repression of state 3 respiration rates supported by palmitoylcarnitine and malate (81, 82, 91). A decrease in palmitoylcarnitine supported ADP-stimulated respiration was also observed in permeabilized cardiac fibers with intact mitochondrial matrices from 4-6-month-old TazKD mice with preserved cardiac function, as determined by high-resolution respirometry (82). Protein expression of fatty acid binding protein and acyl-CoA synthetase, which mediate intracellular fatty acid transport and fatty acid esterification to CoA, respectively, were similar in left ventricular (LV) tissue from male patients with BTHS and non-failing hearts (86). Furthermore, similar enzymatic activities of CPT1 and CPT2 in LV tissue homogenates from male patients with BTHS cardiomyopathy compared to non-failing controls, is suggestive of an impairment downstream of mitochondrial fatty acid uptake (86). Likewise, respiratory capacity of cardiac mitochondria from TazKD mice was decreased compared to WT littermates using palmitoylcarnitine, which bypasses CPT1, whereas respiration with palmitoyl CoA plus carnitine was not reduced, providing further evidence against a specific defect in mitochondrial fatty acid uptake (82).

Alternatively, impaired tafazzin-mediated CL remodeling in BTHS may result in a selective block in long-chain fatty acid β-oxidation. Protein levels of very long-chain acyl CoA dehydrogenase (VLCAD) were decreased in LV tissue from male BTHS subjects compared to age-matched, non-failing male subjects and male subjects diagnosed with idiopathic dilated cardiomyopathy, as assessed by both immunoblotting and LC-MS/MS based proteomic profiling (86). Likewise, VLCAD protein expression was also decreased in cardiac mitochondria from 4-6-month-old TazKD mice compared to WT, as determined via LC-MS/MS based proteomic profiling (82). This is consistent with evidence of disrupted interactions between VLCAD and ETC supercomplexes in isolated cardiac mitochondria from 3-month-old TazKD mice (79). In addition, an accumulation of 3-hydroxy-palmitoyl-CoA in cardiac tissue from 4-6-month-old TazKD mice (82) and male individuals with BTHS (86) is consistent with a selective impairment of IMM long chain fatty acid β-oxidation, particularly downstream of long-chain hydroxyacyl-CoA dehydrogenase (LCHAD) activity catalyzed by the alpha subunit of the trifunctional protein complex (TFPα) (96).

Of interest, protein expression of the TFPα is elevated in heart tissue from BTHS subjects (86). As TFPα also possesses MLCL acyltransferase activity, further investigation is required to determine whether the accumulation of MLCL in BTHS may impair the β-oxidation function of TFPα by shifting towards MLCL reacylation. Further evidence for a general defect in the enzymatic machinery of fatty acid β-oxidation in BTHS is also seen by the decline in medium chain acyl-CoA dehydrogenase protein expression and a reduction in octanoylcarnitine-supported respiration in cardiac mitochondria from TazKD mice (82). However, it is important to consider that while the above-described studies allude to impaired myocardial fatty acid oxidation in BTHS, there are limitations with assessing intermediary metabolism in isolated mitochondria where key cellular regulators (i.e. malonyl CoA) may be removed, and measures of protein expression do not necessarily reflect flux (97).

The current dogma in the field posits that stimulating myocardial fatty acid oxidation may be a novel approach to improve cardiac function in heart failure via increasing energy production to support contraction (42). Supporting such a strategy as a therapeutic approach in BTHS, the pan-peroxisome proliferator-activated receptor (PPAR) agonist, bezafibrate, is currently being investigated in the CARDIOlipin MANipulation (CARDIOMAN) trial (98). PPAR agonists, in particular of PPARα, promote fatty acid β-oxidation via transcriptional upregulation of genes encoding for enzymes involved in fatty acid β-oxidation (99). Intriguingly, treatment of 3-month-old TazKD mice with bezafibrate for 4-months prevented the development of dilated cardiomyopathy and systolic dysfunction, which was associated with increased expression of genes involved in multiple energy metabolism pathways (100). Although the results of the CARDIOMAN trial are not yet published, a summary of the initial results was released by the Barth Syndrome Foundation. This single center, double-blinded, randomized, placebo-controlled crossover study included 11 participants with BTHS who were treated with bezafibrate for 15-weeks. Assessment of cardiac function by ultrasound echocardiography revealed a significant improvement in heart strain at rest, however not during peak exercise, and a trend towards improved heart chamber size. However, given that neither traditional cardiac parameters nor quality of life was changed significantly, these findings of cardiac improvement may not be clinically relevant (https://www.barthsyndrome.org/research/clinicaltrials/cardioman.html, accessed June 03, 2022). Taken together, these bezafibrate-mediated cardiac improvements in

preclinical and clinical studies are encouraging and suggest that stimulating myocardial fatty acid β-oxidation may have utility in BTHS. Nonetheless, it has been suggested by others that systemic activation of PPARα with fibrates may in fact decrease myocardial fatty acid β-oxidation due to the stimulation of hepatic fatty acid β-oxidation and subsequent reduction in circulating lipids (101). Hence, further studies are still required to delineate whether the specific enhancement of cardiac fatty acid β-oxidation is indeed effective in alleviating BTHS-related cardiomyopathy.

1.2.5 Perturbation of Myocardial Carbohydrate Metabolism in Barth Syndrome

Numerous forms of cardiovascular disease (e.g., ischemic heart disease, heart failure, diabetic cardiomyopathy) are characterized by an impairment in myocardial glucose oxidation, often due to defects in PDH, the rate-limiting enzyme of glucose oxidation (102-104). This metabolic perturbation also appears to be present in BTHS-related cardiomyopathy. Indeed, circulating lactate levels are elevated in individuals with BTHS (105), which is consistent with uncoupled glucose metabolism as glycolytically-derived pyruvate is shunted to lactate rather than being oxidized by PDH. Further evidence for a glucose oxidation defect in BTHS has been reported in several studies utilizing the TazKD mouse model and *Tafazzin* deficient cell lines. Utilizing a XF24 Seahorse bioanalyzer, neonatal cardiac myocytes isolated from TazKD mice demonstrated an ~40% decrease in oxygen consumption coincident with an increase in the extracellular acidification rate, suggestive of uncoupled glucose metabolism due to elevated glycolysis and decreased glucose oxidation (83). Furthermore, ADP-stimulated respiration in isolated cardiac subsarcolemmal and intermyofibrillar mitochondria, as well as permeabilized cardiac muscle fibers, was significantly decreased with pyruvate and malate as substrates in 4-6-month-old TazKD mice versus their WT littermates (82). Conversely, no impairment in pyruvate-supported ADP-stimulated respiration was observed in isolated cardiac mitochondria from 2-month-old TazKD mice compared to their WT littermates (81). In addition, C2C12 mouse myoblasts subjected to CRISPR/Cas9-mediated knockout of *Tafazzin* demonstrated decreased incorporation of [U-^{13}C]glucose into acetyl CoA (106). This reduction was associated with increased inhibitory phosphorylation of PDH at serine 293, resulting in an approximate 50% decrease in enzymatic activity that could be rescued by incubation with exogenous CL. Deficiency of mature CL may also blunt Ca^{2+}-dependent PDH dephosphorylation by reducing the abundance and stability of mitochondrial calcium uptake protein 1, the primary regulator of the MCU, thereby impairing

mitochondrial Ca^{2+} uptake and PDH activation in response to an acute increase in cellular energy demand (107). A cardiac-specific downregulation of the MCU pore-forming MCUa subunit has also been observed in 10-week-old TazKD mice, which abrogates Ca^{2+} uptake in isolated cardiac mitochondria (108) and could further explain impairments in PDH activity in BTHS. This defect in normal Ca^{2+} handling was associated with increased myofilament Ca^{2+} sensitivity and decreased cross-bridge cycling velocity, thereby contributing to diastolic dysfunction in TazKD mice which is consistent with observations that a cardiac-specific deficiency of PDH promotes impaired diastolic function (109).

Positron emission tomography imaging studies with [1-^{11}C]glucose in individuals with BTHS (age 18-36 years) contrast the majority of findings in preclinical models of BTHS, as myocardial glucose extraction fraction, uptake and utilization were significantly elevated compared to healthy age-matched controls (76). Interestingly, these alterations in glucose metabolism were significantly associated with reduced parameters of cardiac function including global strain and ejection fraction. However, given that myocardial glucose oxidation rates were not directly assessed in these subjects, it is plausible that the elevated myocardial glycolytic rates observed in BTHS may explain the observed increase in myocardial glucose utilization.

As the stimulation of glucose oxidation in the heart has been shown to improve cardiac function in ischemic heart disease, heart failure, and diabetic cardiomyopathy (102, 104, 110-112), this may be an exciting metabolic approach to alleviate BTHS-related cardiomyopathy, though this has not yet been thoroughly investigated. Dichloroacetate (DCA) is a pyruvate analogue that inhibits PDH kinase, thereby resulting in reduced PDH phosphorylation and the stimulation of PDH activity and glucose oxidation. Treatment with DCA has been beneficial in alleviating diabetic cardiomyopathy and attenuating heart failure progression in rat models (112), and reducing infarct size in mice subjected to experimental ischemia-reperfusion injury (104). Therefore, treatment with DCA may represent a novel intervention for BTHS, however, further investigation will be required to determine whether the pharmacological optimization of glucose oxidation is an effective therapeutic approach to mitigate BTHS-related cardiomyopathy.

1.2.6 Perturbation of Myocardial Ketone Body Metabolism in Barth Syndrome

Observations that the failing heart increases its reliance on ketones as an oxidative fuel source (113, 114) has led to increased investigation of potential perturbations in myocardial ketone metabolism during the pathology of cardiovascular disease. Whether a similar shift in myocardial substrate utilization occurs in BTHS remains enigmatic, though metabolomics studies in 23 individuals with BTHS demonstrated a 1.8-fold increase in circulating βOHB levels in comparison to 15 age-matched individuals not known to have an inborn error of metabolism (115). An increase in myocardial βOHB content was also observed in LV samples from BTHS subjects compared to age-matched non-failing control heart samples (86). This result was associated with a downregulation of the TCA cycle enzyme, succinyl coenzyme A synthetase, which may imply that TCA cycle intermediates could be diverted to promote the succinyl-CoA-dependent oxidation of βOHB in the tafazzin-deficient heart.

It has been proposed that the salutary actions of sodium-glucose cotransporter-2 (SGLT2) inhibitors in heart failure with reduced or preserved ejection fraction in the presence or absence of diabetes may be due in part to increasing circulating ketone levels and subsequent myocardial ketone oxidation (116-118). Accordingly, interventions that optimize cardiac ketone oxidation may represent a potential target to alleviate BTHS-related cardiomyopathy. Moreover, such a strategy may prove to be a more viable metabolic target due to the enzymes of ketone oxidation not being as reliant on interactions with CL for their activity as they are primarily localized to the mitochondrial matrix (119, 120).

1.2.7 Perturbation of Myocardial Amino Acid Metabolism in Barth Syndrome

Although amino acids contribute minimally to cardiac ATP production under normal physiological conditions (41), combined glutamate and malate-supported state 3 respiration was upregulated by 45-68% in cardiac mitochondria isolated from TazKD mice 4-6 months of age compared to their WT littermates (82). Because *TAFAZZIN* deficiency may reduce CoA availability, it was postulated that the increased reliance on glutamate metabolism may manifest since glutamate can be oxidized through the malate-aspartate shuttle, which generates NADH through CoA-independent reactions. The activity of the TCA cycle enzyme, α-ketoglutarate dehydrogenase (α-KGDH), regulates flux of the metabolic intermediate, α-ketoglutarate, between the malate

aspartate shuttle (MAS) and the TCA cycle, whereby reduced activity of α-KGDH facilitates the diversion of α-ketoglutarate into the MAS (121). The upregulated glutamate oxidation in cardiac mitochondria from TazKD mice was associated with increased and decreased protein expression of the key MAS enzyme, malate dehydrogenase (MDH), and dihydrolipoyl succinyl transferase, a critical subunit of the α-KGDH complex, respectively, which is consistent with an enhancement of MAS flux and subsequent glutamate oxidation (82). Likewise, a 25% increase in glutamate-stimulated state 3 respiration was also reported in isolated cardiac mitochondria from 2-month-old TazKD mice (81). This particular study also reported a 6-fold increase in glutamate-stimulated activity of the CL-regulated adenine nucleotide translocase in TazKD mouse cardiac mitochondria, thus suggesting that aberrant CL remodeling may influence substrate selectivity of the adenine nucleotide translocase and overall ETC flux.

Circulating BCAAs are positively associated with cardiovascular disease (114, 122), and there appears to be both transcriptional and proteomic downregulation of pathways involved in BCAA metabolism in hearts from TazKD mice at 2-3 months of age (79, 81). A decrease in cardiac BCAA metabolism, depending on where the restriction is, may lead to increased levels of myocardial BCAAs and their correspondent keto acids, the latter of which are proposed to explain how BCAA metabolism promotes cardiac insulin resistance and cardiac hypertrophy (123). Alternatively, it has been suggested that amino acid utilization is enhanced in individuals with BTHS versus activity matched healthy control subjects as they exhibited decreased serum levels of amino acids involved in TCA Cycle anaplerosis including arginine, ornithine and citrulline (124). Nonetheless, an increased reliance on amino acid metabolism to support energetic demands could potentially result in increased proteolysis of skeletal and cardiac muscle, which may contribute to the decreased lean mass and cardiac dysfunction characteristic of the BTHS phenotype (125). Supporting this perspective, a higher whole-body leucine rate of appearance per kg of fat-free mass, a measure of proteolysis, demonstrated a trend towards an association with worsened LV function as determined by lower LV global strain in adolescents and young adults with BTHS (124). While there appears to be several disturbances in myocardial amino acid metabolism present in BTHS, further investigation will be required to determine whether such disturbances are a viable metabolic target to alleviate BTHS-related cardiomyopathy.

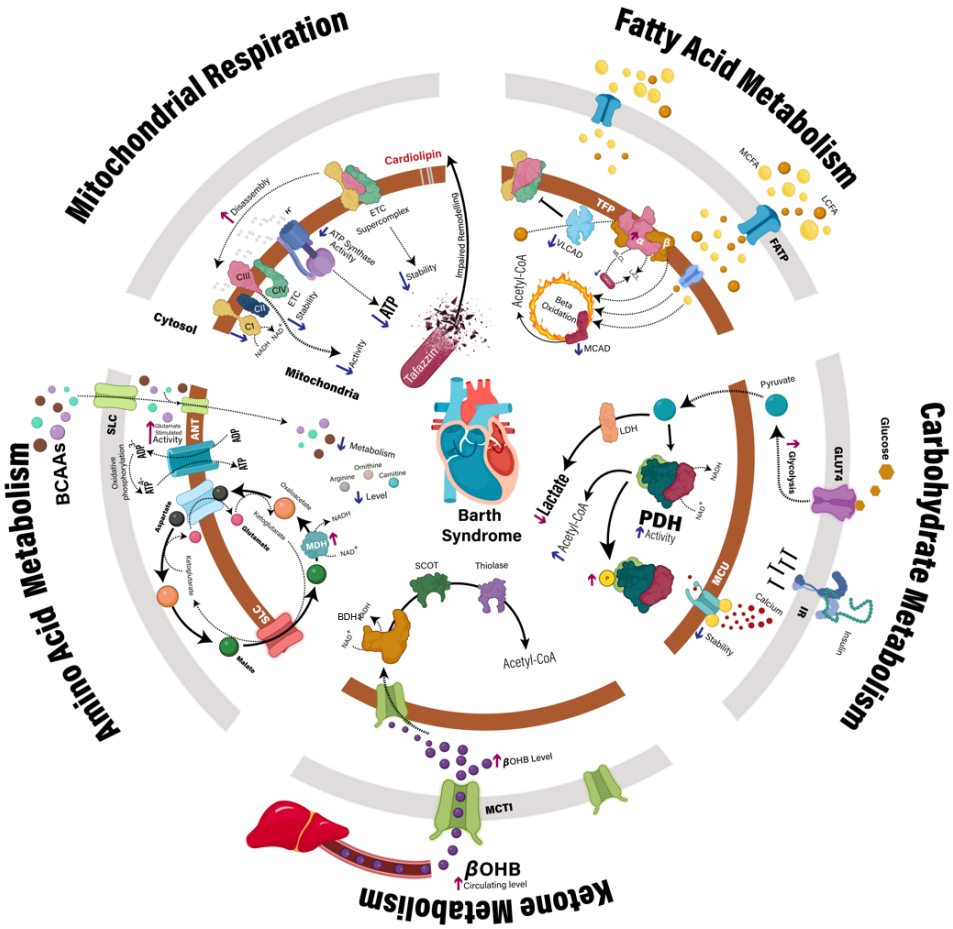

Figure 1.5. *Myocardial metabolic disturbances in Barth syndrome.* Clinical and preclinical studies have identified multiple mechanisms that may contribute to impaired cardiac ATP production in the context of *TAFAZZIN* deficiency. In addition to direct impairment of the mitochondrial electron transport chain, specific defects have also been identified relating to the intermediary metabolism of fatty acids, carbohydrates, ketones, and amino acids. ANT, adenine nucleotide translocase; BCAA, branched chain amino acid, BDH1, β-hydroxybutyrate dehydrogenase; βOHB, β-hydroxybutyrate; CI-IV, complex 1–4; GLUT4, glucose transporter type 4; IR, insulin receptor; LCFA, long-chain fatty acid; LDH, lactate dehydrogenase; MCAD, medium-chain acyl-CoA dehydrogenase; MCFA, medium-chain fatty acid; MCU, mitochondrial calcium uniporter; MDH, malate dehydrogenase; P, phosphate group; PDH, pyruvate dehydrogenase; SCOT, succinyl-CoA:3-ketoacid CoA transferase; SLC, solute carrier; TFP, mitochondrial trifunctional protein; VLCAD, very long-chain acyl-CoA dehydrogenase. Created with BioRender.com. Created by Dr. Seyed Amirhossein Tabatabaei Dakhili. Published in Greenwell e*t al.* 2022 (126).

1.3 Pathophysiology of Diabetic Cardiomyopathy

1.3.1 Overview of Diabetic Heart Disease

Since its initial description in a small cohort of diabetic heart failure patients in 1972 (127), diabetic cardiomyopathy, characterized by concomitant diabetes mellitus and myocardial morphological and functional abnormalities that occur independent of other cardiac risk factors, has become increasingly recognized as a distinct clinical entity with a complex pathophysiology. The Framingham Heart Study demonstrated a 2.4 and 5-fold increased risk of heart failure for diabetic male and female participants, respectively, that could not be accounted for by other macrovascular complications of diabetes including hypertension and coronary artery disease (128, 129). Diabetes has also been identified as an independent predictor of cardiovascular morbidity and mortality in individuals with chronic symptomatic heart failure and either reduced or preserved ejection fraction (130). However, despite the significant association between diabetes and cardiac dysfunction, a comprehensive understanding of the full spectrum of pathophysiological mechanisms contributing to the diabetes-related cardiac phenotype has yet to be resolved. Impaired glycemic control is correlated with the severity of heart failure risk as each 1% increase in glycated hemoglobin A_{1c} was associated with a 30% increased risk of heart failure in individuals with type 1 diabetes mellitus (T1D) and an 8% increased risk for those with type 2 diabetes mellitus (T2D) after adjustment for hypertension, myocardial infarction, obesity, and other risk factors for the development of heart failure (131, 132). However, intensive glycemic therapy has often failed to prevent the incidence of heart failure, particularly in T2D (133-135), and a degree of cardiac dysfunction remains evident even in individuals with well-controlled T1D and T2D (136-138), therefore emphasizing the complexity of the disorder and the urgent need for therapies that directly target diabetes-related cardiac dysfunction and subsequent heart failure.

In the early stages of the disease, diabetic cardiomyopathy is often clinically asymptomatic and characterized by subclinical impairments in diastolic function including prolonged and delayed LV filling and relaxation, and an elevation of LV end-diastolic pressure (137, 139-143) **(Figure 1.6)**. With disease progression, cardiac hypertrophic remodeling and reduced LV compliance lead to the advancement of diastolic dysfunction and towards the clinical manifestation of heart failure with preserved ejection fraction (HFpEF) (144-146). Structural and morphological defects

including cardiac fibrosis, cardiac myocyte hypertrophy and impaired coronary microvascular perfusion often accompany and likely contribute to the functional decline in cardiac function (147-149). Although a clear association between diabetes and the development of heart failure with reduced ejection fraction (HFrEF) has been clearly established in clinical studies, there is limited evidence of a progressive decline of systolic function in diabetic cardiomyopathy (150). However, several studies involving individuals with T2D have provided evidence of subclinical systolic dysfunction demonstrated by reduced values of midwall fractional shortening and systolic strain with normal ejection fraction (151, 152). As previously discussed, the multifactorial mechanisms underlying the development and progression of diabetic cardiomyopathy have not been fully elucidated. Nonetheless, pathological mediators including oxidative stress, inflammation, impaired Ca^{2+} handling, endoplasmic reticulum stress, neurohormonal mechanisms, mitochondrial dysfunction, activation of myocardial cell death pathways, and epigenetic and miRNA-mediated mechanisms have all been implicated (145, 146). Notably, altered cardiac energy metabolism has been identified as a well-established contributor to the development of diabetic cardiomyopathy (153, 154).

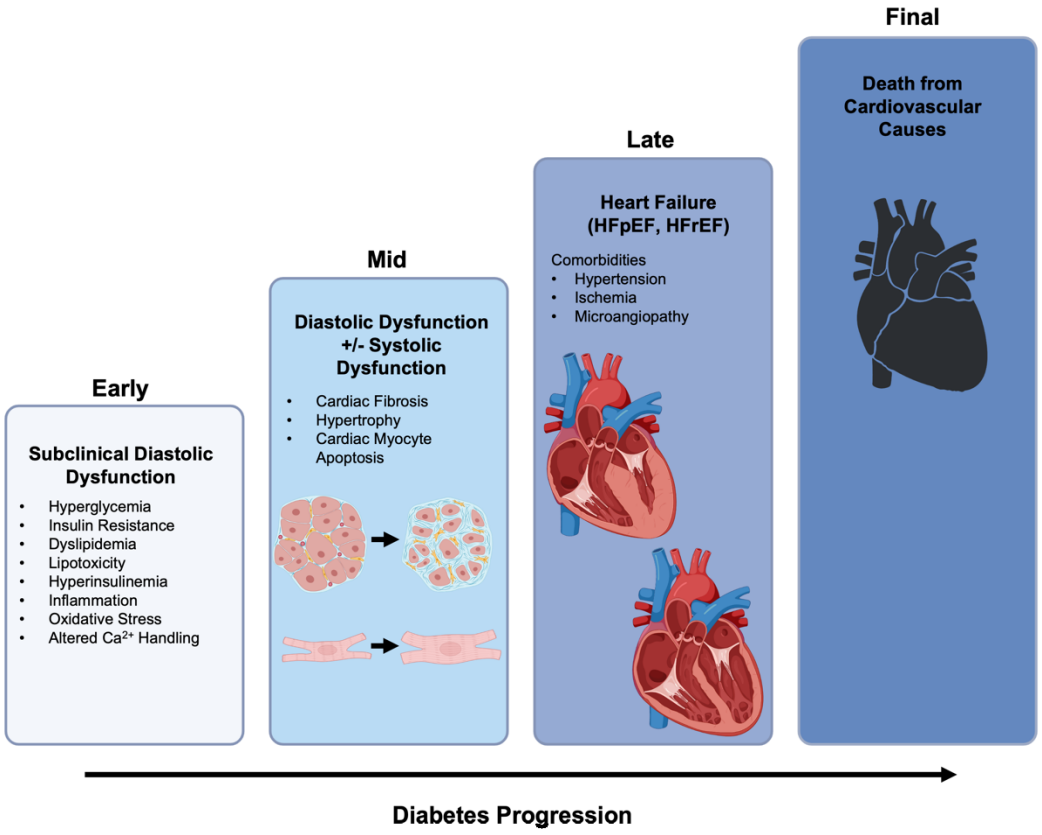

Figure 1.6. *Current understanding of the progression of cardiac dysfunction associated with the early through to the late stages of diabetes.* Adapted from Ritchie *et al*. (2020) (146) and Gopal *et al*. (2020) (155). Created with BioRender.com

1.3.2 Myocardial Energy Metabolism in Diabetic Cardiomyopathy

To sustain maximal energy production during different physiological states, the heart possesses the ability to switch between energy substrates depending on conditions such as workload, substrate availability and hormonal status (156). Conversely, this vital capacity for metabolic flexibility is impaired in the heart by the effect of the diabetic milieu resulting in an excessive dependence on fatty acid oxidation and a concomitant reduction in glucose oxidation (154). These diabetes-associated metabolic changes in the heart are apparent very early on in the disease course and often precede the decline in cardiac function, therefore emphasizing the principal pathogenic role of altered cardiac energy metabolism in the development of diabetic cardiomyopathy (50, 157, 158). Notably, an overreliance on fatty acid metabolism can increase the oxygen cost of ATP

production, thereby reducing myocardial energy efficiency and leading to cardiac dysfunction as has been demonstrated in obese, insulin resistant, and T1D and T2D mice (50, 159, 160). Diabetic cardiomyopathy is also characterized by a state of energy deficiency as evident in individuals with T2D by a reduction in the cardiac PCr/ATP ratio (137).

1.3.3 Perturbation of Myocardial Fatty Acid Metabolism in in Diabetic Cardiomyopathy

The vast majority of literature has demonstrated that obesity and diabetes lead to marked increases in myocardial fatty acid oxidation. Studies in genetic models of obesity/T2D have demonstrated that fatty acid oxidation rates are increased during aerobic perfusion of isolated working hearts from either 4-week-old or 15-week-old male *db*/*db* and *ob*/*ob* mice (50). Similarly, fatty acid oxidation rates are increased during aerobic isolated working heart perfusions from male C57BL/6J mice after 2-weeks of high-fat feeding (45% kcal from lard) or 3-weeks of high-fat feeding (60% kcal from lard) (161, 162). These observations also translate to models of T1D, as aerobic isolated working heart perfusions from rodents subjected to streptozotocin (STZ)-mediated destruction of islet β-cells, and Akita mice harbouring a genetic mutation in the insulin 2 gene, demonstrate significant increases in fatty acid oxidation rates (160, 163, 164). These observations have been recapitulated in humans, as positron emission tomography imaging with [1-^{11}C]palmitate in obese women without cardiovascular disease, T1D subjects, or T2D subjects with nonischemic cardiomyopathy, demonstrated significant increases in both myocardial fatty acid uptake and subsequent oxidation (158, 165, 166). It should be noted that many of these studies do not account for endogenous fatty acid oxidation from intracellular TAG stores, making it likely that fatty acid oxidation rates in preclinical and clinical studies of obesity/diabetes are underestimated given that myocardial TAG stores are often increased in this setting (167). Furthermore, PET imaging studies with [1-^{11}C]palmitate and [^{1}H] magnetic resonance spectroscopy in obese patients without cardiovascular disease reported that endogenous fatty acid oxidation rates are greater than exogenous plasma fatty acid oxidation rates, though a lean, healthy group for comparison was not included (168). As such, these observations suggest that obesity/T2D increases the heart's reliance on fatty acids from all sources (exogenous and endogenous) for energy metabolism.

Several mechanisms contribute to an overreliance on fatty acid utilization by the heart in the context of obesity and diabetes. Enhanced adipose tissue lipolysis, largely as a result of systemic insulin resistance, results in the elevation of circulating levels of free fatty acids and thus enhances fatty acid delivery to the myocardium. In addition, fatty acid availability and uptake by the heart is elevated by an increase in cardiac myocyte lipoprotein lipase activity (169, 170) and sarcolemmal CD36 protein expression and membrane localization (171, 172), respectively. At a molecular level, genes that facilitate cardiac fatty acid uptake, storage and oxidation in the heart are positively regulated by the transcription factor, PPARα (18, 154, 173). Myocardial expression of PPARα is increased in both T1D and T2D, and cardiac-specific PPARα overexpressing mice exhibit a cardiac phenotype mimicking that seen in diabetic cardiomyopathy (174, 175). PPARα may also be a key mediator in the increased reliance on TAG-derived fatty acid oxidation in obesity/T2D as ^{13}C nuclear magnetic resonance spectroscopy studies revealed increased TAG turnover in cardiac-specific PPARα overexpressing male mice fed a high-fat diet for 2-weeks (25). Attenuated allosteric inhibition of CPT1 and mitochondrial fatty acid uptake by decreased cardiac malonyl CoA levels also contributes to the accelerated myocardial fatty acid oxidation rates (18, 154, 173). In the setting of diabetes, a concomitant decrease and increase in ACC and MCD activity, respectively, contributes to the decline in malonyl CoA content in the heart (164, 173). The activity of fatty acid oxidation enzymes can also be enhanced through post-translational modifications including increased acetylation due to decreased sirtuin 3 levels (176-178). Lastly, as fatty acid supply in obesity and diabetes often exceeds increases in myocardial fatty acid oxidation rates, the build-up of myocardial TAG stores and lipid intermediates (e.g., ceramide and diacylglycerol) frequently characterizes the diabetic myocardium (179, 180). The accumulation of toxic lipid intermediates in the heart can promote myocardial insulin resistance, lipotoxicity and cardiac myocyte apoptosis in diabetic cardiomyopathy (180-182).

With regard to diabetic cardiomyopathy, numerous preclinical studies have demonstrated that correcting the elevated myocardial fatty acid oxidation rates yields salutary actions on cardiac function. Treatment for 3-weeks with the antianginal agent, trimetazidine (15 mg/kg once daily), which decreases fatty acid oxidation by inhibiting 3-ketoacyl-CoA thiolase, prevented diastolic dysfunction in 26-week-old male C57BL/6J mice fed a high-fat diet for 13-weeks (183). These findings may translate to humans with T2D as trimetazidine treatment for 6-months (20 mg 3x

daily) in subjects with T2D and idiopathic dilated cardiomyopathy ameliorated both systolic and diastolic dysfunction (184). Moreover, mice with a whole-body deficiency of MCD demonstrated reductions in fatty acid oxidation due to elevated malonyl CoA levels, while also displaying marked improvements in cardiac efficiency following high-fat diet-induced obesity (185). On the contrary, increasing myocardial fatty acid oxidation via cardiac-specific deletion of ACC2 alleviates both systolic and diastolic dysfunction in a mouse model of obesity-induced cardiomyopathy following 24-weeks of supplementation with a high-fat diet (186). The improvement in cardiac function was associated with an improved balance between lipid supply and consumption in the heart leading to a reduction in myocardial dysfunction induced by accumulation of toxic lipid species. Taken together, modulation of cardiac fatty acid oxidation may represent a promising therapeutic approach for the treatment of diabetic cardiomyopathy, however, further investigation is required to determine how to effectively target fatty acid metabolism in obesity and diabetes.

1.3.4 Perturbation of Myocardial Carbohydrate Metabolism in Diabetic Cardiomyopathy

Impaired cardiac glucose metabolism is well-established in diabetic heart disease. Indeed, marked declines in glucose oxidation rates have been demonstrated in numerous preclinical models of obesity, T1D and T2D (50, 102, 110, 112, 164, 185, 187). Induction of T1D in male Sprague Dawley rats (~230-250 g) by a single administration of STZ (55 mg/kg) led to a robust decline in glucose oxidation rates assessed during aerobic isolated working heart perfusions with glucose oxidation accounting for less than 5% of overall oxidative energy production (164). Experimental T2D resulting from high-fat diet provision plus a single low-dose injection of STZ (25 mg/kg in rats or 75 mg/kg in mice) also produced a robust decline in myocardial glucose oxidation rates as assessed using either ^{13}C hyperpolarized nuclear magnetic resonance (NMR) (in rats) (112), or perfusion with [U-^{14}C]glucose in isolated working hearts (in mice) (102, 110). Furthermore, ^{13}C hyperpolarized NMR has also been successfully used to measure and confirm an impairment of myocardial pyruvate metabolism in humans with diabetes (188). A recent study involving 13 participants with T2D and 12 control participants fasted for at least 9 hours prior to an oral glucose tolerance test (75g glucose) demonstrated significant reductions in myocardial glucose oxidation using ^{13}C hyperpolarized NMR (189).

The impairment of myocardial glucose oxidation in the setting of obesity and diabetes can occur secondary to insulin resistance, which would result in decreased myocardial glucose uptake (27). Furthermore, the glucose-fatty acid cycle, also known as the "Randle Cycle" phenomenon (49), represents another mechanism for the decline in glucose oxidation as the elevation of myocardial fatty acid oxidation rates in T1D and T2D decreases glucose oxidation through substrate competition (145, 146, 179, 180). Molecular perturbations also contribute to impaired cardiac glucose oxidation in diabetes, and primarily reflect a decrease in the activity of the PDH complex. It has been observed in mice with experimental T2D via high-fat diet provision plus low-dose STZ (75 mg/kg) that protein expression of the MCU complex inhibitory subunit (MCUb) increases, thereby decreasing mitochondrial matrix calcium levels and reducing myocardial PDH activity (190). Similar findings were also reported in mice with experimental T1D, whereby decreased MCU protein expression and mitochondrial calcium levels in intact paced-contracting cardiac myocytes from T1D mice were associated with reduced myocardial PDH activity and glucose oxidation rates during isolated working heart perfusions (34). Of interest, administration of an adeno-associated virus expressing murine MCU mRNA normalized cardiac PDH activity and glucose oxidation rates in T1D mice which led to an improvement in cardiac function (34). To further support the notion that impaired myocardial PDH activity and subsequent reductions in glucose oxidation contribute to the pathology of diabetic cardiomyopathy, cardiac-specific deletion of PDH ($PDH^{Cardiac-/-}$) in mice produces a diabetic cardiomyopathy-like phenotype (109). Male $PDH^{Cardiac-/-}$ mice exhibit a near complete abolishment of glucose oxidation during isolated working heart perfusion studies, and these mice also display signs of diastolic dysfunction following ultrasound echocardiography analysis (reduced E/A ratio). In addition, robust cardiac hypertrophy is also present in male $PDH^{Cardiac-/-}$ mice.

Surmounting evidence has demonstrated that diabetic cardiomyopathy can be alleviated by the enhancement of myocardial glucose oxidation (112). Forkhead box protein O1 (FoxO1) is a key transcription factor that regulates *Pdk4* expression in the heart without altering *Pdk1*, *Pdk2*, or *Pdk3* (31). Indeed, targeting this FoxO1-PDHK4 axis through treatment of T2D mice with the FoxO1 antagonist, AS1842856 (100 mg/kg) increased PDH activity and glucose oxidation rates assessed during isolated working heart perfusions (102). An alleviation of diastolic dysfunction was also observed as reflected by an increase in the mitral E/A ratio and the e'/a' ratio and a

decrease in the E/e' ratio. Confirming that the increase in myocardial glucose oxidation was required for the FoxO1 inhibition-induced protection against diabetic cardiomyopathy, AS1842856 treatment failed to alleviate diastolic dysfunction in $PDH^{Cardiac-/-}$ mice subjected to this same model of experimental T2D. Similarly, inhibiting FoxO1 to promote PDH activity and glucose oxidation also appears to be beneficial in preclinical models of T1D (191). Furthermore, enhancement of myocardial glucose oxidation rates by systemic treatment with the glucagon-like peptide 1 receptor (GLP-1R) agonist, liraglutide, also mitigated diastolic dysfunction in mice with experimental T2D (110).

The predominant view in the field as to why increases in myocardial glucose oxidation impart protection against diabetic cardiomyopathy centers on an improvement in cardiac efficiency (51, 104, 192), however this remains to be conclusively determined. Furthermore, as diabetic cardiomyopathy is characterized by diastolic dysfunction, it will be imperative for future studies to investigate the mechanisms by which increasing glucose oxidation may facilitate improved ventricular relaxation. Of relevance, myocardial relaxation during diastole is also an energy dependent process (193), thus it may be possible that an improvement in cardiac efficiency is also mechanistically involved. It is also likely that increased myocardial glucose oxidation-mediated protection against diabetic heart disease is multifactorial as increases in myocardial PDH activity has been shown to alleviate cardiomyocyte apoptosis and may even lead to decreased cardiac fibrosis (102, 111). While the aforementioned studies support that promoting myocardial glucose oxidation has salutary actions against diabetic cardiomyopathy, there are potential concerns with such a strategy that need to be considered. The most prominent concern stems from Randle's glucose-fatty acid cycle (49) since increases in myocardial glucose oxidation often result in a corresponding decline in fatty acid oxidation in order to match energy production with demand. A decline in myocardial fatty acid oxidation may increase steatosis and lipid accumulation, thereby promoting cardiac lipotoxicity. Nonetheless, most studies that have focused on stimulating myocardial glucose oxidation to treat diabetic heart disease have not reported any notable cardiac lipotoxicity that exacerbated the disease pathology.

1.3.5 Perturbation of Myocardial Ketone Body Metabolism in Diabetic Cardiomyopathy

Although perturbations in myocardial fatty acid and glucose oxidation are well-characterized in the context of diabetes, determination of how ketone body oxidation is altered in diabetic cardiomyopathy and whether these potential alterations contribute to the development of cardiac dysfunction remain active areas of investigation. Intriguingly, evidence from several studies have suggested that myocardial ketone body metabolism may in fact be reduced in diabetic cardiomyopathy. The rate of cardiac βOHB oxidation was found to be markedly attenuated in *db/db* mice compared to C57BL/6J mice (118). In addition, measurement of cardiac energy metabolism in isolated working hearts extracted from mice with STZ-induced T1D revealed a strong trend for decreased βOHB oxidation which was associated with reduced cardiac *Bdh1* and *Oxct1* expression and decreased myocardial BDH1 activity and protein level (194). A similar transcriptional suppression of *Bdh1* and *Oxct1* was also exhibited in LV tissue from mice with high-fat diet-induced glucose intolerance and LV biopsy samples from individuals with T2D and end-stage heart failure. Interestingly, enhanced cellular glucose delivery in transgenic mice with cardiac myocyte-specific overexpression of GLUT4 decreased *ex vivo* cardiac βOHB oxidation rates associated with suppressed BDH1 and SCOT mRNA and protein expression, and BDH1 activity (194). Together with findings that *Bdh1* gene expression may be regulated by protein *O*-GlcNAcylation, these findings suggest that BDH1-related alterations of cardiac ketone body oxidation in diabetes could be a direct result of hyperglycemia on the myocardium.

In contrast, catheterization studies for blood sampling from the coronary sinus and aortic root in subjects with T2D and mild diastolic dysfunction revealed increased myocardial uptake of acetoacetate and βOHB suggestive of increased myocardial ketone body utilization (195). Furthermore, a recent study in non-obese diabetic male Goto-Kakizaki rats using hyperpolarized [3-^{13}C]acetoacetate demonstrated increased myocardial ketone body utilization, as well as increases in myocardial SCOT activity (195). However, as these rats also demonstrated cardiac hypertrophy and systolic dysfunction, whether their metabolic perturbations are due to diabetes or systolic dysfunction cannot be discerned.

1.3.6 Perturbation of Myocardial Amino Acid Metabolism in Diabetic Cardiomyopathy

Alterations in BCAA catabolism have been implicated in the development of whole-body and cardiac insulin resistance in obesity and diabetes (196-198). In the heart, cardiac BCAA oxidation rates were decreased in a mouse model of high-fat diet-induced obesity and associated with impaired myocardial insulin signaling as evident from a decrease in the phosphorylation of glycogen synthase kinase-3β (GSK-3β) relative to total GSK-3β levels (46). Cardiac BCAA oxidation contributes minimally to overall cardiac energy production (~1-3%) (46, 199), therefore, alterations in BCAA oxidation rates are unlikely to compete with and thus significantly affect myocardial fatty acid and glucose oxidation rates. However, an accumulation of cardiac BCAAs due to decreased oxidation is postulated to directly impair insulin sensitivity in the heart by enhancing inhibitory phosphorylation of insulin receptor substrate 1 through activation of the mammalian target of rapamycin pathway (200). Cardiac levels of BCAAs were increased in transgenic mice with impaired glucose-stimulated pancreatic β-cell insulin secretion (βv59M mice) and rats with STZ-induced diabetes when compared to non-diabetic counterparts, thus providing further support for the myocardial accumulation of BCAAs in the setting of diabetes (187, 201). Depending on the specific location of the block within the BCAA catabolism pathway, an accumulation of the intermediates of BCAA oxidation, namely BCKAs, may also contribute to insulin resistance by promoting mitochondrial dysfunction (202). BCAAs may also disrupt PDH activity which can negatively influence glucose oxidation (203). Pharmacological stimulation of BCAA oxidation reduced myocardial BCAA accumulation and improved cardiac function in mice subjected to transverse aortic constriction-induced heart failure (200), therefore modulation of cardiac BCAA catabolism may have therapeutic potential for treating diabetic cardiomyopathy.

1.4 Succinyl-CoA:3-ketoacid CoA Transferase Inhibition as a Novel Therapeutic Approach for Type 2 Diabetes and Related Diabetic Heart Disease

1.4.1 Current Therapeutic Approaches for Diabetic Heart Disease

Given that individuals with diabetes are at a significant risk of developing cardiovascular disease, there is a critical demand for anti-diabetic treatments that also improve cardiovascular outcomes. Therapies specifically designed to target diabetic cardiomyopathy or diabetes-related heart failure are exceptionally limited. Furthermore, health regulatory agencies have now mandated that all

therapies in development for diabetes undergo rigorous evaluation in large-scale multicenter cardiovascular outcomes trials (CVOT) to assess cardiovascular safety (204). Among the anti-diabetic agents, positive results have been reported in CVOTs assessing GLP-1R agonists (205-209) and SGLT2 inhibitors (210-212), however, despite their efficacy in controlling hyperglycemia, other agents such as dipeptidyl peptidase 4 inhibitors were noninferior compared to placebo in CVOTs and thus failed to demonstrate any obvious cardiovascular benefits (209). In addition, the thiazolidinedione, rosiglitazone, was associated with an increased risk of heart failure in patients with T2D in the Rosiglitazone Evaluation for Cardiac Outcomes and Regulation of Glycaemia in Diabetes (RECORD) trial (213). Taken together, the outcomes of these clinical trials highlight the significant need for the further development of strategies to prevent and treat diabetes-related cardiovascular complications.

1.4.2 The Effect of the Ketogenic Diet on Cardiovascular Risk Factors

Dietary interventions including the very low carbohydrate, high-fat ketogenic diet have gained considerable popularity in the recent years as a strategy to mitigate cardiovascular risk factors including obesity, insulin resistance and diabetes (214, 215). Although various forms of the ketogenic diet have been investigated and utilized, the classic composition generally consists of a 4:1 or 3:1 ratio, by weight, of dietary fat to combined dietary protein and carbohydrate which equates to 85-90% energy from fat, 2-5% energy from carbohydrates and 6-12% energy from protein (216). However, other formulations can include those that allow for 70-80% energy from fat, <10% energy from carbohydrates and ~10% energy from protein and are still known to produce ketosis in humans (216, 217). Adherence to a low carbohydrate diet can diminish circulating insulin levels (217), as well as a state of nutritional ketosis has been postulated to supress appetite (218) and increase energy expenditure (219), which may be beneficial for promoting body weight loss and improving glucose homeostasis in obesity and T2D. Indeed, in humans and animal models, the ketogenic diet has been shown to promote body weight loss, as well as improve glycemic control and insulin resistance in obesity and T2D (220-222). However, other studies have reported that the ketogenic diet was no more effective than other dietary interventions at inducing body weight loss (223, 224), and that improvements in metabolic parameters may not be sustained with long-term adherence (225). Furthermore, although the effect of the ketogenic diet on plasma

lipid concentrations has been debated, reports that the diet increases LDL cholesterol has generated concern about its cardiovascular safety (216, 226).

1.4.3 Pimozide as a Potential Treatment for Type 2 Diabetes

Pimozide was first developed in 1963 as a conventional antipsychotic of the diphenylbutylpiperidine class for the treatment of schizophrenia and Tourette syndrome (227, 228). Although pimozide is a known antagonist of the dopamine D2 receptor subfamily (D2, D3 and D4 receptors) and the 5-HT7 serotonin receptor (228), recent findings from our laboratory have also identified pimozide as a novel non-competitive inhibitor of SCOT (Ki = 312.9 $\pm$ 28.2 nM) (229), a critical enzyme in ketone body oxidation. Given that SCOT is not present in the liver, pharmacological antagonism of SCOT activity can selectively reduce systemic ketone body oxidation without altering hepatic ketogenesis. Of interest, treatment with pimozide reduced skeletal muscle SCOT activity leading to improved glucose tolerance independent of body weight loss, lipid accumulation and brain SCOT activity in mice with obesity-induced hyperglycemia and T2D. An improved glucose profile was also evident in obese mice with a skeletal-muscle specific knockout of SCOT ($SCOT^{Muscle-/-}$), thereby further supporting a beneficial role for skeletal muscle SCOT inhibition in the alleviation of obesity/T2D-induced glucose intolerance. Although the mechanistic link between ketone body metabolism and glucose homoeostasis requires further investigation, pharmacological inhibition of ketone body oxidation may be an exciting novel approach for glucose lowering therapy in individuals with T2D. However, if pimozide is to be repurposed as a treatment for T2D, it is imperative that the impact of SCOT inhibition on the development and progression of diabetic heart disease be assessed.

1.5 Statement of Hypotheses and Aims

Perturbation of myocardial intermediary energy metabolism leading to metabolic inflexibility and impaired cardiac energy production is a unifying pathological mechanism driving disease progression in several cardiomyopathies with diverse etiologies. Evidence to support altered myocardial energy metabolism has been provided for Barth syndrome and diabetic cardiomyopathy, however, a comprehensive understanding of the broad spectrum of metabolic changes remains to be elucidated, as well as the mechanisms that underlie the shifts in substrate utilization. In addition, further investigation is required to determine whether the pharmacological

optimization of cardiac energy metabolism, or modulation of the systemic nutrient environment to mitigate cardiovascular risk factors represent promising targets for therapeutic intervention. The overarching hypotheses that were investigated are described below:

1. Cardiac intermediary energy metabolism is altered in Barth syndrome cardiomyopathy and pharmacological interventions that aim to optimize myocardial substrate utilization will be effective in mitigating the development and/or progression of cardiac structural and functional defects **(Chapters 2 and 3)**.
2. Modulation of the systemic nutrient environment by maintenance on a ketogenic diet may mitigate cardiovascular risk factors including obesity and impaired glucose homeostasis, however, potential detrimental effects of the ketogenic milieu directly on the myocardium may prevent an overall improvement of cardiac function in the setting of obesity/prediabetes **(Chapter 4)**.
3. Myocardial ketone body oxidation is altered in and contributes to the development of diabetic cardiomyopathy **(Chapter 5)**.

The aims of each study, which addressed specific portions of the overarching hypotheses, are listed below by chapter:

Chapter 2: Barth Syndrome-Related Cardiomyopathy is Associated with a Reduction in Myocardial Glucose Oxidation

1. Examine the cardiomyopathy demonstrated by TazKD mice and assess the relevance of the mouse model to the clinical phenotype.
2. To identify the alterations in cardiac intermediary energy metabolism that characterize the cardiomyopathy associated with Barth syndrome.
3. To provide insight into the underlying mechanisms that may contribute to the development of altered cardiac energy metabolism in Barth syndrome.

Chapter 3: Stimulating Myocardial Pyruvate Dehydrogenase Activity Fails to Alleviate Cardiac Abnormalities in a Mouse Model of Human Barth Syndrome

1. To determine whether reversal of impaired glucose oxidation via treatment with dichloroacetate can mitigate cardiac structural abnormalities in TazKD mice.

Chapter 4: An Isoproteic Cocoa Butter-based Ketogenic Diet Fails to Improve Glucose Homeostasis and Promote Weight Loss in Obese Mice

1. To compare the efficacy of a low-fat diet versus a ketogenic diet in mitigating cardiovascular risk factors including obesity and obesity-induced impairments in glucose tolerance and insulin sensitivity.
2. To identify the effect of the ketogenic diet on food intake and energy expenditure.
3. To examine the effects of high-fat diet-induced obesity on cardiac structure and function.
4. To assess the impact of the ketogenic diet on cardiac structure and function in obese mice.

Chapter 5: Pharmacological Inhibition of Myocardial Ketone Body Oxidation with Pimozide Improves Diastolic Function in a Mouse Model of Type 2 Diabetes

1. To determine whether myocardial ketone body oxidation is altered in a mouse model of experimental T2D.
2. To assess the effect of the diabetic milieu on the activity and expression of ketolytic enzymes in the myocardium.
3. To elucidate the effects of pharmacological SCOT inhibition on cardiac structural and functional abnormalities in T2D.

Chapter 2: Barth Syndrome-Related Cardiomyopathy is Associated with a Reduction in Myocardial Glucose Oxidation

Amanda A. Greenwell[1,3,4], Keshav Gopal[1,3,4], Tariq Altamimi[2,3], Christina T. Saed[1,3,4], Faqi Wang[3,6,7], Seyed Amirhossein Tabatabaei Dakhili[1,3,4], Kim L. Ho[2,3,4,6], Liyan Zhang[2,3,4,6], Farah Eaton[1,3,4], Jennifer Kruger[5], Rami Al Batran[1,3,4,8], Gary D. Lopaschuk[2,3,4,6], Gavin Y. Oudit[3,6,7], John R. Ussher[1,3,4]

[1]Faculty of Pharmacy and Pharmaceutical Sciences, University of Alberta, Edmonton, AB, Canada
[2]Department of Pediatrics, University of Alberta, Edmonton, AB, Canada
[3]Cardiovascular Research Centre, University of Alberta, Edmonton, AB, Canada
[4]Women and Children's Health Research Institute, University of Alberta, Edmonton, AB, Canada
[5]Health Sciences Laboratory Animal Services, University of Alberta, Edmonton, AB, Canada
[6]Divsion of Cardiology, Department of Medicine, University of Alberta, Edmonton, Canada
[7]Mazankowski Alberta Heart Institute, University of Alberta, Edmonton, Canada
[8]Present Address, Faculty of Pharmacy, Université de Montréal, Montréal, QC Canada

PUBLISHED: Greenwell AA, Gopal K, Altamimi TR, Saed CT, Wang F, Tabatabaei Dakhili SA, Ho KL, Zhang L, Eaton F, Kruger J, Al Batran R, Lopaschuk GD, Oudit GY, and Ussher JR. Barth syndrome-related cardiomyopathy is associated with a reduction in myocardial glucose oxidation. Am J Physiol Heart Circ Physiol 320: H2255-H2269, 2021.

2.1 Abstract

Heart failure presents as the leading cause of infant mortality in individuals with Barth syndrome (BTHS), a rare genetic disorder due to mutations in the tafazzin (*TAFAZZIN*) gene affecting mitochondrial structure and function. Investigations into the perturbed bioenergetics in the BTHS heart remain limited. Hence, our objective was to identify the potential alterations in myocardial energy metabolism and molecular underpinnings that may contribute to the early cardiomyopathy and heart failure development in BTHS. Cardiac function and myocardial energy metabolism were assessed via ultrasound echocardiography and isolated working heart perfusions, respectively, in a mouse model of BTHS (doxycycline inducible Taz knockdown (TazKD) mice). In addition, we also performed mRNA/protein expression profiling for key regulators of energy metabolism in hearts from TazKD mice and their wild-type (WT) littermates. TazKD mice developed hypertrophic cardiomyopathy as evidenced by increased left ventricular anterior and posterior wall thickness, as well as increased cardiac myocyte cross sectional area, though no functional impairments were observed. Glucose oxidation rates were markedly reduced in isolated working hearts from TazKD mice compared to their WT littermates in the presence of insulin, which was associated with decreased pyruvate dehydrogenase activity. Conversely, myocardial fatty acid oxidation rates were elevated in TazKD mice, whereas no differences in glycolytic flux or ketone body oxidation rates were observed. Our findings demonstrate that myocardial glucose oxidation is impaired prior to the development of overt cardiac dysfunction in TazKD mice and may thus represent a pharmacological target for mitigating the development of cardiomyopathy in BTHS.

2.2 Introduction

Barth Syndrome (BTHS) is a rare, X-linked, genetic disorder phenotypically characterized by cardiac and skeletal myopathy, neutropenia, and pre-pubertal growth retardation (125). Despite a wide variability in phenotypic expression, BTHS is frequently associated with infantile-onset cardiomyopathy, and heart failure represents a significant cause of morbidity and mortality in those diagnosed with the condition (94, 125). The causative mutation underlying the development of BTHS is linked to the tafazzin (*TAFAZZIN)* gene, which encodes a mitochondrial acyltransferase that plays a key role in the remodeling of cardiolipin (94, 125). Cardiolipin is a structurally distinct phospholipid particularly enriched in the inner mitochondrial membrane, with important functions in maintaining mitochondrial integrity and function. As such, *TAFAZZIN* mutations in BTHS result in impaired production of tetra-linoleoyl cardiolipin, which is the predominant cardiolipin species present in the heart and skeletal muscle, thereby impairing mitochondrial function by interfering with electron transport chain activity, particularly at complex III (79, 83, 94). Importantly, derangements in mitochondrial function and subsequent myocardial energy metabolism have been demonstrated to contribute to the progression of cardiac dysfunction in numerous cardiac pathologies (18, 94, 180). Hence, it is likely that perturbations in myocardial energy metabolism are also present in BTHS, and these perturbations may contribute to the cardiomyopathy phenotype present in these individuals.

The heart is the most metabolically demanding organ in the body on a per gram basis, whose energy needs are met primarily by the oxidation of fatty acids and carbohydrates (glucose) (17, 18). Indeed, studies have suggested that fatty acid oxidation is reduced in tafazzin deficient mice, a murine model of BTHS (herein referred to as TazKD mice), as cardiac myocytes isolated from these mice exhibit reduced oxygen consumption rates (83). In addition, isolated mitochondria from hearts of TazKD mice exhibit a reduction in fatty acid oxidation during state 3 respiration with palmitoyl-L-carnitine as a substrate using high-resolution respirometry (81). Glucose oxidation may also be impaired in BTHS, as C2C12 myoblasts exhibit reductions in pyruvate dehydrogenase (PDH) activity following CRISPR/cas9 mediated *Taz* knockout, which is associated with increased PDH phosphorylation (106) (indicative of decreased PDH activity (29, 30)). Despite the aforementioned studies providing evidence of perturbed myocardial energy metabolism in BTHS, there are limitations with the methods that have currently been used to assess energy metabolism

in BTHS. Isolated mitochondria are often devoid of key intracellular factors, such as malonyl CoA, a potent endogenous inhibitor of mitochondrial fatty acid uptake by inhibiting carnitine palmitoyltransferase 1 (CPT1), whereas changes in mRNA/protein expression do not necessarily equate to changes in flux (97). Furthermore, as rates of oxidative metabolism are highly dependent on workload, measuring oxidative rates and oxygen consumption in cardiac myocytes in vitro is limited due to their markedly reduced metabolic demand compared to the intact or ex vivo heart (97).

To address these limitations, our goal was to assess intermediary energy metabolism in isolated working hearts from TazKD mice. The isolated working heart model allows for actual investigations of flux through various metabolic pathways by using highly sensitive radiolabeled tracers, while the heart performs actual external work at a metabolic demand more closely mimicking that seen in the intact organism (97). Previous reports have indicated that TazKD mice do not develop overt heart failure until ~7-8 months of age (100, 230, 231). Therefore, our goal was to characterize myocardial energy metabolism in TazKD mice at an earlier age (~8-10 weeks of age), which would allow us to infer whether perturbations in myocardial energy metabolism may contribute to BTHS-related heart failure, rather than being a consequence of heart failure. Moreover, interventions that correct perturbations in energy metabolism have been demonstrated to improve cardiac performance in preclinical and clinical studies of cardiomyopathy and heart failure (28, 180, 232). We herein demonstrate that hearts from TazKD mice are characterized by a marked impairment and elevation of glucose oxidation and fatty acid oxidation, respectively, which may represent potential pharmacological metabolic targets for treating and/or reversing the development or progression of BTHS-related cardiomyopathy and/or heart failure.

2.3 Methods

2.3.1 Animal Care and Experimentation

All animal procedures were approved by the University of Alberta Health Sciences Animal Welfare Committee and performed in accordance with the regulations of the Canadian Council on Animal Care. Animals were housed in a temperature-controlled unit under a 12-hour light/dark cycle with free access to drinking water and food. The doxycycline-inducible short hair pin RNA

(shRNA)-mediated tafazzin (gene name *Taz*) knockdown mouse model (TazKD; The Jackson Laboratory, stock no. 014648) has been described previously (230). To induce *Taz* silencing during the early embryonic stage, female C57BL/6J mice were placed on rodent chow supplemented with doxycycline (625 mg/kg) for 1-week prior to mating with transgenic male mice heterozygous for the *Taz* shRNA transgene. Male pups were continuously maintained on doxycycline-containing chow for the remainder of the experimental procedure. This approach has been demonstrated to induce an 85 – 90% silencing of *Taz* in the heart (230). Male littermates that did not possess the *Taz* shRNA transgene were maintained on doxycycline-containing chow and used as the wild-type (WT) controls for all experiments. Upon study completion, all mice were euthanized following an intraperitoneal (IP) injection of sodium pentobarbital (12 mg) after a 16-hr fast and 4-hr refeed, following which the heart and other peripheral tissues (e.g., skeletal muscle, liver) were immediately snap-frozen in liquid N_2 using liquid N_2-cooled Wollenberger tongs and stored at -80°C.

2.3.2 Ultrasound Echocardiography

Cardiac structure and function were assessed in 8 to 10-week-old mice utilizing non-invasive transthoracic echocardiography with an MX 550S probe and the VisualSonics Vevo 3100 rodent ultrasound imaging system. Mice were initially anesthetized with 2 – 3% isoflurane and maintained on 1 – 1.5% isoflurane for the remainder of the assessment. During image acquisition, body temperature, respiratory rate and heart rate were consistently monitored. M-mode images were acquired for measurements of left ventricular (LV) internal diameter (LVID) and LV anterior (LVAW) and posterior (LVPW) wall thickness during systole (s) and diastole (d) and used for the calculation of the following parameters:

$$LV\ Volume\ (Vol)\ (\mu L) = \left(\frac{7.0}{2.4 + LVID}\right) \times LVID^3$$

$$LV\ Ejection\ Fraction\ (EF)\ (\%) = 100 \times \left(\frac{LV\ Vol;d - LV\ Vol;s}{LV\ Vol;d}\right)$$

$$LV\ Fractional\ Shortening\ (FS)\ (\%) = 100\ \times \left(\frac{LVID;d - LVID;s}{LVID;d}\right)$$

$$LV\ Mass\ Uncorrected\ (mg) = 1.053 \times [(LVID;d + LVPW;d + LVAW;d)^3 - LVID;d^3]$$

$$LV\ Mass\ Corrected\ (mg) = LV\ Mass\ \times 0.8$$

Diastolic function was assessed using pulsed-wave (PW) and tissue Doppler (TDI) imaging of the mitral inflow and mitral annular velocities, respectively, during early diastolic filling (PW: E; TDI: e') and late diastolic filling due to atrial contraction (PW: A; TDI: a').

2.3.3 Isolated Working Heart Perfusions and Assessment of Energy Metabolism

All mice were euthanized after an overnight fast via IP injection of sodium pentobarbital (12 mg) at 8 to 10 weeks of age, following which the hearts were immediately excised and perfused aerobically in the working mode for 60 minutes as previously described (233-235). To further elaborate, hearts were placed in ice-cold Krebs-Henseleit bicarbonate solution (118 mM NaCl, 25 mM $NaHCO_3$, 4.7 mM KCl, 1.2 mM $MgSO_4 \bullet 7H_2O$, 2.5 mM $CaCl_2 \bullet 2H_2O$, 1.2mM KH_2PO_4, and 5mM glucose) after excision. Subsequently, hearts were trimmed of extraneous tissues (pericardium, lung, trachea, etc.) and the opening to the left atrium and the aorta was canulated. The aorta was then perfused with Krebs-Henseleit bicarbonate solution (37°C) in the retrograde Langendorff mode (60 mmHg perfusion pressure), following which hearts were switched to the working mode after equilibration by clamping the aortic inflow line from the Langendorff reservoir and opening the left atrial inflow (preload) line and the aortic inflow line (afterload). Hearts were perfused with Krebs-Henseleit buffer containing 5.0 mM glucose, 0.8 mM palmitate pre-bound to 3% bovine serum albumin (BSA) as previously described (233), and 0.8 mM β-hydroxybutyrate (βOHB) with the appropriate radiolabeled tracers for the measurement of either glycolysis ([5-^{3}H]glucose) and glucose oxidation ([U-^{14}C]glucose), or fatty acid ([9,10-^{3}H]palmitate) and ketone body oxidation ([3-^{14}C]βOHB) and gassed with 95% O_2 and 5% CO_2 (pH = 7.4) in a glass oxygenator. Insulin (100 μU/ml) was added to the perfusate delivered to the left atrium after 30 min of perfusion at a preload pressure of 11.5 mmHg. Perfusate was recirculated after being ejected from spontaneously beating hearts into a compliance chamber and the aortic outflow line against a hydrostatic afterload pressure of 50 mmHg. At 10 min intervals during the 60-minute perfusion period, a 5 mL sample of perfusate was withdrawn through an injection port and stored in a

scintillation vial under 500uL of paraffin oil to prevent the loss of $^{14}CO_2$. The $^{14}CO_2$ dissolved in the perfusate was extracted by acidification with 1 mL of 9*N* H_2SO_4 in a 25 mL stoppered flask with a hyamine hydroxide-soaked filter paper in the central well to absorb the $^{14}CO_2$ released during acidification (235). Quantitative measurement of $^{14}CO_2$ released as a gas in the oxygenation chamber and dissolved as $H^{14}CO_3^-$ in the perfusate were used to assess glucose oxidation rates. Liberated gaseous $^{14}CO_2$ was trapped in a 1 M hyamine hydroxide solution in the air outlet line. At the completion of perfusion, hearts were immediately snap frozen with liquid N_2 and stored at -80°C.

Assessment of glycolysis and fatty acid oxidation was determined through the quantitative collection of ^3H_2O, whereas glucose and ketone body oxidation were determined through the quantitative collection of $^{14}CO_2$ (234, 235). ^3H_2O was separated from [5-^{3}H]glucose and [9,10-^{3}H]palmitate in perfusate samples using a water vapor exchange method (234). In brief, 200 µL of perfusate was added to a capless 1.5 mL microcentrifuge tube and placed in a 5 mL scintillation vial containing 500 µL of distilled water. The scintillation vials were capped and stored at 50°C for 24 hours and then 4°C for 24 hours to facilitate vapor exchange between the perfusate and distilled water and vapor condensation, respectively. After the storage periods, the perfusate-containing microcentrifuge tubes were removed and scintillation fluid (Ecolite, ICN) was added to the vials and counted for radioactivity in a liquid scintillation counter.

2.3.4 Mechanical Function Measurements in Isolated Working Mouse Hearts

A Gould P21 pressure transducer (Harvard Apparatus) connected to the aortic outflow line was utilized to measure heart rate and aortic pressure (mmHg). Coronary flow (mL/min) was calculated by subtracting aortic flow (mL/min) from cardiac output which were measured with Transonic T206 ultrasonic flow probes in the afterload and preload lines, respectively. Cardiac power was calculated as the product of LV developed pressure (difference between aortic systolic pressure and preload pressure) and cardiac output. An AcqKnowledge MP100 system (BIOPAC Systems Inc.) was utilized for data collection.

2.3.5 RNA Isolation and Real-Time Quantitative PCR

TRIzol™ reagent (Invitrogen) was used to homogenize frozen, powdered cardiac tissue (~15-20 mg) for 2 minutes. Chloroform was added after homogenization, following which the samples were left to sit for 10 min to allow the homogenate to separate. The clear upper aqueous layer containing RNA was removed and RNA was precipitated with the addition of isopropanol. The precipitated RNA was washed with 75% ethanol to remove impurities and resuspended in 30 µL of DNase/RNase-free water. First-strand cDNA (2 µg) was synthesized from extracted RNA using the High-Capacity cDNA Reverse Transcription Kit (Applied Biosystems). A CFX Connect Real-Time PCR machine (Bio-Rad Laboratories Inc.) was used to perform real-time PCR utilizing TaqMan Gene Expression Assays (4369016; Applied Biosystems) or SYBR Green (KK4601; Kapa Viosystems, Inc.). Primer sequences are reported in **Table 2.1**. Cyclophilin A (*Ppia*) was used as an internal housekeeping gene to determine relative mRNA transcript levels quantified with the $2^{-\Delta\Delta Ct}$ method as previously described (236).

2.3.6 Whole Cell Homogenate Preparation and Immunoblot Analysis

Frozen, powdered cardiac tissue (~15-20 mg) was homogenized in a protein lysis buffer containing 50 mM Tris HCl (pH 8 at 4°C), 1 mM EDTA, 10% glycerol (w/v), 0.02% Brij-35 (w/v), 1 mM dithiothreitol, and protease and phosphatase inhibitors (Sigma-Aldrich). After homogenization for 2 minutes, the homogenate was left on ice for 30 minutes and subsequently centrifuged at 12 000 x g for 20 minutes. The protein-containing supernatant was removed and used for western blotting. Protein was quantified using a Bradford protein assay kit (Bio-Rad), following which samples (15 µg) were denatured at 95°C for 5 minutes, resolved via 12% sodium dodecyl sulfate polyacrylamide gel electrophoresis (SDS-PAGE) and transferred onto a 0.45 µm nitrocellulose membrane. Membranes were blocked with 5% fat-free milk for 45 minutes and probed overnight with the following antibodies: succinyl CoA:3-ketoacid CoA transferase (SCOT; 12175-1-AP, Proteintech), βOHB dehydrogenase 1 (BDH1; NBP188673, Novus Biologicals), acetoacetyl CoA thiolase 1 (ACAT1; PA5-19227, Invitrogen), β-hydroxyacyl CoA dehydrogenase (βHAD; ab37673, Abcam), long chain acyl CoA dehydrogenase (LCAD; ab129711, Abcam), phospho-PDH (serine 293) (AP1062, Sigma-Aldrich), phospho-PDH (serine 232) (AP1063, Sigma-Aldrich), phospho-PDH (serine 300) (AP1064, Sigma-Aldrich) PDH (3205S, Cell Signaling), Sirtuin-3 (SIRT3) (ab86671, Abcam), acetyl CoA carboxylase (ACC) (3662S, Cell Signaling),

phospho-ACC (3661S; Cell Signaling), and vinculin (1390S, Cell Signaling). All antibodies were prepared in a 1/1000 dilution in 3% bovine serum albumin (BSA) with the exception of βHAD, LCAD, vinculin, phospho-PDH (serine 232) and phospho-PDH (serine 300), which were prepared in a 1/2000 dilution. The next day, membranes were washed with TBST wash buffer (1X Tris-Buffered Saline, 0.1% Tween® 20 Detergent) for 3 x 10-minute intervals and subsequently probed with either goat anti-rabbit (70747S, Cell Signaling), mouse anti-goat (sc-2354, Santa Cruz Biotechnology) or goat anti-chicken (sc-2428, Santa Cruz Biotechnology) secondary antibody in a 1:2000 dilution with 5% fat-free milk for 1.5 hours. Immunoblots were visualized with SuperSignal™ West Pico PLUS chemiluminescent substrate kit (34580, ThermoFisher Scientific) and quantified with Image Studio Lite software (Licor).

2.3.7 Pyruvate Dehydrogenase Activity

PDH activity was measured in myocardial homogenates prepared with phosphatase (P0044, Sigma-Aldrich), and protease (A32953, Thermo Fisher) inhibitors using a PDH enzyme activity microplate assay kit as per manufacturer's instructions (ab109902, Abcam). In brief, prepared samples of a concentration of 100 μg/200 μL were loaded onto microplate wells coated with an anti-PDH monoclonal antibody. The microplate was incubated for 3 hrs at room temperature, following which PDH activity was determined by measuring the rate of reduction of NAD^+ to NADH, coupled to the reduction of a reporter dye, through monitoring the increase in absorbance of the reaction product over 30 min at an optical density of 450 nm. Relative PDH activity was calculated by determining the slopes of the generated curves between the 5- and 15-min time points where the increase in absorbance was linear.

2.3.8 Pyruvate Dehydrogenase Acetylation

Myocardial tissue samples were pre-cleared for 4 hrs with A/G agarose beads (sc-2003, Santa Cruz), following which the lysate was incubated overnight with acetyl-lysine antibody (AB3879, Sigma-Aldrich). The antibody-protein complexes were subsequently pulled down with A/G agarose beads by incubating overnight. The next day, samples were washed three times and subsequently eluted using 5x sample buffer. The samples were then subjected to SDS-PAGE, transferred to a nitrocellulose membrane, and incubated in PDH antibody (3205S, Cell Signaling) to detect acetylated-PDH.

2.3.9 Short Chain CoA Content

Free CoA, succinyl CoA, malonyl CoA and acetyl CoA content were quantified from powdered frozen myocardial tissue (~15 mg) homogenized in 6% perchloric acid. The homogenate was kept on ice for 10 min and centrifuged at 12,000 x g for 5 min at 4°C prior to analysis via high performance liquid chromatography as previously described (185).

2.3.10 Assessment of Circulating Insulin and Glucose Levels

Plasma insulin levels were determined using a commercially available enzyme-linked immunosorbent assay kit (Alpco Diagnostics). Plasma was collected from mice during euthanasia following a 16 hr fast and 4 hr refeed. Samples (5 μL) were added to wells with 75 μL of a provided enzyme conjugate, following which the 96 well plate was incubated for 2 hrs at room temperature on an orbital microplate shaker at 700 revolutions per minute. After the plate was washed with a provided working strength wash buffer, the reaction was initiated with the addition of a provided substrate and terminated after 30 min with a provided stop solution. The optical density at 450 nm of each sample was determined and used to calculate plasma insulin levels. Fasting blood glucose levels were measured from tail whole-blood following a 20 hr fast using the Contour Next blood glucose monitoring system (Bayer, NJ, USA).

2.3.11 Measurement of Myocardial Triacylglycerol Content and the Incorporation of [9,10-^{3}H]Palmitate into Triacylglycerol

Triacylglycerol (TAG) content was measured in frozen ventricular tissue from mouse hearts perfused with [9,10-^{3}H]palmitate with an enzymatic assay kit (Wako Pure Chemical Industries, Richmond, Virginia) as previously described (103). The incorporation of [9,10-^{3}H]palmitate into the TAG pool was measured based on the specific activity of [9,10-^{3}H]palmitate using a separate portion of the lipid extraction counted with scintillation fluid as previously described (103).

2.3.12 Measurement of Myocardial Glycogen Content and the Incorporation of Glycogen from [U-^{14}C]Glucose

Glycogen content was measured in frozen ventricular tissue from the perfused hearts with [U-^{14}C]glucose present in the perfusate using a glucose assay kit (Sigma-Aldrich) as previously described (103). The incorporation of [U-^{14}C]glucose into the glycogen pool was subsequently

measured based on the specific activity of [U-^{14}C]glucose using a separate portion of the glucose extraction counted with scintillation fluid as previously described (103).

2.3.13 Masson's Trichrome and Wheat-Germ Agglutinin Staining

Hearts were extracted from mice arrested in diastole using 1 M KCl, fixed in 10% buffered formalin and subsequently embedded in paraffin. Sections (10 μM thick) were stained with Masson's trichrome and visualized with light microscopy (DM4000 B, Leica) as previously described (237) for the assessment of myocardial fibrosis. In addition, optimal cutting temperature (23-730-571, Thermo Fisher)-embedded sections (5 μM thick) were stained with Oregon Green 488-conjugated wheat-germ agglutinin (WGA; #W11261, Thermo Fisher) and 4',6-Diamidino-2-Phenyllindole, Dilactate (DAPI; D3571, Thermo Fisher) and visualized using fluorescence microscopy (Olympus IX81, MetaMorph Basic (version 7.7.0.0), Olympus Canada Inc., Richmond Hill, ON, Canada) to measure cardiac myocyte cross sectional area as previously described (237).

2.3.14 Statistical Analysis

All values are presented as mean ± standard error of the mean. The significance of differences was assessed by an unpaired two-tailed Student's t-test or a two-way analysis of variance (ANOVA) followed by a Bonferroni post-hoc analysis. Once the variances of were assessed between comparisons involving two groups, a non-parametric Mann Whitney test was used to assess statistical significance if appropriate. Differences were considered significant when $P < 0.05$.

Table 2.1. *Primer Sequences*

Gene Name	Forward	Reverse	Taqman Assay ID
Ppia	GAGCTGTTTGCAGACAAAGTTC	CCCTGGCACATGAATCCTGG	NA
Pdk1	CTGTGATACGGATCAGAAACCG	TCCACCAAACAATAAAGAGTGCT	NA
Pdk2	ATGAAAGAGATCAACCTGCTTCC	GGCTCTGGACATACCAGCTC	NA
Pdk4	GGAGCATTTCTCGCGCTACA	ACAGGCAATTCTTGTCGCAAA	NA
Foxo1	ACCACTCTGGACGGCATACT	TGAGTCTGGGGCTAGTTTGA	NA
Acadm	GCTGGAGACATTGCCAATCA	GGCGTCCCTCATCAGCTTCT	NA
Col1a1	TGCTAACGTGGTTCGTGACCGT	ACATCTTGAGGTCGCGGCATGT	NA
Col1a2	TTGCTGAGGGCAACAGCAGGTT	AATGTCAAGGAACGGCAGGCGA	NA
Ccn2	TGACCCCTGCGACCCACA	TACACCGACCCACCGAAGACACAG	NA
Ppargc1a	TATGGAGTGACATAGAGTGTGCT	CCACTTCAATCCACCCAGAAAG	NA
Acta1	CGACGGGCAGGTCATCA	ACCGATAAAGGAAGGCTGGAA	NA
Nrf1	AGCACGGAGTGACCCAAAC	TGTACGTGGCTACATGGACCT	NA
Ppara	GCAGTGCCCTGAACATCGA	CGCCGAAAGAAGCCCTTAC	NA
Nppb	GAGGTCACTCCTATCCTCTGG	GCCATTTCCTCCGACTTTTCTC	NA
Myh7	CCGAGTCCCAGGTCAACAA	CTTCACGGGCACCCTTGGA	NA
Cpt1b	ACAGACTTGCTACAGCACCTC	CGTCGAGGATTCTCTGGAAC	NA
Srebf1	GGAGCCATGGATTGCACATT	GGCCCGGGAAGTCACTGT	NA
Cd36	TTAGATGTGGAACCCATAACTGGA	TTGACCAATATGTTGACCTGCAG	NA
Fasn	GGTTACACTGTGCTAGGTGTTG	TCCAGGCGCATGAGGCTCAGC	NA

Dgat1	GCTCTGGCATCATACTCCATC	CGGTAGGTCAGGTTGTCTGG	NA
Gpam	TGCTGAAGTGGCTGCGGAGTTG	TTAGTAACACCCAGCCAGTCAG	NA
Slc2a4	TTCATTGTCGGCATGGGTTT	ACGGCAAATAGAAGGAAGACGTA	NA
Slc2a1	TCAACACGGCCTTCACTG	CACGATGCTCAGATAGGACATC	NA
Oxct1	CCAAGGAAGTAAATGAAGATGCTCCTA	ACGTGTATGTTACAAGAAATGGCTTACC	NA
Ppia	NA	NA	Mm02342430_g1
Taz	NA	NA	Mm00504978_m1
PnPla2	NA	NA	Mm00503040_m1
Lipe	NA	NA	Mm00495359_m1
Acat1	NA	NA	Mm00507463_m1
Bdh1	NA	NA	Mm00558330_m1

2.4 Results

2.4.1 TazKD Mice Exhibit a Hypertrophic Cardiomyopathy Without Notable Cardiac Dysfunction

Using real-time PCR, we confirmed successful knockdown of *Taz* mRNA expression >90% in the hearts and soleus muscles of 8 to 10-week-old TazKD mice, whereas not as robust reductions were observed in the lung and liver **(Figure 2.1A)**. By 8 to 10 weeks of age, TazKD mice developed a hypertrophic cardiomyopathy characterized by an increase in LV anterior and posterior wall thickness, as well as a reduction in LV internal diameter **(Figure 2.1, B–H)**. LV volume was reduced by nearly 32% and 60% during diastole and systole, respectively, in TazKD mice compared to their WT littermates **(Figure 2.1, I and J)**. However, these structural alterations did not translate into any notable functional impairments. With regards to systolic function, cardiac output and stroke volume were comparable between TazKD mice and their WT littermates **(Table 2.2)**. Parameters of diastolic function including the mitral E/A ratio, isovolumic relaxation time and the E/e' ratio (mitral inflow E wave/tissue Doppler mitral annulus velocity) were also similar between TazKD mice and their WT littermates. Consistent with previously published models of cardiac hypertrophy (238, 239), TazKD mice exhibited hypercontractile function as evidenced by an increase in LV ejection fraction and fractional shortening **(Table 2.2)**. Furthermore, WGA staining revealed that cardiac myocyte cross-sectional area was increased in TazKD mice **(Figure 2.2A)**, which was associated with increased mRNA expression of markers of cardiac hypertrophy including skeletal α-actin (*Acta1*), a trend to increased brain natriuretic peptide (*Nppb*), but no change in β-myosin heavy chain (*Myh7*) **(Figure 2.2B)**. Masson's trichrome staining of LV cross sections from hearts of TazKD mice demonstrated no changes in fibrosis compared to hearts from WT mice **(Figure 2.2C)**, which was associated with similar collagen type 1 α1 (*Col1a1*), a trend to reduced collagen type 1 α2 (*Col1a2*) and increased connective tissue growth factor (*Ccn2*) mRNA expression **(Figure 2.2D)**.

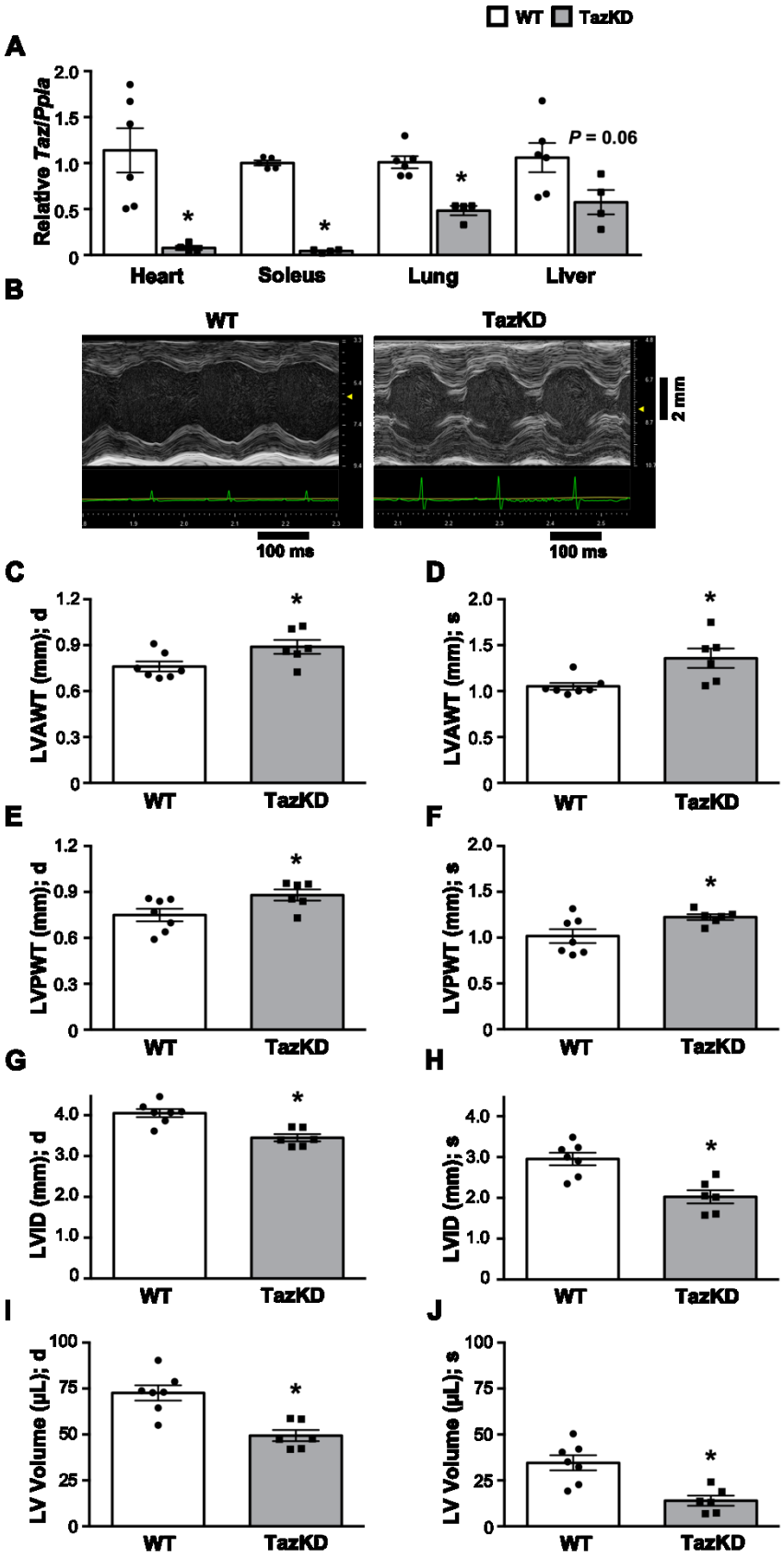
WT
TazKD
A
Relative Taz/Ppia
2.0
1.5
1.0
0.5
0
P = 0.06
*
Heart
Soleus
Lung
Liver
B
WT
TazKD
2 mm
100 ms
100 ms
C
LVAWT (mm); d
1.2
0.9
0.6
0.3
0
WT
TazKD
D
LVAWT (mm); s
2.0
1.5
1.0
0.5
0
E
LVPWT (mm); d
F
LVPWT (mm); s
G
LVID (mm); d
4.0
3.0
2.0
1.0
H
LVID (mm); s
I
LV Volume (µL); d
100
75
50
25
J
LV Volume (µL); s

Figure 2.1. *In vivo cardiac structural dimensions in male TazKD mice.* **A:** Relative *Taz* mRNA expression in heart, soleus, lung, and liver tissue extracted from WT and TazKD mice (n = 4–6). **B:** Representative M-mode images from WT and TazKD mice acquired utilizing ultrasound echocardiography. Left ventricular (LV) anterior wall thickness during diastole **(C)** and systole **(D)** (n = 4–7). LV posterior wall thickness during diastole **(E)** and systole **(F)** (n = 4–7). LV internal diameter during diastole **(G)** and systole **(H)** (n = 4–7). LV volume during diastole **(I)** and systole **(J)** (n = 4–7). Values represent mean ± SEM. Differences were determined by an unpaired two-tailed Student's t-test or by a Mann-Whitney test. *$P < 0.05$, significantly different from WT mice.

Table 2.2. *In vivo* cardiac function in WT and TazKD mice

Parameter	WT	TazKD
Heart Rate (bpm)	381.6 ± 11.69	382.6 ± 15.22
LVID (mm), s	2.952 ± 0.1526	2.028 ± 0.1613*
LVID (mm), d	4.052 ± 0.0997	3.449 ± 0.0879*
Volume (μL); s	34.58 ± 4.142	13.97 ± 2.727*
Volume (μL); d	72.61 ± 4.175	49.39 ± 3.059*
Stroke Volume (μL)	38.03 ± 1.191	35.42 ± 1.741
EF (%)	53.41 ± 3.388	72.47 ± 4.070*
FS (%)	27.43 ± 2.175	41.44 ± 3.584*
CO (ml/min)	14.49 ± 0.5574	13.44 ± 0.3373
LVAWT (mm); s	1.052 ± 0.0376	1.358 ± 0.1054*
LVAWT (mm); d	0.7610 ± 0.0323	0.8893 ± 0.0456*
LVPWT (mm); s	1.017 ± 0.0754	1.224 ± 0.0315*
LVPWT (mm); d	0.7496 ± 0.0411	0.8796 ± 0.0364*
e'/a'	1.413 ± 0.0796	1.446 ± 0.0506
E/e'	28.55 ± 5.013	21.03 ± 3.590
E/A	1.774 ± 0.1827	2.403 ± 0.3335
IVCT (ms)	21.14 ± 1.603	16.51 ± 0.8226*
IVRT (ms)	18.03 ± 1.400	18.80 ± 1.407
MV ET (ms)	60.09 ± 2.382	57.34 ± 1.330

In vivo cardiac function and LV wall measurements in WT and TazKD mice (n = 4–7). Values represent mean ± SEM. Differences were determined by an unpaired two-tailed Student's t-test or by a Mann-Whitney test. *$P < 0.05$, significantly different from WT mice. Bpm, beats per minute; CO, cardiac output; d, diastole, EF, ejection fraction; FS, fractional shortening; IVCT, isovolumic contraction time; IVRT, isovolumic relaxation time; LV, left ventricle; LVID, LV internal diameter; LVEF, LVAWT, LV anterior wall thickness; LVPWT, LV posterior wall thickness; MV ET, mitral valve ejection time; s, systole.

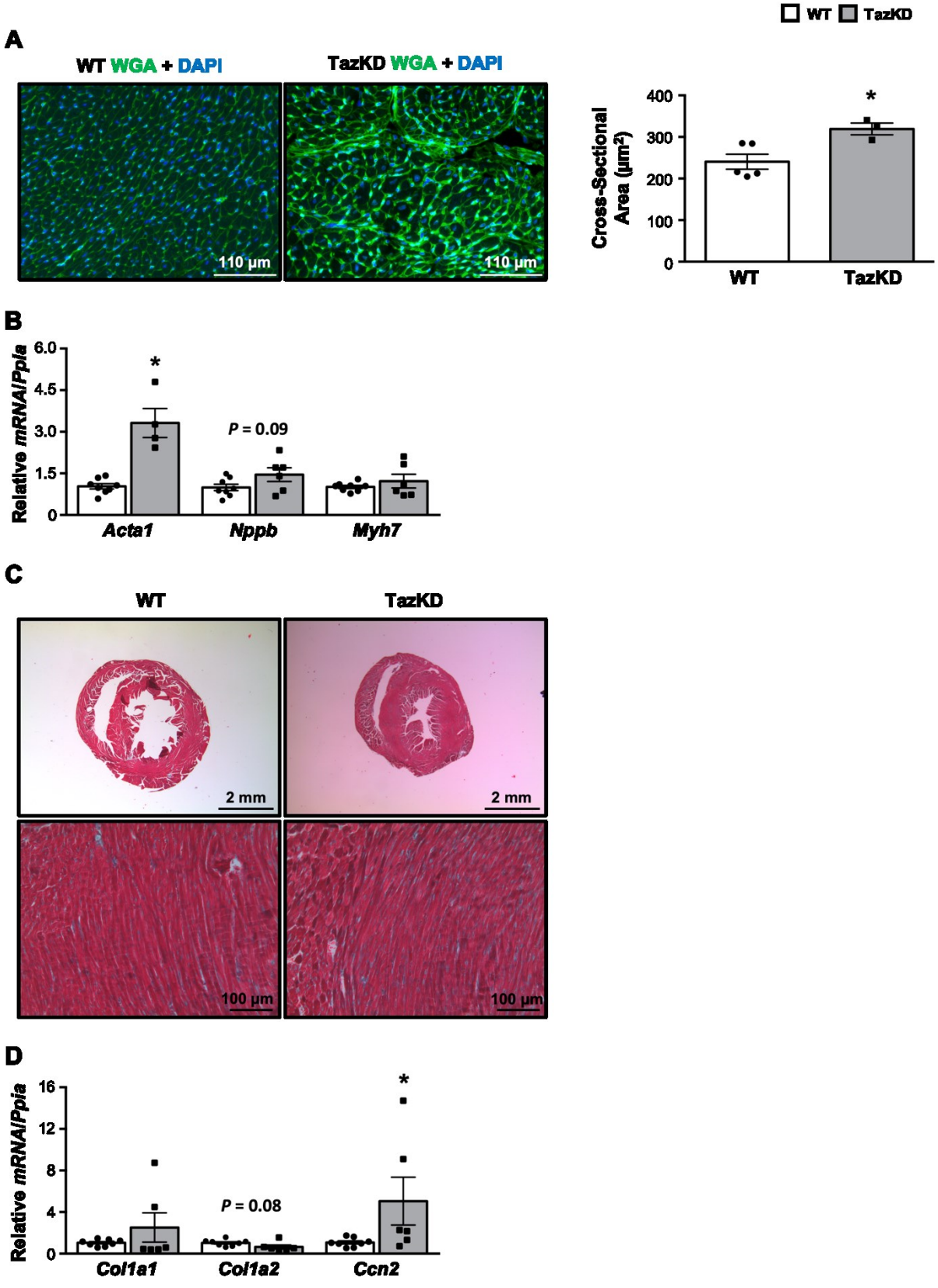
A
WT WGA + DAPI
TazKD WGA + DAPI
110 µm
110 µm
WT
TazKD
Cross-Sectional Area (µm²)
400
300
200
100
0
*
WT
TazKD
B
Relative mRNA/Ppia
6.0
4.5
3.0
1.5
0
*
P = 0.09
Acta1
Nppb
Myh7
C
WT
TazKD
2 mm
2 mm
100 µm
100 µm
D
Relative mRNA/Ppia
16
12
8
4
0
*
P = 0.08
Col1a1
Col1a2
Ccn2

Figure 2.2. *Increased ventricular and cardiac myocyte hypertrophy in male TazKD mice*. **A:** WGA staining (representative images and quantification) and cardiac myocyte cross-sectional area in hearts from TazKD mice and their WT littermates (n = 3–5). **B:** Relative mRNA expression of gene markers for cardiac myocyte hypertrophy [skeletal a-actin (*Acta1*), brain natriuretic peptide (*Nppb*), and b-myosin heavy chain (*Myh7*)] in WT and TazKD mice (n = 4–8). **C:** Masson's trichrome staining demonstrates similar myocardial fibrosis between WT and TazKD mice. **D:** Relative mRNA expression of gene markers for cardiac fibrosis [collagen type 1 a1 (*Col1a1*), collagen type 1 a2 (*Col1a2*), and connective tissue growth factor (*Ccn2*)] in WT and TazKD mice (n = 6–8). Values are represented as means ± SE. Differences were determined by an unpaired two-tailed Student's t test or by a Mann–Whitney test. $P < 0.05$, significantly different from WT mice.

2.4.2 Myocardial Energy Metabolism is Perturbed in TazKD Mice

To investigate potential alterations in myocardial energy metabolism resulting from *Taz* deficiency, isolated hearts from 8 to 10-week-old TazKD mice and their WT littermates were aerobically perfused in the working mode. In the absence of insulin, TazKD mice exhibited no major differences in palmitate oxidation rates, β-hydroxybutyrate (βOHB) oxidation rates, or glycolysis rates, though they did display a trending reduction in glucose oxidation rates compared to their WT littermates **(Figure 2.3, A–D)**. Upon the addition of insulin (100 μU/mL), a mild but nonsignificant decrease in palmitate oxidation was observed in WT littermates ($P = 0.16$), whereas palmitate oxidation rates were now surprisingly increased in TazKD mice **(Figure 2.3A)**. Myocardial βOHB oxidation rates and glycolysis rates continued to remain similar, while glucose oxidation rates were less insulin responsive and further decreased in TazKD mice versus their WT littermates **(Figure 2.3, B–E)**. In addition, there were no differences in glycogen content or the incorporation of [U-^{14}C]glucose into the glycogen pool, indicating that the reduction in glucose oxidation was not siphoning more glucose towards glycogen storage **(Figure 2.3, F and G)**. Importantly, the metabolic perturbations observed in TazKD mouse hearts were independent of differences in workload, as there were no changes in *ex vivo* cardiac work between TazKD mice and their WT littermates **(Table 2.3)**. In addition, other parameters of *ex vivo* cardiac function, including cardiac output, the rate pressure product, as well as the aortic and coronary flows during the aerobic perfusion, remained similar between TazKD mice and their WT littermates, though peak systolic pressure was mildly elevated in TazKD mice **(Table 2.3)**.

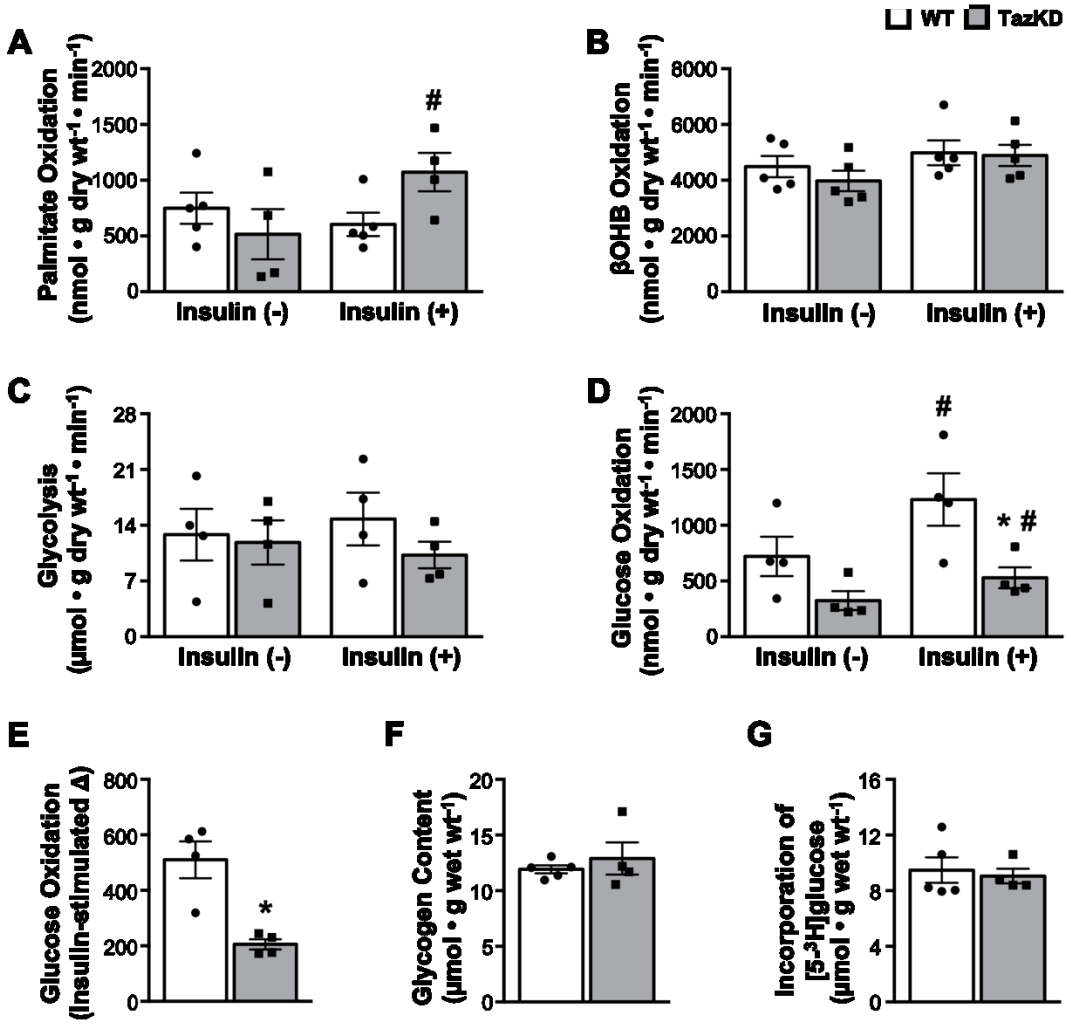

Figur *azKD mice.* Palmitate oxidation rates **(A)**, βOHB oxidation rates **(B)**, glycolysis rates **(C)**, and glucose oxidation rates **(D)** during aerobic perfusion of isolated working hearts from either WT or TazKD mice ($n = 4–5$). **E:** Insulin-stimulated increase (delta) in glucose oxidation rates ($n = 4$). Myocardial glycogen content **(F)**, and the incorporation of [U-14C]glucose into the glycogen pool **(G)** during the isolated working heart perfusion ($n = 4–5$). Values are represented as means ± SE. Differences were determined by a repeated measures two-way ANOVA followed by a Bonferroni post hoc analysis, an unpaired two-tailed Student's t test or by a Mann–Whitney test**.** *$P < 0.05$, significantly different from WT mice. $^{\#}P < 0.05$, significantly different from without-insulin counterpart.

Table 2.3. *Ex vivo cardiac function in isolated working hearts from WT or TazKD mice*

Parameter	WT	TazKD
Heart Rate (bpm)	308 ± 16	284 ± 18
Peak Systolic Pressure (mmHg)	68.9 ± 1.0	73.6 ± 1.4*
Developed Pressure (mmHg)	21.4 ± 1.9	25.2 ± 1.9
HR x PSP (bpm • mmHg • 10^{-3})	21.28 ± 1.16	20.81 ± 1.22
HR x DP (bpm • mmHg • 10^{-3})	6.66 ± 0.69	7.10 ± 0.60
CO (mL/min)	8.6 ± 0.9	8.8 ± 0.8
Aortic Outflow (mL/min)	6.0 ± 0.8	6.1 ± 0.8
Coronary Flow (mL/min)	2.6 ± 0.4	2.7 ± 0.2
Cardiac Work (mJ/min)	66.7 ± 7.5	73.2 ± 8.1
Cardiac Work (J • g dry wt^{-1} • min^{-1})	2.551 ± 0.321	2.896 ± 0.281

Parameters of cardiac function in the ex vivo isolated working heart from WT and TazKD mice 8 to 10 weeks of age (n = 4–5). Values represent mean ± SEM. Differences were determined by an unpaired two-tailed Student's t-test. *$P < 0.05$, significantly different from WT mice. Bpm, beats per minute; CO, cardiac output; DP, developed pressure; HR, heart rate; PSP, peak systolic pressure.

2.4.3 The Impairment of Myocardial Glucose Oxidation in TazKD Mice is Associated with Reduced Pyruvate Dehydrogenase Activity but Not Changes in the Molecular Control of Glucose Metabolism

Consistent with impaired myocardial glucose oxidation rates, PDH activity was significantly reduced in myocardial extracts from TazKD mice versus their WT littermates **(Figure 2.4A)**. Of interest, this reduction in PDH activity was independent of changes in PDH phosphorylation, as all 3 PDH phosphorylation sites (serine 293, serine 300, and serine 232) were similar in TazKD mouse hearts **(Figure 2.4B)**. We also observed unexpected decreases in both myocardial *Pdk1* and *Pdk4* mRNA expression, whereas *Pdk2* mRNA expression remained similar in TazKD mice versus their WT littermates **(Figure 2.4C)**. In addition, mRNA expression of forkhead box O1 (*Foxo1*), a key transcription factor regulating *Pdk4* gene expression (31, 102), was also unaltered in hearts from TazKD mice **(Figure 2.4C)**. We also examined PDH acetylation, which negatively regulates PDH activity, as well as expression of sirtuin 3 (SIRT3), a major deacetylase that acts on PDH (32), though once again both remained unchanged in myocardial extracts from TazKD mice **(Figure 2.4, D and E)**. Reductions in glucose uptake could also account for decreases in glucose oxidation, and while mRNA expression of glucose transporter (GLUT) 1 was unchanged, GLUT4 mRNA expression was decreased in myocardial extracts of TazKD mice versus their WT littermates **(Figure 2.4F)**. Circulating insulin and glucose levels were also decreased and increased, respectively, in TazKD mice **(Figure 2.4, G and H)**, suggestive of abnormal insulin signaling in BTHS.

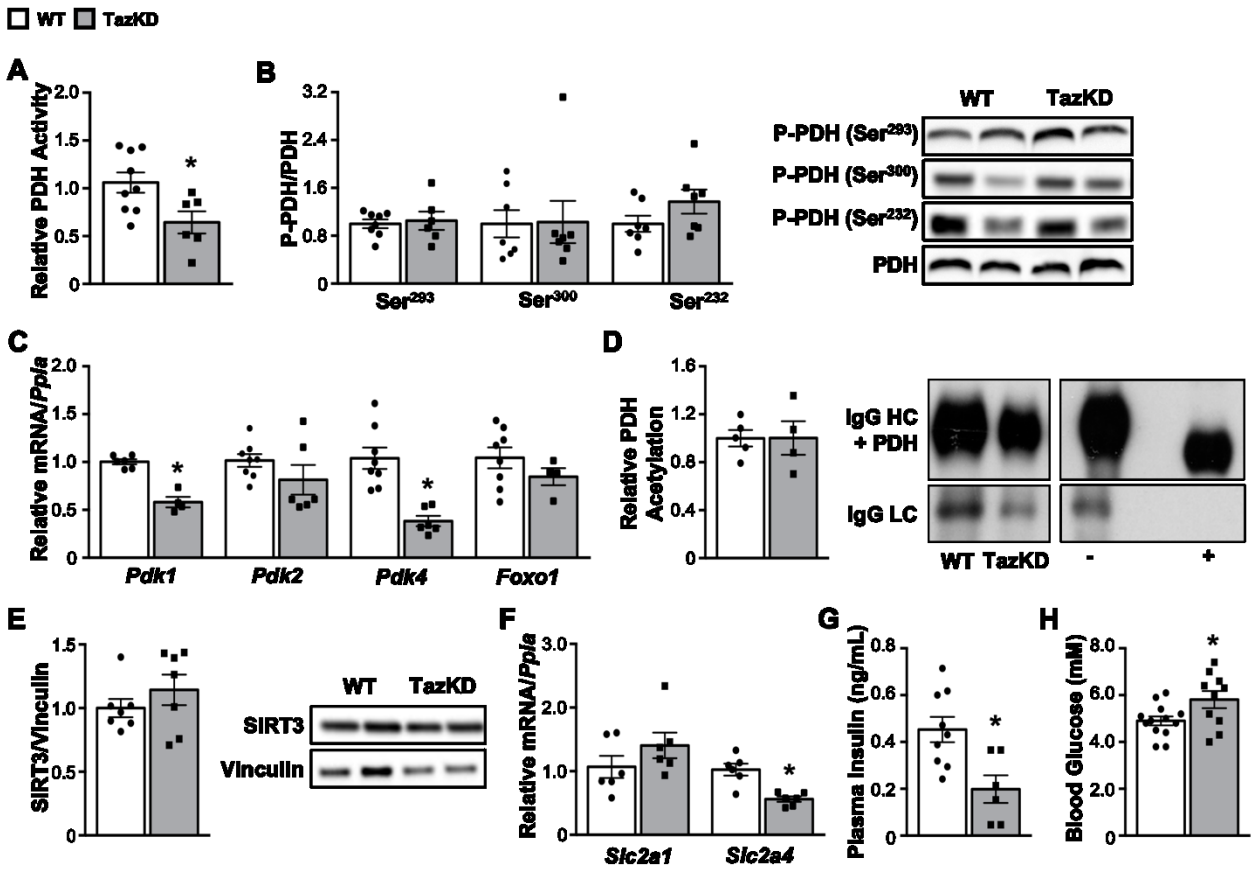

Figure 2.4. *Myocardial PDH activity is impaired in male TazKD mice.* **A:** Pyruvate dehydrogenase (PDH) enzymatic activity in hearts from TazKD and WT mice following a 16-h fast to 4-h refeed (n = 6–9). **B:** PDH phosphorylation at serine (Ser) 293, Ser 300, and Ser 232 in myocardial extracts from WT and TazKD mice *(*n = 6–8). **C:** Expression of genes involved in the regulation of PDH activity [PDH kinase 1 (*Pdk1*), PDH kinase 2 (*Pdk2*), PDH kinase 4 (*Pdk4*), and forkhead box protein O1 (*Foxo1*)] in hearts from WT and TazKD mice (n = 4–8). **D:** Relative assessment of PDH acetylation in WT and TazKD hearts normalized to the light chain of the antibody used to pull down lysine-acetylated proteins (n = 4–5). **E:** Sirtuin 3 (SIRT3) protein expression in myocardial extracts from WT and TazKD mice (n = 7). **F:** Expression of genes involved in the regulation of glucose uptake [glucose transporter 1 (*Slc2a1*) and glucose transporter 4 (*Slc2a4*)] (n = 6). **G:** Plasma insulin levels assessed following a 16-h fast and 4-h refeed in WT and TazKD mice (n = 6–9). **H:** Plasma glucose levels in WT mice and TazKD mice following a 20-h fast (n = 10–13). Values are represented as means ± SE. Differences were determined by an unpaired two-tailed Student's t test. *$P < 0.05$, significantly different from WT mice.

2.4.4 The Increase in Myocardial Fatty Acid Oxidation in TazKD mice is Not Associated with Increased Expression of Fatty Acid Oxidation Enzymes or Decreased Malonyl CoA Levels

The increase in myocardial fatty acid oxidation rates observed in TazKD mice was interestingly associated with decreased mRNA expression of the peroxisome proliferator-activated receptor α (*PPARα*)-regulated fatty acid oxidation enzymes, medium chain acyl CoA dehydrogenase (*Acadm*) and carnitine palmitoyl transferase 1 (CPT1/*Cpt1b*) **(Figure 2.5A)**. Nuclear respiratory factor 1 (*Nrf1*) mRNA expression was also decreased, whereas mRNA expression of PPARα (*Ppara*) and PPARγ coactivator-1α (*Ppargc1a*) were similar in hearts of TazKD mice versus their WT littermates **(Figure 2.5A)**. Moreover, myocardial protein expression of the PPARα-regulated fatty acid oxidation enzymes, LCAD and βHAD, was also similar in TazKD mice **(Figure 2.5B)**. ACC is another key regulator of fatty acid oxidation through controlling the formation of malonyl CoA, an endogenous inhibitor of CPT1 (18), though ACC phosphorylation (indicative of ACC activity) remained similar in TazKD mouse hearts, consistent with no differences in malonyl CoA content **(Figure 2.5, C and D)**. Assessment of other short chain CoA esters revealed no changes in free CoA and succinyl CoA content, whereas acetyl CoA content trended towards a reduction ($P = 0.18$) in TazKD mouse hearts versus their WT littermates **(Figure 2.5, E–G)**.

Although palmitate oxidation rates were increased in TazKD mouse hearts in the presence of insulin, we observed an unexpected increase in myocardial TAG content, which was associated with an increased incorporation of [9,10-^{3}H]palmitate into the TAG pool **(Figure 2.5, H and I)**. The increases in myocardial TAG content in TazKD mice does not appear to be due to changes in myocardial fatty acid uptake, as mRNA expression of cluster of differentiation 36 (*Cd36*) was actually decreased in TazKD versus WT littermate mouse hearts **(Figure 2.5J)**. Furthermore, regulators of lipogenesis (sterol regulatory element-binding protein 1c (*Srebf1*), fatty acid synthase (*Fasn*), glycerol-3-phosphate acyltransferase (*Gpam*), and diacylglycerol acyltransferase 1 (*Dgat1*)) were also either decreased or remained similar in TazKD mouse hearts **(Figure 2.5K)**. Conversely, elevations in myocardial TAG content could reflect reductions in lipolysis, and we observed decreased mRNA expression of hormone sensitive lipase (*Lipe*) and adipose TAG lipase (*Pnpla2*) in myocardial extracts from TazKD mice **(Figure 2.5L)**.

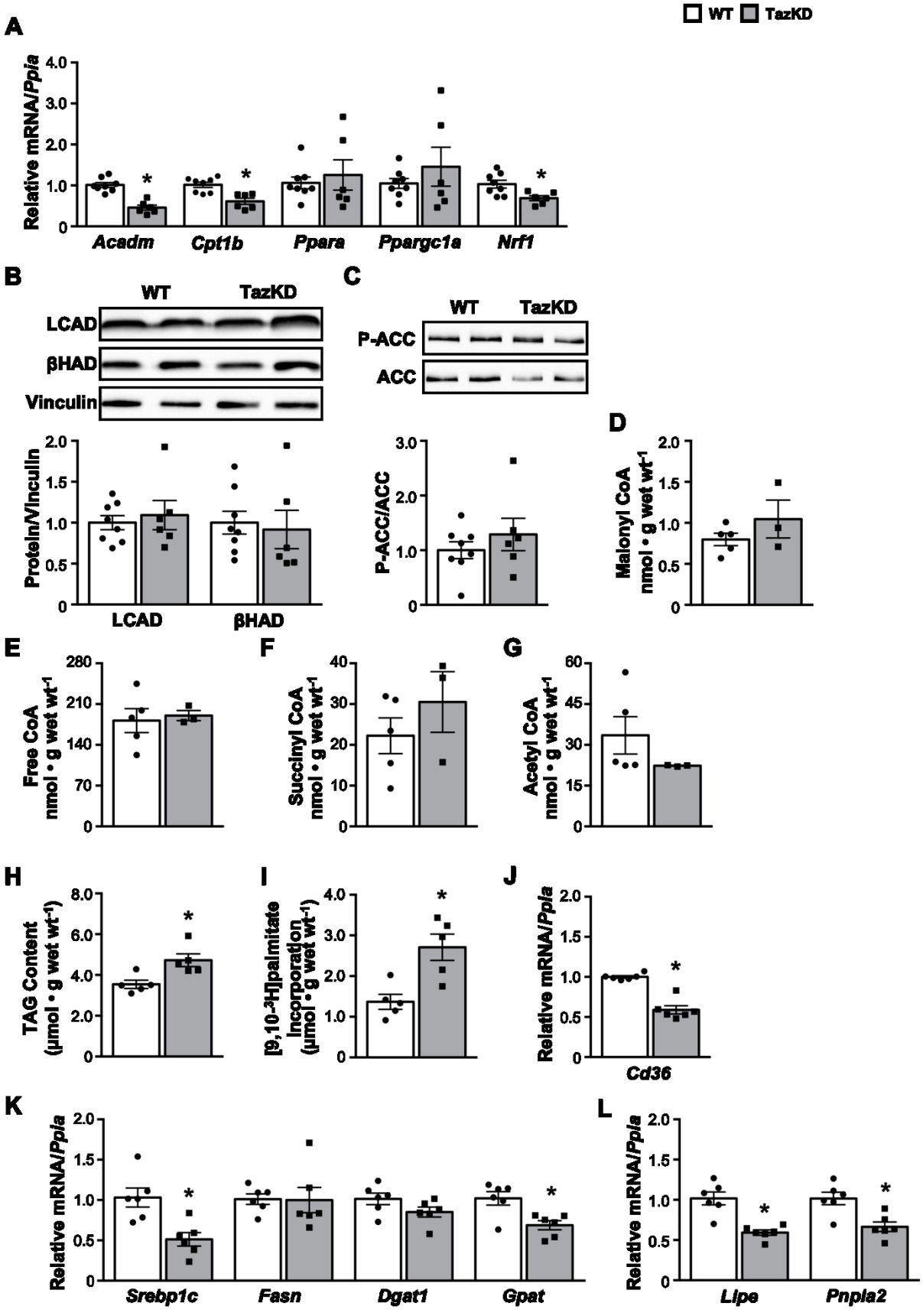
WT
TazKD
A
Relative mRNA/Ppia
Acadm
Cpt1b
Ppara
Ppargc1a
Nrf1
B
LCAD
βHAD
Vinculin
Protein/Vinculin
C
P-ACC
ACC
P-ACC/ACC
D
Malonyl CoA
nmol • g wet wt-1
E
Free CoA
F
Succinyl CoA
G
Acetyl CoA
H
TAG Content
(µmol • g wet wt-1)
I
[9,10-3H]palmitate
Incorporation
J
Cd36
K
Srebp1c
Fasn
Dgat1
Gpat
L
Lipe
Pnpla2

Figure 2.5. *Molecular regulation of fatty acid oxidation in hearts from male TazKD mice.* **A:** mRNA expression of genes involved in the regulation of fatty acid oxidation [medium chain acyl CoA dehydrogenase (*Acadm*), carnitine palmitoyl transferase 1 (*Cpt1b*), peroxisome proliferator-activated receptor α (*Ppara*), PPARγ coactivator-1α (*Ppargc1a*), and nuclear respiratory factor 1 (*Nrf1*)] in hearts from WT and TazKD mice (n = 6–8). **B:** Protein expression of fatty acid b-oxidation enzymes [long-chain acyl CoA dehydrogenase (LCAD) and β-hydroxyacyl CoA dehydrogenase (βHAD)] in hearts from WT and TazKD mice (n = 6–8). **C:** phosphorylation of acetyl-CoA carboxylase (ACC) at serine 79 in hearts from WT and TazKD mice (n = 6–8). **D:** Malonyl CoA content in hearts from WT and TazKD mice (n = 3–5). Free CoA **(D)**, malonyl CoA **(E)**, succinyl CoA **(F)**, and acetyl CoA **(G)** content in hearts from WT and TazKD mice (n = 3–5). Myocardial triacylglycerol (TAG) content **(H)** and the incorporation of [9,10-3H]palmitate into the TAG pool **(I)** in mouse hearts perfused with [9,10-3H]palmitate (n = 5). mRNA expression of genes involved in the regulation of fatty acid uptake [cluster of differentiation 36 (*Cd36*)] **(J)**, lipogenesis [sterol regulatory element-binding protein 1c (*Srebf1*), fatty acid synthase (*Fasn*), diacylglycerol acyltransferase 1 (*Dgat1*), glycerol-3-phosphate acyltransferase (*Gpam*)] **(K)**, and lipolysis [hormone sensitive lipase (*Lipe*), adipose TAG lipase (*Pnpla2*)] **(L)** in myocardial extracts from WT and TazKD mice (n = 6). Values are represented as means ± SE. Differences were determined by an unpaired two-tailed Student's t test or a Mann–Whitney test. $P < 0.05$, significantly different from WT mice.

2.4.5 BDH1 expression is increased in hearts of TazKD mice

Despite TazKD mouse hearts exhibiting similar ketone body oxidation rates as their WT littermates, we did observe a robust ~4-fold increase in BDH1 protein expression **(Figure 2.6A)**. This observation is consistent with previous studies reporting that models of cardiomyopathy and/or heart failure result in an increase in both BDH1 expression and myocardial ketone body oxidation (113, 240). In contrast, we observed a mild decrease in myocardial ACAT1 and no change in SCOT protein expression in TazKD mice versus their WT littermates **(Figure 2.6A)**. The reduction in ACAT1 protein expression was associated with a decrease in *Acat1* mRNA expression, whereas the increased protein expression of BDH1 was not associated with increased *BDH1* mRNA expression, while SCOT mRNA expression (*Oxct1*) was unaffected in TazKD mice **(Figure 2.6B)**.

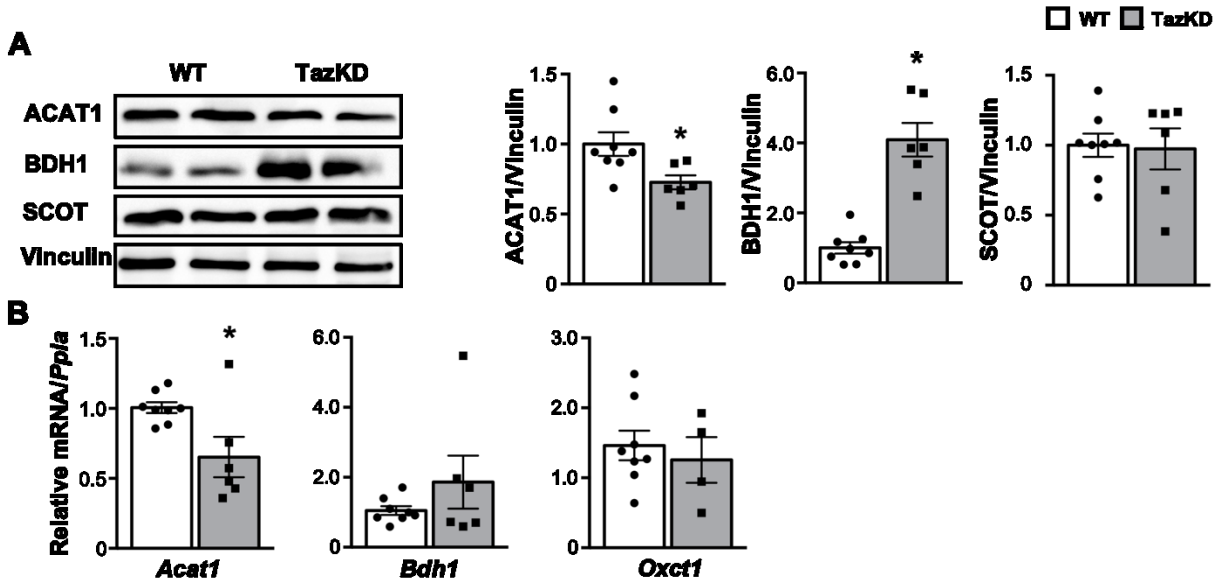

Figure 2.6. *Molecular regulation of ketone body oxidation in hearts from male TazKD mice.* **A:** protein expression of ACAT1, BDH1, and SCOT in hearts from TazKD and WT mice (n = 6–8). **B:** mRNA expression of *Acat1*, *Bdh1*, and *Oxct1* in hearts from WT and TazKD mice (n = 4–8). Values are represented as means ± SE. Differences were determined by an unpaired two-tailed Student's t test or a Mann–Whitney test. $P < 0.05$, significantly different from WT mice. ACAT1, acetoacetyl CoA thiolase 1; BDH1, βOHB dehydrogenase 1; SCOT, succinyl CoA:3-ketoacid CoA transferase.

2.5 Discussion

Our findings advance our understanding of cardiac energy metabolism perturbations in the context of BTHS, as we performed the first assessment of flux through glucose and fatty acid oxidation in intact isolated working hearts from TazKD mice using radioisotopes. Although derangements of myocardial intermediary energy metabolism have been implicated in clinical and preclinical studies of BTHS (76, 79, 81, 106), specific flux measurements in the BTHS heart are lacking. In support of reduced PDH activity in C2C12 myoblasts following CRISPR/cas9 mediated *Taz* knockout (106), we did observe a marked reduction in glucose oxidation rates in working hearts from TazKD mice. This may potentially contribute to the pathology of BTHS-related cardiomyopathy, as we demonstrated that TazKD mice develop a striking hypertrophic cardiomyopathy without overt functional impairments by ~8 – 10 weeks of age.

The reduction in PDH activity in C2C12 myoblasts following CRISPR/cas9 mediated *Taz* knockout was attributed to increases in PDH phosphorylation (106). In contrast, the reduction in myocardial PDH activity in TazKD mice appears to be independent of changes in phosphorylation, as all 3 PDH phosphorylation sites were unaffected. Although PDH kinase-mediated phosphorylation and PDH phosphatase mediated-dephosphorylation have been extensively studied, PDH is also subject to control by other regulatory mechanisms including allosteric control and other post-translational modifications (29, 30). However, PDH acetylation and SIRT3 expression were also unaltered in TazKD mouse hearts. It also remains possible that increases in the glutathionylation of PDH may explain their decreased PDH activity (32, 110, 241), which will need to be explored in future studies. *In vivo* assessment of cardiac energetics using positron emission tomography imaging in young adults with BTHS and without overt heart failure, demonstrated significantly increased myocardial glucose uptake and utilization compared to healthy age-matched controls (76). Although these results suggest potential increases in myocardial glucose oxidation in BTHS, they could also simply reflect increases in glycolysis, which markedly increases in heart failure (17, 18). Consistent with an increased reliance on glycolysis for energy production in BTHS, enhanced extracellular acidification rates, reflective of elevations in glycolysis, were observed in neonatal cardiac myocytes isolated from TazKD mice (83). Similarly, glucose uptake and lactate production are elevated in induced pluripotent stem cell-derived cardiac myocytes subjected to CRISPR/cas9 mediated *Taz* mutation (242).

Conversely, in our study TazKD mouse hearts exhibited a trend towards decreased glycolysis rates in the presence of insulin, as well as a reduction in GLUT4 mRNA levels, though we were underpowered to make a firm conclusion on whether this trend contributes to their decreased glucose oxidation. The reduction in myocardial glucose oxidation in TazKD mice is consistent with previous studies demonstrating that transverse aortic constriction-induced cardiac hypertrophy impairs glucose oxidation rates (243). Moreover, cardiac-specific deletion of PDH induces a robust cardiac hypertrophy (109), suggesting that reductions in myocardial glucose oxidation may directly contribute to hypertrophic growth of the myocardium.

The increase in fatty acid oxidation we observed in working hearts from TazKD mice was not expected based on previous studies (79, 81, 83), and we are unable to reconcile at a molecular level why fatty acid oxidation rates are increased in hearts from TazKD mice. Myocardial extracts from TazKD mice did not exhibit increased transcription of PPARα regulated fatty acid oxidation genes, which were decreased, while myocardial malonyl CoA content was similar to that observed in WT littermates. It should be noted though, that malonyl CoA within the vicinity of CPT1 may have differed and contributed to elevated fatty acid oxidation rates in TazKD mouse hearts, however measuring sub-compartmentalization of malonyl CoA is notoriously difficult due to the strong affinity CoA esters have for membranes (244). Hyperacetylation of fatty acid oxidation enzymes in the heart has also been associated with increased fatty acid oxidation (245, 246), potentially through a reduction in SIRT3 expression (247). However, SIRT3 protein expression was similar in TazKD and WT littermate mouse hearts, while myocardial acetyl CoA levels trended towards being decreased in TazKD mice. As acetyl CoA may also regulate acetylation by mass action as substrate for protein acetylation (248), when combined with normal SIRT3 expression levels, it is unlikely that increases in acetylation explain the increase in fatty acid oxidation observed in TazKD mouse hearts. Another aspect to take into consideration involves insulin resistance, as the elevated fatty acid oxidation in TazKD mouse hearts was only observed in the presence of insulin. In the absence of insulin fatty acid oxidation rates were actually similar between TazKD and WT littermate mouse hearts, and in response to insulin a trend to a mild reduction was observed in WT mice. This was expected based on insulin's actions on myocardial energy metabolism (18, 27), though insulin failed to inhibit fatty acid oxidation rates in working hearts from TazKD mice. Reasons for why fatty acid oxidation rates would increase in response

to insulin are difficult to reconcile, but it may simply be the result of the "Randle Cycle" phenomenon, whereby increases in either glucose or fatty acid oxidation lead to a reciprocal reduction in utilization of the competing fuel source (18, 249). As cardiomyopathy and heart failure are characterized by insulin resistance (156), insulin's failure to stimulate glucose oxidation rates to the same extent in working hearts from TazKD mice versus their WT littermates, may have necessitated an increased reliance on fatty acid oxidation to meet the heart's energy demands. In further support of impaired insulin action in BTHS, previous studies have demonstrated reduced islet insulin content and insulin secretion in TazKD mice (250), reinforcing our observations of lower circulating insulin levels in TazKD mice.

It remains unclear as to why we did not observe a decrease in fatty acid oxidation in TazKD mouse hearts, which has frequently been reported by others. While cardiac mitochondria isolated from TazKD mice demonstrated a reduction in palmitoyl-L-carnitine-mediated respiration (81, 82), studies in isolated mitochondria are devoid of key intracellular regulators of fatty acid oxidation such as malonyl CoA, which would be present in the intact isolated working heart (97). Furthermore, the rate of flux through glucose and fatty acid oxidation are heavily influenced by cardiac workload, which is much lower *in vitro* in cardiac myocytes or isolated mitochondria versus the intact heart *ex vivo* or *in vivo* (97). Last, the differences in fatty acid oxidation that we observed in working hearts from TazKD mice appear to be exacerbated in the presence of insulin, whereas the vast majority of studies that have assessed myocardial fatty acid oxidation in TazKD mice did not include insulin. Therefore, the reported discrepancies in fatty acid oxidation in BTHS may simply be attributed to differences in techniques utilized to assess myocardial energy metabolism or the absence of insulin, and we believe our observations using the working heart model provide important advances towards understanding the metabolic perturbations present in the BTHS heart.

We also observed a marked increase in myocardial protein expression of the ketone body oxidation enzyme, BDH1, in TazKD mice. This is consistent with a number of recent reports demonstrating that cardiac hypertrophy and heart failure are associated with marked increases in ketone body oxidation, which are postulated to be an adaptive response to improve energy production in myocardium that might be low on fuel supply (17, 113, 240). In support of this, cardiac-specific

overexpression of BDH1 in mice increases myocardial ketone body oxidation rates and protects against transverse aortic constriction-induced adverse remodeling and cardiac dysfunction (251). However, βOHB oxidation rates were not increased in isolated working hearts from TazKD mice despite having elevated BDH1 expression. It is plausible that since the concentration of ketone bodies provided in the perfusate was equivalent (0.8 mM), βOHB oxidation rates remained similar. Circulating ketone body levels are a major determinant of myocardial ketone body oxidation rates, whereby ketone bodies can become a major energy source for the heart when provided at concentrations seen with prolonged fasting (21), and thus *in vivo* myocardial ketone body oxidation rates may be elevated in BTHS. Moreover, increased circulating βOHB levels observed in individuals with BTHS supports that ketones could serve as an important fuel source for the heart in the context of *TAZ* deficiency (115).

The observed molecular alterations in the hearts of TazKD mice are not directly related to *Taz* deficiency and impaired remodeling of mature cardiolipin per se, as similar patterns were not observed in their soleus muscle. Although skeletal muscle is another highly oxidative organ, BDH1 expression was not increased in the soleus muscles of TazKD mice, and mRNA expression of genes regulating fatty acid oxidation (e.g., *Acadm* and *Cpt1b*) were not downregulated **(Appendix Figure 1.1)**. It is likely that the hypertrophic cardiomyopathy also contributes to the molecular changes that we observed in TazKD mouse hearts. As such, it will be important for future studies to better understand the causal nature of these changes, and the interplay between cardiac hypertrophy and energy metabolism in BTHS.

Of interest, the cardiac phenotype described in our TazKD mice is consistent with the hypertrophic cardiomyopathy reported by Johnson *et al*. (238) and Cole *et al*. (252), but in contrast to the dilated cardiomyopathy with systolic dysfunction observed originally by Acehan *et al*. (230) and others (100, 231). The reason for the discrepancy in phenotypes is unclear, however is unlikely to be attributed to differences in *Taz* knockdown efficiency, as we utilized a similar doxycycline administration strategy and achieved a similar degree of knockdown as that seen by Acehan *et al*. (230). Given that the development of systolic dysfunction in TazKD mice is not observed until the mice are 7 to 8 months of age (100, 230, 231), it is possible that our TazKD mice will also develop systolic dysfunction with prolonged age, as their hypertrophic cardiomyopathy in the absence of

systolic dysfunction was observed at 2 to 2.5 months of age. Nonetheless, the difference in phenotypes may simply represent a transition from compensatory hypertrophic cardiac remodeling to decompensated heart failure, as an undulating phenotype from hypertrophic to dilated cardiomyopathy has been described in a BTHS case report (64).

Taken together, our findings reveal that *Taz* deficiency results in a selective impairment of myocardial glucose oxidation with a concomitant increase in fatty acid oxidation. Our specific goal was to elucidate whether BTHS may be characterized by perturbations in myocardial energy metabolism, paralleling observations with cardiomyopathy/heart failure in general (18, 40, 156). Currently, there are a variety of pharmacological agents available that can increase myocardial glucose oxidation (dichloroacetate) or decrease fatty acid oxidation (trimetazidine). Thus, future studies should aim to determine whether correcting these metabolic perturbations can alleviate the pathology of BTHS-related cardiomyopathy. Supporting this premise, interventions that increase myocardial glucose oxidation have been reported to attenuate diabetic cardiomyopathy or improve cardiac function in experimental heart failure (110-112). Similarly, heart failure with preserved ejection fraction, which currently has no approved therapies, is also characterized by increased myocardial glucose oxidation that normalizes upon alleviation of diastolic dysfunction (253). Likewise, interventions that decrease fatty acid oxidation rates have also been reported to mitigate obesity-induced cardiomyopathy, while improving cardiac function in heart failure (183, 254). Accordingly, therapeutic interventions that aim to optimize cardiac intermediary metabolism may represent a novel approach to prevent and/or reverse cardiomyopathy development in BTHS and other cardiac disorders associated with perturbed cardiolipin biosynthesis.

Acknowledgements & Grants

This study was supported by an Innovation Grant from the Women and Children's Health Research Institute to J.R.U. A.A.G. is supported by a Canada Graduate Scholarship from the Canadian Institutes of Health Research, and a Graduate Studentship from the Women and Children's Health Research Institute. J.R.U. is a Tier 2 Canada Research Chair (Pharmacotherapy of Energy Metabolism in Obesity).

Disclosures

No conflicts of interest, financial or otherwise, are declared by the authors.

Chapter 3: Stimulating Myocardial Pyruvate Dehydrogenase Activity Fails to Alleviate Cardiac Abnormalities in a Mouse Model of Human Barth Syndrome

Amanda A. Greenwell[1,2,3], Seyed Amirhossein Tabatabaei Dakhili[1,2,3*], Keshav Gopal[1,2,3], Christina T. Saed[1,2,3], Jordan S.F. Chan[1,2,3], Nick Kazungu Mugabo[1], Pavel Zhabyeyev[2,5,6], Farah Eaton[1,2,3], Jennifer Kruger[4], Gavin Y. Oudit[2,5,6], John R. Ussher[1,2,3]

[1]Faculty of Pharmacy and Pharmaceutical Sciences, University of Alberta, Edmonton, AB, Canada
[2]Cardiovascular Research Centre, University of Alberta, Edmonton, AB, Canada
[3]Women and Children's Health Research Institute, University of Alberta, Edmonton, AB, Canada
[4]Health Sciences Laboratory Animal Services, University of Alberta, Edmonton, AB, Canada
[5]Divsion of Cardiology, Department of Medicine, University of Alberta, Edmonton, Canada
[6]Mazankowski Alberta Heart Institute, University of Alberta, Edmonton, Canada

PUBLISHED: Greenwell AA*, Tabatabaei Dakhili SA*, Gopal K, Saed CT, Chan JSF, Kazungu Mugabo N, Zhabyeyev P, Eaton F, Kruger J, Oudit GY, and Ussher JR. Stimulating myocardial pyruvate dehydrogenase activity fails to alleviate cardiac abnormalities in a mouse model of human Barth syndrome. *Frontiers in Cardiovascular Medicine* 23: 2659, 2022.
*Denotes equal contribution

3.1 Abstract

Barth syndrome (BTHS) is a rare genetic disorder due to mutations in the *TAFAZZIN* gene, leading to impaired maturation of cardiolipin and thereby adversely affecting mitochondrial function and energy metabolism, often resulting in cardiomyopathy. In a murine model of BTHS involving short-hairpin RNA mediated knockdown of *Tafazzin* (TazKD mice), myocardial glucose oxidation rates were markedly reduced, likely secondary to an impairment in the activity of pyruvate dehydrogenase (PDH), the rate-limiting enzyme of glucose oxidation. Furthermore, TazKD mice exhibited cardiac hypertrophy with minimal cardiac dysfunction. Because the stimulation of myocardial glucose oxidation has been shown to alleviate diabetic cardiomyopathy and heart failure, we hypothesized that stimulating PDH activity would alleviate the cardiac hypertrophy present in TazKD mice. In order to address our hypothesis, 6-week-old male TazKD mice and their wild-type (WT) littermates were treated with dichloroacetate (DCA; 70 mM in the drinking water), which stimulates PDH activity via inhibiting PDH kinase to prevent inhibitory phosphorylation of PDH. We utilized ultrasound echocardiography to assess cardiac function and left ventricular wall structure in all mice prior to and following 6-weeks of treatment. Consistent with systemic activation of PDH and glucose oxidation, DCA treatment lowered glycemia in both TazKD mice and their WT littermates, and decreased PDH phosphorylation equivalently at all 3 of its inhibitory sites (serine 293/300/232). However, DCA treatment had no impact on left ventricular structure, or systolic and diastolic function in TazKD mice. Therefore, it is unlikely that stimulating glucose oxidation is a viable target to improve BTHS-related cardiomyopathy.

3.2 Introduction

Severe, infantile-onset cardiomyopathy, often leading to heart failure, is the dominant clinical manifestation of the rare genetic disorder, Barth syndrome (BTHS) (55, 58). Pathogenic variants of *TAFAZZIN* on chromosome Xq28.12 cause BTHS by impairing the enzymatic activity of tafazzin, leading to defective cardiolipin (CL) remodeling and consequent mitochondrial abnormalities (66). Similar to other cardiac pathologies (20, 40), deficient myocardial energy production is a characteristic feature of BTHS-related cardiomyopathy (76, 77). However, the specific mechanisms by which tafazzin deficiency precipitates a cardiac energy deficit and whether optimization of oxidative metabolism represents a potential therapeutic target requires further investigation.

Although disruption of tafazzin mediated CL remodeling is associated with electron transport chain (ETC) dysfunction (79, 89, 91), evidence has identified that derangements in oxidative metabolism may be substrate-specific, thus implicating upstream intermediary metabolism pathway defects in the pathogenesis of BTHS-related cardiomyopathy (80-82). Notably, studies utilizing the *Tafazzin* knockdown (TazKD) mouse model and *Tafazzin* knockout cell lines have identified a selective defect in the activity of pyruvate dehydrogenase (PDH), the rate-limiting enzyme in glucose oxidation (80, 91). Furthermore, glucose oxidation rates are markedly impaired in perfused isolated working hearts from TazKD mice (80).

Dichloroacetate (DCA) is a pyruvate analogue that enhances PDH activity and glucose oxidation by inhibiting all isoforms of PDH kinase (PDHK), which inhibit PDH through reversible phosphorylation (255, 256). Of interest, stimulating myocardial PDH activity and subsequent glucose oxidation has been shown to improve cardiac function in murine models of diabetic cardiomyopathy, ischemia-reperfusion injury, and heart failure (102, 104, 111, 112). We hypothesized that this may also represent a novel approach for the treatment of BTHS-related cardiomyopathy, of which no specific therapies have been identified to date. Accordingly, in the present study we aimed to determine whether enhancement of myocardial PDH activity via treatment with DCA would be effective in attenuating the development and progression of pathological cardiac structural remodeling in TazKD mice.

3.3 Methods

3.3.1 Animal Care and Experimentation

All animal procedures were approved by the University of Alberta Health Sciences Animal Welfare Committee and performed in accordance with the regulations of the Canadian Council on Animal Care. Animals were housed in a 22°C temperature-controlled unit under a 12-hr light/dark cycle with standard environmental enrichment and *ad libitum* access to drinking water and food. The generation of the doxycycline-inducible short hairpin RNA (shRNA)-mediated TazKD mouse model has been described elsewhere (230). Doxycycline (625 mg/kg) was administered as part of the chow provided to the mice throughout the study. Female C57BL/6J mice were placed on doxycycline-containing diet 1-week prior to mating with transgenic male mice heterozygous for the *Tafazzin* shRNA transgene, to produce a *Tafazzin* deficiency in the pups during the early embryonic stage. Male littermates that did not possess the *Tafazzin* shRNA transgene were also maintained on the doxycycline-containing chow and used as our wild-type (WT) controls. Male TazKD and WT mice at 6-weeks of age were randomized to receive a 6-week treatment with sodium DCA (Sigma-Aldrich) which was added to the drinking water (70 mM) and pH-balanced. Daily water consumption for each cage of mice was measured consistently throughout the 6-week treatment period and calculated per mouse by dividing the total amount consumed by the number of mice in each cage. Blood glucose levels were measured from tail whole-blood during the random-fed state using the Contour Next blood glucose monitoring system (Bayer, NJ, USA). At the end of the treatment protocol, mice were euthanized with an intraperitoneal injection of sodium pentobarbital (12 mg) after a 16-hour fast and 4-hour refeed period. Peripheral tissues were subsequently extracted and immediately snap frozen in liquid nitrogen using liquid nitrogen-cooled Wollenberger tongs prior to storage at -80°C.

3.3.2 Ultrasound Echocardiography

Cardiac ultrasound images were acquired utilizing an MX 550S probe and the VisualSonics Vevo 3100 rodent ultrasound imaging system as previously described in **Chapter 2.3.2**. Mice were initially anesthetized with 2 – 3% isoflurane and maintained on 1 – 1.5% isoflurane for the remainder of the assessment. Body temperature, respiratory rate and heart rate were consistently monitored during image acquisition. Cardiac structure and left ventricular (LV) systolic and

diastolic function were determined in 5-week-old WT and TazKD mice (baseline) and following 6-weeks of DCA treatment. Several parameters were assessed including, but not limited to, anterior and posterior wall dimensions, left ventricular (LV) ejection fraction (EF), LV fractional shortening (FS), cardiac output (CO), mitral E/A ratio, tissue Doppler e'/a' ratio, and the E/e' ratio as described previously (80, 102). Because the E and e' waves can become fused with A and a' waves at higher heart rates, respectively, the E/A, E/e' and e'/a' ratios could not be accurately measured for some mice (257).

3.3.3 Magnetic Resonance Imaging and Body Composition Analysis

Total fat and lean mass were quantified by quantitative nuclear magnetic resonance relaxometry utilizing an EchoMRI-4in1/700 body composition analyzer. Fat mass is representative of the total mass of all fat molecules in the body expressed as an equivalent weight of canola oil. Lean mass represents a muscle tissue mass equivalent of all body parts containing water, excluding fat, bone mineral content and NMR undetectable substances such as hair and claws.

3.3.4 Whole Cell Homogenate Preparation and Immunoblot Analysis

A protein lysis buffer containing 50 mM Tris HCl (pH 8 at 4°C), 1 mM EDTA, 10% glycerol (w/v), 0.02% Brij-35 (w/v), 1 mM dithiothreitol, and protease and phosphatase inhibitors (Sigma-Aldrich) was used to extract protein from powdered, frozen cardiac tissue (~15-20 mg). Protein was quantified using a Bradford protein assay kit (Bio-Rad) and samples (30 µg) were subsequently denatured and subjected to western blotting protocols as previously described in **Chapter 2.3.6**. Membranes were probed with the following antibodies: PDH (3205S, Cell Signalling), phospho-PDH-E1α (Serine 293) (AP1062, Sigma-Aldrich), phospho-PDH-E1α (Serine 232) (AP1063, Sigma-Aldrich), phospho-PDH-E1α (Serine 300) (AP1064, Sigma-Aldrich), PDHK4 (ab214938, Abcam), vinculin (1390S, Cell Signaling), All antibodies were prepared in a 1/1000 dilution in 3% BSA except for vinculin, which was prepared in a 1/2000 dilution.

3.3.5 RNA Isolation and Real-Time Quantitative PCR

First-strand cDNA was synthesized from RNA extracted from powdered frozen cardiac (~15-20 mg) tissue using the iScript Reverse Transcription Supermix (Bio-Rad Laboratories Inc., Hercules,

CA) as described in **Chapter 2.3.5**. A CFX Connect Real-Time PCR machine (Bio-Rad Laboratories Inc.) was used to perform real-time PCR utilizing SYBR Green (KK4601; Kapa Viosystems, Inc.). Cyclophilin A (*Ppia*) was used as an internal housekeeping gene to determine relative mRNA transcript levels quantified with the $2^{-\Delta\Delta Ct}$ method as previously described (236). Primer sequences used include the following: *Ppia* forward; GCTGGACCAAACACAAACG, *Ppia* reverse; ATGCCTTCTTTCACCTTCCC, *Acta1* forward; CGACGGGCAGGTCATCA, *Acta1* reverse; ACCGATAAAGGAAGGCTGGAA, *Nppb* forward; GAGGTCACTCCTATCCTCTGG, *Nppb* reverse; GCCATTTCCTCCGACTTTTCTC.

3.3.6 Protein Carbonylation

Myocardial protein carbonylation was determined using the protein carbonyl content assay kit (MAK094, Sigma-Aldrich). Approximately 20 mg of frozen heart tissue per sample was lysed with protein lysis buffer and the resulting supernatant was analyzed according to the manufacturer's protocol, with absorbance measured at $\lambda = 375$ nm using a Synergy H1 microplate reader (BioTek). Protein carbonyl levels in myocardial samples were expressed as nmol/mg protein.

3.3.7 Statistical Analysis

All values are presented as mean ± standard error of the mean (SEM). An unpaired, two-tailed Student's *t* test or a two-way ANOVA was used to assess statistical significance and differences were considered significant when $P < 0.05$. Statistical analysis was completed utilizing GraphPad Prism 9 software.

3.4 Results

3.4.1 TazKD Mice Present with Cardiac Hypertrophy at 5-Weeks of Age

5-week-old TazKD mice displayed significant reductions in body weight, lean mass, and fat mass in comparison to their age-matched WT littermates **(Figure 3.1, A–C)**. Consistent with the generalized growth defect observed in subjects with Barth Syndrome (125), despite lean and fat mass being reduced in TazKD mice, the relative proportions of lean and fat mass normalized to body weight were similar between TazKD mice and their WT littermates **(Figure 3.1D)**. As our

previous findings identified that TazKD mice demonstrate cardiac hypertrophy by 8-10 weeks of age (80), we first performed ultrasound echocardiography studies in 5-week-old TazKD mice to determine whether this cardiac hypertrophy was present earlier. Despite LV mass being similar in 5-week-old TazKD mice and their WT littermates, when taking the generalized growth defect into account and normalizing LV mass to body weight, the TazKD mice demonstrated a clear cardiac hypertrophy (4.02 ± 0.12 mg/g [WT] versus 4.65 ± 0.18 mg/g [TazKD]; $P = 0.01$). Furthermore, other indices of cardiac hypertrophy were evident in TazKD mice, including a decreased LV internal diameter (LVID) and volumes during diastole, as well as an increased LV anterior wall (LVAW) and posterior wall (LVPW) thickness when normalized to body weight **(Figure 3.1, E–H, Table 3.1)**. These structural abnormalities resulted in a 26% and 22% reduction in CO and stroke volume (SV), respectively, which is consistent with previous reports that TazKD mice do exhibit cardiac hypertrophy (238) **(Figure 3.1I, Table 3.1)**. Parameters of systolic function including LVEF and LVFS were not different between TazKD and WT mice. Likewise, the E/A and E/e' ratios were also similar between TazKD mice and their WT littermates, indicating normal diastolic dysfunction **(Figure 3.1, H and I)**.

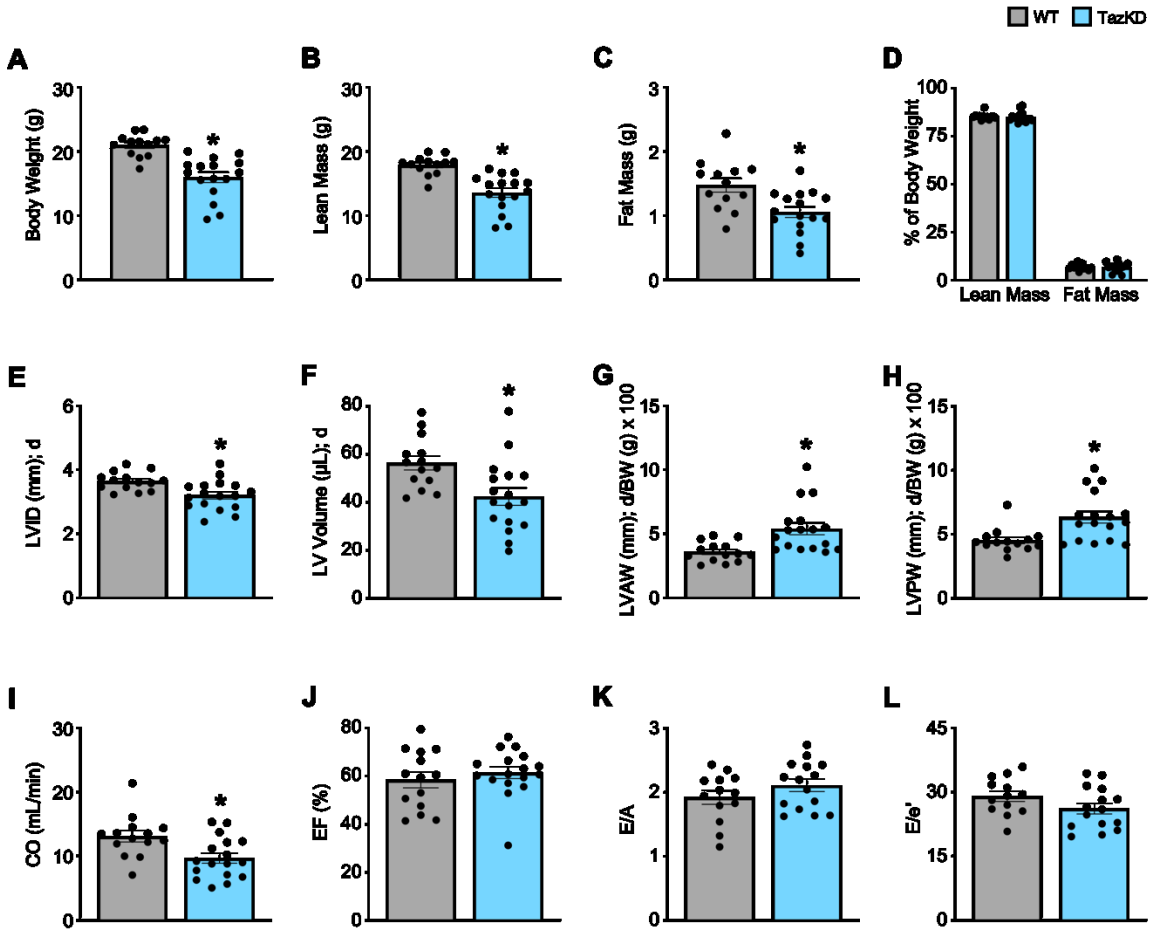

Figure 3.1. *Cardiac hypertrophy is already present in TazKD mice at 5 weeks of age*. **A–D:** Body weight and body composition (lean mass, fat mass) analysis in 5-week-old TazKD mice and their WT littermates (WT: $n = 13$, TazKD: $n = 16$). Ultrasound echocardiography was used to assess left ventricular (LV) chamber and wall dimensions including **(E)** LV internal diameter (LVID), **(F)** LV volume, **(G)** LV anterior wall thickness (LVAW) normalized to body weight (BW), **(H)** and LV posterior wall thickness (LVPW) normalized to BW during diastole (d), in addition to functional parameters including **(I)** cardiac output (CO), **(J)** ejection fraction (EF), **(K)** E/A, and **(L)** E/e' in 5-week old TazKD mice and their WT littermates. For structural and systolic function parameters (WT: $n = 14$, TazKD: $n = 17$); for diastolic function parameters (WT: $n = 13$, TazKD: $n = 15$). Values represent mean ± SEM. Differences were determined using an unpaired, two-tailed Student's *t* test. $^*P < 0.05$ significantly different from WT littermates.

Table 3.1. *In vivo baseline assessment of cardiac structural and functional parameters in WT and TazKD mice.*

	WT	TazKD
Heart Rate (beats/min)	401 ± 9	382 ± 6
BW (g)	19.8 ± 0.8	14.7 ± 0.9*
LVID (mm); s	2.53 ± 0.11	2.18 ± 0.11*
LVID (mm); d	3.64 ± 0.08	3.20 ± 0.11*
Volume (μL); s	24.0 ± 2.6	17.1 ± 2.6
Volume (μL); d	56.4 ± 2.9	42.4 ± 3.6*
Stroke Volume (μL)	32.4 ± 1.9	25.3 ± 1.9*
EF (%)	58.4 ± 3.3	61.4 ± 2.4
FS (%)	30.9 ± 2.3	32.3 ± 1.6
CO (ml/min)	13.1 ± 0.9	9.7 ± 0.8*
LVAW/BW x 10^2 (mm/g); s	5.44 ± 0.30	7.57 ± 0.59*
LVAW/BW x 10^2 (mm/g); d	3.59 ± 0.21	5.39 ± 0.46*
LVPW/BW x 10^2 (mm/g); s	5.89 ± 0.26	8.15 ± 0.58*
LVPW/BW x 10^2 (mm/g); d	4.52 ± 0.25	6.33 ± 0.46*
E/A	1.92 ± 0.11	2.11 ± 0.10
e'/a'	1.54 ± 0.10	2.09 ± 0.16*
E/e'	29.0 ± 1.2	26.1 ± 1.3

In vivo cardiac function and LV wall measurements in 5-week-old WT and TazKD mice (n = 13–17). Values represent mean ± SEM. *$P < 0.05$, significantly different from WT. BW, body weight; CO, cardiac output; EF, ejection fraction; FS, fractional shortening; LV, left ventricular; LVAW, LV anterior wall thickness; LVID, LV internal diameter; LVPW, LV posterior wall thickness; s, systole; d, diastole.

3.4.2 Treatment with DCA Decreases Myocardial PDH Phosphorylation in TazKD Mice

In order to correct the impairments in myocardial PDH activity we previously observed in TazKD mice (80), we treated 6-week-old TazKD mice and their WT littermates with the PDHK inhibitor, DCA (70 mM in the drinking water), for 6-weeks. Although WT and TazKD mice treated with DCA via the drinking water tended to consume slightly less water than control mice on average, water consumption was similar across the 6-week treatment period, thus ensuring that the dose of DCA each mouse received remained consistent throughout the study **(Figure 3.2A)**. In line with a systemic enhancement of glucose oxidation, blood glucose levels were significantly decreased in both WT and TazKD mice treated with DCA **(Figure 3.2B)**. As glucose is a more oxygen efficient fuel than fat (51), stimulating PDH activity often leads to a reduction in oxygen consumption, and we also observed with indirect calorimetry that DCA treatment decreased whole-body oxygen consumption rates in both WT and TazKD mice (*data not shown*). Furthermore, we observed a marked reduction in the inhibitory phosphorylation of PDH at all three phosphorylation sites (Serine 293, Serine 232, and Serine 300) in myocardial tissue from DCA-treated WT and TazKD mice without altering PDHK4 protein expression **(Figure 3.2, C–F)**. Taken together, these findings are highly suggestive of an increase in myocardial PDH activity and a subsequent enhancement of myocardial glucose oxidation.

3.4.3 Treatment with DCA Does Not Improve the Cardiac Structural Abnormalities in TazKD Mice

In opposition of our hypothesis, the adverse hypertrophic cardiac remodeling present in TazKD mice was not improved by treatment with DCA. The decreased LVID and LV volume during systole and diastole in TazKD mice were unaffected by DCA treatment **(Figure 3.2, G and H. Table 3.2)**. Furthermore, the increased LVAW and LVPW thickness present in TazKD mice were also not improved following treatment with DCA (Figure 2I/J). Consistent with unattenuated cardiac hypertrophy, CO and SV remained decreased in DCA treated TazKD mice **(Figure 3.2K, Table 3.2)**. Systolic function represented by LVEF and LVFS, as well as diastolic function represented by the E/A, e'/a', and E/e', were similar between TazKD mice and their WT littermates, while being unaffected via DCA treatment **(Figure 3. 2, L–N, Table 2)**.

We next assessed markers of cardiac remodeling and cardiac dysfunction, whereby mRNA expression of skeletal α-actin (*Acta1*), a marker of cardiomyocyte hypertrophy, remained markedly elevated in myocardial tissue from TazKD mice and was unaffected by DCA treatment **(Figure 3.2O)**. In addition, myocardial mRNA expression of brain natriuretic peptide (*Nppb*) was not different between WT and TazKD mice, nor was its expression affected by DCA treatment **(Figure 3.2P)**. As TazKD mice exhibit increases in myocardial oxidative stress (238), we also assessed myocardial protein carbonylation levels, which were increased in control treated TazKD mice versus their WT littermates but prevented via treatment with DCA **(Figure 3.2Q)**.

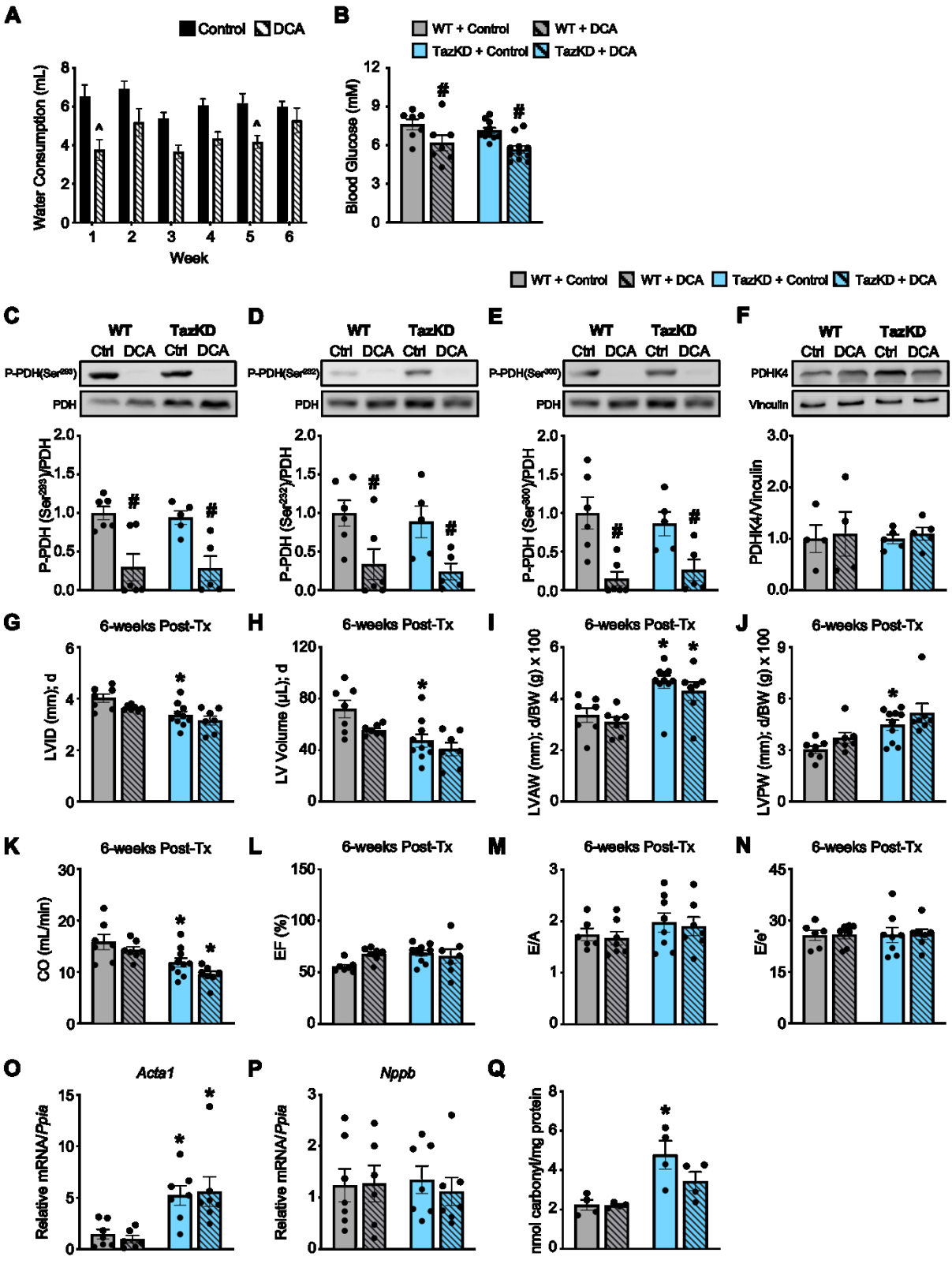
A
Control
DCA
Water Consumption (mL)
Week
B
WT + Control
WT + DCA
TazKD + Control
TazKD + DCA
Blood Glucose (mM)
C
D
E
F
WT
TazKD
Ctrl
DCA
P-PDH(Ser293)
P-PDH(Ser232)
P-PDH(Ser300)
PDH
PDHK4
Vinculin
P-PDH (Ser293)/PDH
P-PDH (Ser232)/PDH
P-PDH (Ser300)/PDH
PDHK4/Vinculin
G
H
I
J
6-weeks Post-Tx
LVID (mm); d
LV Volume (µL); d
LVAW (mm); d/BW (g) x 100
LVPW (mm); d/BW (g) x 100
K
L
M
N
CO (mL/min)
EF (%)
E/A
E/e'
O
P
Q
Acta1
Nppb
Relative mRNA/Ppia
nmol carbonyl/mg protein

Figure 3.2. *DCA treatment decreases inhibitory PDH phosphorylation but fails to alleviate the cardiac structural abnormalities in TazKD mice*. **A:** Average daily consumption of water or water supplemented with DCA (70 mM) reported per individual mouse for each week of the experimental protocol (n = 17–18). **B:** Random-fed blood glucose measurements of WT and TazKD mice either subjected to control or DCA treatment (n = 7–11). Pyruvate dehydrogenase (PDH) phosphorylation at **(C)** serine 293, **(D)** serine 232, and **(E)** serine 300 relative to total PDH in myocardial tissue from WT and TazKD mice treated with control or DCA for 6-weeks (n = 5–6). **F:** PDHK4 protein expression relative to vinculin in myocardial tissue from WT and TazKD mice treated with control or DCA for 6-weeks (n = 4–5). Ultrasound echocardiography was used to assess left ventricular (LV) chamber and wall dimensions including **(G)** LV internal diameter (LVID), **(H)** LV volume, **(I)** LV anterior wall thickness (LVAW) normalized to body weight, and **(J)** LV posterior wall thickness (LVPW) normalized to body weight during diastole (d), in addition to functional parameters including **(K)** cardiac output (CO), **(L)** ejection fraction (EF), **(M)** E/A, and **(N)** E/e' in WT and TazKD mice treated with control of DCA. For structural and systolic function parameters (WT control: n = 7, WT DCA: n = 7, TazKD control: n = 10, TazKD DCA: n = 7); for diastolic function parameters (WT control: n = 6, WT DCA: n = 7, TazKD control: n = 8, TazKD DCA: n = 7). Relative mRNA expression of **(O)** skeletal α-actin (*Acta1*) and **(P)** brain natriuretic peptide (*Nppb*) normalized to cyclophilin A (*Ppia*), and **(Q)** total protein carbonylation in myocardial tissue from WT and TazKD mice treated with control or DCA for 6-weeks (n = 4–7). Values represent mean ± SEM. Differences were determined using a two-way ANOVA. $^{\wedge}P < 0.05$, significantly different from control treated mice. $^{\#}P < 0.05$, significantly different from control treated counterpart. $^{*}P < 0.05$, significantly different from WT counterpart.

Table 3.2. *In vivo assessment of cardiac structural and functional parameters in WT and TazKD mice following treatment with DCA.*

	WT Control	WT DCA	TazKD Control	TazKD DCA
Heart Rate (beats/min)	400 ± 14	378 ± 8	377 ± 11	379 ± 8
BW (g)	26.0 ± 0.7	22.6 ± 1.0$^{\#}$	21.2 ± 0.7*	20.0 ± 0.9
LVID (mm); s	2.87 ± 0.15	2.28 ± 0.08	2.11 ± 0.15*	2.02 ± 0.28
LVID (mm); d	4.02 ± 0.17	3.63 ± 0.04	3.36 ± 0.14*	3.15 ± 0.18
Volume (μL); s	32.4 ± 4.0	17.9 ± 1.6$^{\#}$	15.8 ± 3.0*	15.9 ± 4.4
Volume (μL); d	71.9 ± 6.8	55.6 ± 1.5	47.3 ± 4.9*	40.7 ± 5.2
Stroke Volume (μL)	39.5 ± 3.2	37.7 ± 1.5	31.5 ± 2.3	24.9 ± 1.7*
EF (%)	55.5 ± 2.1	67.8 ± 2.5	68.6 ± 2.8	65.7 ± 6.7
FS (%)	28.7 ± 1.4	37.3 ± 1.9	37.9 ± 2.1	37.5 ± 6.1
CO (ml/min)	15.8 ± 1.5	14.2 ± 0.7	11.8 ± 0.9*	9.44 ± 0.7*
LVAW/BW x 10^2 (mm/g); s	4.82 ± 0.30	5.02 ± 0.41	6.79 ± 0.29*	6.36 ± 0.49
LVAW/BW x 10^2 (mm/g); d	3.36 ± 0.28	3.09 ± 0.19	4.66 ± 0.25*	4.30 ± 0.35*
LVPW/BW x 10^2 (mm/g); s	4.19 ± 0.31	5.49 ± 0.39	6.27 ± 0.39*	6.65 ± 0.50
LVPW/BW x 10^2 (mm/g); d	3.03 ± 0.22	3.72 ± 0.31	4.46 ± 0.30*	5.16 ± 0.55^
E/A	1.74 ± 0.12	1.67 ± 0.13	1.98 ± 0.19	1.90 ± 0.18
e'/a'	1.40 ± 0.13	1.56 ± 0.11	1.86 ± 0.15	1.90 ± 0.18
E/e'	25.7 ± 1.5	25.9 ± 1.2	25.7 ± 2.2	26.0 ± 1.5

In vivo cardiac function and LV wall measurements in WT and TazKD mice subjected to control or DCA treatment for 6-weeks (n = 6–10). Values represent mean ± SEM. *$P < 0.05$, significantly different from WT counterpart. $^{\#}P < 0.05$, significantly different from control treated counterpart. ^$P = 0.07$, versus WT counterpart. BW, body weight; CO, cardiac output; EF, ejection fraction;

FS, fractional shortening; LV, left ventricular; LVAW, LV anterior wall thickness; LVID, LV internal diameter; LVPW, LV posterior wall thickness; s, systole; d, diastole.

3.5 Discussion

Perturbations in myocardial energy metabolism play a significant role in the development and progression of numerous cardiovascular disorders, and therefore represent a promising target for therapeutic intervention (42, 114). This study sought to elucidate whether optimization of cardiac glucose oxidation, through treatment with DCA to stimulate PDH activity, could improve the pathological structural remodeling of the heart associated with *Tafazzin* deficiency observed in BTHS. Our results demonstrated that treatment of TazKD mice with DCA for 6-weeks did not attenuate or reverse their cardiac hypertrophy despite a restoration of myocardial PDH activity.

We were particularly surprised by these negative findings, since stimulating myocardial PDH activity has been shown to improve cardiac abnormalities in numerous experimental settings. For example, inhibition of the transcription factor forkhead box O1 prevents transcription of *Pdk4*, which encodes for PDHK4, leading to increased myocardial glucose oxidation and alleviation of the diastolic dysfunction associated with experimental diabetic cardiomyopathy in mice (102). Similarly, the glucagon-like peptide-1 receptor agonist liraglutide, an antidiabetic agent that promotes insulin secretion, also stimulates myocardial PDH activity and glucose oxidation, thereby alleviating the diastolic dysfunction in a murine model of diabetic cardiomyopathy (110). Treatment with DCA itself has also been shown to alleviate experimental diabetic cardiomyopathy in rats (112), while decreasing infarct size in mice subjected to experimental ischemia-reperfusion injury via temporary occlusion of the left anterior descending coronary artery (104). In addition, DCA treatment of Dahl salt-sensitive rats fed a high-salt diet increased myocardial PDH activity, which attenuated heart failure progression as indicated by increased systolic function, decreased cardiac hypertrophy, and improved survival (111).

Because isolated working hearts from TazKD mice exhibit marked reductions in glucose oxidation rates (80), it seemed well rationalized to presume that DCA treatment might alleviate their cardiac abnormalities. This raises the important question as to why stimulating myocardial PDH activity would fail to yield benefit in TazKD mice, considering numerous other cardiac pathologies are

corrected by such a metabolic strategy? We posit that the persistent destabilization of ETC supercomplexes and reduced ETC complex activity coupled with consequent elevations of mitochondrial reactive oxygen species and oxidative stress (72, 81, 83, 91, 95), likely supersede intermediary metabolism defects present in BTHS. This may explain the failure of DCA treatment to attenuate the LV hypertrophic remodeling in TazKD mice despite an improvement of myocardial glucose oxidation. Therefore, the results of our study suggest that any therapeutic intervention aiming to optimize myocardial intermediary energy metabolism may be ineffective at alleviating BTHS-related cardiomyopathy, unless the defects in the respiratory chain are addressed. In other words, even if the BTHS heart is capable of oxidizing more of the carbohydrate or fatty acid fuel delivered to it, if the generated reducing equivalents (i.e. NADH) are unable to result in ATP generation due to the ETC respiratory defects, no improvement in cardiac pathology can be expected. However, our preliminary observations addressing this question suggest that DCA can still increase myocardial ATP levels in TazKD mice (control treated mean of 2.53 mM [n = 2] versus DCA treated mean of 4.00 mM [n = 3]), and thus we plan to interrogate this more extensively in future studies.

In order for metabolic interventions to yield clinical utility in BTHS, it may need to be coupled with strategies that ultimately correct the adverse CL remodeling responsible for BTHS-related ETC respiratory dysfunction. One such strategy that may show promise is the agent, elamipretide, which is a cell-permeable, aromatic-cationic mitochondria-targeting tetrapeptide that localizes to the inner mitochondrial membrane where it selectively associates with CL to improve respiratory chain function (258, 259). Presently, the ongoing TAZPOWER clinical trial (NCT03098797) is investigating the efficacy of directly targeting mitochondrial dysfunction with elamipretide as a treatment for BTHS (60). Intriguingly, in participants with genetically confirmed BTHS, a 16% improvement in average SV indexed to body surface area at week 36 of the open extension phase of the trial compared to baseline was reported with elamipretide treatment (mean age 19.5 years, range 12-35 years). Furthermore, elamipretide treatment produced a trend towards an increase in SV over time when a slope model of individual regression lines for each subject was utilized (60). It is possible that the utilization of a metabolic therapy such as DCA in combination with elamipretide may ensure that augmented substrate oxidation maximally translates to enhanced ATP production. This may thus represent a more effective approach to mitigate BTHS-related

cardiomyopathy, which we emphasize should be a key direction for metabolic investigations to reorient their research towards.

An earlier intervention with DCA may also need to be considered, since we already observed cardiac hypertrophy in TazKD mice at 5-weeks of age. Thus, administering DCA immediately after birth or the weaning of TazKD mice may allow us to prevent the progression of their cardiac hypertrophy before it develops. Alternatively, it may be that glucose oxidation is simply not a viable metabolic target for BTHS-related cardiomyopathy, but not myocardial intermediary metabolism *per se*. Indeed, increasing fatty acid oxidation by treatment of 3-month-old TazKD mice with a pan-peroxisome proliferator activated receptor (PPAR) agonist, bezafibrate, prevented the development of dilated cardiomyopathy and systolic dysfunction over the course of 4-months (99, 100). A complementary study also determined that bezafibrate treatment prevented the exacerbation of cardiac dysfunction in 4.5-month-old TazKD mice in combination with infusion of isoproterenol (231). Bezafibrate is also presently being investigated as a potential therapy for BTHS in the CARDIOlipin MANipulation (CARDIOMAN) trial (98). Therefore, interrogation of other intermediary metabolism pathways rather than glucose oxidation may be a more beneficial target. However, bezafibrate treatment also induced an increase in mitochondrial biogenesis, the enzymatic activity of ETC complexes I-III and trended to increase the protein expression of all ETC complexes in the hearts of TazKD mice, therefore, it is difficult to determine the specific mechanism(s) underpinning the cardioprotective actions of bezafibrate (231). A limitation of our study is that we did not assess ETC function or other parameters of mitochondrial status in response to DCA treatment (e.g., were defects in complex I-V activity in TazKD mice mitigated by DCA?). Conversely, it has also been demonstrated that fibrates actually decrease myocardial fatty acid oxidation, since PPAR activation in the liver increases fatty acid oxidation, which decreases hepatic triacylglycerol secretion and subsequent fatty acid delivery to the myocardium (101). As such, it is difficult to determine the specific mechanism(s) underpinning the cardioprotective actions of bezafibrate in BTHS.

In summary, the findings of the present study reveal that treatment with DCA is ineffective in reversing cardiac hypertrophy present in TazKD mice, and thus may not represent an effective treatment for BTHS-related cardiomyopathy. Although a precise mechanism to explain why DCA

failed to alleviate cardiac remodeling in the *Tafazzin* deficient heart is unknown, persistent respiratory chain dysfunction may have limited energy production despite an enhancement of flux through PDH. As such, further investigation is required to determine whether DCA in combination with a therapy that stabilizes the ETC, such as elamipretide, may represent a beneficial therapeutic approach for BTHS-related cardiomyopathy.

Acknowledgements & Grants

This study was supported by an Innovation Grant from the Women and Children's Health Research Institute to J.R.U. A.A.G is supported by a Vanier Canada Graduate Scholarship from the Canadian Institutes of Health Research, and a Graduate Studentship from the Women and Children's Health Research Institute. J.R.U. is a Tier 2 Canada Research Chair (Pharmacotherapy of Energy Metabolism in Obesity).

Disclosures

No conflicts of interest, financial or otherwise, are declared by the authors.

Chapter 4: An Isoproteic Cocoa Butter-Based Ketogenic Diet Fails to Improve Glucose Homeostasis and Promote Weight Loss in Obese Mice

Amanda A. Greenwell[1,2], Christina T. Saed[1,2], Seyed Amirhossein Tabatabaei Dakhili[1,2], Kim L. Ho[2,3], Keshav Gopal[1,2], Jordan S. F. Chan[1,2], Oksana O. Kaczmar[1], Scott A. Dyer[1], Farah Eaton[1,2], Gary D. Lopaschuk[2,3], Rami Al Batran[4], John R. Ussher[1,2]

[1]Faculty of Pharmacy and Pharmaceutical Sciences, University of Alberta, Edmonton, AB, Canada

[2]Alberta Diabetes Institute, University of Alberta, Edmonton, AB, Canada

[3]Department of Pediatrics, Faculty of Medicine and Dentistry, University of Alberta, Edmonton, AB, Canada

[4]Faculty of Pharmacy, University of Montreal, Montreal, QC, Canada

PUBLISHED: Greenwell AA, Saed CT, Tabatabaei Dakhili SA, Ho KL, Gopal K, Chan JSF, Kaczmar OO, Dyer SA, Eaton F, Lopaschuk GD, Al Batran R, and Ussher JR. An isoproteic cocoa butter-based ketogenic diet fails to improve glucose homeostasis and promote weight loss in obese mice. *Am J Physiol Endocrinol Metab* 323: E8-E20, 2022.

4.1 Abstract

High-fat and very low-carbohydrate based ketogenic diets have gained considerable popularity as a non-pharmacological strategy for obesity, due to their potential to enhance weight loss and improve glucose homeostasis and cardiovascular risk factors. However, the effectiveness of a ketogenic diet towards metabolic health is equivocal. To better understand the impact of ketogenic diets in obesity, male and female mice were fed a 60% cocoa butter-based high-fat diet for 16-weeks to induce obesity, following which mice were transitioned to either an 85% cocoa butter fat-based ketogenic diet, a 10% cocoa butter fat-based low-fat diet, or maintained on a high-fat diet for an additional 8-weeks. All experimental diets were matched for sucrose and protein content, and contained an identical micronutrient profile, with complex carbohydrates being the primary carbohydrate source in the low-fat diet. The transition to a ketogenic diet was ineffective at inducing significant body fat loss and improving glucose homeostasis in obese male and female mice and led to an enhancement of myocardial triacylglycerol content in male mice. Alternatively, obese male and female mice transitioned to a low-fat and high-complex carbohydrate diet exhibited beneficial body composition changes and improved glucose tolerance that may, in part, be attributed to a mild decrease in food intake and a mild increase in energy expenditure. Our findings support the consumption of a diet low in saturated fat and rich in complex carbohydrates as a potential dietary intervention for the treatment of obesity and obesity-induced impairments in glycemia. Furthermore, our results suggest that careful consideration should be taken when considering a ketogenic diet as a non-pharmacological strategy for obesity.

4.2 Introduction

Obesity is a significant risk factor for a plethora of disorders including type 2 diabetes (T2D), hypertension, stroke, cardiovascular disease, and even certain types of cancer (260). In light of the rising obesity epidemic and limited efficacy of pharmacotherapy, there has been an increased willingness amongst the general population to pursue dietary interventions as a non-pharmacological approach for weight loss, such as the high-fat and very-low carbohydrate ketogenic diet. Many variations of the ketogenic diet exist, however, the typical macronutrient breakdown consists of approximately 70-80% of energy from fat, 10% from protein and a restriction of dietary carbohydrates to less than 10% of daily energy intake (216). Support for the use of a ketogenic diet in overweight individuals arose from the Carbohydrate-Insulin Model of obesity, which predicts that overconsumption of a carbohydrate-rich diet results in augmented insulin secretion, thereby driving fat accumulation (261). Although, in contrast to this model, the high palatability and weak effect on satiety of calorically dense high-fat foods may contribute to passive overconsumption (262).

The effectiveness of a ketogenic diet in promoting weight loss and improving obesity-induced metabolic impairments and cardiovascular risk factors has been demonstrated in several clinical trials and animal models of obesity and/or T2D (220-222, 263-266). Preclinical studies have even demonstrated that chronic consumption of a ketogenic diet can enhance longevity and improve cognitive function (267, 268). However, other studies have dampened enthusiasm for the diet's effectiveness. A meta-analysis of 8 randomized clinical trials including participants with obesity and T2D reported that the ketogenic diet results in a greater decrease in hemoglobin A1c and weight loss up to 6 months after initiation of the diet, however, no meaningful difference between the ketogenic and control diet was detected after 12 months (225). Negative effects associated with consumption of a ketogenic diet including an increase in circulating low-density lipoprotein cholesterol levels, hepatic steatosis, insulin resistance, inflammation, cardiac hypertrophy, and a loss of glycemic control have all been reported in either rodent or human studies (269-273).

A significant limitation with many previous ketogenic diet studies that may account for inconsistencies of reported findings, relates to the use of experimental diets that differ in terms of macronutrient source, protein content, and differences in micronutrient composition versus the diet

they are being compared to. Commonly used rodent ketogenic diets are often markedly low in protein. The synergistic effects of protein restriction and choline deficiency have been demonstrated to contribute to the phenotype of mice fed a ketogenic diet (274). In contrast to previous studies, the sources of macronutrients were kept constant in every experimental diet used in the present study. All experimental diets were also matched for simple sugar (sucrose) content, micronutrient composition, and contained an adequate amount of protein. Therefore, any phenotypic differences observed in this study with regards to whole-body physiology should be directly attributable to alterations in the relative abundance of fat and complex carbohydrates of the diets studied, as well as the process of nutritional ketosis.

We herein demonstrate that a transition of obese male and female mice from a high-fat cocoa butter-based diet to a ketogenic cocoa butter-based diet is ineffective at inducing weight loss and improving glucose homeostasis. In contrast, we observed favorable body composition changes and a marked improvement in glucose tolerance when obese mice were transitioned to a high-complex carbohydrate, low-fat cocoa butter-based diet. Overall, our findings suggest that caution should be taken when recommending the ketogenic diet for the purposes of promoting weight loss in obesity.

4.3 Methods

4.3.1 Animal Care and Experimentation

All animal procedures were approved by the University of Alberta Health Sciences Animal Welfare Committee and performed in accordance with the regulations of the Canadian Council on Animal Care. Animals were housed in a 22°C temperature-controlled unit under a 12-hr light/dark cycle with standard environmental enrichment and *ad libitum* access to drinking water and food. Male and female C57BL/6J mice (The Jackson Laboratory) at 10-12 weeks of age were fed a high-fat diet (60% kcal from cocoa butter, Research Diets D18072402) for 16-weeks to induce obesity. After 16-weeks of the dietary protocol, baseline body composition, glucose tolerance and cardiac function were assessed, following which mice were randomized into 3 dietary intervention groups for 8-weeks. Mice were either maintained on the high-fat diet, switched to a ketogenic diet (85% kcal from cocoa butter, Research Diets D18072401), or switched to a low-fat diet (10% kcal from cocoa butter, Research Diets D18072403). Mice maintained on a low-fat control diet for the entire

duration of the study were used as a lean control group for comparison. Within the 8-week dietary intervention, glucose tolerance was assessed through intraperitoneal and oral glucose tolerance tests (IPGTTs and OGTTs) at 2- and 4-weeks post-diet transition, respectively. Body composition measurements and *in vivo* metabolic assessments were performed at 3-weeks post-diet transition, whereas insulin sensitivity was determined during an insulin tolerance test (ITT) at 6-weeks post-diet transition. Daily food and water intake, as well as circulating glucose and ketone body levels were serially measured throughout the study. After 8-weeks post-diet transition, cardiac function was assessed and mice were subsequently euthanized following a 16-hour fast and 4-hour refeed with an intraperitoneal injection of sodium pentobarbital (12 mg), following which tissues were extracted and immediately snap frozen in liquid N_2 using liquid N_2-cooled Wollenberger tongs.

4.3.2 Diet Composition

A detailed composition of the three diets is indicated in **Table 4.1**. The sucrose content (5%) and percentage of calories derived from protein (10%) were kept constant among all diets. Therefore, diets only differed in the relative abundance of complex carbohydrates and fat (from cocoa butter). The ketogenic diet was formulated with 85% of its calories from fat and 5% from carbohydrates, while the high-fat diet was formulated with 60% of its calories from fat and 30% from carbohydrates, and the low-fat diet contained 10% of its calories from fat and 80% from carbohydrates. The sources of macronutrients were identical across all diets (protein source – casein, L-Cystine; complex carbohydrate source – corn starch; fat source – cocoa butter).

4.3.3 Assessment of Glucose Homeostasis

Glucose tolerance tests (IPGTTs and OGTTs) and ITTs were performed in mice fasted overnight or for 6 hours, respectively. Mice were administered glucose (2 g/kg) via IP injection or oral gavage, or insulin via IP injection (0.5 U/kg). Blood glucose levels were measured from tail whole-blood following the fast (0 minutes) and at 15, 30, 60, 90 and 120 minutes after the administration of glucose or insulin using the Contour Next blood glucose monitoring system (Bayer, NJ, USA). For the assessment of circulating insulin levels, plasma was collected during the OGTT at the 0- and 15-minute time points and analyzed using a commercially available enzyme-linked immunosorbent assay kit according to the manufacturer's instructions (Alpco Diagnostics). In brief, plasma (5 μL) was added to the microplate wells along with 75 μL of a provided enzyme

conjugate, following which the microplate was incubated at room temperature on an orbital microplate shaker at 700 rpm for 2 hours. After the incubation period, the plate was washed 6 times with a provided working strength wash buffer and a reaction was initiated by the addition of 100 µL of a provided substrate. The reaction was terminated after 30 minutes by adding 100 µL of a provided stop solution to each well and plasma insulin levels were determined by measuring the optical density at 450 nm of each sample. The HOMA-IR (homeostasis model assessment of insulin resistance) was calculated as follows: HOMA = ((fasting blood glucose (mM) × fasting insulin (µU/mL))/22.5).

4.3.4 Assessment of Ketosis

Circulating β-hydroxybutyrate (βOHB) (FreeStyle Precision Blood β-Ketone, Abbot Diabetes Care Ltd.) levels were measured from tail whole-blood after either an overnight fast, or a 16-hour fast and a 4-hour refeed as previously described (229).

4.3.5 Magnetic Resonance Imaging and Body Composition Analysis

Total fat and lean mass were quantified by quantitative nuclear magnetic resonance relaxometry utilizing an EchoMRI-4in1/700 body composition analyzer as described in **Chapter 3.3.3**.

4.3.6 Whole Body In Vivo Metabolic Assessment

Indirect calorimetry was performed utilizing the Oxymax comprehensive laboratory animal monitoring system (Columbus Instruments) for *in vivo* metabolic assessment. After an initial 24-hour acclimatization period, animal activity, energy expenditure, whole-body oxygen (VO_2) consumption and carbon dioxide (VCO_2) production rates, and respiratory exchange ratios (RER) were quantified for 24 hours for animals with free access to food and drinking water. Hourly outputs from indirect calorimetry files were generated utilizing the web based CalR tool (275).

Oxygen consumption and carbon dioxide production were calculated utilizing both the input (V_i) and output (V_o) flows (litres per minute) to the chamber with the following equations where O_{2i} and CO_{2i}, and O_{2o} and CO_{2o} represent the reference and sample oxygen and carbon dioxide concentrations (%), respectively:

$$VO_2 = V_i O_{2i} - V_o O_{2o}$$

$$VCO_2 = V_oCO_{2o} - V_iCO_{2i}$$

Standard conversion factors were included in the calculations to result in the units specified by the software configuration (mL/hr).

The RER was calculated as the ratio between carbon dioxide production and oxygen consumption.

$$RER = VCO_2/VO_2$$

Energy expenditure (kcal/hr) was calculated as follows:

$$\text{Energy Expenditure (heat)} = \text{Calorific Value (CV)} \times VO_2$$

$$CV = 3.815 + 1.232 \times RER$$

4.3.7 Whole Cell Homogenate Preparation and Immunoblot Analysis

Protein was extracted from powdered, frozen gastrocnemius muscle (~20 mg) using protein lysis buffer containing 50 mM Tris HCL (pH 8 at 4°C), 1 mM EDTA, 10% glycerol (w/v), 0.02% Brij-35 (w/v), 1 mM dithiothreitol, and protease and phosphatase inhibitors (Sigma-Aldrich) as previously described in **Chapter 2.3.6**. Protein was quantified using a Bradford protein assay kit (Bio-Rad) following extraction. Protein samples (30 µg) were subsequently denatured and subjected to western blotting protocols as previously described in **Chapter 2.3.6**. Membranes were probed with the following antibodies: glycogen synthase kinase-3α (GSK-3α) (D80E6, Cell Signaling), phospho-GSK-3α (serine 21) (36E9, Cell Signaling), protein kinase B (Akt) (9272, Cell Signaling), and phospho-Akt (serine 473) (4060, Cell Signaling). All antibodies were prepared in a 1/1000 dilution in 3% BSA.

4.3.8 Ultrasound Echocardiography

Cardiac ultrasound images were acquired utilizing an MX 550S probe and the VisualSonics Vevo 3100 rodent ultrasound imaging system as previously described in Chapter 2.3.2. Male mice were

initially anesthetized with 2 – 3% isoflurane and maintained on 1 – 1.5% isoflurane for the remainder of the assessment. Body temperature, respiratory rate and heart rate were consistently monitored during image acquisition. Cardiac structure and LV systolic and diastolic function were determined both prior to and following the 8-week dietary intervention. Several parameters were assessed including, but not limited to, anterior and posterior wall dimensions, left ventricular (LV) ejection fraction (EF), LV fractional shortening (FS), cardiac output (CO), mitral E/A ratio, tissue Doppler e'/a' ratio, and the E/e' ratio as described previously in **Chapter 2.3.2**.

4.3.9 Assessment of Myocardial Triacylglycerol Content

Powdered, frozen heart tissue (~20 mg) was homogenized in a 20-fold volume of 2:1 chloroform:methanol solution, following which a 0.2 volume of methanol was added and the samples were kept on ice for 10 minutes before being centrifuged at 3500g for 10 min. After centrifugation, the supernatant was collected and a 0.2 volume of 0.04% *(w/v)* $CaCl_2$ was added. The mixture was then centrifuged at 2400g for 20 min. The upper phase was subsequently discarded, and the interface was washed twice with 150 µL of pure solvent upper phase consisting of 1.5 ml chloroform, 24.0 ml methanol, and 23.5 ml water. Finally, 50 µl of methanol was added to obtain a singular phase. The samples were then dried under N_2 gas at 60°C and the remaining triacylglycerol (TAG) containing pellets were redissolved in 50 µl of 3:2 tert-butyl alcohol:triton X-100/methyl alcohol (1:1). The samples were stored overnight at 4°C and quantified for TAG content the following day using a commercially available enzymatic colorimetric assay kit (Wako Pure Chemical Industries).

4.3.10 Statistical Analysis

All values were presented as mean ± standard error of the mean (SEM). An unpaired, two-tailed Student's *t* test or a two-way ANOVA was used to assess statistical significance between the 1 or 3 experimental groups, respectively, compared to the lean control group. Multiple time points were compared using a repeated measures two-way ANOVA followed by a Bonferroni post-hoc analysis. The above data analysis was completed utilizing GraphPad Prism 9 software. For the analysis of energy expenditure, analysis-of-covariance (ANCOVA) utilizing body weight as a covariate was conducted using IBM Statistical Package for the Social Sciences software. Differences were considered significant when $P < 0.05$.

Table 4.1. *Diet Compositions*

	Ketogenic Diet		High-Fat Diet		Low-Fat Diet	
Ingredient	gm	kcal	gm	kcal	gm	kcal
Casein	100	400	100	400	100	400
L-Cystine	1.5	6	1.5	6	1.5	6
Corn Starch	0	0	204.24	817	50	2000
Maltodextrin 10	0	0	50	200	150	600
Sucrose	49.9	200	49.9	200	49.9	200
Dextrose	0	0	0	0	111.95	448
Cellulose, BW200	50	0	50	0	50	0
Soybean Oil	25	225	25	225	25	225
Cocoa Butter	358.8	3229	245.9	2213	20.2	182
Mineral Mix, S10026	10	0	10	0	10	0
DiCalcium Phosphate	13	0	13	0	13	0
Calcium Carbonate	5.5	0	5.5	0	5.5	0
Potassium Citrate, 1 H2O	16.5	0	16.5	0	16.5	0
Vitamin Mix, V10001C	1	4	1	4	1	4
Choline Bitartrate	2	0	2	0	2	0

Composition of the ketogenic, high-fat, and low-fat diets used herein.

4.4 Results

4.4.1 Supplementation with a 60% Cocoa Butter Fat-Based Diet Induces Metabolic Dysfunction in Both Male and Female Mice

Male and female mice maintained on a 60% cocoa butter fat-based diet for 16-weeks exhibited significant increases in body weight, predominantly attributed to increases in fat mass, when compared to mice fed a 10% cocoa butter fat-based diet **(Figure 4.1, A–D)**. This increase in fat mass and subsequent obesity resulted in impaired glucose tolerance in both male and female mice **(Figure 4.1, E and F)**.

4.4.2 An 85% Cocoa Butter Fat-Based Ketogenic Diet Induces a State of Nutritional Ketosis in Obese Male and Female Mice

Maintenance on a ketogenic diet (85% cocoa butter fat) sufficiently induced an increase in circulating βOHB in male and female mice during both the refed and fasted state when compared to lean control mice **(Figure 4.2, A–E)**. In contrast, no increase in circulating βOHB levels was observed in obese male and female mice that either remained on a high-fat diet (60% cocoa butter fat) or were transitioned to a low-fat diet (10% cocoa butter fat) during the refed state, though the latter in females did result in a trend to increased circulating βOHB levels during fasting **(Figure 4.2, B–E)**. With regards to glycemia, obese male but not female mice maintained on the ketogenic diet exhibited lower circulating glucose levels during refeeding, whereas no changes were observed during the fasted state in obese male or female mice maintained on any of the 3 diets **(Figure 4.2, F–I)**.

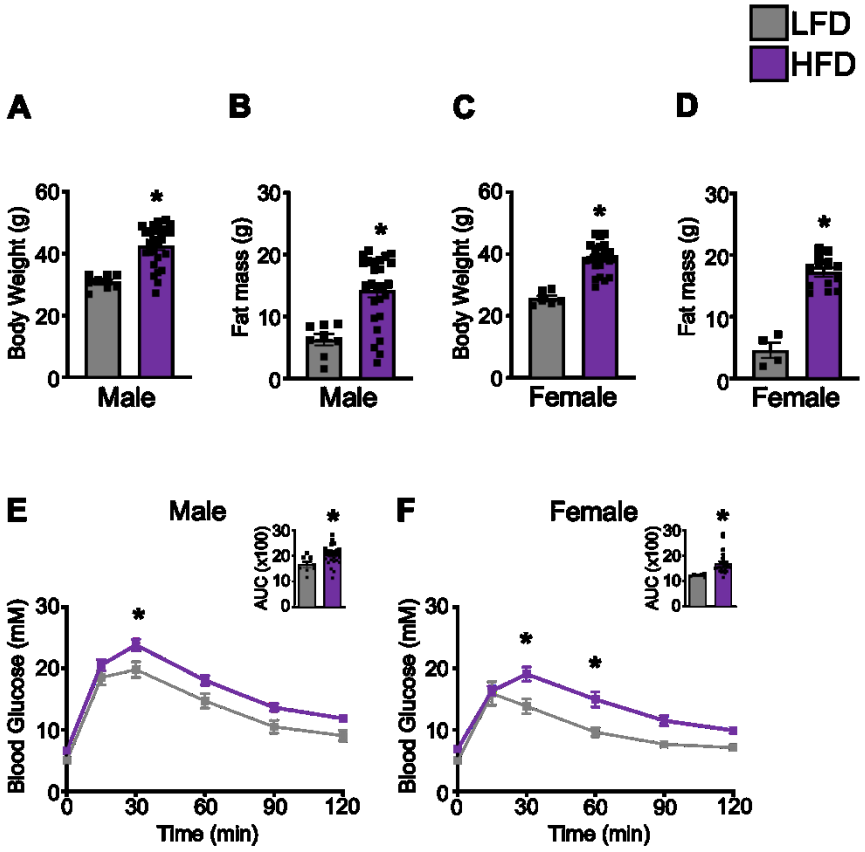

Figure 4.1. *A cocoa butter-based HFD induces metabolic dysfunction in male and female mice*. Body weight and total fat mass were measured in male **(A–B)** and female **(C–D)** mice maintained on either a HFD or LFD for 16-weeks (Body Weight: n = 8–26 [males], n = 6–22 [females]; Fat Mass: n = 8–26 [males], n = 4–13 [females]). Glucose tolerance was assessed during an intraperitoneal glucose tolerance test in HFD and LFD-fed male **(E)** and female **(F)** mice (n = 8–26 [males], n = 6–22 [females]). Values represent mean ± SEM. Differences were determined using an unpaired, two-tailed Student's t test or a two-way ANOVA. *$P < 0.05$, significantly different from LFD-fed, lean mice. AUC, area under the curve; HFD, high-fat diet; LFD, low-fat diet.

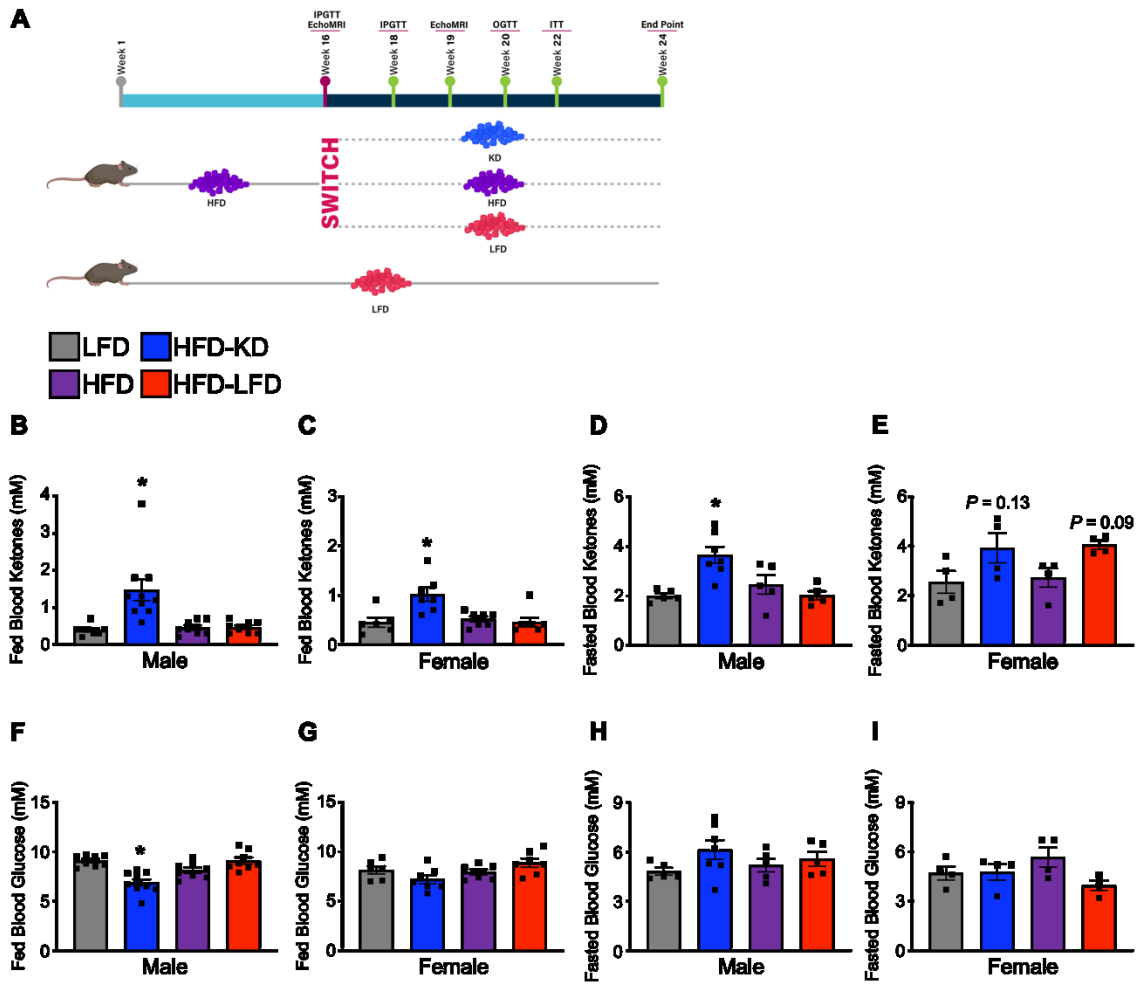

Figure 4.2. *Obese male and female mice fed a KD exhibit a marked increase in circulating ketone levels.* **A:** Schematic illustration of the experimental protocol and dietary intervention. Created with BioRender.com. Blood β-hydroxybutyrate (βOHB) levels were measured after a 16-hour fast and 4-hour refeed and after a 16-hour fast in male **(B, D)** and female **(C, E)** mice. Blood glucose levels were measured after a 16-hour fast and 4-hour refeed and after a 16-hour fast in male **(F, H)** and female **(G, I)** mice (n = 5–10 [males], n = 4–7 [females]). Values represent mean ± SEM. Differences were determined using a one-way ANOVA. *$P < 0.05$, significantly different from LFD-fed, lean mice. HFD, high-fat diet; IPGTT, intraperitoneal glucose tolerance test; ITT, insulin tolerance test; KD, ketogenic diet; LFD, low-fat diet; OGTT, oral glucose tolerance test.

4.4.3 Transitioning to a Low-Fat Diet Is More Effective Than a Ketogenic Diet in Inducing Beneficial Body Composition Changes in Obese Male and Female Mice

Obese male mice that remained on a high-fat diet or were fed a ketogenic diet did not demonstrate any significant changes to body weight, fat mass or lean mass after 3 weeks of the dietary intervention **(Figure 4.3, A–D)**. On the contrary, obese male mice transitioned to a low-fat diet for 3-weeks displayed a marked decrease in body weight **(Figure 4.3A)**, which was primarily attributed to a loss of fat mass but also a mild decrease in lean body mass **(Figure 4.3, B–D)**. Of interest, this reduction in body weight in obese male mice transitioned to a low-fat diet persisted over the entire 8-week dietary intervention, whereas long-term supplementation with a ketogenic diet for 8-weeks continued to have no impact on body weight in obese male mice **(Figure 4.3A)**.

This pattern of body composition changes was similarly recapitulated in obese female mice, whereby dietary transition to a low-fat diet caused significant body weight loss due to a pronounced loss of fat mass but not lean body mass after 3-weeks of intervention **(Figure 4.3, E–H)**. Obese female mice that were transitioned to the ketogenic diet did demonstrate a mild reduction in body weight after 3-weeks of intervention versus their baseline **(Figure 4.3E)**, which may be attributed to a trend to reduced fat mass, but no differences were observed when compared to their obese counterparts that remained on the high-fat diet **(Figure 4.3, F and G)**. However, after 8-weeks of dietary intervention, obese female mice transitioned to the ketogenic diet saw their body weight return to their baseline level, whereas the body weight loss in obese female mice transitioned to a low-fat diet persisted over this same time frame **(Figure 4.3E)**.

Changes in appetite do not appear to play a major role towards our body weight observations in obese male mice. We observed no major differences in food/caloric intake, or water intake between obese mice that transitioned to either a ketogenic diet or a low-fat diet over 10-days of the dietary intervention, though both groups of mice demonstrated reduced caloric and water intake versus the obese mice that remained on a high-fat diet **(Figure 4.3, I–K)**. These observations were not recapitulated in the obese females, as mice that transitioned to a ketogenic diet now had increased food/caloric intake versus mice that remained on the high-fat diet during 10-days of the dietary intervention **(Fig. 4.3, L–N)**, yet they displayed mild weight loss. Consistent with obese female mice that transitioned to a low-fat diet demonstrating robust body weight loss, we observed a

nonsignificant 27% reduction in caloric intake (but not water intake) versus their obese female counterparts that were maintained on a high-fat diet **(Figure 4.3, L–N)**.

4.4.4 Maintenance on a Ketogenic Diet Does Not Exacerbate In Vivo Energy Metabolism Alterations Already Induced by Maintenance on a High Fat Diet in Obese Male Mice

As expected, based on fat being the primary source of energy in both our ketogenic and high-fat diets, obese male mice fed either of these diets exhibited a reduced respiratory exchange ratio (RER) when compared to lean control mice during both the light and dark cycle **(Figure 4.4, A and B)**. In contrast, obese mice that were transitioned to a low-fat diet demonstrated an increase in the RER, which was comparable to that observed in our lean control mice and consistent with their diet being primarily comprised of carbohydrates **(Figure 4.4, A and B)**. Whole-body O_2 consumption and energy expenditure rates over 24-hrs were similar in obese male mice transitioned to a ketogenic diet or maintained on a high-fat diet, even when normalized to lean body mass **(Figure 4.4, C–F)**. Although not significant, energy expenditure rates normalized to lean body mass were ~12% and ~14% greater during the light and dark cycle, respectively, in mice that were transitioned to a low-fat diet when compared to their obese counterparts maintained on a high-fat diet **(Figure 4.4F)**. Due to known methodological limitations of mass-specific ratio analysis, we also performed co-variate analyses (ANCOVA) to correct energy expenditure for body weight variances among mice (276, 277). Following ANCOVA, potential differences in light and dark cycle energy expenditure rates between our experimental groups were not observed after accounting for differences in body weight ($P > 0.05$) **(Figure 4.4, G and H)**. Furthermore, we observed no differences in ambulatory activity between lean control mice and obese mice regardless of their dietary intervention **(Figure 4.4, I and J)**.

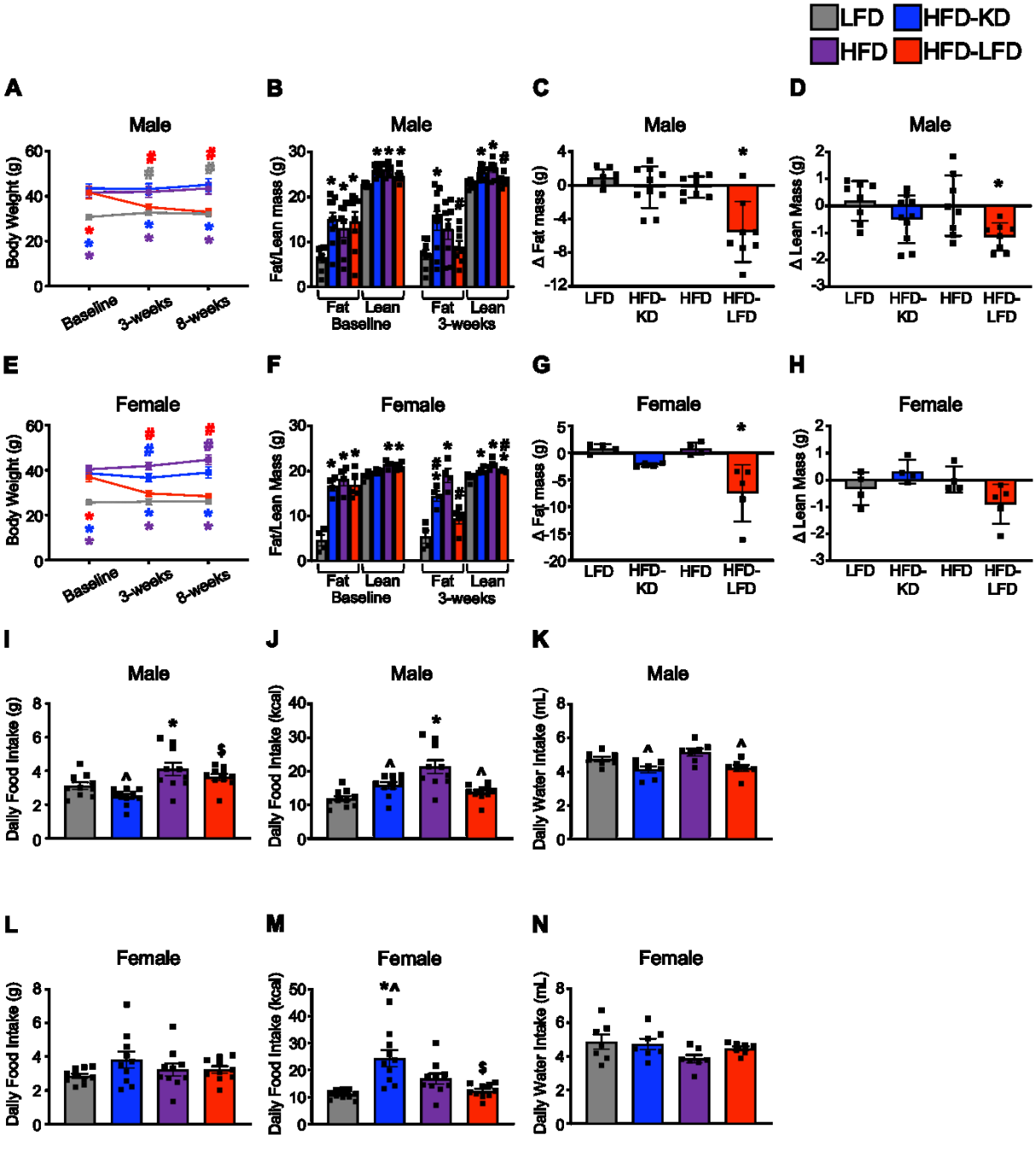
LFD
HFD-KD
HFD
HFD-LFD
A
Male
Body Weight (g)
Baseline
3-weeks
8-weeks
B
Male
Fat/Lean mass (g)
Fat
Lean
Baseline
3-weeks
C
Male
Δ Fat mass (g)
LFD
HFD-KD
HFD
HFD-LFD
D
Male
Δ Lean Mass (g)
E
Female
F
Female
G
Female
H
Female
I
Male
Daily Food Intake (g)
J
Male
Daily Food Intake (kcal)
K
Male
Daily Water Intake (mL)
L
Female
M
Female
N
Female

Figure 4.3. *Transition to an LFD, but not a KD, induces significant body weight and fat mass loss in obese male and female mice.* Body weight measurements at baseline and after 3- and 8-week post-dietary intervention, total fat and lean mass and the change in fat and lean mass relative to baseline after 3-week of dietary intervention in lean and obese male **(A–D)** and female **(E–H)** mice [body weight: $n = 8–10$ (males), $n = 6–8$ (females); fat/lean mass: $n = 8–10$ (males), $n = 4–5$ (females)]. Daily average food intake in grams and caloric density consumed, and water intake were measured in male **(I–K)** and female **(L–N)** mice subjected to our dietary interventions. Values represent means ± SEM. Differences were determined using a one-way or two-way ANOVA. $^{*}P < 0.05$, significantly different from LFD-fed, lean mice. $^{\#}P < 0.05$, significantly different from baseline. $^{\wedge}P < 0.05$, significantly different from HFD-fed, obese mice. $^{\$}P < 0.05$, significantly different from obese mice transitioned to a KD. Colored symbols indicate which specific group is being compared in **A** and **E**. HFD, high-fat diet; KD, ketogenic diet; LFD, low-fat diet.

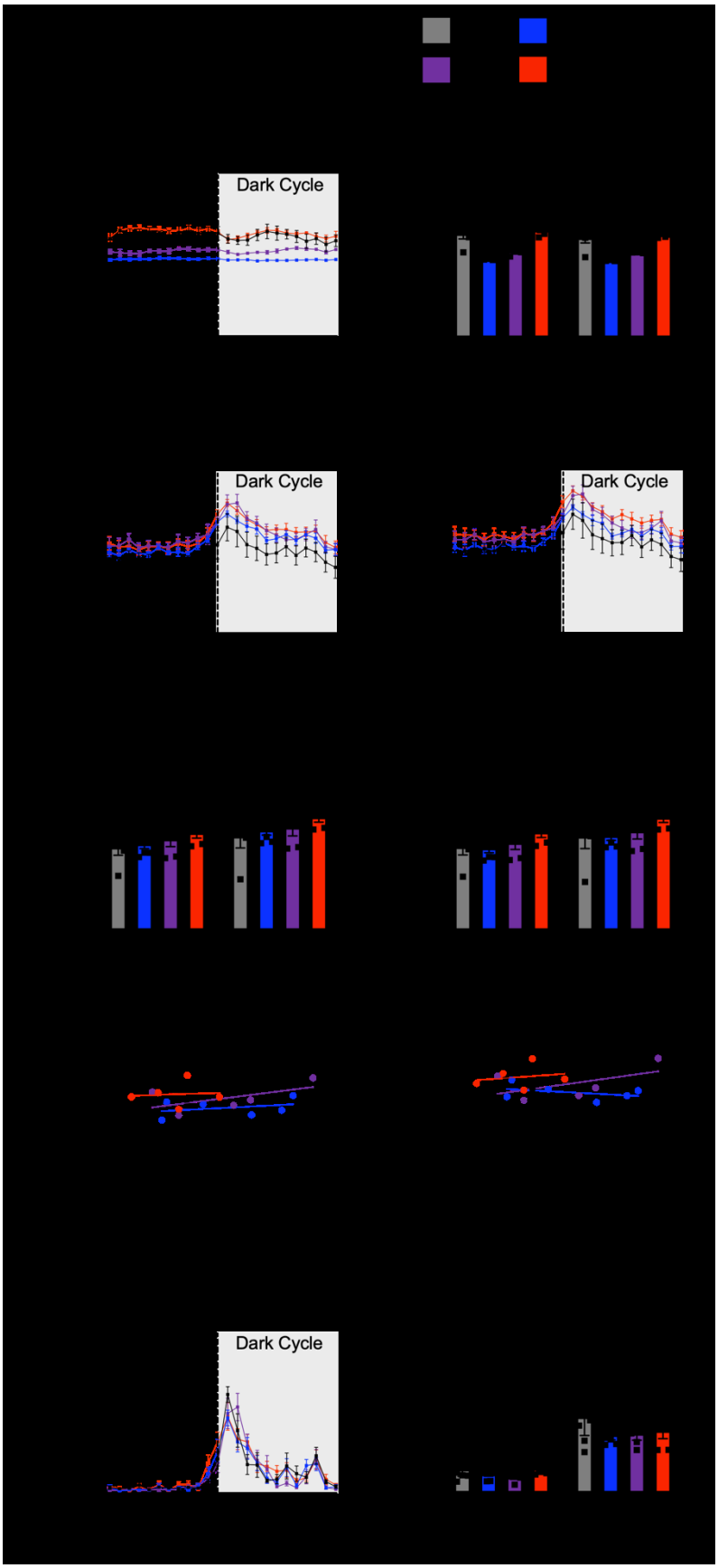
Dark Cycle
Dark Cycle
Dark Cycle
Dark Cycle

Figure 4.4. *Indirect calorimetry in obese male mice subjected to various dietary interventions.* RER over 24 hours **(A)** and average RER during the light and dark cycle **(B)**. Whole-body O_2 consumption **(C)** and energy expenditure **(D)** rates over 24 hours, and the respective rates normalized to LBM **(E, F)**. Scatter plots of body weight and energy expenditure rates during the light **(G)** and dark **(H)** cycle. Ambulatory activity of obese and lean male mice over 24 hours, and **(I)** and totaled over the light and dark cycle **(J)**. Values represent mean ± SEM (n = 5–6). Differences were determined using a one-way ANOVA or ANCOVA. *$P < 0.05$, significantly different from LFD-fed, lean mice. HFD, high-fat diet; KD, ketogenic diet; LBM, lean body mass; LFD, low-fat diet; RER, respiratory exchange ratio.

4.4.5 Maintenance on a Ketogenic Diet Does Not Improve Glucose Tolerance or Insulin Sensitivity in Obese Male and Female Mice

The hyperglycemia during an IPGTT that we previously observed in obese male mice due to supplementation with a high-fat diet was unaffected by a transition to a ketogenic diet for 2-weeks, whereas obese male mice that transitioned to a low-fat diet demonstrated a marked improvement of glucose tolerance **(Figure 4.5A)**. As changes in the complex carbohydrate and fatty acid composition of the diet can also influence incretin hormone (e.g., glucagon-like peptide-1 [GLP-1]) secretion (278-280), we also measured glucose homeostasis in response to an OGTT. Interestingly, obese male mice did not exhibit any major glucose intolerance in response to an OGTT when maintained on either a ketogenic diet or high-fat diet for 4-weeks, though glucose and insulin levels were consistently lower but not significant during the OGTT in obese male mice that transitioned to a low-fat diet **(Figure 4.5, B and C)**. As such, there was no discernible differences in HOMA-IR values between any of the groups **(Figure 4.5D)**. We next performed an assessment of insulin sensitivity via IPITT after 6-weeks of dietary intervention and observed that obese male mice that transitioned to a ketogenic diet were just as insulin resistant as their obese counterparts that remained on a high-fat diet **(Figure 4.5E)**. Despite obese male mice that transitioned to a low-fat diet demonstrating improved glucose tolerance, this was not reflected at the level of insulin sensitivity, as their glucose levels during the IPITT were increased versus lean control mice **(Figure 4.5E)**. As a further index of insulin sensitivity, we also assessed insulin signaling in gastrocnemius muscles at study completion, which demonstrated no differences in Akt and GSK-3α phosphorylation at serine 473 and serine 21, respectively, in any of our experimental groups **(Figure 4.5, F and G)**.

Assessment of glucose homeostasis in obese female mice paralleled some of our observations in their male counterparts. For example, transitioning to a low-fat diet for 2-weeks produced glucose tolerance profiles that matched those of lean control mice during an IPGTT, whereas glucose tolerance trended to now be worsened in obese female mice that transitioned to the ketogenic diet **(Figure 4.5H)**. A similar glucose tolerance pattern was also observed in obese female mice transitioned to either a ketogenic diet or a low-fat diet for 4-weeks in response to an OGTT, with no overall impact on HOMA-IR values **(Figure 4.5, I–K)**. While transitioning to a ketogenic diet did not improve insulin sensitivity during an IPITT in obese female mice after 6-weeks of dietary

intervention and thus matching what we observed in obese males, transitioning to a low-fat diet did now produce an improvement in insulin sensitivity **(Figure 4.5L)**. Further supporting this observation, Akt phosphorylation at serine 473, but not GSK-3α phosphorylation at serine 21, was increased in gastrocnemius muscles from obese female that transitioned to a low-fat diet **(Figure 4.5, M and N)**.

4.4.6 The Ketogenic Diet Increased Myocardial Triacylglycerol Content Without Significantly Altering Cardiac Structure and Function in Obese Mice

At baseline, after 16 weeks of HFD feeding, LV internal dimensions, wall thickness, and left ventricular (LV) mass in addition to systolic and diastolic function were not different between the groups of obese mice compared to lean control mice maintained on a LFD **(Figure 4.6, A–I)**. After 8-weeks following the transition to the respective dietary interventions, obese mice maintained on a HFD displayed a significant increase in diastolic LV internal diameter (LVID) and LV volume compared to lean control mice that was not observed in obese mice on a ketogenic diet **(Figure 4.6, A and B)**. Obese mice transitioned to a low-fat diet also displayed a mild increase in LV volume compared to baseline values **(Figure 4.6B)**. Markers of LV hypertrophy including LV anterior and posterior wall thickness, and LV mass did not differ between the dietary intervention groups and lean control mice after the transition, nor were the measurements different from baseline values **(Figure 4.6, C–B)**. Parameters of systolic and diastolic function including EF, and E/A and e'/a', respectively were also not significantly altered by the dietary interventions **(Figure 4.6 F–G)**. However, compared to lean control mice, ketogenic diet and HFD-fed mice demonstrated a trend towards an increase in the E/e' ratio which may indicate a mild worsening of diastolic function **(Figure 4.6I)**. Of interest, maintenance on a ketogenic diet resulted in a significant increase in myocardial triacylglycerol (TAG) content **(Figure 4.6J)**.

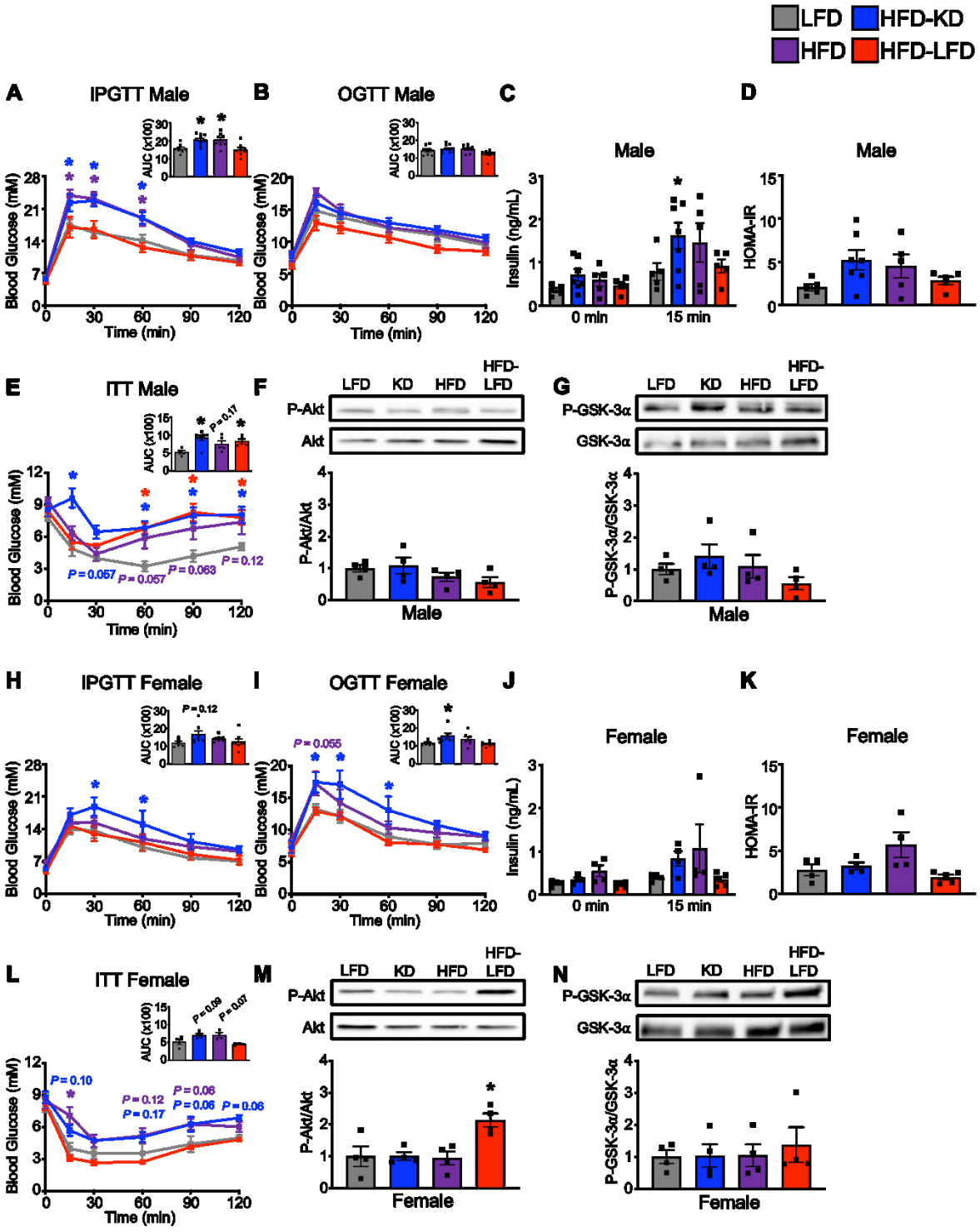
LFD
HFD-KD
HFD
HFD-LFD
A
IPGTT Male
B
OGTT Male
C
Male
D
Male
Blood Glucose (mM)
Time (min)
AUC (x100)
Insulin (ng/mL)
0 min
15 min
HOMA-IR
E
ITT Male
F
G
LFD
KD
HFD
HFD-LFD
P-Akt
Akt
P-Akt/Akt
Male
P-GSK-3α
GSK-3α
P-GSK-3α/GSK-3α
H
IPGTT Female
I
OGTT Female
J
Female
K
Female
L
ITT Female
M
N
Female

Figure 4.5. *Transition to a LFD, but not a KD, improves glucose homeostasis in obese male and female mice.* IPGTTs **(A)** and OGTTs **(B)** in obese and lean male mice performed after 2-weeks and 4-weeks, respectively, of dietary intervention (n = 8–10). Circulating insulin levels **(C)** during the OGTT prior to and at 15 min post-glucose administration (n = 5–7), and **(D)** HOMA-IR values calculated during the OGTT in obese and lean male mice (n = 5–7). Insulin sensitivity assessed by an ITT **(E)** at 6-weeks of the dietary intervention in obese and lean male mice and its corresponding AUC (n = 4–7). Akt phosphorylation at serine 473 relative to total Akt **(F)**, and GSK-3α phosphorylation at serine 21 relative to total GSK-3α **(G)**, in gastrocnemius muscle from obese and lean male mice at study completion (n = 4). IPGTTs **(H)** and OGTTs **(I)** in obese and lean female mice performed after 2-weeks and 4-weeks, respectively, of dietary intervention (n = 6–8). Circulating insulin levels **(J)** during the OGTT prior to and at 15 min post-glucose administration (n = 4–5), and **(K)** HOMA-IR values calculated during the OGTT in obese and lean female mice (n = 4–5). Insulin sensitivity assessed by an ITT **(L)** at 6-weeks of the dietary intervention in obese and lean female mice and its corresponding AUC (n = 4). Akt phosphorylation at serine 473 relative to total Akt **(M)**, and GSK-3α phosphorylation at serine 21 relative to total GSK-3α **(N)**, in gastrocnemius muscle from obese and lean male mice at study completion (n = 4). Values represent mean ± SEM. Differences were determined using a two-way ANOVA. Differences in AUC analysis and comparison of circulating insulin levels were determined using a one-way ANOVA. *$P < 0.05$, significantly different from LFD-fed, lean mice. Colored symbols or P values indicate which specific group is being compared in panels **(A)**, **(E)**, **(H)**, **(I)**, and **(L)**. AUC, area under the curve; HFD, high-fat diet; HOMA-IR, homeostasis model assessment of insulin resistance; IPGTT, intraperitoneal glucose tolerance test; ITT, insulin tolerance test; KD, ketogenic diet; LFD, low-fat diet; OGTT, oral glucose tolerance test.

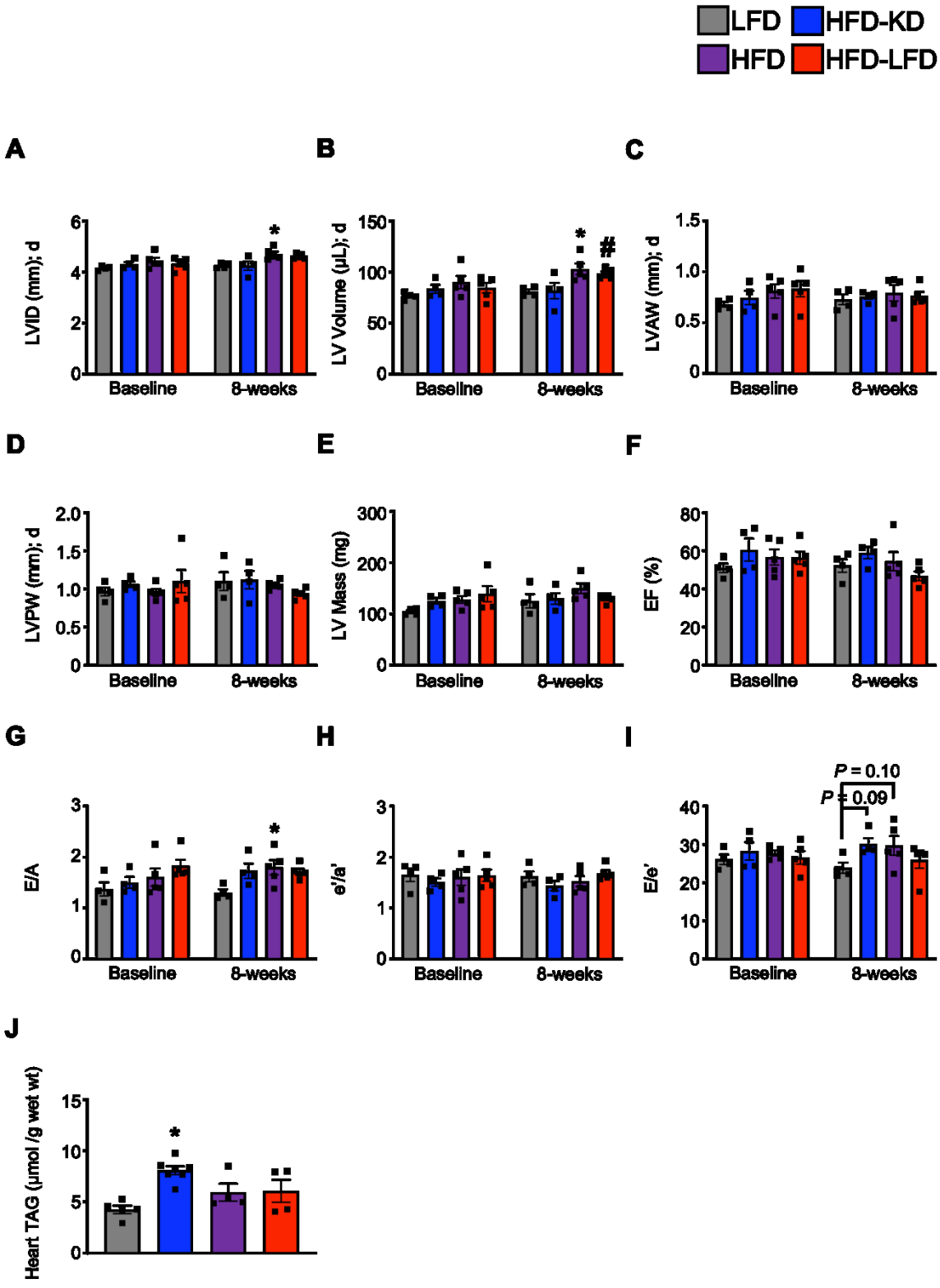
LFD
HFD-KD
HFD
HFD-LFD
A
LVID (mm); d
Baseline
8-weeks
B
LV Volume (µL); d
C
LVAW (mm); d
D
LVPW (mm); d
E
LV Mass (mg)
F
EF (%)
G
E/A
H
e'/a'
I
E/e'
P = 0.10
P = 0.09
J
Heart TAG (µmol /g wet wt)

Figure 4.6. *Transition to a KD increased myocardial triacylglycerol content without significantly affecting cardiac structure and function.* Ultrasound echocardiography was used to assess parameters of cardiac structure and function including LVID **(A)**, LV volume **(B)**, LVAW **(C)**, LVPW **(D)** during diastole, and LV mass **(E)**, EF **(F)**, E/A ratio **(G)**, e'/a' ratio **(H)**, and E/e' ratio **(I)** in obese and lean mice at baseline and after the 8-week dietary intervention (n = 4–5). **J:** Myocardial triacylglycerol content measured after the 8-week dietary intervention in cardiac tissue extracted from obese and lean mice (n = 4–7). Differences were determined using a one-way or two-way ANOVA. $*P < 0.05$, significantly different from LFD-fed, lean mice. LVID, left ventricular (LV) internal diameter; LVAW, LV anterior wall thickness; LVPW, LV posterior wall thickness; EF, ejection fraction; d, diastole; TAG, triacylglycerol.

4.5 Discussion

The ketogenic diet has sparked interest as a non-pharmacological strategy for obesity due to its potential to enhance body weight loss and improve glycemia (281, 282). However, current evidence on the efficacy and long-term safety of a very-low carbohydrate, high-fat diet (i.e., ketogenic diet) as a nutritional strategy for obesity has yielded conflicting results (216). In the current study, we demonstrated the failure of the ketogenic diet to induce significant body fat loss and improve glucose homeostasis in mice subjected to experimental obesity. In contrast, obese mice subjected to a dietary intervention with a low-fat, high-complex carbohydrate diet that was sucrose matched to both our ketogenic and high-fat diets, produced robust body weight loss primarily attributed to a loss of adiposity, while also restoring glucose homeostasis to levels observed in lean control mice.

It has been conjectured that a ketogenic diet may promote weight loss, as its very-low carbohydrate content will keep circulating insulin levels low. This would allow for unregulated adipose tissue lipolysis to increase circulating free fatty acids that the liver would then convert into ketone bodies (39, 283). Indeed, beneficial effects of the ketogenic diet on body weight management have been reported in humans and rodents (221, 266, 284). In particular, it was reported by Kennedy *et al*. that obese mice transitioned to a ketogenic diet for 5-weeks after 12-weeks of supplementation with a high-fat diet experienced significant body weight loss that was associated with an increase in energy expenditure (266). Our findings are in clear deviation of these previous studies, as we demonstrated that 8-weeks of a nutritional intervention with a ketogenic diet was largely ineffective at promoting body weight loss in both obese male and female mice. Similar findings were also observed in male leptin-deficient *ob/ob* mice, whereby 60 days of ketogenic diet feeding did not lead to a significant change in body weight (263), and in obese male mice subjected to experimental T2D, whereby the transition from a high fat diet to a ketogenic diet for 14-weeks reduced blood glucose independent of weight loss (222). It remains plausible that an 8-week dietary intervention may not be sufficient in duration for a ketogenic diet to induce significant weight loss, explaining the lack of benefit in our study. However, based on C57BL/6J mice having an average lifespan of ~2.5 years (285), our 8-week dietary intervention represents a significant fraction of their lifespan (~6%). Because human clinical nutrition studies often range anywhere from 6-months to 2-years (286), which is a smaller fraction of the average human lifespan, the

duration of our dietary intervention is both comparable and translationally relevant. Thus, it is unlikely that extending the duration of our ketogenic diet intervention would eventually produce notable weight loss in obese mice.

Although it remains unclear why our findings contrast with others that have observed beneficial actions on weight loss in response to a ketogenic diet, differences in dietary protein content may underlie such inconsistencies. The ketogenic diet used in the present study provided a protein content (10% of kcal) on the low end of the acceptable macronutrient distribution range (10 – 35% of kcal) (287), but importantly was kept constant among all experimental diets. Conversely, the ketogenic diet utilized by Kennedy *et al*. (266) contained a very-low protein content (5% of kcal) that markedly differed from that of the high-fat diet used to induce obesity (24% of kcal), thus potentially inducing a negative nitrogen balance that contributed to a major loss of lean body mass. In addition, only rats fed a low-carbohydrate, high-fat diet with a very low-protein content (5.5% vs. 19.1% of kcal) exhibited significantly lower body weights compared to control animals at the end of a 4-week dietary intervention (288). The blunted body weight gain of rats provided this ketogenic diet was once again associated with an exacerbated loss of lean body mass in comparison to animals provided the higher protein, low-carbohydrate, high-fat diet. In a clinical setting, a recent crossover study involving inpatients admitted to the National Institutes of Health Metabolic Clinical Research Unit also reported significant body weight loss in weight-stable adults provided with either a minimally processed, animal-based ketogenic diet, or a plant-based, low-fat diet for 2-weeks (223). However, the weight loss induced by the ketogenic diet was mainly attributed to a loss of fat-free mass, whereas the low-fat diet favorably resulted in significant body fat loss and a maintenance of fat-free mass (223). Although we did observe a slight, significant decrease in the lean body mass of obese mice transitioned to a low-fat diet, the reduction was minimal compared to the marked decrease in fat mass that occurred. Moreover, no change in fat or lean mass was observed in obese male and female mice transitioned from a high-fat diet to an isoproteic ketogenic diet. Therefore, our findings support the superiority of a high-complex carbohydrate, low-fat diet over a ketogenic diet for promoting weight loss in obesity when protein intake is sufficient.

Although the low-carbohydrate content and ensuing low circulating insulin levels attributed to ketogenic diets have also been suggested to improve glucose homeostasis (226, 289), transition to

a ketogenic diet failed to improve obesity-induced impairments in glucose homeostasis in male and female mice. Our observations are in agreement with several studies that have observed insulin resistance and a loss of glycemic control in response to long-term ketogenic diet feeding in healthy mice (270, 272), whereas other studies have reported intact insulin responsiveness despite glucose intolerance (268, 271). Alternatively, studies examining the effect of the ketogenic diet in T2D and *ob/ob* mice observed that the diet improved the metabolic phenotype (222, 263). Although the reason for these discrepancies are unclear, differences in the utilized animal models may account for such discrepancies, as well as the fact that some studies perform their comparisons following intervention in lean healthy mice (268), whereas we made our animals obese prior to our dietary intervention. Furthermore, differences in the composition of the various ketogenic diets used may also explain some of the inconsistencies between studies. The source and proportion of fat used in these diets is often a neglected and uncontrolled component of experimental studies that have been demonstrated to have a profound effect on the outcome of ketogenic diet feeding in rodents. In support of this, Li *et al*. demonstrated that after 5-weeks of dietary intervention, 8-week-old C57BL/6J male mice fed a ketogenic diet comprised of 89.5% fat from Primex brand vegetable shortening and corn oil, exhibited marked glucose intolerance and insulin resistance compared to animals on the respective control diet. Similar findings were not observed in mice fed a ketogenic diet with the same fat content, but comprised from a different nutrient source (hydrogenated vegetable shortening and corn oil) (290). It was speculated by Li *et al*. that the increased presence of trans fatty acids in the Primex-based ketogenic diet may have contributed to the differences in metabolic phenotypes. The high saturated fat content of the cocoa butter-based ketogenic diet used in the present study may have contributed to the lack of benefit observed with regards to both weight loss and glucose homeostasis, and it remains possible that an unsaturated fat-based ketogenic diet would have produced entirely different results. Unfortunately, unsaturated fat-based ketogenic diets are extremely difficult to pellet, and thus we specifically chose a saturated fat-based diet for our studies, which would easily allow us to determine whether potential ketogenic diet-induced reductions in body weight were due to changes in caloric intake.

Despite a ketogenic diet not producing salutary actions against weight gain and hyperglycemia in the setting of obesity, we observed robust benefit if obese mice were transitioned to a low-fat, high-carbohydrate diet. This does not imply that high-carbohydrate diets are better for obese

individuals, and caution must be exercised with the interpretation of our data, as increased intake of simple sugars (e.g., sucrose or fructose) is closely linked with the prevalence of obesity in our population (291, 292). Accordingly, we specifically designed our various diets to be matched for sucrose (5% of kcal), with changes in carbohydrate composition attributed to differences in complex carbohydrates, which in our study were primarily corn starch and maltodextrin. While obese male mice that transitioned to either a ketogenic diet or a low-fat diet both demonstrated significant reductions in caloric intake versus obese male mice that remained on a high-fat diet, it remains unclear as to why only the transition to a low-fat diet caused robust weight loss. One possibility may relate to energy expenditure, as energy expenditure normalized to lean body mass was ~12% and ~14% higher during the light and dark cycle, respectively. Taking this into consideration over an 8-week period, a simple explanation is that both of these in combination partly contribute to the robust weight loss observed in obese mice transitioned to the low-fat diet. We say partly and not entirely, as obese female mice transitioned to a low-fat diet experienced just as robust weight loss as their male counterparts, but the percent reductions in caloric intake versus their obese counterparts maintained on a high-fat diet were not as large and not statistically significant. It also remains possible that an increase in energy expenditure may have been greater in the obese female mice that transitioned to a low-fat diet, though a limitation of our study is that we did not assess indirect calorimetry in the female mice. We do hope to address this in future studies since the obese female mice that transitioned to a ketogenic diet did demonstrate mild weight loss after 3-weeks of dietary intervention (but not at 8-weeks) despite increased food/caloric intake. Because sex-specific differences were observed with our ketogenic diet relating to food/caloric intake, there may also be sex-specific differences in energy expenditure in response to a ketogenic diet.

Another potential explanation for the weight loss observed following transition to a low-fat diet may involve increases in GLP-1 secretion, as the primary carbohydrate sources of this diet, starch and maltodextrin, have both been shown to promote GLP-1 secretion (293, 294). However, circulating insulin levels during an OGTT (where GLP-1 secretion is relevant (295)) were not elevated in obese mice transitioned to the low-fat diet. Hence, while the consistent but nonsignificant reductions in appetite could be attributed to increased GLP-1 secretion, the absence of an insulin response during the OGTT in obese mice subjected to this dietary intervention,

suggests that any involvement of GLP-1 is likely mild. Conversely, the more relevant scenario to measure GLP-1 secretion in our mice would be in response to nutrient ingestion from their respective diets versus an oral gavage of glucose, and it will be necessary in future studies to measure circulating GLP-1 levels following meal intake. Another alternative explanation for the rapid weight loss induced by the transition to a low-fat diet may relate to the insulin resistance that developed in response to the preceding obesity. In such a scenario these mice may have been unable to utilize the dietary glucose as a result of metabolic inflexibility, resulting in an energy deficit that would promote adipocyte lipolysis. The subsequent improvement in glucose homeostasis would thus likely have occurred secondary to the significant body weight loss. This would also restore metabolic flexibility, and account for why the RER values in obese mice transitioned to a low-fat diet after 3-weeks of dietary intervention were similar to that observed in insulin sensitive lean mice. It will be important for future studies to assess substrate preference via indirect calorimetry during the immediate transition to the low-fat diet. Furthermore, the improved glycemia in obese mice that transitioned to the low-fat diet was primarily observed in response to an IPGTT, and we did not confirm whether this improvement was solely dependent on weight loss, or whether other mechanisms may contribute. Our data in response to an OGTT suggests that changes in insulin secretion are not involved, though we did not measure circulating insulin levels during the IPGTT. We also did not assess hepatic glucose output or perform more sophisticated techniques to assess insulin sensitivity (e.g., hyperinsulinemic-euglycemic clamps), all of which are important limitations of the current study.

Despite male and female mice demonstrating a number of similar observations in response to our dietary interventions, these phenotypes were not consistent across the board, and it is possible that sex-specific differences in diet-induced alterations in the gut microbiome could be a contributing factor. Indeed, sex-specific differences in gut microbial composition have been demonstrated to contribute to the differing sensitivities among male and female mice to metabolic impairments induced by a high-fat diet (296). Furthermore, obese men and women showed opposite correlations between gut microbiota plasticity, measured by β-diversity metrics, and a 12-month dietary change to a low-fat diet (297). Sex-specific differences were also reported in the diet-induced changes to the abundance of specific genera of gut bacteria in high-fat, high-sugar fed male and female mice compared to their low-fat, low-sugar fed counterparts (298). Another example of a sex-specific

difference present in our study was observed in the obese female mice that transitioned a low-fat, high-carbohydrate diet, as they exhibited a trend to increased circulating βOHB levels following an overnight fast, which was not observed in their obese male counterparts. An explanation for this may relate to differences in lipolysis, as lipolysis rates have been shown to be elevated in women versus men (299, 300), thereby providing excess fatty acid substrate to the liver for the generation of βOHB. There are also sex-specific differences in how males and females store adipose tissue, with females generally having a higher percentage of body fat than males, while storing a greater proportion of their fat subcutaneously (300, 301). Unfortunately, another limitation of our study is that we did not measure the weight of specific adipose depots, nor did we perform histological assessments or molecular profiling of adipose tissues from our mice, which we plan to address in future studies.

Obesity is a leading contributor to the development of major risk factors for cardiovascular disease (302, 303). A direct effect of obesity on the heart has also been recognized that can result in LV hypertrophy, increased cardiac adiposity, and variable effects on systolic and diastolic function (304-306). With the rising interest in the use of the ketogenic diet for the management of obesity, it is imperative that the effects of the diet on cardiac structure and function be investigated given the strong association between obesity and cardiovascular disease. We did not observe a significant cardiac phenotype in our model of diet-induced obesity after 16-weeks of supplementation with a high fat diet, however the transition to a ketogenic diet for 8-weeks did not lead to the further development of significant cardiac abnormalities. Mice maintained on a high fat did exhibit an increase in LV internal dimensions compared to lean control mice that was not exhibited by ketogenic diet-fed mice after the diet transition. Although these findings could indicate that the ketogenic diet resulted in a mild attenuation of obesity-related LV enlargement, both the high fat and ketogenic diet-fed groups exhibited a trend towards decreased diastolic function was groups displayed a trend towards decreased diastolic function. Notably, the ketogenic diet did result in a significant increase in myocardial TAG content. Increased myocardial TAG accumulation can represent a marker for increased deposition of toxic lipid intermediates in the heart which can promote lipotoxicity, cardiac myocyte apoptosis and myocardial insulin resistance (181, 307). Indeed, diabetic rats fed a ketogenic diet for 62 weeks demonstrated a trend towards increased myocardial TAG content that was associated with an exacerbation of cardiac hypertrophy,

oxidative stress, and a trend towards increased cardiac fibrosis (269). Therefore, it is possible that enhanced myocardial lipid accumulation would eventually lead to a deterioration in cardiac function if the mice were maintained on a ketogenic diet for a longer duration.

In summary, our findings reveal that an isoproteic, high-saturated fat-based ketogenic diet is ineffective in reversing obesity and obesity-induced impairments in glucose homeostasis and may lead to a myocardial lipid accumulation. Accordingly, careful consideration and caution should be taken when recommending the ketogenic diet as a non-pharmacological approach for the treatment of obesity. On the contrary, our results support the utilization of a diet low in saturated fat and rich in complex carbohydrates as a potential dietary intervention for the treatment of obesity. Although the specific mechanism(s) underlying the metabolic benefits afforded by a transition to a low-fat, high-complex carbohydrate diet remain unknown, they likely extend beyond a reduction in energy intake and increase in energy expenditure.

Acknowledgements & Grants

This study was supported by a Project Grant from the Canadian Institutes of Health Research (CIHR) to J.R.U. A.A.G is supported by a Vanier Canada Graduate Scholarship from the CIHR, and a Graduate Studentship from the Women and Children's Health Research Institute. J.R.U. is a Tier 2 Canada Research Chair (Pharmacotherapy of Energy Metabolism in Obesity). The graphical abstract and Figure 3.2A were created with BioRender.com.

Disclosures

No conflicts of interest, financial or otherwise, are declared by the authors.

Chapter 5: Pharmacological Inhibition of Myocardial Ketone Body Oxidation with Pimozide Improves Diastolic Function in a Mouse Model of Type 2 Diabetes

Amanda A. Greenwell[1,2], Seyed Amirhossein Tabatabaei Dakhili[1,2], Cory S. Wagg[2,3], Christina T. Saed[1,2], Jordan S.F. Chan[1,2], Kunyan Yang[1,2], Keshav Gopal[1,2], Farah Eaton[1,2], Gary D. Lopaschuk[2,3], John R. Ussher[1,2]

[1]Faculty of Pharmacy and Pharmaceutical Sciences, University of Alberta, Edmonton, AB, Canada

[2]Cardiovascular Research Centre, University of Alberta, Edmonton, AB, Canada

[3]Department of Pediatrics, University of Alberta, Edmonton, AB, Canada

UNDER PREPARATION FOR PUBLICATION

5.1 Abstract

Perturbations in myocardial substrate utilization has been identified as a primary pathological mediator in the development and progression of cardiac structural and functional abnormalities in diabetes mellitus. The role of altered cardiac glucose and fatty acid metabolism in the impairment of myocardial efficiency and energy production in diabetic cardiomyopathy is well-established, however, determination of how ketone body oxidation is altered and whether these potential alterations contribute to the pathogenesis of diabetic cardiomyopathy remains to be thoroughly investigated. Utilizing a combined high-fat diet and low-dose streptozotocin-induced mouse model of experimental type 2 diabetes (T2D), we sought to characterize cardiac ketone body oxidation rates in diabetic cardiomyopathy. In addition, we treated T2D mice with pimozide (10 mg/kg once every 2 days via oral gavage for 4 weeks), a newly identified antagonist of the critical ketone body oxidation enzyme, succinyl CoA:3-ketoacid CoA transferase (SCOT), to elucidate whether potential alterations in cardiac ketone body oxidation may be reflective of an adaptive or maladaptive response of the heart in the context of T2D. We report that myocardial ketone body oxidation is blunted in isolated working hearts from T2D mice. However, this decreased reliance on ketone bodies as an energy substrate may not be necessarily unfavorable for the myocardium given that further inhibition of myocardial SCOT activity by treatment with pimozide neglected to impair, but rather alleviated cardiac hypertrophy and diastolic dysfunction in diabetic cardiomyopathy. Our results offer fundamental insight against a maladaptive role for decreased cardiac ketone body utilization in diabetic cardiomyopathy, as well as provide evidence to support pharmacological SCOT inhibition as a novel therapeutic target for the treatment of diabetes-related cardiac dysfunction.

5.2 Introduction

Individuals with diabetes mellitus are at a significant risk of developing a myriad of debilitating cardiovascular complications (308, 309). Although diabetes mellitus predisposes affected individuals to coronary artery disease, ischemic heart disease and peripheral artery disease which can independently increase the risk of heart failure, the diabetic environment can also directly impact the myocardium. Diabetic cardiomyopathy refers to impairments in cardiac structure and function in diabetic individuals that occurs independent of other cardiac risk factors including hypertension, coronary artery disease and atherosclerosis (145, 146).

The complex and multifactorial pathophysiology driving the development of diabetic cardiomyopathy remains largely unresolved, nonetheless, abnormal myocardial intermediary energy metabolism has been identified as a key contributing mechanism (145, 146, 153, 310, 311). The heart possesses a unique capacity to oxidize a variety of substrates for energy including fatty acids, carbohydrates, ketone bodies and amino acids, and disturbances in this metabolic flexibility can precipitate cardiac dysfunction (156). In the setting of diabetes mellitus, systemic insulin resistance and hyperlipidemia promote an overreliance of the myocardium on fatty acid oxidation at the expense of glucose oxidation, thus prompting a metabolic phenotype that predisposes the heart to energy inefficiency, reduced cardiac performance, and lipotoxicity (50, 312-314). However, given that the majority of research regarding metabolic perturbations in diabetic cardiomyopathy have focused on fatty acid and glucose oxidation, further investigation is required to establish how the utilization of other key energy substrates, namely ketone bodies (acetoacetate and β-hydroxybutyrate (βOHB)), is altered in diabetes mellitus.

Ketone bodies are becoming increasingly recognized as a critical energy substrate for the failing heart (42, 113). Cardiac ketone body oxidation is elevated in heart failure with reduced ejection fraction, a response postulated to be adaptive since increasing ketone body circulating levels and myocardial oxidation rates improves contractile function (315-318). However, whether a similar therapeutic approach would be beneficial in diabetic cardiomyopathy is unknown. Acetoacetate and βOHB delivery to the heart, as well as the collective and individual myocardial uptake of the two ketone bodies were enhanced in individuals with type 2 diabetes (T2D) undergoing cardiac catherization for heart diseases compared to non-diabetic controls (319). Furthermore, acetoacetate

utilization and activity of the key ketolytic enzyme, succinyl-CoA:3-ketoacid-CoA transferase (SCOT), was increased in non-obese diabetic rats (195). Although the aforementioned studies may suggest that ketone body oxidation is upregulated in diabetic cardiomyopathy, evidence from several other studies have contradicted this viewpoint (194, 320). Myocardial ketone body oxidation was decreased in isolated cardiac myocytes and mitochondria from diabetic rats, as well as during aerobic perfusion of isolated working hearts from diabetic mice (118, 194). In addition to the ongoing debate regarding the direction in which ketone body metabolism is altered in diabetic cardiomyopathy, whether these alterations reflect an adaptive or maladaptive response also remains to be determined.

In the present study, we utilized pimozide, an FDA-approved antipsychotic agent that we recently identified as a novel SCOT antagonist and anti-hyperglycemia agent (229), to ascertain the role of altered ketone body oxidation in the pathology of diabetic cardiomyopathy. Our previous findings indicate that pimozide-mediated SCOT inhibition may improve glycemia in obese mice by increasing skeletal muscle glucose oxidation (229). Pharmacological optimization of cardiac glucose oxidation ameliorated diastolic dysfunction in mice with experimental T2D, as evidenced by an improvement in the E/A and e'/a' ratio (102). Additionally, augmentation of cardiac glucose oxidation through treatment with the glucagon-like peptide-1 receptor agonist, liraglutide, was associated with improved cardiac function in a mouse model of T2D (110). Therefore, if the effects of pimozide on glucose oxidation in skeletal muscle can be recapitulated in the heart, pimozide may also be cardioprotective in diabetic cardiomyopathy. Furthermore, inhibition of cardiac ketone body oxidation may reduce inflammatory and pro-hypertrophic signaling in the heart. βOHB has been found to possess anti-inflammatory effects and, as a specific inhibitor of class 1 histone deacetylases (HDAC), can transcriptionally promote resistance to oxidative stress and inhibition of cardiac myocyte hypertrophy (321-323). Therefore, cardiac βOHB accumulation as a result of decreased oxidation could mitigate the inflammation, oxidative damage and pathological hypertrophic remodeling that is characteristic of the myocardium in diabetes mellitus.

Alternatively, given that ketone bodies may serve as an important additional energy substrate for the heart, it is possible that the pharmacological inhibition of cardiac ketone body oxidation will further impair cardiac metabolic flexibility and exacerbate cardiac dysfunction in diabetic

cardiomyopathy. Therefore, by inhibiting myocardial SCOT activity and subsequent ketone body oxidation with pimozide in mice with experimental T2D, we aimed to elucidate how cardiac ketone body oxidation is altered in diabetes, whether these alterations are compensatory or detrimental in the progression of diabetic cardiomyopathy, and to define the cardiac effects of pimozide which will be instrumental in determining whether it can be repurposed as a therapy for T2D.

5.3 Methods

5.3.1 Animal Care and Experimentation

All animal procedures were conducted in accordance with the regulations of the Canadian Council on Animal Care and approved by the University of Alberta Health Sciences Animal Welfare Committee. Mice were housed under a 12-hr light/dark cycle in a 22°C temperature-controlled unit with standard environmental enrichment and *ad libitum* access to drinking water and food. Male C57BL/6J mice (The Jackson Laboratory) at 12 weeks-of-age were subjected to experimental type 2 diabetes (T2D) induced by high-fat diet feeding (HFD, 60% kcal from lard, Research Diets D12450J) for 10-weeks, with a single low-dose intraperitoneal (IP) injection of the pancreatic β-cell toxin, streptozotocin (STZ, 75mg/kg dissolved in sodium citrate (0.1M) at a pH of 5.0), provided at 4-weeks into the dietary protocol. Lean control mice were fed a standard chow diet and provided with an IP injection of vehicle control (sodium citrate). Following 4 weeks after STZ administration, mice were randomized to receive treatment with vehicle control (VC; corn oil) or pimozide (10 mg/kg once every 2 days) via oral gavage for 4 weeks. We have previously shown that treatment at this dose results in skeletal muscle SCOT inhibition and increases circulating concentrations of ketone bodies (229). Mice were maintained on their respective HFD or chow diet after completion of the experimental T2D induction protocol for the remainder of the study. After the 4-week treatment period, mice were euthanized after a 4-hour fast and 1-hour refeed with Ensure® (200 μL) via oral gavage with an IP injection of sodium pentobarbital (12 mg), following which hearts were extracted and immediately snap frozen in liquid nitrogen using liquid nitrogen-cooled Wollenberger tongs prior to storage at -80°C. At study completion, a separate cohort of mice was euthanized and their isolated hearts were perfused in the working mode for the assessment of myocardial energy metabolism.

5.3.2 Ultrasound Echocardiography

Cardiac structure and function were assessed at 4-weeks after STZ administration (baseline) and following 4-weeks of treatment with pimozide or VC utilizing non-invasive transthoracic echocardiography with an MX 550S probe and the VisualSonics Vevo 3100 rodent ultrasound imaging system as described in **Chapter 2.3.2**. Mice were initially anesthetized with 2 – 3% isoflurane and maintained on 1 – 1.5% isoflurane for the remainder of the assessment. During image acquisition, body temperature, respiratory rate and heart rate were consistently monitored. M-mode images were acquired for measurements of left ventricular (LV) internal diameter (LVID) and LV anterior (LVAW) and posterior (LVPW) wall thickness during systole (s) and diastole (d). Left atrial size was measured by m-mode imaging in the parasternal long-axis view as the maximal anteroposterior left atrial diameter.

5.3.3 Whole Cell Homogenate Preparation and Immunoblot Analysis

A protein lysis buffer containing 50 mM Tris HCl (pH 8 at 4°C), 1 mM EDTA, 10% glycerol (w/v), 0.02% Brij-35 (w/v), 1 mM dithiothreitol, and protease and phosphatase inhibitors (Sigma-Aldrich) was used to extract protein from powdered, frozen cardiac tissue (~15-20 mg). Protein was quantified using a Bradford protein assay kit (Bio-Rad) and samples (30 µg) were subsequently denatured and subjected to western blotting protocols as previously described in **Chapter 2.3.6**. Membranes were probed with the following antibodies: succinyl CoA:3-ketoacid CoA transferase (SCOT; 12175-1-AP, Proteintech), βOHB dehydrogenase 1 (BDH1; NBP188673, Novus Biologicals), acetoacetyl CoA thiolase (ACAT1; 44276S, Cell Signaling), pyruvate dehydrogenase (PDH; 3205S, Cell Signaling), phospho-PDH-E1α (Serine 293) (AP1062, Sigma-Aldrich), and vinculin (1390S, Cell Signaling). All antibodies were prepared in a 1/1000 dilution in 3% BSA except for vinculin, which was prepared in a 1/2000 dilution.

5.3.4 RNA Isolation and Real-Time Quantitative PCR

TRIzol™ reagent (Invitrogen) was used to homogenize frozen, powdered cardiac tissue (~15-20 mg) for 2 minutes. Chloroform was added after homogenization, following which the samples were left to sit for 10 min to allow the homogenate to separate. The clear upper aqueous layer containing RNA was removed and RNA was precipitated with the addition of isopropanol. The precipitated RNA was washed with 75% ethanol to remove impurities and resuspended in 30 µL

of DNase/RNase-free water. First-strand cDNA (2 μg) was synthesized from extracted RNA using the High-Capacity cDNA Reverse Transcription Kit (Applied Biosystems). A CFX Connect Real-Time PCR machine (Bio-Rad Laboratories Inc.) was used to perform real-time PCR utilizing SYBR Green (KK4601; Kapa Viosystems, Inc.). Cyclophilin A (*Ppia*) was used as an internal housekeeping gene to determine relative mRNA transcript levels quantified with the $2^{-\Delta\Delta Ct}$ method as previously described (236). Primer sequences are listed in **Table 5.1**.

5.3.5 Magnetic Resonance Imaging and Body Composition Analysis

Total fat and lean mass were quantified by quantitative nuclear magnetic resonance relaxometry utilizing an EchoMRI-4in1/700 body composition analyzer. Fat mass is representative of the total mass of all fat molecules in the body expressed as an equivalent weight of canola oil. Lean mass represents a muscle tissue mass equivalent of all body parts containing water, excluding fat, bone mineral content and NMR undetectable substances such as hair and claws.

5.3.6 Succinyl-CoA:3-ketoacid-CoA Transferase Activity Assay

Frozen, powdered cardiac tissue (30 mg) was homogenized in phosphate buffered saline (PBS) with protease inhibitors (Sigma-Aldrich) for 2 minutes, following which samples were left on ice for 30 minutes and then centrifuged at 20 000 x g at 4°C for 20 minutes. The supernatant was collected from each sample and the protein concentration was quantified using a Bradford protein assay kit (Bio-Rad). The protein concentration was adjusted with PBS to ensure a similar concentration among all samples. For the quantification of SCOT activity, 6 μL of each sample was added to the bottom of a cuvette along with 14 μL of a master mix containing 50 mM Tris HCl (pH 8.0), 10 mM MgCl2, 0.1–10 mM lithium acetoacetate, and 4 mM iodoacetamide. The catalytic reaction was initiated by the addition of 0.2 mM succinyl-CoA and SCOT activity was determined by the production rate of acetoacetyl-CoA, which was measured spectrophotometrically by monitoring the absorbance changes at 313 nm at room temperature and normalized to an acetoacetyl-CoA standard curve. The absorbance changes were recorded every 5 seconds for 3 minutes.

5.3.7 Isolated Working Heart Perfusions and Assessment of Energy Metabolism

Mice were euthanized via IP injection of sodium pentobarbital (12 mg) after the 4-week treatment with pimozide or VC, following which the hearts were immediately excised and perfused aerobically in the working mode for 60 min as previously described in **Chapter 2.3.3**. Insulin (100 μU/ml) was added to the perfusate at 30 min of perfusion. Hearts were perfused with oxygenated Krebs-Henseleit buffer containing 11 mM glucose, 1.2 mM palmitate bound to 3% bovine serum albumin (BSA) and 0.8 mM β-hydroxybutyrate (βOHB) with the appropriate radiolabeled tracers for the measurement of glycolysis ([5-^{3}H]glucose), glucose oxidation ([U-^{14}C]glucose), fatty acid oxidation ([9,10-^{3}H]palmitate) and ketone body oxidation ([3-^{14}C]βOHB). Assessment of glycolysis and fatty acid oxidation was determined through the quantitative collection of $^{3}H_2O$, whereas glucose and ketone body oxidation were determined through the quantitative collection of $^{14}CO_2$ as previously described (240, 324). At the completion of perfusion, hearts were immediately snap frozen with liquid N_2 and stored at -80°C.

5.3.8 Assessment of Glucose Homeostasis

Mice were administered glucose (1g/kg) via IP injection in a glucose tolerance test (IPGTT) following an overnight fast. Blood glucose levels were measured from tail whole-blood following the fast (0 minutes) and at 15, 30, 60, 90 and 120 minutes after the administration of glucose using the Contour Next blood glucose monitoring system (Bayer, NJ, USA). For the assessment of circulating insulin levels, plasma was collected during the IPGTT at the 0- and 15-minute time points and analyzed using a commercially available enzyme-linked immunosorbent assay kit according to the manufacturer's instructions (Alpco Diagnostics). In brief, plasma (5 μL) was added to the microplate wells along with 75 μL of a provided enzyme conjugate, following which the microplate was incubated at room temperature on an orbital microplate shaker at 700 rpm for 2 hours. After the incubation period, the plate was washed 6 times with a provided working strength wash buffer and a reaction was initiated by the addition of 100 μL of a provided substrate. The reaction was terminated after 30 minutes by adding 100 μL of a provided stop solution to each well and plasma insulin levels (ng/mL) were determined by measuring the optical density at 450 nm of each sample.

5.3.9 Statistical Analysis

All values are presented as mean ± standard error of the mean (SEM). The significance of differences was determined using an unpaired, two-tailed Student's *t* test, a two-way ANOVA or a repeated measures two-way ANOVA followed by a Bonferroni post-hoc analysis where appropriate. Data analysis was completed utilizing GraphPad Prism 9 software.

Table 5.1. *Primer sequences*

Gene Name	Forward	Reverse
Ppia	GCT GGA CCA AAC ACA AAC G	ATG CCT TCT TTC ACC TTC CC
Col1a1	TGCTAACGTGGTTCGTGACCGT	ACATCTTGAGGTCGCGGCATGT
Col1a2	TTGCTGAGGGCAACAGCAGGTT	AATGTCAAGGAACGGCAGGCGA
Tgfb	ATT TGG AGC CTG GAC ACA CA	GAG CGC ACA ATC ATG TTG GA
Nlrp3	GAC ACG AGT CCT GGT GAC TT	GTC CAC ACA GAA AGT TCT CTT AGC
Il-1b	TGG CAA CTG TTC CTG AAC TCA A	AGC AGC CCT TCA TCT TTT GG
Il-6	AGT TGC CTT CTT GGG ACT GA	TCC ACG ATT TCC CAG AGA AC
Ccl2	AGGTCCCTGTCATGCTTCTG	TCTGGACCCATTCCTTCTTG
Ccl5	TGCCCACGTCAAGGAGTATTT	TTCTCTGGGTTGGCACACACT
Tnfa	AGCCCCCAGTCTGTATCCTT	CTCCCTTTGCAGAACTCAGG
Slc2a1	TCA ACA CGG CCT TCA CTG	CAC GAT GCT CAG ATA GGA CAT C
Slc2a4	TTCATTGTCGGCATGGGTTT	ACGGCAAATAGAAGGAAGACGTA
Foxo3	GGG GAA CCT GTC CTA TGC C	TCA TTC TGA ACG CGC ATG AAG
Sod2	CAG ACC TGC CTT ACG ACT ATG G	CTC GGT GGC GTT GAG ATT GTT

5.4 Results

5.4.1 Mice with Experimental T2D Exhibit Left Ventricular Hypertrophy and Diastolic Dysfunction Associated with Increased Markers of Cardiac Fibrosis and Inflammation

Echocardiography was utilized to investigate the baseline differences in cardiac structure and function between lean control mice and mice with experimental T2D after 8-weeks of HFD supplementation with a single low-dose injection of STZ provided after 4-weeks. Parameters indicative of systolic function including cardiac output (CO) and ejection fraction (EF) were preserved in T2D compared to lean mice, consistent with previous studies using the HFD diet/STZ rodent model of T2D **(Figure 5.1, A and B, Table 5.2)** (102, 112). Alternatively, T2D mice exhibited mild LV hypertrophy demonstrated by a significant increase in diastolic LV posterior wall (LVPW) thickness and a trending increase in LV anterior wall (LVAW) ($P = 0.18$) and LVPW thickness ($P = 0.10$) during systole compared to their lean counterparts **(Table 5.2)**. However, systolic and diastolic LV internal diameter and volume remined unchanged when compared to lean mice, as well as the ratio between LV mass and lean body mass (LBM), although the latter is likely attributable to T2D mice having increased LBM **(Figure 5.1, C–E, Table 5.2)**. T2D mice demonstrated impaired diastolic function evidenced by an increase and decrease in the E/e' and e'/a' ratio, respectively, although the E/A ratio was unchanged **(Figure 5.1, F–H, Table 5.2, Appendix Figure 1.2)**. In addition, enlargement of the left atrium (LA) is a commonly used maker of LV diastolic dysfunction (325-327) and LA size was in fact significantly increased in T2D compared to lean mice **(Figure 5.1I, Table 5.2, Appendix Figure 1.2)**.

There is robust clinical and preclinical evidence to suggest that cardiac fibrosis is a characteristic morphological defect of the heart affected by diabetes (328-332). Indeed, assessment of cardiac tissue isolated from T2D mice displayed enhanced mRNA expression of collagen type 1 α1 (*Col1a1*) which encodes for the pro-α1(I) chain component of type I collagen, although transcript levels of collagen type 1 α2 (*Col1a2*) and transforming growth factor-β (*Tgfβ*) were unchanged **(Figure 5.1J)**. Cardiac inflammation has also been identified as a pathophysiological mediator in the development of diabetic heart disease (333-337). To evaluate the association of cardiac inflammation with the aberrant LV structural remodeling and diastolic dysfunction observed in T2D mice, the expression of several gene markers of inflammatory signaling was assessed **(Figure**

5.1K). Notably, the results identified a trending increase in the transcript levels of the nucleotide-binding domain-like receptor protein 3 (*Nlrp3)* inflammasome and interleukin-6 (*Il-6*) **(Figure 5.1K)**. Furthermore, consistent with myocardial insulin resistance and a reduction in glucose utilization, mRNA expression of glucose transporter type 4 (*Slc2a4)*, which is responsible for insulin-dependent glucose uptake, strongly trended to decrease in T2D while glucose transporter type 1 (*Slc2a1*) expression was unchanged **(Figure 5.1L)**.

5.4.2 Myocardial Ketone Body Oxidation is Blunted in Mice with Experimental T2D

Hearts isolated from T2D and lean mice were aerobically perfused in the working mode to investigate the alterations in myocardial intermediary energy metabolism, namely ketone body oxidation, that characterize diabetic heart disease. In support of previous findings suggesting increased cardiac fatty acid oxidation in the setting of diabetes, palmitate oxidation rates trended to increase in T2D mouse hearts compared to lean counterparts **(Figure 5.2A)**. Notably, a marked decrease in βOHB oxidation rates was also observed in T2D mouse hearts, however, was paradoxically associated with an increase in SCOT activity **(Figure 5.2, B–D)**. The reduction in cardiac βOHB oxidation rates was also associated with a decline in the cardiac protein expression of SCOT and β-hydroxybutyrate dehydrogenase (BDH1), which catalyzes the first step in the ketone body oxidation pathway **(Figure 5.2, E–G)**. Cardiac protein levels of acetoacetyl CoA thiolase (ACAT1), another critical enzyme in the oxidation of ketone bodies, was unaffected in the hearts of T2D mice **(Figure 5.2G)**.

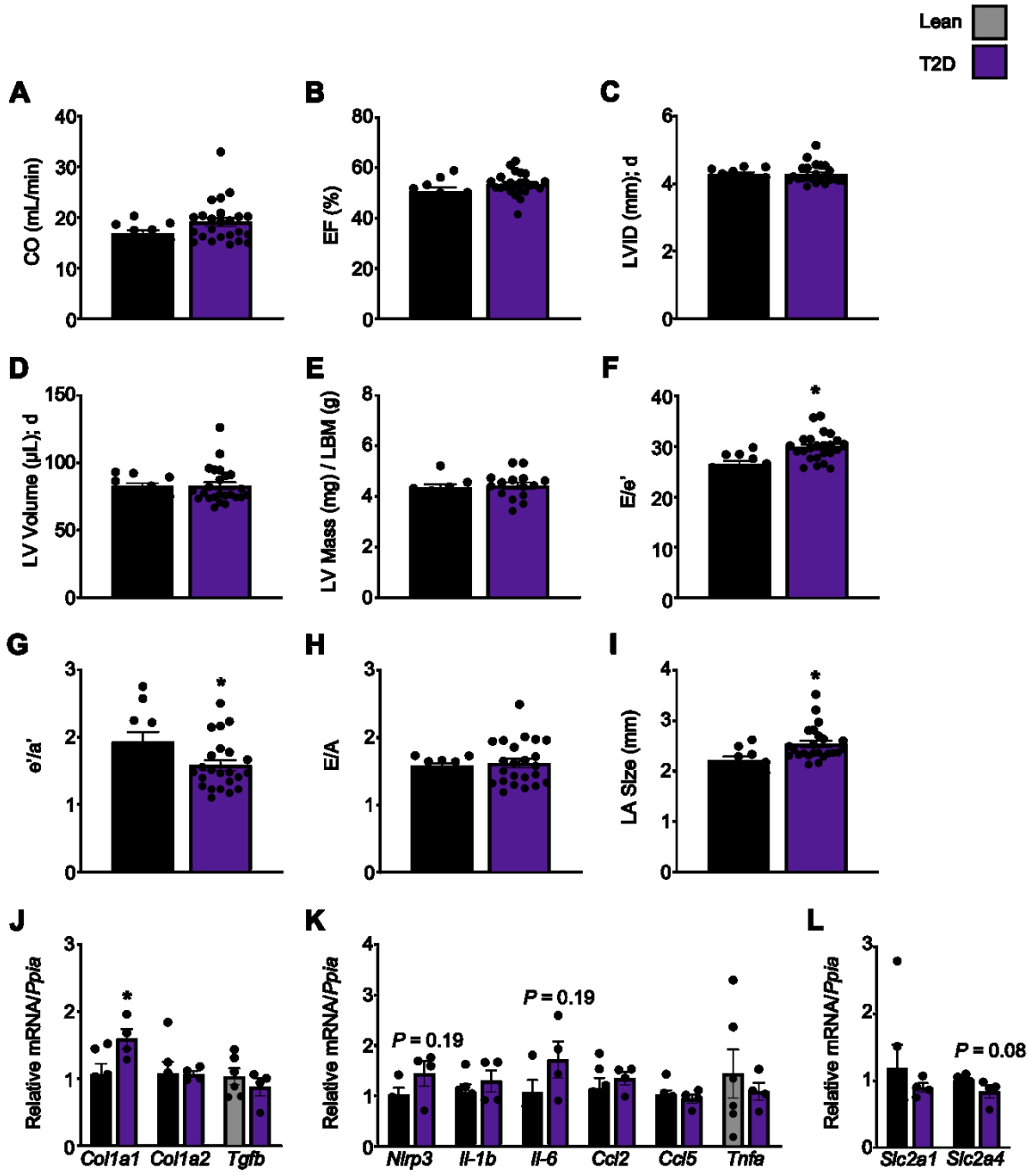
Lean
T2D
A
CO (mL/min)
B
EF (%)
C
LVID (mm); d
D
LV Volume (µL); d
E
LV Mass (mg) / LBM (g)
F
E/e'
G
e'/a'
H
E/A
I
LA Size (mm)
J
Relative mRNA/Ppia
Col1a1
Col1a2
Tgfb
K
Relative mRNA/Ppia
P = 0.19
P = 0.19
Nlrp3
Il-1b
Il-6
Ccl2
Ccl5
Tnfa
L
Relative mRNA/Ppia
P = 0.08
Slc2a1
Slc2a4

Figure 5.1. *Mice with experimental T2D exhibit mild cardiac hypertrophy with notable diastolic dysfunction and preserved systolic function.* Ultrasound echocardiography was used to assess cardiac output (CO) **(A)**, ejection fraction (EF) **(B)**, left ventricular (LV) internal diameter (LVID) **(C)**, LV volume **(D)**, LV mass normalized to lean body mass (LBM) **(E)** (n = 8–15), E/e' **(F)**, e'/a' **(G)**, E/A **(H)**, and left atrial (LA) size **(I)** in mice with experimental T2D compared to lean control mice (n = 10–24). Relative mRNA expression of gene markers of fibrosis (collagen type 1 α1 (*Col1a1*), collagen type 1 α2 (*Col1a2*), and transforming growth factor-β (*Tgfβ*)) **(J)**, inflammation (nucleotide-binding domain-like receptor protein 3 (*Nlrp3)*, interleukin-1β (*Il-1b*), interleukin-6 (*Il-6*), C-C motif chemokine ligand 2 (*Ccl2*), and C-C motif chemokine ligand 5 (*Ccl5*)), and **(L)** glucose uptake (glucose transporter 1 (*Slc2a1*) and glucose transporter 4 (*Slc2a4*) **(K)** (n = 4–6). Values represent mean ± SEM. Differences were determined using an unpaired, two-tailed Student's t test. *P < 0.05, significantly different from lean control mice.

Table 5.2. *In vivo baseline assessment of cardiac structural and functional parameters in lean and T2D mice*

	Lean	T2D
Heart Rate (beats/min)	404 ± 13	430 ± 7
LBM (g)	24.9 ± 0.5	26.5 ± 0.5*
LV Mass (mg) / LBM (g)	4.34 ± 0.15	4.42 ± 0.14
LVID (mm); s	3.19 ± 0.07	3.11 ± 0.05
LVID (mm); d	4.29 ± 0.05	4.28 ± 0.06
Volume (μL); s	40.9 ± 2.2	38.6 ± 1.4
Volume (μL); d	82.6 ± 2.4	82.9 ± 2.8
Stroke Volume (μL)	41.7 ± 1.1	44.3 ± 1.8
CO (ml/min)	16.8 ± 0.7	19.1 ± 0.9
EF (%)	50.7 ± 1.5	53.5 ± 0.9
FS (%)	25.7 ± 0.9	27.4 ± 0.6
LVAW; s (mm)	1.08 ± 0.01	1.13 ± 0.02
LVAW; d (mm)	0.72 ± 0.02	0.77 ± 0.03
LVPW; s (mm)	1.18 ± 0.04	1.27 ± 0.03
LVPW; d (mm)	0.86 ± 0.04	0.95 ± 0.02*
E/A	1.58 ± 0.04	1.62 ± 0.07
e'/a'	1.93 ± 0.15	1.58 ± 0.08*
E/e'	26.5 ± 0.7	29.9 ± 0.6*
LA Size (mm)	2.22 ± 0.07	2.53 ± 0.07*

In vivo cardiac function and LV wall measurements in lean (n = 8-10) and T2D (n = 15-24) mice. Values represent mean ± SEM. Differences were determined using an unpaired, two-tailed Student's t test. *$P < 0.05$, significantly different from lean mice. LBM, lean body mass; CO, cardiac output; EF, ejection fraction; FS, fractional shortening; LV, left ventricular; LVAW, LV anterior wall thickness; LVID, LV internal diameter; LVPW, LV posterior wall thickness; s, systole; d, diastole.

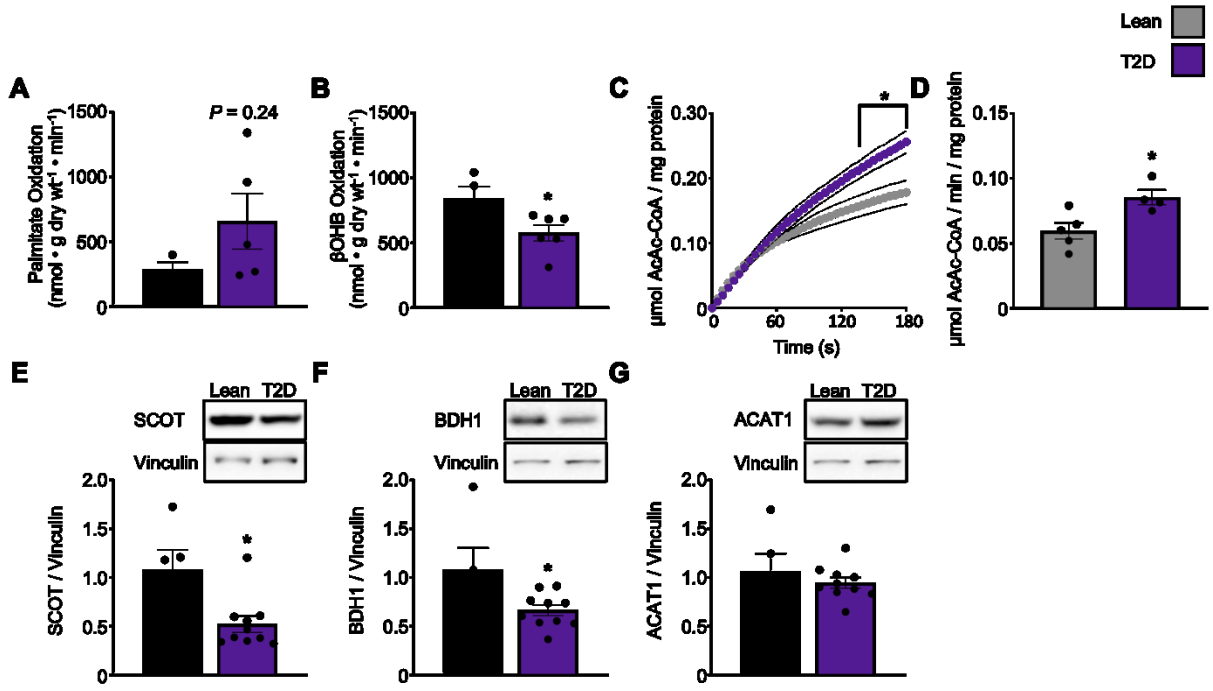

Figure 5.2. *Myocardial ketone body oxidation is blunted in mice with experimental T2D.* Palmitate **(A)** and βOHB **(B)** oxidation rates were determined during aerobic perfusion of isolated working hearts from lean and T2D mice (n = 3–6). SCOT activity in cardiac tissue from lean and T2D mice expressed as the levels **(C)** and rate **(D)** of acetoacetyl CoA (AcAc-CoA) production per mg of protein (n = 4–5). Protein levels of succinyl CoA:3-ketoacid CoA transferase (SCOT) **(E)**, βOHB dehydrogenase 1 (BDH1) **(F)**, and acetoacetyl CoA thiolase (ACAT1) **(G)** relative to vinculin in cardiac tissue from lean and T2D mice (n = 5–10). Values represent mean ± SEM. Differences were determined using a two-way ANOVA or an unpaired, two-tailed Student's t test. *P < 0.05, significantly different from lean control mice.

5.4.3 Treatment with Pimozide Improves Glycemia in T2D Mice Without Significantly Altering Body Composition

Consistent with our previous findings that the pharmacological inhibition of skeletal muscle SCOT activity via treatment with pimozide improves glycemia in mice with HFD-induced obesity, T2D mice treated with pimozide for 2 weeks demonstrated a robust improvement of glucose homeostasis when compared to T2D mice that received VC independent of changes in plasma insulin levels **(Figure 5.3, A–C)**. These results support that in addition to obesity, the anti-hyperglycemic effects of pimozide can be extended to the setting of T2D. The pimozide-mediated improvements in glycemia are likely to be independent of changes in body composition given that only mild, nonsignificant decreases in body weight and fat mass, and no change in lean mass measurements were observed in pimozide-treated T2D mice despite the marked enhancement of glucose tolerance **(Figure 5.3, D–F)**.

5.4.4 Pimozide Effectively Reduces Myocardial SCOT Activity

Treatment of T2D mice with pimozide for 4 weeks effectively inhibited myocardial SCOT activity compared to T2D control mice, thus emulating our previous findings with gastrocnemius muscle from diet-induced obese mice (229) and providing further evidence to support pimozide as a SCOT antagonist. The reduction in myocardial SCOT activity had no effect on palmitate oxidation rates in the isolated T2D working heart, nor were cardiac βOHB oxidation rates affected despite the pronounced pimozide-mediated SCOT inhibition **(Figure 5.4, A–D)**. Protein expression of SCOT, BDH1 and ACAT1 also remained similar between pimozide and VC-treated T2D mice **(Figure 5. 4, E–G)**. To elucidate the effect of pimozide and subsequent SCOT inhibition on myocardial glucose oxidation, we assessed the level of PDH phosphorylation in cardiac tissue extracted from pimozide and VC-treated T2D mice, whereby a reduction in inhibitory phosphorylation is associated with enhanced PDH activity and suggestive of an increase in glucose oxidation. Although our previous findings with diet-induced obese mice identified that treatment with pimozide reduced PDH phosphorylation in gastrocnemius muscle (229), we did not observe a significant difference in the phosphorylation state of cardiac PDH between pimozide and VC-treated T2D mice **(Figure 5.4H)**.

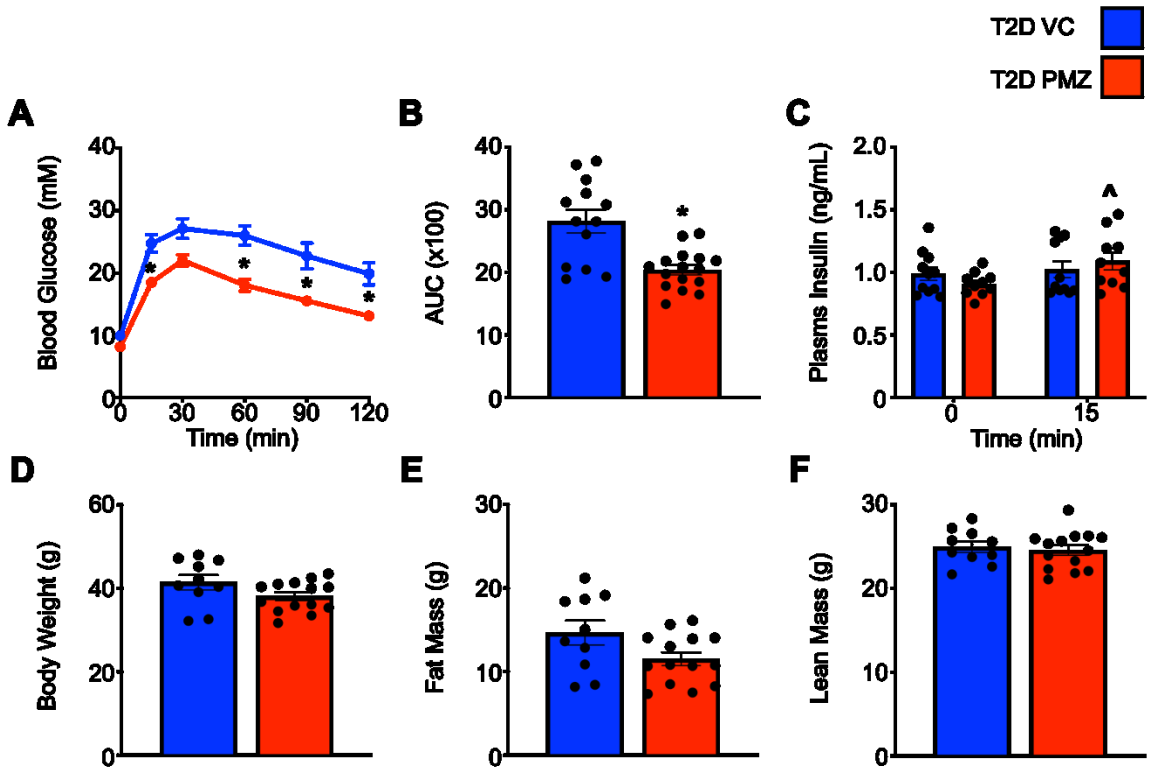

Figure 5.3. *Pimozide improves glucose tolerance in T2D mice independent of marked alterations in body composition.* Glucose tolerance assessed by an intraperitoneal glucose tolerance test (IPGTT) after 2-weeks of treatment with pimozide or vehicle control (VC) in T2D mice **(A)** and the corresponding area under the curve analysis (AUC) **(B)** (n = 13–16). Circulating insulin levels during the IPGTT before and at 15 minutes post glucose administration (**C**) (n = 10–11). Body weight **(D)**, fat mass **(E)** and lean mass **(F)** measured after 4-weeks of treatment with pimozide or VC in T2D mice (n = 10–14). Values represent mean ± SEM. Differences were determined using a two-way ANOVA or an unpaired, two-tailed Student's t test. *P < 0.05, significantly different from VC-treated T2D mice. ^P < 0.05, significantly different from 0-minute time point.

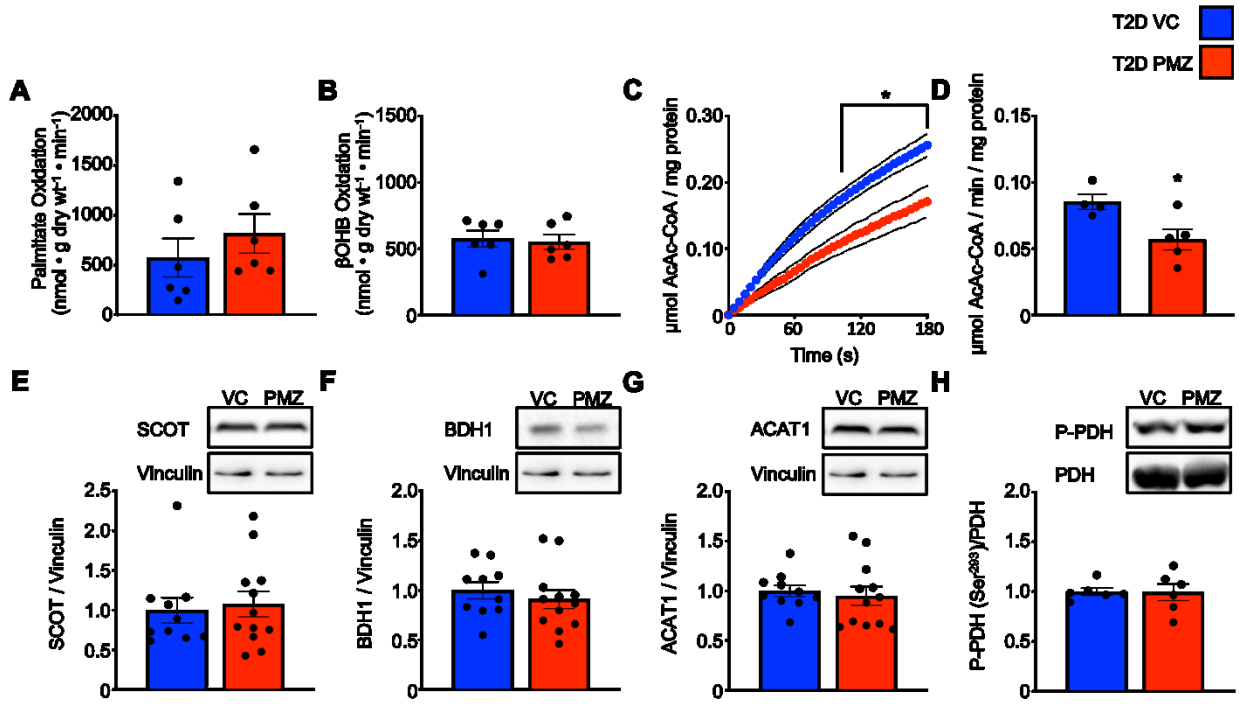

Figure 5.4. *Pimozide reduces myocardial SCOT activity.* Palmitate and **(A)** βOHB **(B)** oxidation rates were determined during aerobic perfusion of isolated working hearts from T2D mice treated with pimozide or vehicle control (VC) (n = 6). Succinyl CoA:3-ketoacid CoA transferase (SCOT) activity in cardiac tissue from pimozide and VC-treated T2D mice expressed as the levels **(C)** and rate **(D)** of acetoacetyl CoA (AcAc-CoA) production per mg of protein (n = 4–5). Protein levels of SCOT **(E)**, βOHB dehydrogenase 1 (BDH1) **(F)**, and acetoacetyl CoA thiolase (ACAT1) **(G)** relative to vinculin in cardiac tissue from pimozide and VC-treated T2D mice (n = 10–12). Pyruvate dehydrogenase (PDH) phosphorylation at serine 293 relative to total PDH in myocardial tissue from T2D mice treated with pimozide or VC **(H)** (n = 6). Values represent mean ± SEM. Differences were determined using a two-way ANOVA or an unpaired, two-tailed Student's t test. *P < 0.05 significantly different from VC-treated T2D mice.

5.4.5 Chronic Reduction of Myocardial SCOT Activity by Pimozide Treatment Improves Aberrant Cardiac Structural Remodeling and Diastolic Function in T2D Mice

Cardiac structure and function were assessed in mice with T2D after a 4-week treatment with pimozide or VC to ascertain whether the blunting of myocardial βOHB oxidation rates is reflective of an adaptive or maladaptive mechanism in diabetic cardiomyopathy. Systolic function, as assessed by CO and EF, as well as diastolic and systolic LVID and volume were not detrimentally impacted by the chronic reduction of myocardial SCOT activity **(Figure 5.5, A–D, Table 5.3)**. Intriguingly, pimozide-treated T2D mice displayed a reduction in the LV mass to LBM ratio indicative of a reduction in cardiac hypertrophy and reversal of aberrant LV structural remodeling when compared to VC-treated T2D littermates **(Figure 5.5E, Table 5.3)**. Likewise, a significant and trending ($P = 0.15$) reduction in LVAW thickness during diastole and systole, respectively, was demonstrated in T2D mice following chronic pimozide administration **(Table 5.3)**. In line with an attenuation of hypertrophic remodeling, diastolic function was also improved as determined by an increase in the E/e' ratio when compared to both VC-treated T2D mice following treatment, and to baseline measurements **(Figure 5.5, F and G)**. The e'/a' ratio also trended to decrease in T2D pimozide-treated mice when compared to control mice suggestive of improved diastolic function, although the E/A ratio was unchanged **(Figure 5.5, H and I)**. Furthermore, the LA enlargement associated with the T2D cardiac phenotype was also effectively attenuated by pimozide, thus providing further evidence to suggest an improvement of diastolic function **(Figure 5.5, J–M)**.

Assessment of the transcript levels of *Col1a1* in the pimozide-treated T2D mouse heart revealed a trend towards reduced expression, however, expression of *Col1a2* and *Tgfβ* were unchanged **(Figure 5.5N)**. In addition, the transcriptional expression of the pro-inflammatory cytokine, *Il-6*, also trended towards a reduction in pimozide-treated mice ($P = 0.18$), whereas expression levels of the glucose transporters (*Slc2a1*, *Slc2a4*) and oxidative stress resistance genes (forkhead box O3 (*Foxo3*) and superoxide dismutase 2 (*Sod2*)) were unaffected **(Figure 5.5, O–Q)**. Overall, these findings highlight that the pharmacological inhibition of myocardial SCOT activity does not exacerbate cardiac dysfunction in the context of T2D and rather permits an improvement in LV function and reversal of pathological cardiac remodeling which may be associated with a mild reduction in fibrosis and inflammation.

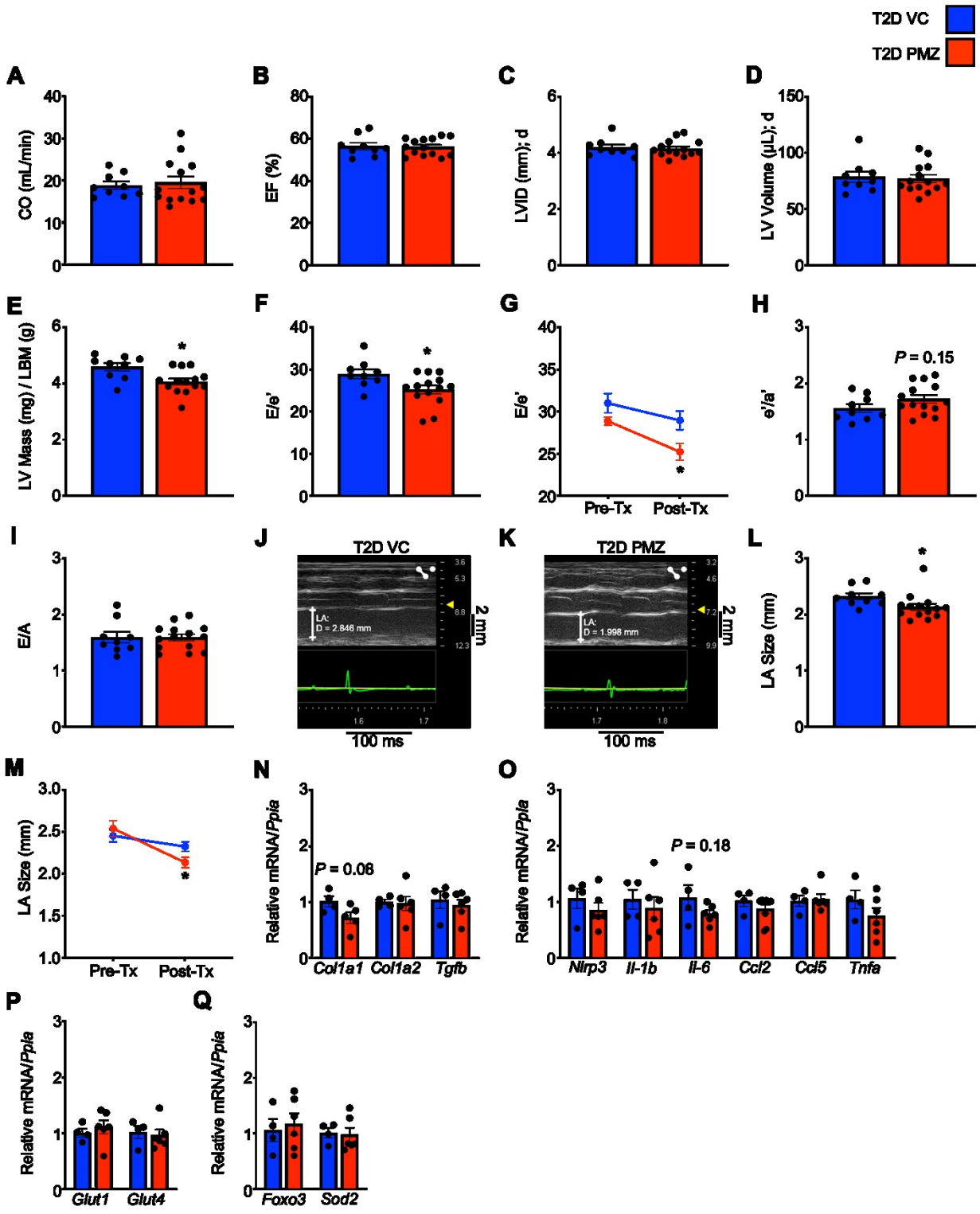
T2D VC
T2D PMZ
A
CO (mL/min)
B
EF (%)
C
LVID (mm); d
D
LV Volume (µL); d
E
LV Mass (mg) / LBM (g)
F
E/e'
G
E/e'
Pre-Tx
Post-Tx
H
e'/a'
P = 0.15
I
E/A
J
T2D VC
LA:
D = 2.846 mm
2 mm
100 ms
K
T2D PMZ
LA:
D = 1.998 mm
2 mm
100 ms
L
LA Size (mm)
M
LA Size (mm)
Pre-Tx
Post-Tx
N
Relative mRNA/Ppia
P = 0.08
Col1a1
Col1a2
Tgfb
O
Relative mRNA/Ppia
P = 0.18
Nlrp3
Il-1b
Il-6
Ccl2
Ccl5
Tnfa
P
Relative mRNA/Ppia
Glut1
Glut4
Q
Relative mRNA/Ppia
Foxo3
Sod2

Figure 5.5. *Pimozide improves diastolic function and supresses adverse cardiac remodeling in T2D mice.* Ultrasound echocardiography was used to assess cardiac output (CO) **(A)**, ejection fraction (EF) **(B)**, left ventricular (LV) internal diameter (LVID) **(C)**, LV volume **(D)**, and LV mass normalized to lean body mass (LBM) **(E)** in T2D mice treated with vehicle control (VC) or pimozide for 4-weeks (n = 9–14). Post-treatment measurements of the E/e' ratio **(F)** and compared to pre-treatment (baseline) values **(G)**, e'/a' ratio **(H)**, and E/A **(I)** measured in VC and pimozide-treated T2D mice (n = 9–14). Representative images of left atrial (LA) size in T2D VC-treated mice **(J)** and T2D pimozide-treated mice **(K)**. Post-treatment measurements of LA size in T2D VC and pimozide-treated mice **(L)** and presented compared to pre-treatment values **(M)** (n = 9–14). Relative mRNA expression of gene markers of fibrosis (collagen type 1 α1 (*Col1a1*), collagen type 1 α2 (*Col1a2*), and transforming growth factor-β (*Tgfβ*)) **(N)**, inflammation (nucleotide-binding domain-like receptor protein 3 (*Nlrp3)*, interleukin-1β (*Il-1b*), interleukin-6 (*Il-6*), C-C motif chemokine ligand 2 (*Ccl2*), and C-C motif chemokine ligand 5 (*Ccl5*)) **(O),** glucose uptake (glucose transporter 1 (*Slc2a1*) and glucose transporter 4 (*Slc2a4*) **(P)**, and oxidative stress (forkhead box O3 (*Foxo3*) and superoxide dismutase 2 (*Sod2*)) **(Q)** (n = 4–6). Values represent mean ± SEM. Differences were determined using a repeated measures two-way ANOVA or an unpaired, two-tailed Student's t test. *P < 0.05, significantly different from VC-treated T2D mice.

Table 5.3 *In vivo assessment of cardiac structural and functional parameters in T2D mice following treatment with vehicle control or pimozide*

	VC	Pimozide
Heart Rate (beats/min)	422 ± 7	451 ± 12
LBM (g)	24.6 ± 0.6	24.6 ± 0.6
LV Mass (mg) / LBM (g)	4.59 ± 0.14	4.07 ± 0.11*
LVID (mm); s	2.95 ± 0.07	2.99 ± 0.06
LVID (mm); d	4.19 ± 0.10	4.15 ± 0.08
Volume (μL); s	33.9 ± 2.0	35.0 ± 1.6
Volume (μL); d	78.5 ± 4.8	77.0 ± 3.5
Stroke Volume (μL)	43.4 ± 1.8	43.9 ± 2.2
CO (ml/min)	18.8 ± 0.9	19.5 ± 1.4
EF (%)	56.4 ± 1.6	56.1 ± 1.1
FS (%)	29.2 ± 1.1	28.7 ± 0.7
LVAW; s (mm)	1.15 ± 0.04	1.06 ± 0.04
LVAW; d (mm)	0.79 ± 0.04	0.70 ± 0.02*
LVPW; s (mm)	1.29 ± 0.06	1.24 ± 0.03
LVPW; d (mm)	0.95 ± 0.05	0.90 ± 0.02
E/A	1.60 ± 0.10	1.59 ± 0.06
e'/a'	1.56 ± 0.07	1.72 ± 0.07
E/e'	29.0 ± 1.1	25.2 ± 1.0*
LA Size (mm)	2.32 ± 0.06	2.14 ± 0.06*

In vivo cardiac function and LV wall measurements in T2D mice treated with vehicle control (VC) ($n = 9$) or pimozide ($n = 14$) for 4 weeks. Values represent mean ± SEM. *$P < 0.05$, significantly different from T2D VC-treated mice. LBM, lean body mass; CO, cardiac output; EF, ejection fraction; FS, fractional shortening; LV, left ventricle; LVAW, LV anterior wall thickness; LVID, LV internal diameter; LVPW, LV posterior wall thickness; s, systole; d, diastole.

5.5 Discussion

Cardiovascular disease manifests in a significant proportion of well-controlled diabetic patients, thus emphasizing the need for further investigation into the pathophysiology underlying diabetic heart disease and the development of targeted therapies (145). A loss of myocardial metabolic flexibility characterized by an excessive reliance on fatty acid oxidation and impaired glucose oxidation is a leading mechanism that contributes to the development and progression of diabetic cardiomyopathy, however, the extent to which perturbations in myocardial ketone body metabolism are also implicated remains enigmatic (154). Recent findings collectively postulate an adaptive role for the increase in cardiac ketone body oxidation demonstrated in heart failure without diabetes (42). In contrast, our results reveal that myocardial ketone body oxidation is in fact suppressed in diabetic cardiomyopathy characterized by moderate cardiac hypertrophy and impaired diastolic function. Intriguingly, this intrinsic shift away from ketone body utilization in the diabetes-affected heart may not be detrimental given that further pharmacological antagonism of cardiac SCOT activity neglected to exacerbate adverse LV remodeling and cardiac dysfunction in T2D mice. Furthermore, we identified that, in addition to its anti-hyperglycemic effects, pimozide also has cardioprotective actions, thus further supporting its potential as a novel therapy for T2D.

Myocardial βOHB oxidation rates were markedly depressed in T2D mice. Of interest, this reduction in ketone body oxidation did not appear to be due to a repression of SCOT given that SCOT catalytic activity was paradoxically increased in the T2D mouse heart. Alternatively, the reduced myocardial ketone body oxidation rates in T2D mice may be explained by the observed decrease in the cardiac protein expression of the upstream enzyme, BDH1. Extrahepatic mitochondrial BDH1 catalyzes the first step in ketone body oxidation by converting βOHB to acetoacetate, which is then activated to acetoacetyl-CoA by SCOT through a CoA exchange with succinyl-CoA (39). Although we did not directly measure BDH1 activity in the T2D heart, a recent study utilizing a streptozotocin-induced mouse model of T1D demonstrated a reduction in cardiac BDH1 expression that translated to a 27% reduction in catalytic activity and a strong trend for decreased βOHB oxidation in isolated working hearts (194). A similar reduction in cardiac BDH1 enzymatic activity was also demonstrated in mice with high-fat diet-induced glucose intolerance and chronically diabetic rats, which is consistent with findings of suppressed *BDH1* gene

expression in LV biopsies from T2D patients with heart failure compared to nondiabetic heart failure patients (194, 320).

Metabolic flux measurements in the isolated working mouse heart suggest that the utilization of ketone bodies for cardiac energy production is decreased in diabetic cardiomyopathy, which is consistent with several recent findings in mouse models of diabetes and heart failure with preserved ejection fraction, a cardiac phenotype enriched in the diabetic population (118, 194, 338). In contrast, cardiac ketone body oxidation was proposed to be increased in diabetic cardiomyopathy following findings that the myocardial uptake of acetoacetate and βOHB was enhanced in individuals with T2D undergoing cardiac catherization for heart disease (319). Furthermore, ketone body oxidation in the heart was determined to be elevated in a non-obese T2D rat model utilizing hyperpolarized [3-^{13}C]acetoacetate (195). However, given that BDH1 catalyzes the conversion of βOHB to acetoacetate in the first step of βOHB oxidation, the use of acetoacetate rather than βOHB, the most abundant circulating ketone body (339), circumvents a potential contribution of BDH1 dysregulation in the assessment of cardiac ketone body oxidation. Therefore, it remains possible that cardiac ketone body oxidation may have actually been decreased in this model of T2D if potential alterations in BDH1 activity had been accounted for.

To elucidate whether a decrease in myocardial ketone oxidation is reflective of an adaptive or maladaptive response in diabetic cardiomyopathy, we further inhibited ketone body metabolism in the heart through pharmacological antagonism of SCOT with pimozide. Notably, we observed that inhibition of the heart's capacity to utilize ketone bodies as an energy source does not provoke a deterioration of cardiac structure and function which suggests against a pathological role for decreased myocardial ketone body metabolism in the development and progression of diabetic cardiomyopathy. An adaptive attenuation of ketone body oxidation may serve to preserve tricarboxylic acid (TCA) cycle flux when plasma concentrations of ketone bodies are elevated as observed in T1D and T2D (340, 341). Isolated working rat hearts perfused exclusively with acetoacetate developed reversible contractile dysfunction associated with an inhibition of the TCA cycle at the level of α-ketoglutarate dehydrogenase (342-345). This defect could be rescued by the addition of anaplerotic substrates to replenish TCA cycle intermediates or CoA synthetic precursors to compensate for the sequestration of intramitochondrial CoA as acetoacetyl-CoA and

acetyl-COA. Furthermore, a downregulation of ketolysis may occur as a result of a compensatory upregulation of cardiac ketogenesis to shift the flux of excess intramitochondrial fatty acid-derived acetyl CoA toward ketone body synthesis. Indeed, transcriptional suppression of ketolytic enzymes has been demonstrated to occur concomitantly with an induction of the fate-committing ketogenic enzyme, mitochondrial 3-hydroxymethylglutaryl-CoA synthase 2 (*Hmgcs2*/HMGCS2), in the myocardium of T1D mice (194, 325, 346, 347).

Increasing myocardial ketone body availability by means of reduced oxidation may have enhanced the function of βOHB as a signaling molecule in the myocardium, thus contributing to the cardioprotective effects of pimozide treatment. Cardiac dysfunction in T2D mice was associated with enhanced expression of the fibrotic marker, *Col1a1*, as well as a trending increase in the gene expression of the pro-inflammatory cytokine, *Il-6*, which were both decreased by pimozide treatment. βOHB can mediate anti-inflammatory effects through activation of the G-protein coupled receptor, GPR109A, and inhibition of the NLRP3 inflammasome on macrophages/monocytes (323, 348), as well as suppress cardiac fibrosis as a specific inhibitor of class 1 histone deacetylases (349, 350). Interestingly, gene expression of several other fibrotic and inflammatory markers was not different between lean and T2D mice, which may indicate that inflammation and fibrosis do not contribute to the development of diabetic cardiomyopathy to the same degree as observed in other preclinical models (329, 332). Nonetheless, expression of markers that were enhanced in T2D mice were the markers reduced by pimozide treatment, therefore, βOHB-mediated suppression of cardiac inflammation and fibrosis may still play a modest role in the improvement of the cardiac phenotype. Notably, HDAC inhibition has been demonstrated to preserve cardiac function and reduce adverse remodeling in diabetic cardiomyopathy through multiple alternative mechanisms including mitigation of oxidative stress, cardiac myocyte hypertrophy, insulin resistance, endothelial hyperpermeability and diabetes-associated derangements in fatty acid metabolism (322, 349, 351-354). However, treatment with pimozide did not enhance the cardiac transcriptional expression of insulin-dependent glucose transporter 4 (*Slc2a4*) or the oxidative stress resistance genes, *Foxo3* and *Sod2*.

Emergent evidence from our laboratory indicates that pimozide may improve glucose homeostasis in obese and T2D mice, at least in part, through the enhancement of skeletal muscle PDH activity

and glucose oxidation (229). Therefore, if the effects of SCOT inhibition on skeletal muscle PDH phosphorylation can be recapitulated in the myocardium, enhancement of cardiac glucose oxidation secondary to PDH activation could represent a potential mechanism through which pimozide may improve cardiac function in diabetic cardiomyopathy. In contrast to our previous findings in gastrocnemius muscle, pimozide treatment did not affect the phosphorylation state of PDH in the hearts of T2D mice. Although this finding suggests against our hypothesis, we were unable to confirm whether myocardial glucose oxidation rates were affected by pimozide treatment during isolated working heart perfusions. Furthermore, given that pimozide improved glucose tolerance in T2D mice, alleviation of hyperglycemia may also contribute to the observed improvements in cardiac structure and function. Lastly, it cannot be excluded that inhibition of other pimozide targets, namely myocardial D_2 receptors (355), may also be involved in mediating the positive cardiac outcomes of pimozide treatment.

In conclusion, our results suggest that myocardial ketone body oxidation is downregulated in diabetic cardiomyopathy, and that this metabolic shift away from the utilization of ketones as an energy substrate may reflect a compensatory response of the myocardium to the diabetic milieu. Furthermore, we identified that systemic SCOT inhibition by treatment with pimozide improves glucose homeostasis, as well as attenuates diastolic dysfunction and hypertrophic remodeling in T2D mice, therefore highlighting the therapeutic potential of pimozide for the treatment of T2D. Further investigation is required to elucidate the mechanisms underlying pimozide-mediated cardioprotection in diabetic cardiomyopathy. Nevertheless, therapies specifically designed to target diabetic cardiomyopathy and subsequent heart failure are very limited, therefore, the findings of this study are highly relevant towards the development of novel anti-diabetic therapies.

Acknowledgements & Grants

This study was supported by a Project Grant from the Canadian Institutes of Health Research (CIHR) to J.R.U. A.A.G is supported by a Vanier Canada Graduate Scholarship from the CIHR. J.R.U. is a Tier 2 Canada Research Chair (Pharmacotherapy of Energy Metabolism in Obesity).

Disclosures

No conflicts of interest, financial or otherwise, are declared by the authors.

Chapter 6: Discussion

6.1 Barth Syndrome Cardiomyopathy

6.1.1 Overview

Derangement of mitochondrial membrane lipid composition is a critical mechanism contributing to the impairment of myocardial energy production and subsequent progression of cardiac dysfunction (356-359). Cardiolipin is a structurally distinct phospholipid primarily localized to the inner mitochondrial membrane with essential roles in providing structural and functional support to numerous proteins involved in mitochondrial bioenergetics (72). Aberrant cardiolipin content and composition in the heart, particularly a reduction of the predominant tetralinoleoyl cardiolipin species, has been reported in a variety of cardiac pathologies, including idiopathic dilated cardiomyopathy (356), diabetic cardiomyopathy (360) and heart failure (71), therefore highlighting the fundamental role of cardiolipin in cardiovascular health and disease. Moreover, defective cardiolipin biosynthesis and remodeling is also implicated in the development of cardiomyopathy associated with several genetic disorders such as Dilated Cardiomyopathy with Ataxia and Sengers syndrome (361). Notably, the X-linked recessive disorder, Barth syndrome (BTHS), provides direct evidence for a pathological role of perturbed cardiolipin remodeling in heart disease (94). In BTHS, deficiency of tetralinoleoyl cardiolipin caused by *TAFAZZIN* mutations is the primary mechanism for mitochondrial dysfunction leading to the infantile development of cardiomyopathy (66, 67). Therefore, further investigation to delineate the pathophysiological mechanisms linking altered cardiolipin biosynthesis to cardiac dysfunction in BTHS has broad implications for a plethora of cardiac pathologies associated with defects in the cardiolipin pool.

The work presented in the two studies herein **(Chapters 2 and 3)**, in addition to previous literature (81, 82, 86, 106), identifies alterations in myocardial intermediary energy metabolism as a primary pathological mediator and potential therapeutic target for BTHS-related cardiomyopathy. Whereas previous findings have predominately been dependent on *in vitro* studies (81, 82, 106), the results reported in **Chapter 2** provide noteworthy contributions towards the field as we performed the first investigations of metabolic flux in the *ex vivo* isolated working heart. Importantly, we

demonstrated that tafazzin-deficiency in BTHS is associated with an impairment of insulin-stimulated cardiac glucose oxidation and a concomitant elevation of cardiac fatty acid metabolism in the presence of insulin. Similar to findings in tafazzin-deficient C2C12 mouse myoblasts (106), decreased myocardial glucose oxidation in TazKD mice was accompanied by a reduction in PDH activity, however, in contrast to the aforementioned study, decreased PDH catalytic activity was independent of alterations in the phosphorylation or acetylation state of the enzyme. Interestingly, although proteins involved in fatty acid uptake and oxidation were either unchanged or decreased, palmitate oxidation rates in perfused working hearts from TazKD mice strongly trended to increase compared to WT mice in the presence of insulin. Insulin exerts an inhibitory effect on fatty acid oxidation by increasing the level of malonyl-CoA through enhancement of ACC activity, thereby decreasing mitochondrial fatty acid uptake via CPT1 (362, 363). Therefore, the elevation of palmitate oxidation in the TazKD working heart may be suggestive of cardiac insulin resistance. The insulin-stimulated enhancement of glucose oxidation rates was also blunted in the TazKD isolated working heart which coincided with a reduction in the gene expression of GLUT4, therefore providing further evidence to suggest a degree of cardiac insulin resistance in BTHS. Furthermore, given that myocardial TAG content was elevated in TazKD mice, it is possible that accumulation of toxic lipid intermediates such as ceramide and diacylglycerol contribute to the development of cardiac insulin resistance in BTHS (180).

Evidence of increased and decreased circulating glucose and insulin levels, respectively, in our TazKD mouse model, and of reduced pancreatic islet insulin secretion in TazKD mice (250) provide further support for the paradigm of impaired insulin action in the context of tafazzin deficiency. Although, overt insulin deficiency was not reported in one study involving adolescents and young adults with BTHS (124). Lastly, regarding cardiac ketone body metabolism in BTHS, we observed a near four-fold increase in the myocardial protein expression of the ketone body oxidation enzyme, BDH1, which did not translate into an increase in βOHB oxidation rates assessed during isolated working heart perfusions. Nonetheless, the increased BDH1 levels may indicate an increased capacity of the heart to oxidize ketones for energy and, therefore, modulation of ketone body oxidation may represent a novel target for therapeutic intervention in BTHS.

In **Chapter 3**, we explored whether pharmacological enhancement of myocardial glucose oxidation with DCA would be sufficient to attenuate pathological cardiac remodeling in the TazKD mouse heart. In contrast to our hypothesis, DCA treatment did not alleviate hypertrophic cardiac remodeling in TazKD mice despite a reduction in PDH phosphorylation, indicative of an enhancement of PDH activity, and a trend towards reduced oxidative stress. The latter result supports the argument against a significant role of mitochondrial reactive oxygen species in the pathophysiology of BTHS-related cardiomyopathy, which recapitulates previous findings that the overexpression of catalase and amelioration of oxidative stress in the heart did not improve the cardiac phenotype in TazKD mice (238).

As discussed in **Chapter 3**, a potential reason why DCA treatment failed to improve cardiac outcomes in TazKD mice may be due to the possibility that despite PDH activity and glucose oxidation being elevated, persistent ETC defects may prevent a net improvement in ATP production. However, alternative explanations for the lack of benefit may be attributed to direct cardiolipin-deficiency associated impairments of TCA cycle enzymes including aconitase and succinate dehydrogenase (364, 365) and/or recent findings of impaired calcium handling in TazKD cardiac myocytes (107, 108, 366). To accommodate for variations in cardiac workload, ADP-induced stimulation of the ETC is coupled with mitochondrial Ca^{2+} uptake though the MCU to enhance the activity of PDH and TCA cycle dehydrogenases, thereby accelerating the regeneration of reducing equivalents in a process termed "mechano-energetic coupling" (72). Downregulation of the pore-forming subunit of the MCU complex abrogates mitochondrial Ca^{2+} uptake in cardiac mitochondria from TazKD mice, therefore impairing adaptation of TCA cycle activity to ATP consumption in response to increased cardiac workload (108). A reduction in the abundance of the MCU and mitochondrial calcium uptake protein 1, the principal regulator of the MCU channel, was also demonstrated in a C2C12 *Tafazzin*-knockout murine myoblast cell line and BTHS patient-derived cells and cardiac tissue (107, 366). Therefore, although the heart's ability to oxidize glucose for energy was enhanced by DCA treatment, a principal defect in mechano-energetic coupling, rather than ATP-production-capacity, per se, may limit the increased energy production required to enhance contractile performance during elevated demand, thus resulting in cardiac myocyte hypertrophy (367). Furthermore, defective Ca^{2+}-dependent energy supply and demand matching in the hearts of TazKD mice may also explain why our finding of a potential increase in

basal myocardial ATP levels by DCA treatment did not translate into a reversal of hypertrophic cardiac remodeling.

In addition, although assessment of the level of PDH phosphorylation is considered a reliable indicator of PDH activity and subsequent glucose oxidation (29, 102), we did not directly measure cardiac PDH flux or glucose oxidation in TazKD and WT mice treated with DCA or vehicle control. This limitation of the experimental design in **Chapter 3** may also contribute to the negative findings as it is possible that the DCA-mediated reduction in myocardial PDH phosphorylation did not result in a restoration of cardiac glucose oxidation. PDH closely associates with the inner mitochondrial membrane (368), and its activity can be directly regulated by mature cardiolipin (106), therefore an intrinsic defect in PDH due to impaired cardiolipin remodeling may ultimately impair PDH activity despite alterations in the phosphorylation state. Furthermore, as described in **Chapter 2**, we identified that myocardial PDH activity is downregulated in TazKD mice independent of PDH phosphorylation, therefore an alternative post-translational modification (i.e., S-glutathionylation (369)) may have ultimately superseded the effect of DCA on PDH phosphorylation in the regulation of PDH activity. Cardiolipin has also been demonstrated to interact with the mitochondrial pyruvate carrier (370). Reduced transport of cytosolic-derived pyruvate into the mitochondria for conversion to acetyl CoA by PDH could reduce pyruvate oxidation despite increased availability of active PDH. Direct measurement of glucose oxidation in the *ex vivo* isolated working heart of DCA-treated mice and the direct *in vivo* assessment of myocardial PDH flux utilizing hyperpolarized ^{13}C-magnetic resonance spectroscopy (371) could address these limitations. The potential contributing factors that may underlie the failure of DCA to improve pathological structural remodeling in TazKD mice are outlined in **Figure 6.1**.

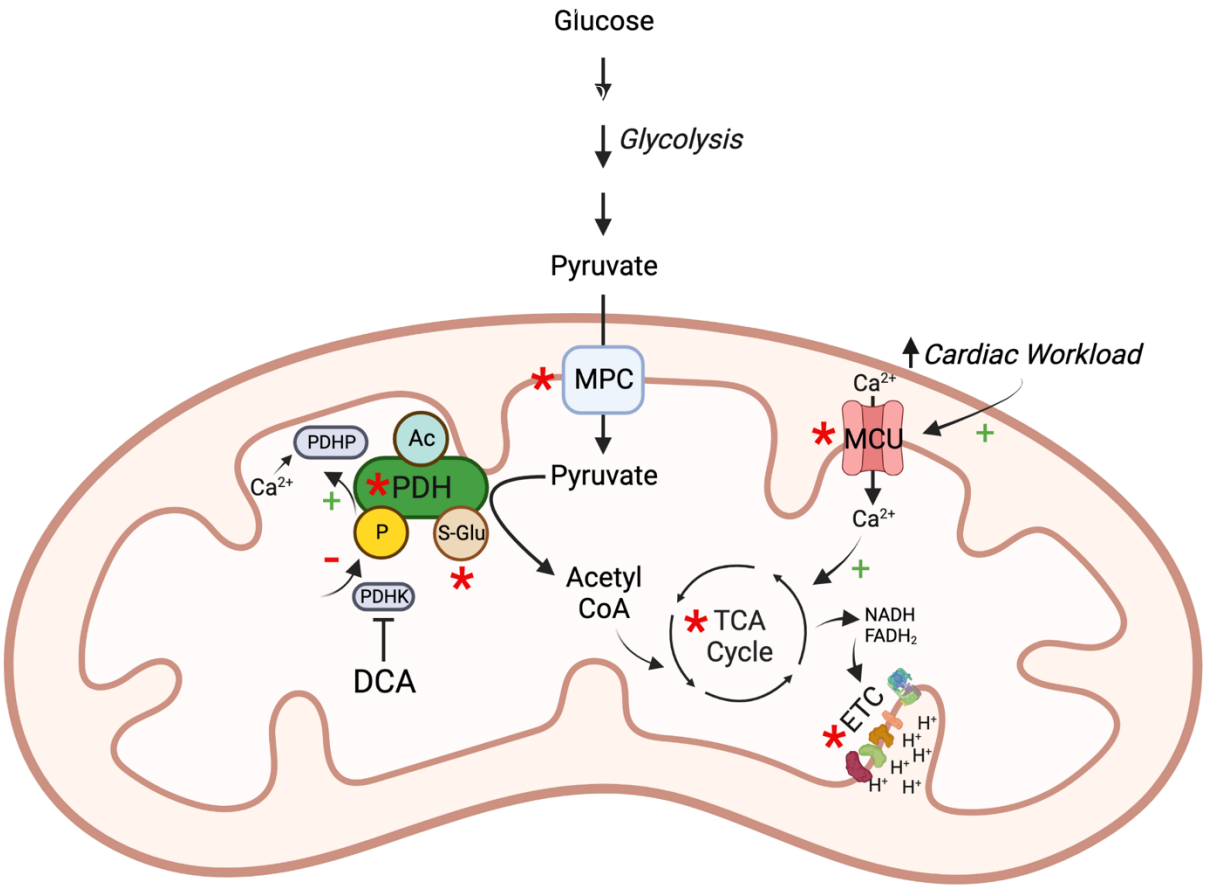

Figure 6.1. *Potential factors that may limit the effectiveness of DCA as a therapeutic agent for Barth syndrome cardiomyopathy.* Mechanisms that may explain the lack of benefit observed with DCA treatment in TazKD mice with regard to pathological cardiac structural remodeling are denoted with a red asterisk. In brief, DCA enhances PDH activity through inhibition of all isoforms of PDHK which inhibit PDH through reversible phosphorylation. However, impaired pyruvate uptake through the MPC, intrinsic defects in PDH, alternative regulatory PDH post-translational modifications (acetylation, S-glutathionylation), impaired mitochondrial Ca^{2+} handling and associated activation of TCA cycle dehydrogenases, decreased activities of TCA cycle enzymes, and defects in ETC function may contribute to the negative findings described in **Chapter 3**. MPC, mitochondrial pyruvate carrier; PDH, pyruvate dehydrogenase; PDHK, PDH kinase; PDHP, PDH phosphatase; P, phosphate group; Ac, acetyl group; S-Glu, glutathione; MCU, mitochondrial calcium uniporter; TCA cycle, tricarboxylic acid cycle; ETC, electron transport chain. Created with BioRender.com.

6.1.2 Future Directions

Although the mechanisms underlying the cardioprotective effects of SGLT2 inhibitors, including empagliflozin, in the setting of heart failure with reduced and preserved ejection fraction (210, 372) have not yet been comprehensively elucidated, one hypothesis suggests that SGLT2 inhibitors may enhance cardiac ketone body oxidation, thereby improving myocardial energetics, by increasing circulating levels and thus the cardiac delivery of βOHB (373, 374). Given our findings that the ability of the heart to oxidize ketone bodies is likely intact, and potentially enhanced in the energy-deficient heart in BTHS, SGLT2 inhibitors may represent a promising therapeutic approach for BTHS-related cardiomyopathy. Indeed, empagliflozin treatment increased cardiac utilization of ketone bodies and myocardial ATP content in a nondiabetic porcine model of heart failure which was associated with an improvement in cardiac function and reversal of adverse remodeling (117). Empagliflozin may also improve mechano-energetic coupling in BTHS by enhancing mitochondrial Ca^{2+} concentration in cardiac myocytes secondary to reduced myocardial Na^{+} levels due to direct inhibition of the Na^{+}/H^{+} exchanger (375). However, given that circulating ketone body levels are already increased in BTHS (115), there is a possibility that further enhancement of plasma ketone body levels by treatment with SGLT2 inhibitors could lead to ketoacidosis. In addition, given that empagliflozin treatment can stimulate adipose tissue lipolysis to mobilize fatty acids for hepatic ketogenesis (376), this could be detrimental for individuals with BTHS whom already possess a very lean body composition (124). Therefore, treatment of TazKD mice with empagliflozin and subsequent assessment of body composition, myocardial energetics and cardiac function could be performed to help determine whether SGLT2 inhibitors are cardioprotective in the context of BTHS.

6.2 Obesity and Diabetic Cardiomyopathy

6.2.1 Overview

Chapter 4 describes the effect of the ketogenic diet on body composition, glycemic control, and cardiac function in the setting of obesity/prediabetes. We observed that 8-weeks of supplementation with a ketogenic diet did not promote significant body weight loss or improve glucose homeostasis in a mouse model of high-fat diet-induced obesity. Alternatively, transition to a low-fat, high complex carbohydrate diet produced marked body weight loss in obese mice that

was primarily attributable to a decrease in fat mass, and reversed obesity-induced derangements in glucose tolerance. The ketogenic diet also promoted an accumulation of myocardial TAG content without significantly affecting cardiac function in obese mice.

Our findings are in contrast to a recent study that used a similar experimental approach to investigate the effects of the ketogenic diet on obesity and obesity-related cardiovascular risk factors. C57Bl6/J mice rendered obese by a high-fat diet and subjected to surgical destabilization of the medial meniscus to induce osteoarthritis were transitioned to either a ketogenic or chow diet, or were maintained on a high-fat diet for an additional 8-weeks (377). Similar to chow-fed mice, ketogenic diet-fed mice also exhibited decreased body weight and fat mass, and improved glucose homeostasis as assessed by an IPGTT. An increase in histone β-hydroxybutyrylation, a protein post-translational modification involved in the regulation of gene expression (378), in the liver and kidney may have contributed to the metabolic effects. We did not assess modulation of the epigenome by β-hydroxybutyrylation in our study, therefore, it cannot be determined whether differences in histone β-hydroxybutyrylation may account for the discrepancies. In contrast to the ketogenic diet utilized in our study (85% calories from fat, 5% from carbohydrates and 10% from protein), the ketogenic diet utilized by Nasser *et al.* (2022) was formulated with 94% of its energy provided by fat, 5% by protein and <1% of energy provided by carbohydrates. The 9% difference in fat content between the diets may have altered the level of ketosis achieved in each study which may also have contributed to the contrasting findings (379).

A specific obesity-induced cardiac phenotype is difficult to determine given that obesity is often associated with several comorbidities that can increase the risk for cardiovascular complications including hypertension, impaired glucose tolerance and diabetes (304). Although several preclinical and clinical studies have proposed that obesity may be independently associated with increased left ventricular mass and cardiac adiposity (304, 380-383), findings regarding the effect on systolic and diastolic function are variable (304). In the mouse model of high-fat diet-induced obesity utilized in **Chapter 4**, impairments in cardiac function were not observed, which is consistent with several studies where a similar preclinical model was used (185, 384, 385). Of interest, transition to a ketogenic diet after chronic high-fat diet feeding did not induce marked abnormalities in cardiac structure and function.

However, given that we were unable to complete a comprehensive molecular analysis of the cardiac tissue samples, it remains a possibility that maintenance on a ketogenic diet prompted pathological molecular alterations that had not yet manifested into overt cardiac functional defects. Indeed, spontaneously hypertensive rats (SHR) subjected to a ketogenic diet exhibited aggravated hypertension, cardiac hypertrophy and myocardial interstitial fibrosis compared to SHR rats fed a control diet (386, 387). Furthermore, the ketogenic diet increased activity of the mammalian target of rapamycin complex 2 pathway which may have contributed to the enhancement of mitochondrial reactive oxygen species production and inflammatory signaling in the hearts of SHR rats as evidenced by increased protein levels of monocyte chemoattractant protein 1 and TNFα, and increased neutrophil and macrophage infiltration (387). Maintenance on a ketogenic diet for 12 weeks also exacerbated diastolic dysfunction and cardiac interstitial fibrosis in *db/db* mice despite mild improvement of some metabolic parameters (fasting glucose, fasting insulin, HOMA-IR) and was associated with suppression of T-regulatory cell expansion and function (388). In contrast, 8-week supplementation with the ketogenic diet improved systolic function and reduced levels of cardiac fibrosis in *db/db* mice by improving mitochondrial dynamics and function, reducing oxidative stress, and attenuating cardiac myocyte apoptosis (389). Although the reason for the discrepancies between studies is unclear, the latter study also reported a decrease in fasting blood glucose and serum insulin levels following the ketogenic dietary intervention in *db/db* mice, therefore, improved glucose homeostasis may account for an initial recovery of cardiac function, however, with extended ketogenic diet feeding, the negative effects induced by the diet may ultimately supersede the beneficial outcomes of improved metabolic control.

In addition, although we did not observe impaired cardiac function in ketogenic diet-fed obese mice at rest, it is possible that with increased myocardial stress, functional defects would have been revealed. Abdurrachim *et al.* (2018) reported that the ketogenic diet attenuated the decrease in end-diastolic volume measured in diabetic Goto-Kakizaki rats using MRI during infusion of the β-1 agonist, dobutamine, indicative of an increase in cardiac preload and reduced cardiac compliance (269). However, cardiac function parameters were similar between chow-fed and ketogenic diet-fed diabetic rats at rest. This study highlights the importance of assessing the cardiovascular effects of the ketogenic diet during different physiological (exercise) and pathological states that individuals with obesity and diabetes are at an increased risk to develop

(myocardial ischemia, hypertension, and heart failure) in order to comprehensively assess the cardiovascular safety profile of the ketogenic diet.

In **Chapter 5**, we aimed to elucidate the alterations in ketone body metabolism present in diabetic cardiomyopathy and provide insight regarding whether these alterations may reflect a beneficial or detrimental response of the myocardium. Consistent with previous findings (118, 194), we confirmed that ketone body oxidation is reduced in the heart affected by obesity and T2D **(Figure 6.2)**. Furthermore, we identified that this metabolic shift away from ketone body utilization in the heart may be adaptive given that further inhibition of myocardial SCOT activity did not exacerbate, but rather improved cardiac functional and structural abnormalities in a mouse model of diabetic cardiomyopathy. Lastly, we proposed that the anti-psychotic agent, pimozide, may represent a novel therapeutic approach for the treatment of diabetes given its antihyperglycemic and cardioprotective effects.

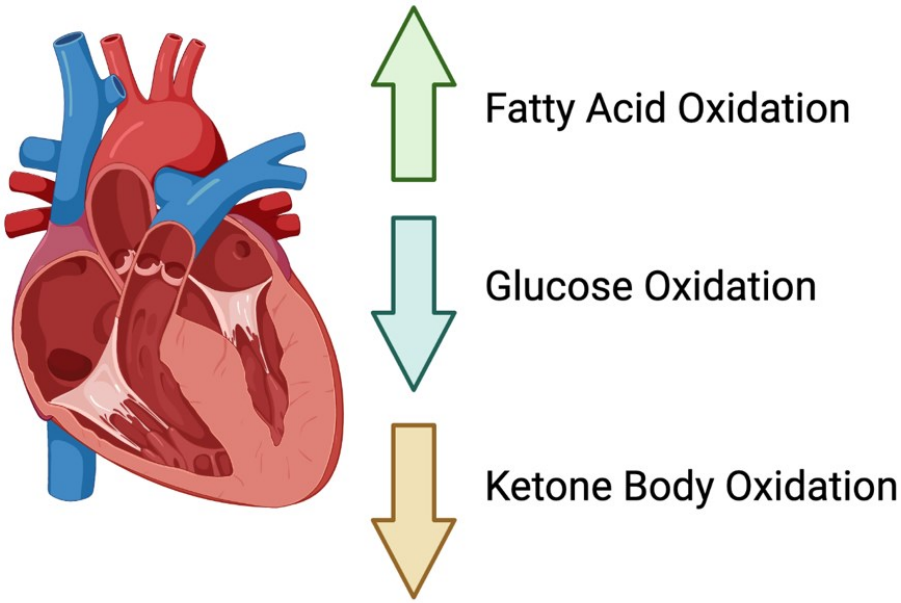

Figure 6.2. *Myocardial energy metabolism in diabetic cardiomyopathy.* Created with BioRender.com

The notion that a decrease in ketone body utilization for energy production could be adaptive in diabetic cardiomyopathy is interesting given that enhanced ketone body oxidation is postulated to be protective in HFrEF (42), nonetheless recent findings have tended towards this hypothesis. Myocardial ketone body oxidation as assessed by ^{13}C NMR isotopomer analysis was decreased in a 3-Hit murine model of HFpEF (involving age, long-term high-fat diet, and deoxycorticosterone pivalate (75 mg/kg) challenge to accentuate hypertension and systemic inflammation) (338). Of interest, sirtuin 3 knockout mice subjected to the same 3-Hit protocol exhibited increased myocardial ketone body oxidation, however, developed a more severe cardiac phenotype involving further exacerbation of cardiac hypertrophy and fibrosis and a decrease in diastolic function (338). It is important to consider that mitochondrial protein hyperacetylation as a result of the sirtuin 3 knockdown can affect multiple pathways which would influence the cardiac phenotype, however, it is interesting that an increase in cardiac ketone oxidation failed to benefit the heart in HFpEF, a cardiac phenotype enriched in the diabetic population (146). Another study also demonstrated that enhancing circulating ketone bodies through treatment with empagliflozin improved cardiac function in *db/db* mice without reversing the reduction in βOHB oxidation rates in isolated working hearts (118). Furthermore, in individuals with T2D undergoing cardiac catherization for heart failure compared to non-diabetic controls, a significant positive correlation was observed between total ketone body cardiac uptake and plasma levels of brain natriuretic peptide, a biomarker for cardiac dysfunction, thus suggesting that increased cardiac ketone body utilization may be associated with cardiac functional deterioration in T2D (319). Lastly, enhancing circulating ketone body concentrations is associated with an improvement of cardiac function in the setting of diabetes (390, 391), which may highlight the role of the βOHB-mediated activation of signaling pathways in the heart as the primary contributor to the cardiovascular benefits.

Although we have identified pimozide as a SCOT antagonist (229), it is also possible that the cardioprotective effects of pimozide are mediated by alterative mechanisms beyond an effect on cardiac ketone body metabolism. Pimozide has also been shown to activate PPARγ by selective inhibition of fatty acid binding protein-4 (392). PPARγ activators have been used in the treatment of T2D to improve insulin sensitivity and reduce glucose levels (393). In addition, the PPARγ agonist, pioglitazone, has also been demonstrated to improve myocardial insulin sensitivity and diastolic function in individuals with T2D (394, 395). Furthermore, although we did not report a

difference in PDH phosphorylation state, a limitation of **Chapter 5** was that were unable to determine whether myocardial glucose oxidation rates were altered by pimozide treatment.

Lastly, there are several remaining concerns regarding the use of pimozide as a treatment for diabetic cardiomyopathy that warrant further investigation. Schugar *et al.* (2014) reported that mice with a cardiac myocyte-specific knockout of SCOT (SCOT-Heart-KO) developed more severe ventricular remodeling characterized by left ventricular dilatation and reduced ejection fraction in response to myocardial pressure overload through transverse aortic constriction when compared to αMHC-Cre control mice which exhibited compensatory left ventricular hypertrophy and preserved systolic function (396). However, at baseline, SCOT-Heart-KO mice did not display any abnormalities in left ventricular mass or systolic function. The results of this study suggest that myocardial stress may be required to unmask the full spectrum of cardiac effects induced by limiting the heart's capacity to oxidize ketones. Therefore, it would be important for future studies to investigate the cardiac effects of pimozide treatment in diabetic mice subjected to additional myocardial stressors such as myocardial ischemia and sustained hypertension in order to confirm the cardiovascular safety of pimozide. Furthermore, several reports that pimozide may prolong the cardiac QT interval and increase the risk for arrythmias (397) may also limit the clinical utility of pimozide for the treatment of T2D.

6.2.2 Future Directions

A major concern with the utilization of the ketogenic diet as a therapeutic intervention for obesity and T2D is that individuals with an already elevated risk of cardiovascular disease may unknowingly subject themselves to further detrimental cardiac effects. Although we did not observe compromised cardiac function in ketogenic diet-fed obese mice, it remains possible that maintenance on a ketogenic diet induced maladaptive myocardial metabolic changes that may only manifest into overt cardiac dysfunction with chronic administration or induction of myocardial stress. Therefore, characterization of the cardiac metabolic alterations induced by the ketogenic nutrient environment in the setting of obesity and T2D would represent an important follow-up investigation to the results presented in **Chapter 4**. Maintenance on a ketogenic diet has been shown to increase circulating levels of free fatty acids (398), which can increase cardiac fatty acid availability. This increase in fatty acid delivery to the myocardium could exacerbate diabetes-

induced alterations in myocardial energy metabolism by leading to a further elevation and reduction of fatty acid and glucose oxidation, respectively, through substrate competition. In addition, cardiac lipid accumulation as discussed in **Chapter 4**, could further impair insulin sensitivity in the heart. Moreover, elevated circulating levels of βOHB with ketogenic diet feeding could also directly affect glucose uptake given evidence that chronic *in vitro* exposure to βOHB has been shown to promote insulin resistance and decrease glucose uptake in cardiac myocytes through decreased activation of the phosphatidylinositol 3-kinase (PI3-K)/protein kinase B signaling cascade (399, 400). To provide insight into the effect of the ketogenic diet on the heart in the setting of T2D, alterations in metabolic flux could be measured in isolated working hearts of mice with experimental T2D fed a ketogenic diet and perfused with substrate concentrations reflective of the ketogenic nutrient environment (high levels of palmitate and βOHB).

With regard to **Chapter 5,** assessment of cardiac function in mice with cardiac myocyte-specific overexpression of BDH1 and subjected to experimental T2D would serve to provide further insight into whether the reduction in myocardial ketone body oxidation in diabetic cardiomyopathy is adaptive or maladaptive. Overexpression of BDH1 in the heart would reverse the reduction in cardiac BDH1 protein expression in T2D mice and enhance ketone body oxidation (251). If our hypothesis is correct and the reduction in cardiac ketone body oxidation is indeed beneficial in diabetes, we would expect that T2D BDH1 overexpressing mice would exhibit a more severe cardiac phenotype. On the contrary, if overexpression of BDH1 in the heart is cardioprotective, this may suggest that pimozide mitigates diabetic cardiomyopathy through mechanisms beyond an effect on cardiac ketone body oxidation (i.e., mitigation of inflammation, oxidative stress, and fibrosis and/or systemic improvement in glucose tolerance). Furthermore, if mice with a cardiac myocyte-specific knockout of SCOT and subjected to experimental T2D recapitulate the improvement in cardiac function observed with pimozide-treated T2D mice, this would provide further support for an adaptive role of reduced cardiac ketone body oxidation in diabetes, as well as confirm that pimozide mediates its cardioprotective effects primarily through SCOT inhibition. Alternatively, if treatment of T2D cardiac myocyte-specific SCOT knockout mice with pimozide results in additional improvement in cardiac function, this may suggest that alternative actions of pimozide are also involved.

6.3 Concluding Remarks

Both BTHS-related cardiomyopathy and diabetic cardiomyopathy are characterized by perturbations in myocardial intermediary energy metabolism which may represent potential targets for reversing disease pathology and preventing the progression to clinical heart failure (94, 145, 146). Indeed, investigations involving animal models of BTHS have significantly expanded the collective understanding of pathological metabolic alterations present in BTHS. Accordingly, defects in both ETC respiratory function and intermediary energy metabolism have been postulated as important contributors to cardiomyopathy development in this rare genetic disease (72, 81, 82, 89, 95, 106, 242). Impaired myocardial glucose oxidation appears to be a principal metabolic defect in the BTHS-affected heart. Unfortunately, pharmacological enhancement of cardiac glucose metabolism in BTHS failed to reverse adverse hypertrophic cardiac remodeling. Without correcting the impairments in ETC function, interventions that stimulate cardiac intermediary energy metabolism in BTHS may fail given that enhanced oxidation of fuel substrates may not translate into increased energy production. As such, metabolic therapeutic interventions may need to be provided in conjunction with therapies that stabilize ETC respiratory function (i.e., elamipretide) in order to be beneficial in BTHS.

Previous investigations regarding alterations in myocardial ketone body metabolism in diabetic cardiomyopathy have yielded contrasting results (118, 194, 195). From the results presented herein, the heart affected by T2D appears to shift away from the utilization of ketone bodies as an energy source, which may reflect an adaptive response although further investigation will be necessary to confirm this finding. Myocardial ketone body oxidation could also be modulated by maintenance on a ketogenic diet, whereby increased circulating levels of ketone bodies would enhance myocardial delivery and subsequent cardiac uptake. However, the ketogenic nutrient environment is also characterized by elevated circulating fatty acids, which would influence the overall effect of the dietary intervention on the myocardium. The ketogenic diet did not impair cardiac function in obese/prediabetic mice, however, given that myocardial lipid content was increased, it is possible that pathological molecular alterations were present, and that overt cardiac dysfunction would manifest with long-term administration of the dietary intervention.

In conclusion, although alterations of myocardial energy metabolism represent a shared feature of cardiomyopathies, modulation of intermediary metabolic pathways may not always represent a sufficient therapeutic approach, especially if downstream defects in oxidative phosphorylation are present. Further study of the mechanisms by which cardiac metabolic flexibility or energy production is impaired in various cardiomyopathies will help to ascertain whether therapies designed to target myocardial intermediary energy metabolism will be effective at mitigating cardiac dysfunction.

Bibliography

1. **McCartan C, Mason R, Jayasinghe SR, and Griffiths LR**. Cardiomyopathy classification: ongoing debate in the genomics era. *Biochem Res Int* 2012: 796926, 2012.

2. **Abelmann WH**. Classification and natural history of primary myocardial disease. *Prog Cardiovasc Dis* 27: 73-94, 1984.

3. **Maron BJ, Towbin JA, Thiene G, Antzelevitch C, Corrado D, Arnett D, Moss AJ, Seidman CE, Young JB, American Heart A, Council on Clinical Cardiology HF, Transplantation C, Quality of C, Outcomes R, Functional G, Translational Biology Interdisciplinary Working G, Council on E, and Prevention**. Contemporary definitions and classification of the cardiomyopathies: an American Heart Association Scientific Statement from the Council on Clinical Cardiology, Heart Failure and Transplantation Committee; Quality of Care and Outcomes Research and Functional Genomics and Translational Biology Interdisciplinary Working Groups; and Council on Epidemiology and Prevention. *Circulation* 113: 1807-1816, 2006.

4. **Elliott P**. The 2006 American Heart Association classification of cardiomyopathies is not the gold standard. *Circ Heart Fail* 1: 77-79; discussion 80, 2008.

5. **Maron BJ**. The 2006 American Heart Association classification of cardiomyopathies is the gold standard. *Circ Heart Fail* 1: 72-75; discussion 76, 2008.

6. **Elliott P, Andersson B, Arbustini E, Bilinska Z, Cecchi F, Charron P, Dubourg O, Kuhl U, Maisch B, McKenna WJ, Monserrat L, Pankuweit S, Rapezzi C, Seferovic P, Tavazzi L, and Keren A**. Classification of the cardiomyopathies: a position statement from the European Society Of Cardiology Working Group on Myocardial and Pericardial Diseases. *Eur Heart J* 29: 270-276, 2008.

7. **Braunwald E**. Cardiomyopathies: An Overview. *Circ Res* 121: 711-721, 2017.

8. **Marian AJ, and Braunwald E**. Hypertrophic Cardiomyopathy: Genetics, Pathogenesis, Clinical Manifestations, Diagnosis, and Therapy. *Circ Res* 121: 749-770, 2017.

9. **Corrado D, Basso C, and Judge DP**. Arrhythmogenic Cardiomyopathy. *Circ Res* 121: 784-802, 2017.

10. **Norman M, Simpson M, Mogensen J, Shaw A, Hughes S, Syrris P, Sen-Chowdhry S, Rowland E, Crosby A, and McKenna WJ**. Novel mutation in desmoplakin causes arrhythmogenic left ventricular cardiomyopathy. *Circulation* 112: 636-642, 2005.

11. **Muchtar E, Blauwet LA, and Gertz MA**. Restrictive Cardiomyopathy: Genetics, Pathogenesis, Clinical Manifestations, Diagnosis, and Therapy. *Circ Res* 121: 819-837, 2017.

12. **Maron BJ, Gardin JM, Flack JM, Gidding SS, Kurosaki TT, and Bild DE**. Prevalence of hypertrophic cardiomyopathy in a general population of young adults. Echocardiographic analysis of 4111 subjects in the CARDIA Study. Coronary Artery Risk Development in (Young) Adults. *Circulation* 92: 785-789, 1995.

13. **Semsarian C, Ingles J, Maron MS, and Maron BJ**. New perspectives on the prevalence of hypertrophic cardiomyopathy. *J Am Coll Cardiol* 65: 1249-1254, 2015.

14. **Hershberger RE, Hedges DJ, and Morales A**. Dilated cardiomyopathy: the complexity of a diverse genetic architecture. *Nat Rev Cardiol* 10: 531-547, 2013.

15. **Peters S, Trummel M, and Meyners W**. Prevalence of right ventricular dysplasia-cardiomyopathy in a non-referral hospital. *Int J Cardiol* 97: 499-501, 2004.

16. **McKenna WJ, Maron BJ, and Thiene G**. Classification, Epidemiology, and Global Burden of Cardiomyopathies. *Circ Res* 121: 722-730, 2017.

17. **Lopaschuk GD, and Ussher JR**. Evolving Concepts of Myocardial Energy Metabolism: More Than Just Fats and Carbohydrates. *Circ Res* 119: 1173-1176, 2016.

18. **Lopaschuk GD, Ussher JR, Folmes CD, Jaswal JS, and Stanley WC**. Myocardial fatty acid metabolism in health and disease. *Physiol Rev* 90: 207-258, 2010.

19. **Neubauer S**. The failing heart--an engine out of fuel. *N Engl J Med* 356: 1140-1151, 2007.

20. **Taha M, and Lopaschuk GD**. Alterations in energy metabolism in cardiomyopathies. *Ann Med* 39: 594-607, 2007.

21. **Ho KL, Karwi QG, Wagg C, Zhang L, Vo K, Altamimi T, Uddin GM, Ussher JR, and Lopaschuk GD**. Ketones can become the major fuel source for the heart but do not increase cardiac efficiency. *Cardiovasc Res* 2020.

22. **Teusink B, Voshol PJ, Dahlmans VE, Rensen PC, Pijl H, Romijn JA, and Havekes LM**. Contribution of fatty acids released from lipolysis of plasma triglycerides to total plasma fatty acid flux and tissue-specific fatty acid uptake. *Diabetes* 52: 614-620, 2003.

23. **Kuang M, Febbraio M, Wagg C, Lopaschuk GD, and Dyck JR**. Fatty acid translocase/CD36 deficiency does not energetically or functionally compromise hearts before or after ischemia. *Circulation* 109: 1550-1557, 2004.

24. **Luiken JJ, Turcotte LP, and Bonen A**. Protein-mediated palmitate uptake and expression of fatty acid transport proteins in heart giant vesicles. *J Lipid Res* 40: 1007-1016, 1999.

25. **Banke NH, Wende AR, Leone TC, O'Donnell JM, Abel ED, Kelly DP, and Lewandowski ED**. Preferential oxidation of triacylglyceride-derived fatty acids in heart is augmented by the nuclear receptor PPARalpha. *Circ Res* 107: 233-241, 2010.

26. **Shipp JC, Thomas JM, and Crevasse L**. Oxidation of Carbon-14-Labeled Endogenous Lipids by Isolated Perfused Rat Heart. *Science* 143: 371-373, 1964.

27. **Brownsey RW, Boone AN, and Allard MF**. Actions of insulin on the mammalian heart: metabolism, pathology and biochemical mechanisms. *Cardiovasc Res* 34: 3-24, 1997.

28. **Jaswal JS, Keung W, Wang W, Ussher JR, and Lopaschuk GD**. Targeting fatty acid and carbohydrate oxidation--a novel therapeutic intervention in the ischemic and failing heart. *Biochim Biophys Acta* 1813: 1333-1350, 2011.

29. **Patel MS, and Korotchkina LG**. Regulation of the pyruvate dehydrogenase complex. *Biochemical Society transactions* 34: 217-222, 2006.

30. **Patel MS, Nemeria NS, Furey W, and Jordan F**. The pyruvate dehydrogenase complexes: structure-based function and regulation. *J Biol Chem* 289: 16615-16623, 2014.

31. **Gopal K, Saleme B, Al Batran R, Aburasayn H, Eshreif A, Ho KL, Ma WK, Almutairi M, Eaton F, Gandhi M, Park EA, Sutendra G, and Ussher JR**. FoxO1 regulates myocardial glucose oxidation rates via transcriptional control of pyruvate dehydrogenase kinase 4 expression. *Am J Physiol Heart Circ Physiol* 313: H479-H490, 2017.

32. **Jing E, O'Neill BT, Rardin MJ, Kleinridders A, Ilkeyeva OR, Ussar S, Bain JR, Lee KY, Verdin EM, Newgard CB, Gibson BW, and Kahn CR**. Sirt3 regulates metabolic flexibility of skeletal muscle through reversible enzymatic deacetylation. *Diabetes* 62: 3404-3417, 2013.

33. **Denton RM**. Regulation of mitochondrial dehydrogenases by calcium ions. *Biochim Biophys Acta* 1787: 1309-1316, 2009.

34. **Suarez J, Cividini F, Scott BT, Lehmann K, Diaz-Juarez J, Diemer T, Dai A, Suarez JA, Jain M, and Dillmann WH**. Restoring mitochondrial calcium uniporter expression in diabetic

mouse heart improves mitochondrial calcium handling and cardiac function. *J Biol Chem* 293: 8182-8195, 2018.

35. **Ussher JR, Jaswal JS, and Lopaschuk GD**. Pyridine nucleotide regulation of cardiac intermediary metabolism. *Circ Res* 111: 628-641, 2012.

36. **Gupte SA, Levine RJ, Gupte RS, Young ME, Lionetti V, Labinskyy V, Floyd BC, Ojaimi C, Bellomo M, Wolin MS, and Recchia FA**. Glucose-6-phosphate dehydrogenase-derived NADPH fuels superoxide production in the failing heart. *J Mol Cell Cardiol* 41: 340-349, 2006.

37. **Shipp JC, Delcher HK, and Crevasse LE**. Glucose Metabolism by the Hexose Monophosphate Pathway in the Perfused Rat Heart. *Biochim Biophys Acta* 86: 399-402, 1964.

38. **Halestrap AP**. Pyruvate and ketone-body transport across the mitochondrial membrane. Exchange properties, pH-dependence and mechanism of the carrier. *Biochem J* 172: 377-387, 1978.

39. **Puchalska P, and Crawford PA**. Multi-dimensional Roles of Ketone Bodies in Fuel Metabolism, Signaling, and Therapeutics. *Cell Metab* 25: 262-284, 2017.

40. **Greenwell AA, Gopal K, and Ussher JR**. Myocardial Energy Metabolism in Non-ischemic Cardiomyopathy. *Front Physiol* 11: 570421, 2020.

41. **Karwi QG, and Lopaschuk GD**. Branched-Chain Amino Acid Metabolism in the Failing Heart. *Cardiovasc Drugs Ther* 2022.

42. **Lopaschuk GD, Karwi QG, Tian R, Wende AR, and Abel ED**. Cardiac Energy Metabolism in Heart Failure. *Circ Res* 128: 1487-1513, 2021.

43. **Neinast M, Murashige D, and Arany Z**. Branched Chain Amino Acids. *Annu Rev Physiol* 81: 139-164, 2019.

44. **Lu G, Sun H, She P, Youn JY, Warburton S, Ping P, Vondriska TM, Cai H, Lynch CJ, and Wang Y**. Protein phosphatase 2Cm is a critical regulator of branched-chain amino acid catabolism in mice and cultured cells. *J Clin Invest* 119: 1678-1687, 2009.

45. **Suryawan A, Hawes JW, Harris RA, Shimomura Y, Jenkins AE, and Hutson SM**. A molecular model of human branched-chain amino acid metabolism. *Am J Clin Nutr* 68: 72-81, 1998.

46. **Fillmore N, Wagg CS, Zhang L, Fukushima A, and Lopaschuk GD**. Cardiac branched-chain amino acid oxidation is reduced during insulin resistance in the heart. *Am J Physiol Endocrinol Metab* 315: E1046-E1052, 2018.

47. **Murashige D, Jang C, Neinast M, Edwards JJ, Cowan A, Hyman MC, Rabinowitz JD, Frankel DS, and Arany Z**. Comprehensive quantification of fuel use by the failing and nonfailing human heart. *Science* 370: 364-368, 2020.

48. **Shipp JC, Opie LH, and Challoner D**. Fatty Acid and Glucose Metabolism in the Perfused Heart. *Nature* 189: 1018-1019, 1961.

49. **Randle PJ, Garland PB, Hales CN, and Newsholme EA**. The glucose fatty-acid cycle. Its role in insulin sensitivity and the metabolic disturbances of diabetes mellitus. *Lancet* 1: 785-789, 1963.

50. **Buchanan J, Mazumder PK, Hu P, Chakrabarti G, Roberts MW, Yun UJ, Cooksey RC, Litwin SE, and Abel ED**. Reduced cardiac efficiency and altered substrate metabolism precedes the onset of hyperglycemia and contractile dysfunction in two mouse models of insulin resistance and obesity. *Endocrinology* 146: 5341-5349, 2005.

51. **Liu Q, Docherty JC, Rendell JC, Clanachan AS, and Lopaschuk GD**. High levels of fatty acids delay the recovery of intracellular pH and cardiac efficiency in post-ischemic hearts by inhibiting glucose oxidation. *J Am Coll Cardiol* 39: 718-725, 2002.

52. **Wisneski JA, Gertz EW, Neese RA, Gruenke LD, Morris DL, and Craig JC**. Metabolic fate of extracted glucose in normal human myocardium. *J Clin Invest* 76: 1819-1827, 1985.

53. **Wisneski JA, Stanley WC, Neese RA, and Gertz EW**. Effects of acute hyperglycemia on myocardial glycolytic activity in humans. *J Clin Invest* 85: 1648-1656, 1990.

54. **Barth PG, Scholte HR, Berden JA, Van der Klei-Van Moorsel JM, Luyt-Houwen IE, Van 't Veer-Korthof ET, Van der Harten JJ, and Sobotka-Plojhar MA**. An X-linked mitochondrial disease affecting cardiac muscle, skeletal muscle and neutrophil leucocytes. *J Neurol Sci* 62: 327-355, 1983.

55. **Taylor C, Rao ES, Pierre G, Chronopoulou E, Hornby B, Heyman A, and Vernon HJ**. Clinical presentation and natural history of Barth Syndrome: An overview. *J Inherit Metab Dis* 45: 7-16, 2022.

56. **Finsterer J**. Barth syndrome: mechanisms and management. *Appl Clin Genet* 12: 95-106, 2019.

57. **Kang SL, Forsey J, Dudley D, Steward CG, and Tsai-Goodman B**. Clinical Characteristics and Outcomes of Cardiomyopathy in Barth Syndrome: The UK Experience. *Pediatr Cardiol* 37: 167-176, 2016.

58. **Roberts AE, Nixon C, Steward CG, Gauvreau K, Maisenbacher M, Fletcher M, Geva J, Byrne BJ, and Spencer CT**. The Barth Syndrome Registry: distinguishing disease characteristics and growth data from a longitudinal study. *Am J Med Genet A* 158A: 2726-2732, 2012.

59. **Johnston J, Kelley RI, Feigenbaum A, Cox GF, Iyer GS, Funanage VL, and Proujansky R**. Mutation characterization and genotype-phenotype correlation in Barth syndrome. *Am J Hum Genet* 61: 1053-1058, 1997.

60. **Reid Thompson W, Hornby B, Manuel R, Bradley E, Laux J, Carr J, and Vernon HJ**. A phase 2/3 randomized clinical trial followed by an open-label extension to evaluate the effectiveness of elamipretide in Barth syndrome, a genetic disorder of mitochondrial cardiolipin metabolism. *Genet Med* 23: 471-478, 2021.

61. **Rigaud C, Lebre AS, Touraine R, Beaupain B, Ottolenghi C, Chabli A, Ansquer H, Ozsahin H, Di Filippo S, De Lonlay P, Borm B, Rivier F, Vaillant MC, Mathieu-Dramard M, Goldenberg A, Viot G, Charron P, Rio M, Bonnet D, and Donadieu J**. Natural history of Barth syndrome: a national cohort study of 22 patients. *Orphanet J Rare Dis* 8: 70, 2013.

62. **Ades LC, Gedeon AK, Wilson MJ, Latham M, Partington MW, Mulley JC, Nelson J, Lui K, and Sillence DO**. Barth syndrome: clinical features and confirmation of gene localisation to distal Xq28. *Am J Med Genet* 45: 327-334, 1993.

63. **Spencer CT, Bryant RM, Day J, Gonzalez IL, Colan SD, Thompson WR, Berthy J, Redfearn SP, and Byrne BJ**. Cardiac and clinical phenotype in Barth syndrome. *Pediatrics* 118: e337-346, 2006.

64. **Hanke SP, Gardner AB, Lombardi JP, Manning PB, Nelson DP, Towbin JA, Jefferies JL, and Lorts A**. Left ventricular noncompaction cardiomyopathy in Barth syndrome: an example of an undulating cardiac phenotype necessitating mechanical circulatory support as a bridge to transplantation. *Pediatr Cardiol* 33: 1430-1434, 2012.

65. **Pignatelli RH, McMahon CJ, Dreyer WJ, Denfield SW, Price J, Belmont JW, Craigen WJ, Wu J, El Said H, Bezold LI, Clunie S, Fernbach S, Bowles NE, and Towbin JA**. Clinical

characterization of left ventricular noncompaction in children: a relatively common form of cardiomyopathy. *Circulation* 108: 2672-2678, 2003.

66. **Garlid AO, Schaffer CT, Kim J, Bhatt H, Guevara-Gonzalez V, and Ping P**. TAZ encodes tafazzin, a transacylase essential for cardiolipin formation and central to the etiology of Barth syndrome. *Gene* 726: 144148, 2020.

67. **Gaspard GJ, and McMaster CR**. Cardiolipin metabolism and its causal role in the etiology of the inherited cardiomyopathy Barth syndrome. *Chem Phys Lipids* 193: 1-10, 2015.

68. **McMillin JB, and Dowhan W**. Cardiolipin and apoptosis. *Biochim Biophys Acta* 1585: 97-107, 2002.

69. **Shen Z, Li Y, Gasparski AN, Abeliovich H, and Greenberg ML**. Cardiolipin Regulates Mitophagy through the Protein Kinase C Pathway. *J Biol Chem* 292: 2916-2923, 2017.

70. **Oemer G, Koch J, Wohlfarter Y, Alam MT, Lackner K, Sailer S, Neumann L, Lindner HH, Watschinger K, Haltmeier M, Werner ER, Zschocke J, and Keller MA**. Phospholipid Acyl Chain Diversity Controls the Tissue-Specific Assembly of Mitochondrial Cardiolipins. *Cell Rep* 30: 4281-4291 e4284, 2020.

71. **Sparagna GC, Chicco AJ, Murphy RC, Bristow MR, Johnson CA, Rees ML, Maxey ML, McCune SA, and Moore RL**. Loss of cardiac tetralinoleoyl cardiolipin in human and experimental heart failure. *J Lipid Res* 48: 1559-1570, 2007.

72. **Dudek J, and Maack C**. Mechano-energetic aspects of Barth syndrome. *J Inherit Metab Dis* 45: 82-98, 2022.

73. **Schlame M, Towbin JA, Heerdt PM, Jehle R, DiMauro S, and Blanck TJ**. Deficiency of tetralinoleoyl-cardiolipin in Barth syndrome. *Ann Neurol* 51: 634-637, 2002.

74. **Valianpour F, Mitsakos V, Schlemmer D, Towbin JA, Taylor JM, Ekert PG, Thorburn DR, Munnich A, Wanders RJ, Barth PG, and Vaz FM**. Monolysocardiolipins accumulate in Barth syndrome but do not lead to enhanced apoptosis. *J Lipid Res* 46: 1182-1195, 2005.

75. **Houtkooper RH, Rodenburg RJ, Thiels C, van Lenthe H, Stet F, Poll-The BT, Stone JE, Steward CG, Wanders RJ, Smeitink J, Kulik W, and Vaz FM**. Cardiolipin and monolysocardiolipin analysis in fibroblasts, lymphocytes, and tissues using high-performance liquid chromatography-mass spectrometry as a diagnostic test for Barth syndrome. *Anal Biochem* 387: 230-237, 2009.

76. **Cade WT, Laforest R, Bohnert KL, Reeds DN, Bittel AJ, de Las Fuentes L, Bashir A, Woodard PK, Pacak CA, Byrne BJ, Gropler RJ, and Peterson LR**. Myocardial glucose and fatty acid metabolism is altered and associated with lower cardiac function in young adults with Barth syndrome. *J Nucl Cardiol* 28: 1649-1659, 2021.

77. **Wang G, McCain ML, Yang L, He A, Pasqualini FS, Agarwal A, Yuan H, Jiang D, Zhang D, Zangi L, Geva J, Roberts AE, Ma Q, Ding J, Chen J, Wang DZ, Li K, Wang J, Wanders RJ, Kulik W, Vaz FM, Laflamme MA, Murry CE, Chien KR, Kelley RI, Church GM, Parker KK, and Pu WT**. Modeling the mitochondrial cardiomyopathy of Barth syndrome with induced pluripotent stem cell and heart-on-chip technologies. *Nat Med* 20: 616-623, 2014.

78. **Bashir A, Bohnert KL, Reeds DN, Peterson LR, Bittel AJ, de Las Fuentes L, Pacak CA, Byrne BJ, and Cade WT**. Impaired cardiac and skeletal muscle bioenergetics in children, adolescents, and young adults with Barth syndrome. *Physiol Rep* 5: 2017.

79. **Huang Y, Powers C, Madala SK, Greis KD, Haffey WD, Towbin JA, Purevjav E, Javadov S, Strauss AW, and Khuchua Z**. Cardiac metabolic pathways affected in the mouse model of barth syndrome. *PLoS One* 10: e0128561, 2015.

80. **Greenwell AA, Gopal K, Altamimi TR, Saed CT, Wang F, Tabatabaei Dakhili SA, Ho KL, Zhang L, Eaton F, Kruger J, Al Batran R, Lopaschuk GD, Oudit GY, and Ussher JR**. Barth syndrome-related cardiomyopathy is associated with a reduction in myocardial glucose oxidation. *Am J Physiol Heart Circ Physiol* 320: H2255-H2269, 2021.

81. **Kiebish MA, Yang K, Liu X, Mancuso DJ, Guan S, Zhao Z, Sims HF, Cerqua R, Cade WT, Han X, and Gross RW**. Dysfunctional cardiac mitochondrial bioenergetic, lipidomic, and signaling in a murine model of Barth syndrome. *J Lipid Res* 54: 1312-1325, 2013.

82. **Le CH, Benage LG, Specht KS, Li Puma LC, Mulligan CM, Heuberger AL, Prenni JE, Claypool SM, Chatfield KC, Sparagna GC, and Chicco AJ**. Tafazzin deficiency impairs CoA-dependent oxidative metabolism in cardiac mitochondria. *J Biol Chem* 295: 12485-12497, 2020.

83. **Powers C, Huang Y, Strauss A, and Khuchua Z**. Diminished Exercise Capacity and Mitochondrial bc1 Complex Deficiency in Tafazzin-Knockdown Mice. *Front Physiol* 4: 74, 2013.

84. **Xu Y, Erdjument-Bromage H, Phoon CKL, Neubert TA, Ren M, and Schlame M**. Cardiolipin remodeling enables protein crowding in the inner mitochondrial membrane. *EMBO J* 40: e108428, 2021.

85. **Xu Y, Phoon CKL, Ren M, and Schlame M**. A simple mechanistic explanation for Barth syndrome and cardiolipin remodeling. *J Inherit Metab Dis* 45: 51-59, 2022.

86. **Chatfield KC, Sparagna GC, Specht KS, Whitcomb LA, Omar AK, Miyamoto SD, Wolfe LM, and Chicco AJ**. Long-chain fatty acid oxidation and respiratory complex I deficiencies distinguish Barth Syndrome from idiopathic pediatric cardiomyopathy. *J Inherit Metab Dis* 45: 111-124, 2022.

87. **McKenzie M, Lazarou M, Thorburn DR, and Ryan MT**. Mitochondrial respiratory chain supercomplexes are destabilized in Barth Syndrome patients. *J Mol Biol* 361: 462-469, 2006.

88. **Chatzispyrou IA, Guerrero-Castillo S, Held NM, Ruiter JPN, Denis SW, L IJ, Wanders RJ, van Weeghel M, Ferdinandusse S, Vaz FM, Brandt U, and Houtkooper RH**. Barth syndrome cells display widespread remodeling of mitochondrial complexes without affecting metabolic flux distribution. *Biochim Biophys Acta Mol Basis Dis* 1864: 3650-3658, 2018.

89. **Dudek J, Cheng IF, Balleininger M, Vaz FM, Streckfuss-Bomeke K, Hubscher D, Vukotic M, Wanders RJ, Rehling P, and Guan K**. Cardiolipin deficiency affects respiratory chain function and organization in an induced pluripotent stem cell model of Barth syndrome. *Stem Cell Res* 11: 806-819, 2013.

90. **Mejia EM, Cole LK, and Hatch GM**. Cardiolipin metabolism and the role it plays in heart failure and mitochondrial supercomplex formation. *Cardiovasc Hematol Disord Drug Targets* 14: 98-106, 2014.

91. **Zhu S, Chen Z, Zhu M, Shen Y, Leon LJ, Chi L, Spinozzi S, Tan C, Gu Y, Nguyen A, Zhou Y, Feng W, Vaz FM, Wang X, Gustafsson AB, Evans SM, Kunfu O, and Fang X**. Cardiolipin Remodeling Defects Impair Mitochondrial Architecture and Function in a Murine Model of Barth Syndrome Cardiomyopathy. *Circ Heart Fail* 14: e008289, 2021.

92. **Pfeiffer K, Gohil V, Stuart RA, Hunte C, Brandt U, Greenberg ML, and Schagger H**. Cardiolipin stabilizes respiratory chain supercomplexes. *J Biol Chem* 278: 52873-52880, 2003.

93. **Vercellino I, and Sazanov LA**. The assembly, regulation and function of the mitochondrial respiratory chain. *Nat Rev Mol Cell Biol* 23: 141-161, 2022.

94. **Dudek J, and Maack C**. Barth syndrome cardiomyopathy. *Cardiovasc Res* 113: 399-410, 2017.

95. **Dudek J, Cheng IF, Chowdhury A, Wozny K, Balleininger M, Reinhold R, Grunau S, Callegari S, Toischer K, Wanders RJ, Hasenfuss G, Brugger B, Guan K, and Rehling P**.

Cardiac-specific succinate dehydrogenase deficiency in Barth syndrome. *EMBO Mol Med* 8: 139-154, 2016.

96. **Eaton S, Bursby T, Middleton B, Pourfarzam M, Mills K, Johnson AW, and Bartlett K**. The mitochondrial trifunctional protein: centre of a beta-oxidation metabolon? *Biochemical Society transactions* 28: 177-182, 2000.

97. **Taegtmeyer H, Young ME, Lopaschuk GD, Abel ED, Brunengraber H, Darley-Usmar V, Des Rosiers C, Gerszten R, Glatz JF, Griffin JL, Gropler RJ, Holzhuetter HG, Kizer JR, Lewandowski ED, Malloy CR, Neubauer S, Peterson LR, Portman MA, Recchia FA, Van Eyk JE, Wang TJ, and American Heart Association Council on Basic Cardiovascular S**. Assessing Cardiac Metabolism: A Scientific Statement From the American Heart Association. *Circ Res* 118: 1659-1701, 2016.

98. **Dabner L, Pieles GE, Steward CG, Hamilton-Shield JP, Ness AR, Rogers CA, Bucciarelli-Ducci C, Greenwood R, Ellis L, Sheehan K, and Reeves BC**. Treatment of Barth Syndrome by Cardiolipin Manipulation (CARDIOMAN) With Bezafibrate: Protocol for a Randomized Placebo-Controlled Pilot Trial Conducted in the Nationally Commissioned Barth Syndrome Service. *JMIR Res Protoc* 10: e22533, 2021.

99. **Khuchua Z, Glukhov AI, Strauss AW, and Javadov S**. Elucidating the Beneficial Role of PPAR Agonists in Cardiac Diseases. *Int J Mol Sci* 19: 2018.

100. **Schafer C, Moore V, Dasgupta N, Javadov S, James JF, Glukhov AI, Strauss AW, and Khuchua Z**. The Effects of PPAR Stimulation on Cardiac Metabolic Pathways in Barth Syndrome Mice. *Front Pharmacol* 9: 318, 2018.

101. **Aasum E, Khalid AM, Gudbrandsen OA, How OJ, Berge RK, and Larsen TS**. Fenofibrate modulates cardiac and hepatic metabolism and increases ischemic tolerance in diet-induced obese mice. *J Mol Cell Cardiol* 44: 201-209, 2008.

102. **Gopal K, Al Batran R, Altamimi TR, Greenwell AA, Saed CT, Tabatabaei Dakhili SA, Dimaano MTE, Zhang Y, Eaton F, Sutendra G, and Ussher JR**. FoxO1 inhibition alleviates type 2 diabetes-related diastolic dysfunction by increasing myocardial pyruvate dehydrogenase activity. *Cell Rep* 35: 108935, 2021.

103. **Masoud WG, Ussher JR, Wang W, Jaswal JS, Wagg CS, Dyck JR, Lygate CA, Neubauer S, Clanachan AS, and Lopaschuk GD**. Failing mouse hearts utilize energy

inefficiently and benefit from improved coupling of glycolysis and glucose oxidation. *Cardiovasc Res* 101: 30-38, 2014.

104. **Ussher JR, Wang W, Gandhi M, Keung W, Samokhvalov V, Oka T, Wagg CS, Jaswal JS, Harris RA, Clanachan AS, Dyck JR, and Lopaschuk GD**. Stimulation of glucose oxidation protects against acute myocardial infarction and reperfusion injury. *Cardiovasc Res* 94: 359-369, 2012.

105. **Ferri L, Donati MA, Funghini S, Malvagia S, Catarzi S, Lugli L, Ragni L, Bertini E, Vaz FM, Cooper DN, Guerrini R, and Morrone A**. New clinical and molecular insights on Barth syndrome. *Orphanet J Rare Dis* 8: 27, 2013.

106. **Li Y, Lou W, Raja V, Denis S, Yu W, Schmidtke MW, Reynolds CA, Schlame M, Houtkooper RH, and Greenberg ML**. Cardiolipin-induced activation of pyruvate dehydrogenase links mitochondrial lipid biosynthesis to TCA cycle function. *J Biol Chem* 294: 11568-11578, 2019.

107. **Ghosh S, Zulkifli M, Joshi A, Venkatesan M, Cristel A, Vishnu N, Madesh M, and Gohil VM**. MCU-complex-mediated mitochondrial calcium signaling is impaired in Barth syndrome. *Hum Mol Genet* 31: 376-385, 2022.

108. **Bertero E, Nickel A, Kohlhaas M, Hohl M, Sequeira V, Brune C, Schwemmlein J, Abesser M, Schuh K, Kutschka I, Carlein C, Munker K, Atighetchi S, Muller A, Kazakov A, Kappl R, von der Malsburg K, van der Laan M, Schiuma AF, Bohm M, Laufs U, Hoth M, Rehling P, Kuhn M, Dudek J, von der Malsburg A, Prates Roma L, and Maack C**. Loss of Mitochondrial Ca(2+) Uniporter Limits Inotropic Reserve and Provides Trigger and Substrate for Arrhythmias in Barth Syndrome Cardiomyopathy. *Circulation* 144: 1694-1713, 2021.

109. **Gopal K, Almutairi M, Al Batran R, Eaton F, Gandhi M, and Ussher JR**. Cardiac-Specific Deletion of Pyruvate Dehydrogenase Impairs Glucose Oxidation Rates and Induces Diastolic Dysfunction. *Front Cardiovasc Med* 5: 17, 2018.

110. **Almutairi M, Gopal K, Greenwell AA, Young A, Gill R, Aburasayn H, Al Batran R, Chahade JJ, Gandhi M, Eaton F, Mailloux RJ, and Ussher JR**. The GLP-1 Receptor Agonist Liraglutide Increases Myocardial Glucose Oxidation Rates via Indirect Mechanisms and Mitigates Experimental Diabetic Cardiomyopathy. *Can J Cardiol* 37: 140-150, 2021.

111. **Kato T, Niizuma S, Inuzuka Y, Kawashima T, Okuda J, Tamaki Y, Iwanaga Y, Narazaki M, Matsuda T, Soga T, Kita T, Kimura T, and Shioi T**. Analysis of metabolic

remodeling in compensated left ventricular hypertrophy and heart failure. *Circ Heart Fail* 3: 420-430, 2010.

112. **Le Page LM, Rider OJ, Lewis AJ, Ball V, Clarke K, Johansson E, Carr CA, Heather LC, and Tyler DJ**. Increasing Pyruvate Dehydrogenase Flux as a Treatment for Diabetic Cardiomyopathy: A Combined 13C Hyperpolarized Magnetic Resonance and Echocardiography Study. *Diabetes* 64: 2735-2743, 2015.

113. **Aubert G, Martin OJ, Horton JL, Lai L, Vega RB, Leone TC, Koves T, Gardell SJ, Kruger M, Hoppel CL, Lewandowski ED, Crawford PA, Muoio DM, and Kelly DP**. The Failing Heart Relies on Ketone Bodies as a Fuel. *Circulation* 133: 698-705, 2016.

114. **Ussher JR, Elmariah S, Gerszten RE, and Dyck JR**. The Emerging Role of Metabolomics in the Diagnosis and Prognosis of Cardiovascular Disease. *J Am Coll Cardiol* 68: 2850-2870, 2016.

115. **Sandlers Y, Mercier K, Pathmasiri W, Carlson J, McRitchie S, Sumner S, and Vernon HJ**. Metabolomics Reveals New Mechanisms for Pathogenesis in Barth Syndrome and Introduces Novel Roles for Cardiolipin in Cellular Function. *PLoS One* 11: e0151802, 2016.

116. **Lopaschuk GD, and Verma S**. Mechanisms of Cardiovascular Benefits of Sodium Glucose Co-Transporter 2 (SGLT2) Inhibitors: A State-of-the-Art Review. *JACC Basic Transl Sci* 5: 632-644, 2020.

117. **Santos-Gallego CG, Requena-Ibanez JA, San Antonio R, Ishikawa K, Watanabe S, Picatoste B, Flores E, Garcia-Ropero A, Sanz J, Hajjar RJ, Fuster V, and Badimon JJ**. Empagliflozin Ameliorates Adverse Left Ventricular Remodeling in Nondiabetic Heart Failure by Enhancing Myocardial Energetics. *J Am Coll Cardiol* 73: 1931-1944, 2019.

118. **Verma S, Rawat S, Ho KL, Wagg CS, Zhang L, Teoh H, Dyck JE, Uddin GM, Oudit GY, Mayoux E, Lehrke M, Marx N, and Lopaschuk GD**. Empagliflozin Increases Cardiac Energy Production in Diabetes: Novel Translational Insights Into the Heart Failure Benefits of SGLT2 Inhibitors. *JACC Basic Transl Sci* 3: 575-587, 2018.

119. **Sumegi B, and Srere PA**. Binding of the enzymes of fatty acid beta-oxidation and some related enzymes to pig heart inner mitochondrial membrane. *J Biol Chem* 259: 8748-8752, 1984.

120. **Robinson AM, and Williamson DH**. Physiological roles of ketone bodies as substrates and signals in mammalian tissues. *Physiol Rev* 60: 143-187, 1980.

121. **Lu M, Zhou L, Stanley WC, Cabrera ME, Saidel GM, and Yu X**. Role of the malate-aspartate shuttle on the metabolic response to myocardial ischemia. *J Theor Biol* 254: 466-475, 2008.

122. **Shah SH, Kraus WE, and Newgard CB**. Metabolomic profiling for the identification of novel biomarkers and mechanisms related to common cardiovascular diseases: form and function. *Circulation* 126: 1110-1120, 2012.

123. **Walejko JM, Christopher BA, Crown SB, Zhang GF, Pickar-Oliver A, Yoneshiro T, Foster MW, Page S, van Vliet S, Ilkayeva O, Muehlbauer MJ, Carson MW, Brozinick JT, Hammond CD, Gimeno RE, Moseley MA, Kajimura S, Gersbach CA, Newgard CB, White PJ, and McGarrah RW**. Branched-chain alpha-ketoacids are preferentially reaminated and activate protein synthesis in the heart. *Nat Commun* 12: 1680, 2021.

124. **Cade WT, Spencer CT, Reeds DN, Waggoner AD, O'Connor R, Maisenbacher M, Crowley JR, Byrne BJ, and Peterson LR**. Substrate metabolism during basal and hyperinsulinemic conditions in adolescents and young-adults with Barth syndrome. *J Inherit Metab Dis* 36: 91-101, 2013.

125. **Jefferies JL**. Barth syndrome. *Am J Med Genet C Semin Med Genet* 163C: 198-205, 2013.

126. **Greenwell AA, Tabatabaei Dakhili SA, and Ussher JR**. Myocardial disturbances of intermediary metabolism in Barth syndrome. *Front Cardiovasc Med* 9: 981972, 2022.

127. **Rubler S, Dlugash J, Yuceoglu YZ, Kumral T, Branwood AW, and Grishman A**. New type of cardiomyopathy associated with diabetic glomerulosclerosis. *Am J Cardiol* 30: 595-602, 1972.

128. **Kannel WB, Hjortland M, and Castelli WP**. Role of diabetes in congestive heart failure: the Framingham study. *Am J Cardiol* 34: 29-34, 1974.

129. **Kannel WB, and McGee DL**. Diabetes and glucose tolerance as risk factors for cardiovascular disease: the Framingham study. *Diabetes Care* 2: 120-126, 1979.

130. **MacDonald MR, Petrie MC, Varyani F, Ostergren J, Michelson EL, Young JB, Solomon SD, Granger CB, Swedberg K, Yusuf S, Pfeffer MA, McMurray JJ, and Investigators C**. Impact of diabetes on outcomes in patients with low and preserved ejection fraction heart failure: an analysis of the Candesartan in Heart failure: Assessment of Reduction in Mortality and morbidity (CHARM) programme. *Eur Heart J* 29: 1377-1385, 2008.

131. **Iribarren C, Karter AJ, Go AS, Ferrara A, Liu JY, Sidney S, and Selby JV**. Glycemic control and heart failure among adult patients with diabetes. *Circulation* 103: 2668-2673, 2001.

132. **Lind M, Bounias I, Olsson M, Gudbjornsdottir S, Svensson AM, and Rosengren A**. Glycaemic control and incidence of heart failure in 20,985 patients with type 1 diabetes: an observational study. *Lancet* 378: 140-146, 2011.

133. **Castagno D, Baird-Gunning J, Jhund PS, Biondi-Zoccai G, MacDonald MR, Petrie MC, Gaita F, and McMurray JJ**. Intensive glycemic control has no impact on the risk of heart failure in type 2 diabetic patients: evidence from a 37,229 patient meta-analysis. *Am Heart J* 162: 938-948 e932, 2011.

134. **Control G, Turnbull FM, Abraira C, Anderson RJ, Byington RP, Chalmers JP, Duckworth WC, Evans GW, Gerstein HC, Holman RR, Moritz TE, Neal BC, Ninomiya T, Patel AA, Paul SK, Travert F, and Woodward M**. Intensive glucose control and macrovascular outcomes in type 2 diabetes. *Diabetologia* 52: 2288-2298, 2009.

135. **Gilbert RE, and Krum H**. Heart failure in diabetes: effects of anti-hyperglycaemic drug therapy. *Lancet* 385: 2107-2117, 2015.

136. **Di Cori A, Di Bello V, Miccoli R, Talini E, Palagi C, Delle Donne MG, Penno G, Nardi C, Bianchi C, Mariani M, Del Prato S, and Balbarini A**. Left ventricular function in normotensive young adults with well-controlled type 1 diabetes mellitus. *Am J Cardiol* 99: 84-90, 2007.

137. **Diamant M, Lamb HJ, Groeneveld Y, Endert EL, Smit JW, Bax JJ, Romijn JA, de Roos A, and Radder JK**. Diastolic dysfunction is associated with altered myocardial metabolism in asymptomatic normotensive patients with well-controlled type 2 diabetes mellitus. *J Am Coll Cardiol* 42: 328-335, 2003.

138. **Poirier P, Bogaty P, Garneau C, Marois L, and Dumesnil JG**. Diastolic dysfunction in normotensive men with well-controlled type 2 diabetes: importance of maneuvers in echocardiographic screening for preclinical diabetic cardiomyopathy. *Diabetes Care* 24: 5-10, 2001.

139. **Boyer JK, Thanigaraj S, Schechtman KB, and Perez JE**. Prevalence of ventricular diastolic dysfunction in asymptomatic, normotensive patients with diabetes mellitus. *Am J Cardiol* 93: 870-875, 2004.

140. **Devereux RB, Roman MJ, Paranicas M, O'Grady MJ, Lee ET, Welty TK, Fabsitz RR, Robbins D, Rhoades ER, and Howard BV**. Impact of diabetes on cardiac structure and function: the strong heart study. *Circulation* 101: 2271-2276, 2000.

141. **Galderisi M**. Diastolic dysfunction and diabetic cardiomyopathy: evaluation by Doppler echocardiography. *J Am Coll Cardiol* 48: 1548-1551, 2006.

142. **Liu X, Yang ZG, Gao Y, Xie LJ, Jiang L, Hu BY, Diao KY, Shi K, Xu HY, Shen MT, Ren Y, and Guo YK**. Left ventricular subclinical myocardial dysfunction in uncomplicated type 2 diabetes mellitus is associated with impaired myocardial perfusion: a contrast-enhanced cardiovascular magnetic resonance study. *Cardiovasc Diabetol* 17: 139, 2018.

143. **Zabalgoitia M, Ismaeil MF, Anderson L, and Maklady FA**. Prevalence of diastolic dysfunction in normotensive, asymptomatic patients with well-controlled type 2 diabetes mellitus. *Am J Cardiol* 87: 320-323, 2001.

144. **Holscher ME, Bode C, and Bugger H**. Diabetic Cardiomyopathy: Does the Type of Diabetes Matter? *Int J Mol Sci* 17: 2016.

145. **Jia G, Hill MA, and Sowers JR**. Diabetic Cardiomyopathy: An Update of Mechanisms Contributing to This Clinical Entity. *Circ Res* 122: 624-638, 2018.

146. **Ritchie RH, and Abel ED**. Basic Mechanisms of Diabetic Heart Disease. *Circ Res* 126: 1501-1525, 2020.

147. **Ho KL, Karwi QG, Connolly D, Pherwani S, Ketema EB, Ussher JR, and Lopaschuk GD**. Metabolic, structural and biochemical changes in diabetes and the development of heart failure. *Diabetologia* 65: 411-423, 2022.

148. **Huynh K, Kiriazis H, Du XJ, Love JE, Jandeleit-Dahm KA, Forbes JM, McMullen JR, and Ritchie RH**. Coenzyme Q10 attenuates diastolic dysfunction, cardiomyocyte hypertrophy and cardiac fibrosis in the db/db mouse model of type 2 diabetes. *Diabetologia* 55: 1544-1553, 2012.

149. **Kawaguchi M, Techigawara M, Ishihata T, Asakura T, Saito F, Maehara K, and Maruyama Y**. A comparison of ultrastructural changes on endomyocardial biopsy specimens obtained from patients with diabetes mellitus with and without hypertension. *Heart Vessels* 12: 267-274, 1997.

150. **Seferovic PM, and Paulus WJ**. Clinical diabetic cardiomyopathy: a two-faced disease with restrictive and dilated phenotypes. *Eur Heart J* 36: 1718-1727, 1727a-1727c, 2015.

151. **Ernande L, Rietzschel ER, Bergerot C, De Buyzere ML, Schnell F, Groisne L, Ovize M, Croisille P, Moulin P, Gillebert TC, and Derumeaux G**. Impaired myocardial radial function in asymptomatic patients with type 2 diabetes mellitus: a speckle-tracking imaging study. *J Am Soc Echocardiogr* 23: 1266-1272, 2010.

152. **Ng ACT, Bertini M, Ewe SH, van der Velde ET, Leung DY, Delgado V, and Bax JJ**. Defining Subclinical Myocardial Dysfunction and Implications for Patients With Diabetes Mellitus and Preserved Ejection Fraction. *Am J Cardiol* 124: 892-898, 2019.

153. **An D, and Rodrigues B**. Role of changes in cardiac metabolism in development of diabetic cardiomyopathy. *Am J Physiol Heart Circ Physiol* 291: H1489-1506, 2006.

154. **Karwi QG, Ho KL, Pherwani S, Ketema EB, Sun Q, and Lopaschuk GD**. Concurrent diabetes and heart failure: interplay and novel therapeutic approaches. *Cardiovasc Res* 118: 686-715, 2022.

155. **Gopal K, Chahade JJ, Kim R, and Ussher JR**. The Impact of Antidiabetic Therapies on Diastolic Dysfunction and Diabetic Cardiomyopathy. *Front Physiol* 11: 603247, 2020.

156. **Karwi QG, Uddin GM, Ho KL, and Lopaschuk GD**. Loss of Metabolic Flexibility in the Failing Heart. *Front Cardiovasc Med* 5: 68, 2018.

157. **Aasum E, Hafstad AD, Severson DL, and Larsen TS**. Age-dependent changes in metabolism, contractile function, and ischemic sensitivity in hearts from db/db mice. *Diabetes* 52: 434-441, 2003.

158. **Peterson LR, Herrero P, Schechtman KB, Racette SB, Waggoner AD, Kisrieva-Ware Z, Dence C, Klein S, Marsala J, Meyer T, and Gropler RJ**. Effect of obesity and insulin resistance on myocardial substrate metabolism and efficiency in young women. *Circulation* 109: 2191-2196, 2004.

159. **Boudina S, Sena S, Theobald H, Sheng X, Wright JJ, Hu XX, Aziz S, Johnson JI, Bugger H, Zaha VG, and Abel ED**. Mitochondrial energetics in the heart in obesity-related diabetes: direct evidence for increased uncoupled respiration and activation of uncoupling proteins. *Diabetes* 56: 2457-2466, 2007.

160. **How OJ, Aasum E, Severson DL, Chan WY, Essop MF, and Larsen TS**. Increased myocardial oxygen consumption reduces cardiac efficiency in diabetic mice. *Diabetes* 55: 466-473, 2006.

161. **Wright JJ, Kim J, Buchanan J, Boudina S, Sena S, Bakirtzi K, Ilkun O, Theobald HA, Cooksey RC, Kandror KV, and Abel ED**. Mechanisms for increased myocardial fatty acid utilization following short-term high-fat feeding. *Cardiovasc Res* 82: 351-360, 2009.

162. **Zhang L, Ussher JR, Oka T, Cadete VJ, Wagg C, and Lopaschuk GD**. Cardiac diacylglycerol accumulation in high fat-fed mice is associated with impaired insulin-stimulated glucose oxidation. *Cardiovasc Res* 89: 148-156, 2011.

163. **Basu R, Oudit GY, Wang X, Zhang L, Ussher JR, Lopaschuk GD, and Kassiri Z**. Type 1 diabetic cardiomyopathy in the Akita (Ins2WT/C96Y) mouse model is characterized by lipotoxicity and diastolic dysfunction with preserved systolic function. *Am J Physiol Heart Circ Physiol* 297: H2096-2108, 2009.

164. **Sakamoto J, Barr RL, Kavanagh KM, and Lopaschuk GD**. Contribution of malonyl-CoA decarboxylase to the high fatty acid oxidation rates seen in the diabetic heart. *Am J Physiol Heart Circ Physiol* 278: H1196-1204, 2000.

165. **Herrero P, Peterson LR, McGill JB, Matthew S, Lesniak D, Dence C, and Gropler RJ**. Increased myocardial fatty acid metabolism in patients with type 1 diabetes mellitus. *J Am Coll Cardiol* 47: 598-604, 2006.

166. **Rijzewijk LJ, van der Meer RW, Lamb HJ, de Jong HW, Lubberink M, Romijn JA, Bax JJ, de Roos A, Twisk JW, Heine RJ, Lammertsma AA, Smit JW, and Diamant M**. Altered myocardial substrate metabolism and decreased diastolic function in nonischemic human diabetic cardiomyopathy: studies with cardiac positron emission tomography and magnetic resonance imaging. *J Am Coll Cardiol* 54: 1524-1532, 2009.

167. **Saddik M, and Lopaschuk GD**. Triacylglycerol turnover in isolated working hearts of acutely diabetic rats. *Can J Physiol Pharmacol* 72: 1110-1119, 1994.

168. **Bucci M, Borra R, Nagren K, Parkka JP, Del Ry S, Maggio R, Tuunanen H, Viljanen T, Cabiati M, Rigazio S, Taittonen M, Pagotto U, Parkkola R, Opie LH, Nuutila P, Knuuti J, and Iozzo P**. Trimetazidine reduces endogenous free fatty acid oxidation and improves myocardial efficiency in obese humans. *Cardiovasc Ther* 30: 333-341, 2012.

169. **Kim MS, Wang F, Puthanveetil P, Kewalramani G, Hosseini-Beheshti E, Ng N, Wang Y, Kumar U, Innis S, Proud CG, Abrahani A, and Rodrigues B**. Protein kinase D is a key regulator of cardiomyocyte lipoprotein lipase secretion after diabetes. *Circ Res* 103: 252-260, 2008.

170. **Pulinilkunnil T, and Rodrigues B**. Cardiac lipoprotein lipase: metabolic basis for diabetic heart disease. *Cardiovasc Res* 69: 329-340, 2006.

171. **Luiken JJ, Arumugam Y, Bell RC, Calles-Escandon J, Tandon NN, Glatz JF, and Bonen A**. Changes in fatty acid transport and transporters are related to the severity of insulin deficiency. *Am J Physiol Endocrinol Metab* 283: E612-621, 2002.

172. **Ouwens DM, Diamant M, Fodor M, Habets DDJ, Pelsers M, El Hasnaoui M, Dang ZC, van den Brom CE, Vlasblom R, Rietdijk A, Boer C, Coort SLM, Glatz JFC, and Luiken J**. Cardiac contractile dysfunction in insulin-resistant rats fed a high-fat diet is associated with elevated CD36-mediated fatty acid uptake and esterification. *Diabetologia* 50: 1938-1948, 2007.

173. **Karwi QG, Sun Q, and Lopaschuk GD**. The Contribution of Cardiac Fatty Acid Oxidation to Diabetic Cardiomyopathy Severity. *Cells* 10: 2021.

174. **Finck B, Lehman J, Leone T, Welch M, Bennett M, Kovacs A, Han X, Gross R, Kozak R, and Lopaschuk G**. The cardiac phenotype induced by PPARα overexpression mimics that caused by diabetes mellitus. *Journal of Clinical Investigation* 109: 121-130, 2002.

175. **Finck BN, Han X, Courtois M, Aimond F, Nerbonne JM, Kovacs A, Gross RW, and Kelly DP**. A critical role for PPARalpha-mediated lipotoxicity in the pathogenesis of diabetic cardiomyopathy: modulation by dietary fat content. *Proc Natl Acad Sci U S A* 100: 1226-1231, 2003.

176. **Sun Y, Tian Z, Liu N, Zhang L, Gao Z, Sun X, Yu M, Wu J, Yang F, Zhao Y, Ren H, Chen H, Zhao D, Wang Y, Dong S, Xu C, Lu F, and Zhang W**. Exogenous H2S switches cardiac energy substrate metabolism by regulating SIRT3 expression in db/db mice. *J Mol Med (Berl)* 96: 281-299, 2018.

177. **Vadvalkar SS, Baily CN, Matsuzaki S, West M, Tesiram YA, and Humphries KM**. Metabolic inflexibility and protein lysine acetylation in heart mitochondria of a chronic model of type 1 diabetes. *Biochem J* 449: 253-261, 2013.

178. **Wende AR**. Post-translational modifications of the cardiac proteome in diabetes and heart failure. *Proteomics Clin Appl* 10: 25-38, 2016.

179. **Lopaschuk GD, Folmes CD, and Stanley WC**. Cardiac energy metabolism in obesity. *Circ Res* 101: 335-347, 2007.

180. **Zlobine I, Gopal K, and Ussher JR**. Lipotoxicity in obesity and diabetes-related cardiac dysfunction. *Biochim Biophys Acta* 1861: 1555-1568, 2016.

181. **D'Souza K, Nzirorera C, and Kienesberger PC**. Lipid metabolism and signaling in cardiac lipotoxicity. *Biochim Biophys Acta* 1861: 1513-1524, 2016.

182. **van de Weijer T, Schrauwen-Hinderling VB, and Schrauwen P**. Lipotoxicity in type 2 diabetic cardiomyopathy. *Cardiovasc Res* 92: 10-18, 2011.

183. **Ussher JR, Fillmore N, Keung W, Mori J, Beker DL, Wagg CS, Jaswal JS, and Lopaschuk GD**. Trimetazidine therapy prevents obesity-induced cardiomyopathy in mice. *Can J Cardiol* 30: 940-944, 2014.

184. **Zhao P, Zhang J, Yin XG, Maharaj P, Narraindoo S, Cui LQ, and Tang YS**. The effect of trimetazidine on cardiac function in diabetic patients with idiopathic dilated cardiomyopathy. *Life Sci* 92: 633-638, 2013.

185. **Ussher JR, Koves TR, Jaswal JS, Zhang L, Ilkayeva O, Dyck JR, Muoio DM, and Lopaschuk GD**. Insulin-stimulated cardiac glucose oxidation is increased in high-fat diet-induced obese mice lacking malonyl CoA decarboxylase. *Diabetes* 58: 1766-1775, 2009.

186. **Shao D, Kolwicz SC, Wang P, Roe ND, Villet O, Nishi K, Hsu YA, Flint GV, Caudal A, Wang W, Regnier M, and Tian R**. Increasing Fatty Acid Oxidation Prevents High Fat Diet Induced Cardiomyopathy through Regulating Parkin Mediated Mitophagy. *Circulation* 2020.

187. **Rohm M, Savic D, Ball V, Curtis MK, Bonham S, Fischer R, Legrave N, MacRae JI, Tyler DJ, and Ashcroft FM**. Cardiac Dysfunction and Metabolic Inflexibility in a Mouse Model of Diabetes Without Dyslipidemia. *Diabetes* 67: 1057-1067, 2018.

188. **Cunningham CH, Lau JY, Chen AP, Geraghty BJ, Perks WJ, Roifman I, Wright GA, and Connelly KA**. Hyperpolarized 13C Metabolic MRI of the Human Heart: Initial Experience. *Circ Res* 119: 1177-1182, 2016.

189. **Rider OJ, Apps A, Miller J, Lau JYC, Lewis AJM, Peterzan MA, Dodd MS, Lau AZ, Trumper C, Gallagher FA, Grist JT, Brindle KM, Neubauer S, and Tyler DJ**. Noninvasive In Vivo Assessment of Cardiac Metabolism in the Healthy and Diabetic Human Heart Using Hyperpolarized (13)C MRI. *Circ Res* 126: 725-736, 2020.

190. **Cividini F, Scott BT, Suarez J, Casteel DE, Heinz S, Dai A, Diemer T, Suarez JA, Benner CW, Ghassemian M, and Dillmann WH**. Ncor2/PPARalpha-Dependent Upregulation of MCUb in the Type 2 Diabetic Heart Impacts Cardiac Metabolic Flexibility and Function. *Diabetes* 70: 665-679, 2021.

191. **Yan D, Cai Y, Luo J, Liu J, Li X, Ying F, Xie X, Xu A, Ma X, and Xia Z**. FOXO1 contributes to diabetic cardiomyopathy via inducing imbalanced oxidative metabolism in type 1 diabetes. *J Cell Mol Med* 24: 7850-7861, 2020.

192. **Taniguchi M, Wilson C, Hunter CA, Pehowich DJ, Clanachan AS, and Lopaschuk GD**. Dichloroacetate improves cardiac efficiency after ischemia independent of changes in mitochondrial proton leak. *Am J Physiol Heart Circ Physiol* 280: H1762-1769, 2001.

193. **Pouleur H**. Diastolic dysfunction and myocardial energetics. *Eur Heart J* 11 Suppl C: 30-34, 1990.

194. **Brahma MK, Ha CM, Pepin ME, Mia S, Sun Z, Chatham JC, Habegger KM, Abel ED, Paterson AJ, Young ME, and Wende AR**. Increased Glucose Availability Attenuates Myocardial Ketone Body Utilization. *J Am Heart Assoc* 9: e013039, 2020.

195. **Abdurrachim D, Woo CC, Teo XQ, Chan WX, Radda GK, and Lee PTH**. A new hyperpolarized (13)C ketone body probe reveals an increase in acetoacetate utilization in the diabetic rat heart. *Sci Rep* 9: 5532, 2019.

196. **Bloomgarden Z**. Diabetes and branched-chain amino acids: What is the link? *J Diabetes* 10: 350-352, 2018.

197. **Newgard CB, An J, Bain JR, Muehlbauer MJ, Stevens RD, Lien LF, Haqq AM, Shah SH, Arlotto M, Slentz CA, Rochon J, Gallup D, Ilkayeva O, Wenner BR, Yancy WS, Jr., Eisenson H, Musante G, Surwit RS, Millington DS, Butler MD, and Svetkey LP**. A branched-chain amino acid-related metabolic signature that differentiates obese and lean humans and contributes to insulin resistance. *Cell Metab* 9: 311-326, 2009.

198. **Wurtz P, Soininen P, Kangas AJ, Ronnemaa T, Lehtimaki T, Kahonen M, Viikari JS, Raitakari OT, and Ala-Korpela M**. Branched-chain and aromatic amino acids are predictors of insulin resistance in young adults. *Diabetes Care* 36: 648-655, 2013.

199. **Ichihara K, Neely JR, Siehl DL, and Morgan HE**. Utilization of leucine by working rat heart. *Am J Physiol* 239: E430-436, 1980.

200. **Uddin GM, Zhang L, Shah S, Fukushima A, Wagg CS, Gopal K, Al Batran R, Pherwani S, Ho KL, Boisvenue J, Karwi QG, Altamimi T, Wishart DS, Dyck JRB, Ussher JR, Oudit GY, and Lopaschuk GD**. Impaired branched chain amino acid oxidation contributes to cardiac insulin resistance in heart failure. *Cardiovasc Diabetol* 18: 86, 2019.

201. **Zhao L, Dong M, Xu C, Zheng H, Wei T, Liu K, Yan Z, and Gao H**. Identification of Energy Metabolism Changes in Diabetic Cardiomyopathy Rats Using a Metabonomic Approach. *Cell Physiol Biochem* 48: 934-946, 2018.

202. **Olson KC, Chen G, Xu Y, Hajnal A, and Lynch CJ**. Alloisoleucine differentiates the branched-chain aminoacidemia of Zucker and dietary obese rats. *Obesity (Silver Spring)* 22: 1212-1215, 2014.

203. **Li T, Zhang Z, Kolwicz SC, Jr., Abell L, Roe ND, Kim M, Zhou B, Cao Y, Ritterhoff J, Gu H, Raftery D, Sun H, and Tian R**. Defective Branched-Chain Amino Acid Catabolism Disrupts Glucose Metabolism and Sensitizes the Heart to Ischemia-Reperfusion Injury. *Cell Metab* 25: 374-385, 2017.

204. **Ussher JR, Sutendra G, and Jaswal JS**. The impact of current and novel anti-diabetic therapies on cardiovascular risk. *Future Cardiol* 8: 895-912, 2012.

205. **Gerstein HC, Colhoun HM, Dagenais GR, Diaz R, Lakshmanan M, Pais P, Probstfield J, Botros FT, Riddle MC, Ryden L, Xavier D, Atisso CM, Dyal L, Hall S, Rao-Melacini P, Wong G, Avezum A, Basile J, Chung N, Conget I, Cushman WC, Franek E, Hancu N, Hanefeld M, Holt S, Jansky P, Keltai M, Lanas F, Leiter LA, Lopez-Jaramillo P, Cardona Munoz EG, Pirags V, Pogosova N, Raubenheimer PJ, Shaw JE, Sheu WH, Temelkova-Kurktschiev T, and Investigators R**. Dulaglutide and renal outcomes in type 2 diabetes: an exploratory analysis of the REWIND randomised, placebo-controlled trial. *Lancet* 394: 131-138, 2019.

206. **Hernandez AF, Green JB, Janmohamed S, D'Agostino RB, Sr., Granger CB, Jones NP, Leiter LA, Rosenberg AE, Sigmon KN, Somerville MC, Thorpe KM, McMurray JJV, Del Prato S, Harmony Outcomes c, and investigators**. Albiglutide and cardiovascular outcomes in patients with type 2 diabetes and cardiovascular disease (Harmony Outcomes): a double-blind, randomised placebo-controlled trial. *Lancet* 392: 1519-1529, 2018.

207. **Marso SP, Bain SC, Consoli A, Eliaschewitz FG, Jodar E, Leiter LA, Lingvay I, Rosenstock J, Seufert J, Warren ML, Woo V, Hansen O, Holst AG, Pettersson J, Vilsboll T, and Investigators S-**. Semaglutide and Cardiovascular Outcomes in Patients with Type 2 Diabetes. *N Engl J Med* 375: 1834-1844, 2016.

208. **Marso SP, Daniels GH, Brown-Frandsen K, Kristensen P, Mann JF, Nauck MA, Nissen SE, Pocock S, Poulter NR, Ravn LS, Steinberg WM, Stockner M, Zinman B,**

Bergenstal RM, Buse JB, Committee LS, and Investigators LT. Liraglutide and Cardiovascular Outcomes in Type 2 Diabetes. *N Engl J Med* 375: 311-322, 2016.

209. **Ussher JR, Greenwell AA, Nguyen MA, and Mulvihill EE**. Cardiovascular Effects of Incretin-Based Therapies: Integrating Mechanisms With Cardiovascular Outcome Trials. *Diabetes* 71: 173-183, 2022.

210. **Anker SD, Butler J, Filippatos G, Ferreira JP, Bocchi E, Bohm M, Brunner-La Rocca HP, Choi DJ, Chopra V, Chuquiure-Valenzuela E, Giannetti N, Gomez-Mesa JE, Janssens S, Januzzi JL, Gonzalez-Juanatey JR, Merkely B, Nicholls SJ, Perrone SV, Pina IL, Ponikowski P, Senni M, Sim D, Spinar J, Squire I, Taddei S, Tsutsui H, Verma S, Vinereanu D, Zhang J, Carson P, Lam CSP, Marx N, Zeller C, Sattar N, Jamal W, Schnaidt S, Schnee JM, Brueckmann M, Pocock SJ, Zannad F, Packer M, and Investigators EM-PT**. Empagliflozin in Heart Failure with a Preserved Ejection Fraction. *N Engl J Med* 385: 1451-1461, 2021.

211. **Mazin I, Chernomordik F, Fefer P, Matetzky S, and Beigel R**. The Impact of Novel Anti-Diabetic Medications on CV Outcomes: A New Therapeutic Horizon for Diabetic and Non-Diabetic Cardiac Patients. *J Clin Med* 11: 2022.

212. **Zinman B, Wanner C, Lachin JM, Fitchett D, Bluhmki E, Hantel S, Mattheus M, Devins T, Johansen OE, Woerle HJ, Broedl UC, Inzucchi SE, and Investigators E-RO**. Empagliflozin, Cardiovascular Outcomes, and Mortality in Type 2 Diabetes. *N Engl J Med* 373: 2117-2128, 2015.

213. **Home PD, Pocock SJ, Beck-Nielsen H, Gomis R, Hanefeld M, Jones NP, Komajda M, McMurray JJ, and Group RS**. Rosiglitazone evaluated for cardiovascular outcomes--an interim analysis. *N Engl J Med* 357: 28-38, 2007.

214. **Kosinski C, and Jornayvaz FR**. Effects of Ketogenic Diets on Cardiovascular Risk Factors: Evidence from Animal and Human Studies. *Nutrients* 9: 2017.

215. **Zhang W, Guo X, Chen L, Chen T, Yu J, Wu C, and Zheng J**. Ketogenic Diets and Cardio-Metabolic Diseases. *Front Endocrinol (Lausanne)* 12: 753039, 2021.

216. **Crosby L, Davis B, Joshi S, Jardine M, Paul J, Neola M, and Barnard ND**. Ketogenic Diets and Chronic Disease: Weighing the Benefits Against the Risks. *Front Nutr* 8: 702802, 2021.

217. **Puchalska P, and Crawford PA**. Metabolic and Signaling Roles of Ketone Bodies in Health and Disease. *Annu Rev Nutr* 41: 49-77, 2021.

218. **Gibson AA, Seimon RV, Lee CM, Ayre J, Franklin J, Markovic TP, Caterson ID, and Sainsbury A**. Do ketogenic diets really suppress appetite? A systematic review and meta-analysis. *Obes Rev* 16: 64-76, 2015.

219. **Hall KD, Chen KY, Guo J, Lam YY, Leibel RL, Mayer LE, Reitman ML, Rosenbaum M, Smith SR, Walsh BT, and Ravussin E**. Energy expenditure and body composition changes after an isocaloric ketogenic diet in overweight and obese men. *Am J Clin Nutr* 104: 324-333, 2016.

220. **Choi YJ, Jeon SM, and Shin S**. Impact of a Ketogenic Diet on Metabolic Parameters in Patients with Obesity or Overweight and with or without Type 2 Diabetes: A Meta-Analysis of Randomized Controlled Trials. *Nutrients* 12: 2020.

221. **Dashti HM, Al-Zaid NS, Mathew TC, Al-Mousawi M, Talib H, Asfar SK, and Behbahani AI**. Long term effects of ketogenic diet in obese subjects with high cholesterol level. *Mol Cell Biochem* 286: 1-9, 2006.

222. **Yang Z, Mi J, Wang Y, Xue L, Liu J, Fan M, Zhang D, Wang L, Qian H, and Li Y**. Effects of low-carbohydrate diet and ketogenic diet on glucose and lipid metabolism in type 2 diabetic mice. *Nutrition* 89: 111230, 2021.

223. **Hall KD, Guo J, Courville AB, Boring J, Brychta R, Chen KY, Darcey V, Forde CG, Gharib AM, Gallagher I, Howard R, Joseph PV, Milley L, Ouwerkerk R, Raisinger K, Rozga I, Schick A, Stagliano M, Torres S, Walter M, Walter P, Yang S, and Chung ST**. Effect of a plant-based, low-fat diet versus an animal-based, ketogenic diet on ad libitum energy intake. *Nat Med* 27: 344-353, 2021.

224. **Snorgaard O, Poulsen GM, Andersen HK, and Astrup A**. Systematic review and meta-analysis of dietary carbohydrate restriction in patients with type 2 diabetes. *BMJ Open Diabetes Res Care* 5: e000354, 2017.

225. **Rafiullah M, Musambil M, and David SK**. Effect of a very low-carbohydrate ketogenic diet vs recommended diets in patients with type 2 diabetes: a meta-analysis. *Nutr Rev* 2021.

226. **Hallberg SJ, McKenzie AL, Williams PT, Bhanpuri NH, Peters AL, Campbell WW, Hazbun TL, Volk BM, McCarter JP, Phinney SD, and Volek JS**. Effectiveness and Safety of a Novel Care Model for the Management of Type 2 Diabetes at 1 Year: An Open-Label, Non-Randomized, Controlled Study. *Diabetes Ther* 9: 583-612, 2018.

227. **Chouinard G, and Annable L**. Pimozide in the treatment of newly admitted schizophrenic patients. *Psychopharmacology (Berl)* 76: 13-19, 1982.

228. **Elmaci I, and Altinoz MA**. Targeting the cellular schizophrenia. Likely employment of the antipsychotic agent pimozide in treatment of refractory cancers and glioblastoma. *Crit Rev Oncol Hematol* 128: 96-109, 2018.

229. **Al Batran R, Gopal K, Capozzi ME, Chahade JJ, Saleme B, Tabatabaei-Dakhili SA, Greenwell AA, Niu J, Almutairi M, Byrne NJ, Masson G, Kim R, Eaton F, Mulvihill EE, Garneau L, Masters AR, Desta Z, Velazquez-Martinez CA, Aguer C, Crawford PA, Sutendra G, Campbell JE, Dyck JRB, and Ussher JR**. Pimozide Alleviates Hyperglycemia in Diet-Induced Obesity by Inhibiting Skeletal Muscle Ketone Oxidation. *Cell Metab* 31: 909-919 e908, 2020.

230. **Acehan D, Vaz F, Houtkooper RH, James J, Moore V, Tokunaga C, Kulik W, Wansapura J, Toth MJ, Strauss A, and Khuchua Z**. Cardiac and skeletal muscle defects in a mouse model of human Barth syndrome. *J Biol Chem* 286: 899-908, 2011.

231. **Huang Y, Powers C, Moore V, Schafer C, Ren M, Phoon CK, James JF, Glukhov AV, Javadov S, Vaz FM, Jefferies JL, Strauss AW, and Khuchua Z**. The PPAR pan-agonist bezafibrate ameliorates cardiomyopathy in a mouse model of Barth syndrome. *Orphanet J Rare Dis* 12: 49, 2017.

232. **Glatz JFC, Nabben M, Young ME, Schulze PC, Taegtmeyer H, and Luiken J**. Re-balancing cellular energy substrate metabolism to mend the failing heart. *Biochim Biophys Acta Mol Basis Dis* 1866: 165579, 2020.

233. **Belke DD, Larsen TS, Lopaschuk GD, and Severson DL**. Glucose and fatty acid metabolism in the isolated working mouse heart. *Am J Physiol* 277: R1210-1217, 1999.

234. **Saddik M, and Lopaschuk GD**. Myocardial triglyceride turnover and contribution to energy substrate utilization in isolated working rat hearts. *J Biol Chem* 266: 8162-8170, 1991.

235. **Sambandam N, Morabito D, Wagg C, Finck BN, Kelly DP, and Lopaschuk GD**. Chronic activation of PPARalpha is detrimental to cardiac recovery after ischemia. *Am J Physiol Heart Circ Physiol* 290: H87-95, 2006.

236. **Livak KJ, and Schmittgen TD**. Analysis of relative gene expression data using real-time quantitative PCR and the 2(-Delta Delta C(T)) Method. *Methods* 25: 402-408, 2001.

237. **Patel VB, Bodiga S, Basu R, Das SK, Wang W, Wang Z, Lo J, Grant MB, Zhong J, Kassiri Z, and Oudit GY**. Loss of angiotensin-converting enzyme-2 exacerbates diabetic cardiovascular complications and leads to systolic and vascular dysfunction: a critical role of the angiotensin II/AT1 receptor axis. *Circ Res* 110: 1322-1335, 2012.

238. **Johnson JM, Ferrara PJ, Verkerke ARP, Coleman CB, Wentzler EJ, Neufer PD, Kew KA, de Castro Bras LE, and Funai K**. Targeted overexpression of catalase to mitochondria does not prevent cardioskeletal myopathy in Barth syndrome. *J Mol Cell Cardiol* 121: 94-102, 2018.

239. **Leatherbury L, Yu Q, Chatterjee B, Walker DL, Yu Z, Tian X, and Lo CW**. A novel mouse model of X-linked cardiac hypertrophy. *Am J Physiol Heart Circ Physiol* 294: H2701-2711, 2008.

240. **Ho KL, Zhang L, Wagg C, Al Batran R, Gopal K, Levasseur J, Leone T, Dyck JRB, Ussher JR, Muoio DM, Kelly DP, and Lopaschuk GD**. Increased ketone body oxidation provides additional energy for the failing heart without improving cardiac efficiency. *Cardiovasc Res* 115: 1606-1616, 2019.

241. **Zhang X, Ji R, Liao X, Castillero E, Kennel PJ, Brunjes DL, Franz M, Mobius-Winkler S, Drosatos K, George I, Chen EI, Colombo PC, and Schulze PC**. MicroRNA-195 Regulates Metabolism in Failing Myocardium Via Alterations in Sirtuin 3 Expression and Mitochondrial Protein Acetylation. *Circulation* 137: 2052-2067, 2018.

242. **Fatica EM, DeLeonibus GA, House A, Kodger JV, Pearce RW, Shah RR, Levi L, and Sandlers Y**. Barth Syndrome: Exploring Cardiac Metabolism with Induced Pluripotent Stem Cell-Derived Cardiomyocytes. *Metabolites* 9: 2019.

243. **Zhabyeyev P, Gandhi M, Mori J, Basu R, Kassiri Z, Clanachan A, Lopaschuk GD, and Oudit GY**. Pressure-overload-induced heart failure induces a selective reduction in glucose oxidation at physiological afterload. *Cardiovasc Res* 97: 676-685, 2013.

244. **Idell-Wenger JA, Grotyohann LW, and Neely JR**. Coenzyme A and carnitine distribution in normal and ischemic hearts. *J Biol Chem* 253: 4310-4318, 1978.

245. **Al Batran R, and Ussher JR**. Revisiting protein acetylation and myocardial fatty acid oxidation. *Am J Physiol Heart Circ Physiol* 313: H617-H619, 2017.

246. **Thapa D, Zhang M, Manning JR, Guimaraes DA, Stoner MW, O'Doherty RM, Shiva S, and Scott I**. Acetylation of mitochondrial proteins by GCN5L1 promotes enhanced fatty acid oxidation in the heart. *Am J Physiol Heart Circ Physiol* 313: H265-H274, 2017.

247. **Alrob OA, Sankaralingam S, Ma C, Wagg CS, Fillmore N, Jaswal JS, Sack MN, Lehner R, Gupta MP, Michelakis ED, Padwal RS, Johnstone DE, Sharma AM, and Lopaschuk GD**. Obesity-induced lysine acetylation increases cardiac fatty acid oxidation and impairs insulin signalling. *Cardiovasc Res* 103: 485-497, 2014.

248. **Davies MN, Kjalarsdottir L, Thompson JW, Dubois LG, Stevens RD, Ilkayeva OR, Brosnan MJ, Rolph TP, Grimsrud PA, and Muoio DM**. The Acetyl Group Buffering Action of Carnitine Acetyltransferase Offsets Macronutrient-Induced Lysine Acetylation of Mitochondrial Proteins. *Cell Rep* 14: 243-254, 2016.

249. **Hue L, and Taegtmeyer H**. The Randle cycle revisited: a new head for an old hat. *Am J Physiol Endocrinol Metab* 297: E578-591, 2009.

250. **Cole LK, Agarwal P, Doucette CA, Fonseca M, Xiang B, Sparagna GC, Seshadri N, Vandel M, Dolinsky VW, and Hatch GM**. Tafazzin Deficiency Reduces Basal Insulin Secretion and Mitochondrial Function in Pancreatic Islets From Male Mice. *Endocrinology* 162: 2021.

251. **Uchihashi M, Hoshino A, Okawa Y, Ariyoshi M, Kaimoto S, Tateishi S, Ono K, Yamanaka R, Hato D, Fushimura Y, Honda S, Fukai K, Higuchi Y, Ogata T, Iwai-Kanai E, and Matoba S**. Cardiac-Specific Bdh1 Overexpression Ameliorates Oxidative Stress and Cardiac Remodeling in Pressure Overload-Induced Heart Failure. *Circ Heart Fail* 10: 2017.

252. **Cole LK, Mejia EM, Sparagna GC, Vandel M, Xiang B, Han X, Dedousis N, Kaufman BA, Dolinsky VW, and Hatch GM**. Cardiolipin deficiency elevates susceptibility to a lipotoxic hypertrophic cardiomyopathy. *J Mol Cell Cardiol* 144: 24-34, 2020.

253. **Mori J, Basu R, McLean BA, Das SK, Zhang L, Patel VB, Wagg CS, Kassiri Z, Lopaschuk GD, and Oudit GY**. Agonist-induced hypertrophy and diastolic dysfunction are associated with selective reduction in glucose oxidation: a metabolic contribution to heart failure with normal ejection fraction. *Circ Heart Fail* 5: 493-503, 2012.

254. **Tuunanen H, Engblom E, Naum A, Nagren K, Scheinin M, Hesse B, Juhani Airaksinen KE, Nuutila P, Iozzo P, Ukkonen H, Opie LH, and Knuuti J**. Trimetazidine, a metabolic modulator, has cardiac and extracardiac benefits in idiopathic dilated cardiomyopathy. *Circulation* 118: 1250-1258, 2008.

255. **Kato M, Li J, Chuang JL, and Chuang DT**. Distinct structural mechanisms for inhibition of pyruvate dehydrogenase kinase isoforms by AZD7545, dichloroacetate, and radicicol. *Structure* 15: 992-1004, 2007.

256. **Stacpoole PW, and Greene YJ**. Dichloroacetate. *Diabetes Care* 15: 785-791, 1992.

257. **Schnelle M, Catibog N, Zhang M, Nabeebaccus AA, Anderson G, Richards DA, Sawyer G, Zhang X, Toischer K, Hasenfuss G, Monaghan MJ, and Shah AM**. Echocardiographic evaluation of diastolic function in mouse models of heart disease. *J Mol Cell Cardiol* 114: 20-28, 2018.

258. **Allen ME, Pennington ER, Perry JB, Dadoo S, Makrecka-Kuka M, Dambrova M, Moukdar F, Patel HD, Han X, Kidd GK, Benson EK, Raisch TB, Poelzing S, Brown DA, and Shaikh SR**. The cardiolipin-binding peptide elamipretide mitigates fragmentation of cristae networks following cardiac ischemia reperfusion in rats. *Commun Biol* 3: 389, 2020.

259. **Szeto HH**. First-in-class cardiolipin-protective compound as a therapeutic agent to restore mitochondrial bioenergetics. *Br J Pharmacol* 171: 2029-2050, 2014.

260. **Williams EP, Mesidor M, Winters K, Dubbert PM, and Wyatt SB**. Overweight and Obesity: Prevalence, Consequences, and Causes of a Growing Public Health Problem. *Curr Obes Rep* 4: 363-370, 2015.

261. **Ludwig DS, and Ebbeling CB**. The Carbohydrate-Insulin Model of Obesity: Beyond "Calories In, Calories Out". *JAMA Intern Med* 178: 1098-1103, 2018.

262. **Blundell JE, and Macdiarmid JI**. Passive overconsumption. Fat intake and short-term energy balance. *Ann N Y Acad Sci* 827: 392-407, 1997.

263. **Badman MK, Kennedy AR, Adams AC, Pissios P, and Maratos-Flier E**. A very low carbohydrate ketogenic diet improves glucose tolerance in ob/ob mice independently of weight loss. *Am J Physiol Endocrinol Metab* 297: E1197-1204, 2009.

264. **Dashti HM, Bo-Abbas YY, Asfar SK, Mathew TC, Hussein T, Behbahani A, Khoursheed MA, Al-Sayer HM, and Al-Zaid NS**. Ketogenic diet modifies the risk factors of heart disease in obese patients. *Nutrition* 19: 901-902, 2003.

265. **Dashti HM, Mathew TC, Hussein T, Asfar SK, Behbahani A, Khoursheed MA, Al-Sayer HM, Bo-Abbas YY, and Al-Zaid NS**. Long-term effects of a ketogenic diet in obese patients. *Exp Clin Cardiol* 9: 200-205, 2004.

266. **Kennedy AR, Pissios P, Otu H, Roberson R, Xue B, Asakura K, Furukawa N, Marino FE, Liu FF, Kahn BB, Libermann TA, and Maratos-Flier E**. A high-fat, ketogenic diet induces a unique metabolic state in mice. *Am J Physiol Endocrinol Metab* 292: E1724-1739, 2007.

267. **Newman JC, Covarrubias AJ, Zhao M, Yu X, Gut P, Ng CP, Huang Y, Haldar S, and Verdin E**. Ketogenic Diet Reduces Midlife Mortality and Improves Memory in Aging Mice. *Cell Metab* 26: 547-557 e548, 2017.

268. **Roberts MN, Wallace MA, Tomilov AA, Zhou Z, Marcotte GR, Tran D, Perez G, Gutierrez-Casado E, Koike S, Knotts TA, Imai DM, Griffey SM, Kim K, Hagopian K, McMackin MZ, Haj FG, Baar K, Cortopassi GA, Ramsey JJ, and Lopez-Dominguez JA**. A Ketogenic Diet Extends Longevity and Healthspan in Adult Mice. *Cell Metab* 26: 539-546 e535, 2017.

269. **Abdurrachim D, Teo XQ, Woo CC, Ong SY, Salleh NF, Lalic J, Tan RS, and Lee PTH**. Cardiac metabolic modulation upon low-carbohydrate low-protein ketogenic diet in diabetic rats studied in vivo using hyperpolarized (13) C pyruvate, butyrate and acetoacetate probes. *Diabetes Obes Metab* 21: 949-960, 2019.

270. **Ellenbroek JH, van Dijck L, Tons HA, Rabelink TJ, Carlotti F, Ballieux BE, and de Koning EJ**. Long-term ketogenic diet causes glucose intolerance and reduced beta- and alpha-cell mass but no weight loss in mice. *Am J Physiol Endocrinol Metab* 306: E552-558, 2014.

271. **Garbow JR, Doherty JM, Schugar RC, Travers S, Weber ML, Wentz AE, Ezenwajiaku N, Cotter DG, Brunt EM, and Crawford PA**. Hepatic steatosis, inflammation, and ER stress in mice maintained long term on a very low-carbohydrate ketogenic diet. *Am J Physiol Gastrointest Liver Physiol* 300: G956-967, 2011.

272. **Goldberg EL, Shchukina I, Asher JL, Sidorov S, Artyomov MN, and Dixit VD**. Ketogenesis activates metabolically protective gammadelta T cells in visceral adipose tissue. *Nat Metab* 2: 50-61, 2020.

273. **Park S, Kim DS, Kang S, and Daily JW, 3rd**. A ketogenic diet impairs energy and glucose homeostasis by the attenuation of hypothalamic leptin signaling and hepatic insulin signaling in a rat model of non-obese type 2 diabetes. *Exp Biol Med (Maywood)* 236: 194-204, 2011.

274. **Schugar RC, Huang X, Moll AR, Brunt EM, and Crawford PA**. Role of choline deficiency in the Fatty liver phenotype of mice fed a low protein, very low carbohydrate ketogenic diet. *PLoS One* 8: e74806, 2013.

275. **Mina AI, LeClair RA, LeClair KB, Cohen DE, Lantier L, and Banks AS**. CalR: A Web-Based Analysis Tool for Indirect Calorimetry Experiments. *Cell Metab* 28: 656-666 e651, 2018.

276. **Muller TD, Klingenspor M, and Tschop MH**. Revisiting energy expenditure: how to correct mouse metabolic rate for body mass. *Nat Metab* 3: 1134-1136, 2021.

277. **Virtue S, Lelliott CJ, and Vidal-Puig A**. What is the most appropriate covariate in ANCOVA when analysing metabolic rate? *Nat Metab* 3: 1585, 2021.

278. **Carr RD, Larsen MO, Winzell MS, Jelic K, Lindgren O, Deacon CF, and Ahren B**. Incretin and islet hormonal responses to fat and protein ingestion in healthy men. *Am J Physiol Endocrinol Metab* 295: E779-784, 2008.

279. **Dube PE, and Brubaker PL**. Nutrient, neural and endocrine control of glucagon-like peptide secretion. *Horm Metab Res* 36: 755-760, 2004.

280. **Itoh K, Moriguchi R, Yamada Y, Fujita M, Yamato T, Oumi M, Holst JJ, and Seino Y**. High saturated fatty acid intake induces insulin secretion by elevating gastric inhibitory polypeptide levels in healthy individuals. *Nutr Res* 34: 653-660, 2014.

281. **Paoli A**. Ketogenic diet for obesity: friend or foe? *Int J Environ Res Public Health* 11: 2092-2107, 2014.

282. **Paoli A, Rubini A, Volek JS, and Grimaldi KA**. Beyond weight loss: a review of the therapeutic uses of very-low-carbohydrate (ketogenic) diets. *Eur J Clin Nutr* 67: 789-796, 2013.

283. **Hashim SA, and VanItallie TB**. Ketone body therapy: from the ketogenic diet to the oral administration of ketone ester. *J Lipid Res* 55: 1818-1826, 2014.

284. **Chawla S, Tessarolo Silva F, Amaral Medeiros S, Mekary RA, and Radenkovic D**. The Effect of Low-Fat and Low-Carbohydrate Diets on Weight Loss and Lipid Levels: A Systematic Review and Meta-Analysis. *Nutrients* 12: 2020.

285. **Kunstyr I, and Leuenberger HG**. Gerontological data of C57BL/6J mice. I. Sex differences in survival curves. *J Gerontol* 30: 157-162, 1975.

286. **Bueno NB, de Melo IS, de Oliveira SL, and da Rocha Ataide T**. Very-low-carbohydrate ketogenic diet v. low-fat diet for long-term weight loss: a meta-analysis of randomised controlled trials. *Br J Nutr* 110: 1178-1187, 2013.

287. **Wolfe RR, Cifelli AM, Kostas G, and Kim IY**. Optimizing Protein Intake in Adults: Interpretation and Application of the Recommended Dietary Allowance Compared with the Acceptable Macronutrient Distribution Range. *Adv Nutr* 8: 266-275, 2017.

288. **Bielohuby M, Sisley S, Sandoval D, Herbach N, Zengin A, Fischereder M, Menhofer D, Stoehr BJ, Stemmer K, Wanke R, Tschop MH, Seeley RJ, and Bidlingmaier M**. Impaired glucose tolerance in rats fed low-carbohydrate, high-fat diets. *Am J Physiol Endocrinol Metab* 305: E1059-1070, 2013.

289. **Durrer C, McKelvey S, Singer J, Batterham AM, Johnson JD, Gudmundson K, Wortman J, and Little JP**. A randomized controlled trial of pharmacist-led therapeutic carbohydrate and energy restriction in type 2 diabetes. *Nat Commun* 12: 5367, 2021.

290. **Li Y, Yang X, Zhang J, Jiang T, Zhang Z, Wang Z, Gong M, Zhao L, and Zhang C**. Ketogenic Diets Induced Glucose Intolerance and Lipid Accumulation in Mice with Alterations in Gut Microbiota and Metabolites. *mBio* 12: 2021.

291. **Johnson RJ, Sanchez-Lozada LG, Andrews P, and Lanaspa MA**. Perspective: A Historical and Scientific Perspective of Sugar and Its Relation with Obesity and Diabetes. *Adv Nutr* 8: 412-422, 2017.

292. **Malik VS, Pan A, Willett WC, and Hu FB**. Sugar-sweetened beverages and weight gain in children and adults: a systematic review and meta-analysis. *Am J Clin Nutr* 98: 1084-1102, 2013.

293. **Hira T, Suto R, Kishimoto Y, Kanahori S, and Hara H**. Resistant maltodextrin or fructooligosaccharides promotes GLP-1 production in male rats fed a high-fat and high-sucrose diet, and partially reduces energy intake and adiposity. *Eur J Nutr* 57: 965-979, 2018.

294. **Lim J, Ferruzzi MG, and Hamaker BR**. Dietary starch is weight reducing when distally digested in the small intestine. *Carbohydr Polym* 273: 118599, 2021.

295. **Campbell JE, and Drucker DJ**. Pharmacology, physiology, and mechanisms of incretin hormone action. *Cell Metab* 17: 819-837, 2013.

296. **Peng C, Xu X, Li Y, Li X, Yang X, Chen H, Zhu Y, Lu N, and He C**. Sex-specific association between the gut microbiome and high-fat diet-induced metabolic disorders in mice. *Biol Sex Differ* 11: 5, 2020.

297. **Grembi JA, Nguyen LH, Haggerty TD, Gardner CD, Holmes SP, and Parsonnet J**. Gut microbiota plasticity is correlated with sustained weight loss on a low-carb or low-fat dietary intervention. *Sci Rep* 10: 1405, 2020.

298. **Daly CM, Saxena J, Singh J, Bullard MR, Bondy EO, Saxena A, Buffalino RE, Melville MF, and Freeman LR**. Sex differences in response to a high fat, high sucrose diet in both the gut microbiome and hypothalamic astrocytes and microglia. *Nutr Neurosci* 1-15, 2020.

299. **Horton TJ, Dow S, Armstrong M, and Donahoo WT**. Greater systemic lipolysis in women compared with men during moderate-dose infusion of epinephrine and/or norepinephrine. *J Appl Physiol (1985)* 107: 200-210, 2009.

300. **Karastergiou K, Smith SR, Greenberg AS, and Fried SK**. Sex differences in human adipose tissues - the biology of pear shape. *Biol Sex Differ* 3: 13, 2012.

301. **Blaak E**. Gender differences in fat metabolism. *Curr Opin Clin Nutr Metab Care* 4: 499-502, 2001.

302. **Lavie CJ, Alpert MA, Arena R, Mehra MR, Milani RV, and Ventura HO**. Impact of obesity and the obesity paradox on prevalence and prognosis in heart failure. *JACC Heart Fail* 1: 93-102, 2013.

303. **Powell-Wiley TM, Poirier P, Burke LE, Despres JP, Gordon-Larsen P, Lavie CJ, Lear SA, Ndumele CE, Neeland IJ, Sanders P, St-Onge MP, American Heart Association Council on L, Cardiometabolic H, Council on C, Stroke N, Council on Clinical C, Council on E, Prevention, and Stroke C**. Obesity and Cardiovascular Disease: A Scientific Statement From the American Heart Association. *Circulation* 143: e984-e1010, 2021.

304. **Abel ED, Litwin SE, and Sweeney G**. Cardiac remodeling in obesity. *Physiol Rev* 88: 389-419, 2008.

305. **Alpert MA, Terry BE, and Kelly DL**. Effect of weight loss on cardiac chamber size, wall thickness and left ventricular function in morbid obesity. *Am J Cardiol* 55: 783-786, 1985.

306. **Franssen WMA, Beyens M, Hatawe TA, Frederix I, Verboven K, Dendale P, Eijnde BO, Massa G, and Hansen D**. Cardiac function in adolescents with obesity: cardiometabolic risk factors and impact on physical fitness. *Int J Obes (Lond)* 43: 1400-1410, 2019.

307. **Listenberger LL, and Schaffer JE**. Mechanisms of lipoapoptosis: implications for human heart disease. *Trends Cardiovasc Med* 12: 134-138, 2002.

308. **Einarson TR, Acs A, Ludwig C, and Panton UH**. Prevalence of cardiovascular disease in type 2 diabetes: a systematic literature review of scientific evidence from across the world in 2007-2017. *Cardiovasc Diabetol* 17: 83, 2018.

309. **Ma CX, Ma XN, Guan CH, Li YD, Mauricio D, and Fu SB**. Cardiovascular disease in type 2 diabetes mellitus: progress toward personalized management. *Cardiovasc Diabetol* 21: 74, 2022.

310. **Barsotti A, Giannoni A, Di Napoli P, and Emdin M**. Energy metabolism in the normal and in the diabetic heart. *Curr Pharm Des* 15: 836-840, 2009.

311. **Lopaschuk GD**. Metabolic abnormalities in the diabetic heart. *Heart Fail Rev* 7: 149-159, 2002.

312. **Mazumder PK, O'Neill BT, Roberts MW, Buchanan J, Yun UJ, Cooksey RC, Boudina S, and Abel ED**. Impaired cardiac efficiency and increased fatty acid oxidation in insulin-resistant ob/ob mouse hearts. *Diabetes* 53: 2366-2374, 2004.

313. **Schulze PC, Drosatos K, and Goldberg IJ**. Lipid Use and Misuse by the Heart. *Circ Res* 118: 1736-1751, 2016.

314. **Sharma S, Adrogue JV, Golfman L, Uray I, Lemm J, Youker K, Noon GP, Frazier OH, and Taegtmeyer H**. Intramyocardial lipid accumulation in the failing human heart resembles the lipotoxic rat heart. *FASEB J* 18: 1692-1700, 2004.

315. **Horton JL, Davidson MT, Kurishima C, Vega RB, Powers JC, Matsuura TR, Petucci C, Lewandowski ED, Crawford PA, Muoio DM, Recchia FA, and Kelly DP**. The failing heart utilizes 3-hydroxybutyrate as a metabolic stress defense. *JCI Insight* 4: 2019.

316. **Monzo L, Sedlacek K, Hromanikova K, Tomanova L, Borlaug BA, Jabor A, Kautzner J, and Melenovsky V**. Myocardial ketone body utilization in patients with heart failure: The impact of oral ketone ester. *Metabolism* 115: 154452, 2021.

317. **Nielsen R, Moller N, Gormsen LC, Tolbod LP, Hansson NH, Sorensen J, Harms HJ, Frokiaer J, Eiskjaer H, Jespersen NR, Mellemkjaer S, Lassen TR, Pryds K, Botker HE, and Wiggers H**. Cardiovascular Effects of Treatment With the Ketone Body 3-Hydroxybutyrate in Chronic Heart Failure Patients. *Circulation* 139: 2129-2141, 2019.

318. **Yurista SR, Matsuura TR, Sillje HHW, Nijholt KT, McDaid KS, Shewale SV, Leone TC, Newman JC, Verdin E, van Veldhuisen DJ, de Boer RA, Kelly DP, and Westenbrink**

BD. Ketone Ester Treatment Improves Cardiac Function and Reduces Pathologic Remodeling in Preclinical Models of Heart Failure. *Circ Heart Fail* 14: e007684, 2021.

319. **Mizuno Y, Harada E, Nakagawa H, Morikawa Y, Shono M, Kugimiya F, Yoshimura M, and Yasue H**. The diabetic heart utilizes ketone bodies as an energy source. *Metabolism* 77: 65-72, 2017.

320. **Grinblat L, Pacheco Bolanos LF, and Stoppani AO**. Decreased rate of ketone-body oxidation and decreased activity of D-3-hydroxybutyrate dehydrogenase and succinyl-CoA:3-oxo-acid CoA-transferase in heart mitochondria of diabetic rats. *Biochem J* 240: 49-56, 1986.

321. **Morales CR, Li DL, Pedrozo Z, May HI, Jiang N, Kyrychenko V, Cho GW, Kim SY, Wang ZV, Rotter D, Rothermel BA, Schneider JW, Lavandero S, Gillette TG, and Hill JA**. Inhibition of class I histone deacetylases blunts cardiac hypertrophy through TSC2-dependent mTOR repression. *Sci Signal* 9: ra34, 2016.

322. **Shimazu T, Hirschey MD, Newman J, He W, Shirakawa K, Le Moan N, Grueter CA, Lim H, Saunders LR, Stevens RD, Newgard CB, Farese RV, Jr., de Cabo R, Ulrich S, Akassoglou K, and Verdin E**. Suppression of oxidative stress by beta-hydroxybutyrate, an endogenous histone deacetylase inhibitor. *Science* 339: 211-214, 2013.

323. **Youm YH, Nguyen KY, Grant RW, Goldberg EL, Bodogai M, Kim D, D'Agostino D, Planavsky N, Lupfer C, Kanneganti TD, Kang S, Horvath TL, Fahmy TM, Crawford PA, Biragyn A, Alnemri E, and Dixit VD**. The ketone metabolite beta-hydroxybutyrate blocks NLRP3 inflammasome-mediated inflammatory disease. *Nat Med* 21: 263-269, 2015.

324. **Almutairi M, Gopal K, Greenwell AA, Young A, Gill R, Aburasayn H, Al Batran R, Chahade JJ, Gandhi M, Eaton F, Mailloux RJ, and Ussher JR**. The GLP-1 Receptor Agonist Liraglutide Increases Myocardial Glucose Oxidation Rates via Indirect Mechanisms and Mitigates Experimental Diabetic Cardiomyopathy. *Can J Cardiol* 2020.

325. **Kesherwani V, Shahshahan HR, and Mishra PK**. Cardiac transcriptome profiling of diabetic Akita mice using microarray and next generation sequencing. *PLoS One* 12: e0182828, 2017.

326. **Lindsey ML, Kassiri Z, Virag JAI, de Castro Bras LE, and Scherrer-Crosbie M**. Guidelines for measuring cardiac physiology in mice. *Am J Physiol Heart Circ Physiol* 314: H733-H752, 2018.

327. **Spevack DM, Blum L, Malhotra D, Nazari R, Ostfeld RJ, Doddamani S, Bello R, Cohen HW, and Sonnenblick EH**. Ratio of left atrial to left ventricular size: an anatomical marker of the diastolic left ventricular pressure-volume relationship. *Echocardiography* 25: 366-373, 2008.

328. **Di Bello V, Talarico L, Picano E, Di Muro C, Landini L, Paterni M, Matteucci E, Giusti C, and Giampietro O**. Increased echodensity of myocardial wall in the diabetic heart: an ultrasound tissue characterization study. *J Am Coll Cardiol* 25: 1408-1415, 1995.

329. **Mizushige K, Yao L, Noma T, Kiyomoto H, Yu Y, Hosomi N, Ohmori K, and Matsuo H**. Alteration in left ventricular diastolic filling and accumulation of myocardial collagen at insulin-resistant prediabetic stage of a type II diabetic rat model. *Circulation* 101: 899-907, 2000.

330. **Shimizu M, Umeda K, Sugihara N, Yoshio H, Ino H, Takeda R, Okada Y, and Nakanishi I**. Collagen remodelling in myocardia of patients with diabetes. *J Clin Pathol* 46: 32-36, 1993.

331. **Singh VP, Baker KM, and Kumar R**. Activation of the intracellular renin-angiotensin system in cardiac fibroblasts by high glucose: role in extracellular matrix production. *Am J Physiol Heart Circ Physiol* 294: H1675-1684, 2008.

332. **Westermann D, Rutschow S, Jager S, Linderer A, Anker S, Riad A, Unger T, Schultheiss HP, Pauschinger M, and Tschope C**. Contributions of inflammation and cardiac matrix metalloproteinase activity to cardiac failure in diabetic cardiomyopathy: the role of angiotensin type 1 receptor antagonism. *Diabetes* 56: 641-646, 2007.

333. **Ge Q, Zhao L, Ren XM, Ye P, and Hu ZY**. LCZ696, an angiotensin receptor-neprilysin inhibitor, ameliorates diabetic cardiomyopathy by inhibiting inflammation, oxidative stress and apoptosis. *Exp Biol Med (Maywood)* 244: 1028-1039, 2019.

334. **Jadhav A, Tiwari S, Lee P, and Ndisang JF**. The heme oxygenase system selectively enhances the anti-inflammatory macrophage-M2 phenotype, reduces pericardial adiposity, and ameliorated cardiac injury in diabetic cardiomyopathy in Zucker diabetic fatty rats. *J Pharmacol Exp Ther* 345: 239-249, 2013.

335. **Luo W, Jin Y, Wu G, Zhu W, Qian Y, Zhang Y, Li J, Zhu A, and Liang G**. Blockage of ROS and MAPKs-mediated inflammation via restoring SIRT1 by a new compound LF10 prevents type 1 diabetic cardiomyopathy. *Toxicol Appl Pharmacol* 370: 24-35, 2019.

336. **Mariappan N, Elks CM, Sriramula S, Guggilam A, Liu Z, Borkhsenious O, and Francis J**. NF-kappaB-induced oxidative stress contributes to mitochondrial and cardiac dysfunction in type II diabetes. *Cardiovasc Res* 85: 473-483, 2010.

337. **Westermann D, Rutschow S, Van Linthout S, Linderer A, Bucker-Gartner C, Sobirey M, Riad A, Pauschinger M, Schultheiss HP, and Tschope C**. Inhibition of p38 mitogen-activated protein kinase attenuates left ventricular dysfunction by mediating pro-inflammatory cardiac cytokine levels in a mouse model of diabetes mellitus. *Diabetologia* 49: 2507-2513, 2006.

338. **Deng Y, Xie M, Li Q, Xu X, Ou W, Zhang Y, Xiao H, Yu H, Zheng Y, Liang Y, Jiang C, Chen G, Du D, Zheng W, Wang S, Gong M, Chen Y, Tian R, and Li T**. Targeting Mitochondria-Inflammation Circuit by beta-Hydroxybutyrate Mitigates HFpEF. *Circ Res* 128: 232-245, 2021.

339. **Dedkova EN, and Blatter LA**. Role of beta-hydroxybutyrate, its polymer poly-beta-hydroxybutyrate and inorganic polyphosphate in mammalian health and disease. *Front Physiol* 5: 260, 2014.

340. **Garcia E, Shalaurova I, Matyus SP, Oskardmay DN, Otvos JD, Dullaart RPF, and Connelly MA**. Ketone Bodies Are Mildly Elevated in Subjects with Type 2 Diabetes Mellitus and Are Inversely Associated with Insulin Resistance as Measured by the Lipoprotein Insulin Resistance Index. *J Clin Med* 9: 2020.

341. **Harano Y, Kosugi K, Hyosu T, Suzuki M, Hidaka H, Kashiwagi A, Uno S, and Shigeta Y**. Ketone bodies as markers for type 1 (insulin-dependent) diabetes and their value in the monitoring of diabetic control. *Diabetologia* 26: 343-348, 1984.

342. **Russell RR, 3rd, Mommessin JI, and Taegtmeyer H**. Propionyl-L-carnitine-mediated improvement in contractile function of rat hearts oxidizing acetoacetate. *Am J Physiol* 268: H441-447, 1995.

343. **Russell RR, 3rd, and Taegtmeyer H**. Pyruvate carboxylation prevents the decline in contractile function of rat hearts oxidizing acetoacetate. *Am J Physiol* 261: H1756-1762, 1991.

344. **Russell RR, 3rd, and Taegtmeyer H**. Changes in citric acid cycle flux and anaplerosis antedate the functional decline in isolated rat hearts utilizing acetoacetate. *J Clin Invest* 87: 384-390, 1991.

345. **Russell RR, 3rd, and Taegtmeyer H**. Coenzyme A sequestration in rat hearts oxidizing ketone bodies. *J Clin Invest* 89: 968-973, 1992.

346. **Cook GA, Lavrentyev EN, Pham K, and Park EA**. Streptozotocin diabetes increases mRNA expression of ketogenic enzymes in the rat heart. *Biochim Biophys Acta Gen Subj* 1861: 307-312, 2017.

347. **Shukla SK, Liu W, Sikder K, Addya S, Sarkar A, Wei Y, and Rafiq K**. HMGCS2 is a key ketogenic enzyme potentially involved in type 1 diabetes with high cardiovascular risk. *Sci Rep* 7: 4590, 2017.

348. **Digby JE, Martinez F, Jefferson A, Ruparelia N, Chai J, Wamil M, Greaves DR, and Choudhury RP**. Anti-inflammatory effects of nicotinic acid in human monocytes are mediated by GPR109A dependent mechanisms. *Arterioscler Thromb Vasc Biol* 32: 669-676, 2012.

349. **Chen Y, Du J, Zhao YT, Zhang L, Lv G, Zhuang S, Qin G, and Zhao TC**. Histone deacetylase (HDAC) inhibition improves myocardial function and prevents cardiac remodeling in diabetic mice. *Cardiovasc Diabetol* 14: 99, 2015.

350. **Travers JG, Wennersten SA, Pena B, Bagchi RA, Smith HE, Hirsch RA, Vanderlinden LA, Lin YH, Dobrinskikh E, Demos-Davies KM, Cavasin MA, Mestroni L, Steinkuhler C, Lin CY, Houser SR, Woulfe KC, Lam MPY, and McKinsey TA**. HDAC Inhibition Reverses Preexisting Diastolic Dysfunction and Blocks Covert Extracellular Matrix Remodeling. *Circulation* 143: 1874-1890, 2021.

351. **Lee TI, Kao YH, Tsai WC, Chung CC, Chen YC, and Chen YJ**. HDAC Inhibition Modulates Cardiac PPARs and Fatty Acid Metabolism in Diabetic Cardiomyopathy. *PPAR Res* 2016: 5938740, 2016.

352. **Li B, Yu Y, Liu K, Zhang Y, Geng Q, Zhang F, Li Y, and Qi J**. beta-Hydroxybutyrate inhibits histone deacetylase 3 to promote claudin-5 generation and attenuate cardiac microvascular hyperpermeability in diabetes. *Diabetologia* 64: 226-239, 2021.

353. **Xu Z, Tong Q, Zhang Z, Wang S, Zheng Y, Liu Q, Qian LB, Chen SY, Sun J, and Cai L**. Inhibition of HDAC3 prevents diabetic cardiomyopathy in OVE26 mice via epigenetic regulation of DUSP5-ERK1/2 pathway. *Clin Sci (Lond)* 131: 1841-1857, 2017.

354. **Zhang L, Du J, Yano N, Wang H, Zhao YT, Dubielecka PM, Zhuang S, Chin YE, Qin G, and Zhao TC**. Sodium Butyrate Protects -Against High Fat Diet-Induced Cardiac Dysfunction and Metabolic Disorders in Type II Diabetic Mice. *J Cell Biochem* 118: 2395-2408, 2017.

355. **Cavallotti C, Mancone M, Bruzzone P, Sabbatini M, and Mignini F**. Dopamine receptor subtypes in the native human heart. *Heart Vessels* 25: 432-437, 2010.

356. **Chatfield KC, Sparagna GC, Sucharov CC, Miyamoto SD, Grudis JE, Sobus RD, Hijmans J, and Stauffer BL**. Dysregulation of cardiolipin biosynthesis in pediatric heart failure. *J Mol Cell Cardiol* 74: 251-259, 2014.

357. **Chicco AJ, and Sparagna GC**. Role of cardiolipin alterations in mitochondrial dysfunction and disease. *Am J Physiol Cell Physiol* 292: C33-44, 2007.

358. **Dudek J, Hartmann M, and Rehling P**. The role of mitochondrial cardiolipin in heart function and its implication in cardiac disease. *Biochim Biophys Acta Mol Basis Dis* 1865: 810-821, 2019.

359. **Fillmore N, and Lopaschuk GD**. The link between pediatric heart failure and mitochondrial lipids. *J Mol Cell Cardiol* 76: 71-72, 2014.

360. **He Q, and Han X**. Cardiolipin remodeling in diabetic heart. *Chem Phys Lipids* 179: 75-81, 2014.

361. **Bertero E, Kutschka I, Maack C, and Dudek J**. Cardiolipin remodeling in Barth syndrome and other hereditary cardiomyopathies. *Biochim Biophys Acta Mol Basis Dis* 1866: 165803, 2020.

362. **Dyck JR, Kudo N, Barr AJ, Davies SP, Hardie DG, and Lopaschuk GD**. Phosphorylation control of cardiac acetyl-CoA carboxylase by cAMP-dependent protein kinase and 5'-AMP activated protein kinase. *Eur J Biochem* 262: 184-190, 1999.

363. **Makinde AO, Gamble J, and Lopaschuk GD**. Upregulation of 5'-AMP-activated protein kinase is responsible for the increase in myocardial fatty acid oxidation rates following birth in the newborn rabbit. *Circ Res* 80: 482-489, 1997.

364. **Patil VA, Fox JL, Gohil VM, Winge DR, and Greenberg ML**. Loss of cardiolipin leads to perturbation of mitochondrial and cellular iron homeostasis. *J Biol Chem* 288: 1696-1705, 2013.

365. **Raja V, Salsaa M, Joshi AS, Li Y, van Roermund CWT, Saadat N, Lazcano P, Schmidtke M, Huttemann M, Gupta SV, Wanders RJA, and Greenberg ML**. Cardiolipin-deficient cells depend on anaplerotic pathways to ameliorate defective TCA cycle function. *Biochim Biophys Acta Mol Cell Biol Lipids* 1864: 654-661, 2019.

366. **Ghosh S, Basu Ball W, Madaris TR, Srikantan S, Madesh M, Mootha VK, and Gohil VM**. An essential role for cardiolipin in the stability and function of the mitochondrial calcium uniporter. *Proc Natl Acad Sci U S A* 117: 16383-16390, 2020.

367. **Xu HX, Cui SM, Zhang YM, and Ren J**. Mitochondrial Ca(2+) regulation in the etiology of heart failure: physiological and pathophysiological implications. *Acta Pharmacol Sin* 41: 1301-1309, 2020.

368. **Denton RM, Randle PJ, Bridges BJ, Cooper RH, Kerbey AL, Pask HT, Severson DL, Stansbie D, and Whitehouse S**. Regulation of mammalian pyruvate dehydrogenase. *Mol Cell Biochem* 9: 27-53, 1975.

369. **O'Brien M, Chalker J, Slade L, Gardiner D, and Mailloux RJ**. Protein S-glutathionylation alters superoxide/hydrogen peroxide emission from pyruvate dehydrogenase complex. *Free Radic Biol Med* 106: 302-314, 2017.

370. **Nalecz KA, Bolli R, Wojtczak L, and Azzi A**. The monocarboxylate carrier from bovine heart mitochondria: partial purification and its substrate-transporting properties in a reconstituted system. *Biochim Biophys Acta* 851: 29-37, 1986.

371. **Atherton HJ, Schroeder MA, Dodd MS, Heather LC, Carter EE, Cochlin LE, Nagel S, Sibson NR, Radda GK, Clarke K, and Tyler DJ**. Validation of the in vivo assessment of pyruvate dehydrogenase activity using hyperpolarised 13C MRS. *NMR Biomed* 24: 201-208, 2011.

372. **Packer M, Anker SD, Butler J, Filippatos G, Pocock SJ, Carson P, Januzzi J, Verma S, Tsutsui H, Brueckmann M, Jamal W, Kimura K, Schnee J, Zeller C, Cotton D, Bocchi E, Bohm M, Choi DJ, Chopra V, Chuquiure E, Giannetti N, Janssens S, Zhang J, Gonzalez Juanatey JR, Kaul S, Brunner-La Rocca HP, Merkely B, Nicholls SJ, Perrone S, Pina I, Ponikowski P, Sattar N, Senni M, Seronde MF, Spinar J, Squire I, Taddei S, Wanner C, Zannad F, and Investigators EM-RT**. Cardiovascular and Renal Outcomes with Empagliflozin in Heart Failure. *N Engl J Med* 383: 1413-1424, 2020.

373. **Ferrannini E, Mark M, and Mayoux E**. CV Protection in the EMPA-REG OUTCOME Trial: A "Thrifty Substrate" Hypothesis. *Diabetes Care* 39: 1108-1114, 2016.

374. **Mudaliar S, Alloju S, and Henry RR**. Can a Shift in Fuel Energetics Explain the Beneficial Cardiorenal Outcomes in the EMPA-REG OUTCOME Study? A Unifying Hypothesis. *Diabetes Care* 39: 1115-1122, 2016.

375. **Baartscheer A, Schumacher CA, Wust RC, Fiolet JW, Stienen GJ, Coronel R, and Zuurbier CJ**. Empagliflozin decreases myocardial cytoplasmic Na(+) through inhibition of the cardiac Na(+)/H(+) exchanger in rats and rabbits. *Diabetologia* 60: 568-573, 2017.

376. **Ferrannini E, Baldi S, Frascerra S, Astiarraga B, Heise T, Bizzotto R, Mari A, Pieber TR, and Muscelli E**. Shift to Fatty Substrate Utilization in Response to Sodium-Glucose Cotransporter 2 Inhibition in Subjects Without Diabetes and Patients With Type 2 Diabetes. *Diabetes* 65: 1190-1195, 2016.

377. **Nasser S, Sole T, Vega N, Thomas T, Balcerczyk A, Strigini M, and Pirola L**. Ketogenic diet administration to mice after a high-fat-diet regimen promotes weight loss, glycemic normalization and induces adaptations of ketogenic pathways in liver and kidney. *Mol Metab* 65: 101578, 2022.

378. **Xie Z, Zhang D, Chung D, Tang Z, Huang H, Dai L, Qi S, Li J, Colak G, Chen Y, Xia C, Peng C, Ruan H, Kirkey M, Wang D, Jensen LM, Kwon OK, Lee S, Pletcher SD, Tan M, Lombard DB, White KP, Zhao H, Li J, Roeder RG, Yang X, and Zhao Y**. Metabolic Regulation of Gene Expression by Histone Lysine beta-Hydroxybutyrylation. *Mol Cell* 62: 194-206, 2016.

379. **Bielohuby M, Menhofer D, Kirchner H, Stoehr BJ, Muller TD, Stock P, Hempel M, Stemmer K, Pfluger PT, Kienzle E, Christ B, Tschop MH, and Bidlingmaier M**. Induction of ketosis in rats fed low-carbohydrate, high-fat diets depends on the relative abundance of dietary fat and protein. *Am J Physiol Endocrinol Metab* 300: E65-76, 2011.

380. **Boudina S, Sena S, O'Neill BT, Tathireddy P, Young ME, and Abel ED**. Reduced mitochondrial oxidative capacity and increased mitochondrial uncoupling impair myocardial energetics in obesity. *Circulation* 112: 2686-2695, 2005.

381. **Crisostomo LL, Araujo LM, Camara E, Carvalho C, Silva FA, Vieira M, and Rabelo A, Jr.** Comparison of left ventricular mass and function in obese versus nonobese women <40 years of age. *Am J Cardiol* 84: 1127-1129, A1111, 1999.

382. **Iacobellis G, and Leonetti F**. Epicardial adipose tissue and insulin resistance in obese subjects. *J Clin Endocrinol Metab* 90: 6300-6302, 2005.

383. **Morricone L, Malavazos AE, Coman C, Donati C, Hassan T, and Caviezel F**. Echocardiographic abnormalities in normotensive obese patients: relationship with visceral fat. *Obes Res* 10: 489-498, 2002.

384. **Heather LC, Hafstad AD, Halade GV, Harmancey R, Mellor KM, Mishra PK, Mulvihill EE, Nabben M, Nakamura M, Rider OJ, Ruiz M, Wende AR, and Ussher JR**.

Guidelines on models of diabetic heart disease. *Am J Physiol Heart Circ Physiol* 323: H176-H200, 2022.

385. **Tadinada SM, Weatherford ET, Collins GV, Bhardwaj G, Cochran J, Kutschke W, Zimmerman K, Bosko A, O'Neill BT, Weiss RM, and Abel ED**. Functional resilience of C57BL/6J mouse heart to dietary fat overload. *Am J Physiol Heart Circ Physiol* 321: H850-H864, 2021.

386. **Guo Y, Wang X, Jia P, You Y, Cheng Y, Deng H, Luo S, and Huang B**. Ketogenic diet aggravates hypertension via NF-kappaB-mediated endothelial dysfunction in spontaneously hypertensive rats. *Life Sci* 258: 118124, 2020.

387. **You Y, Guo Y, Jia P, Zhuang B, Cheng Y, Deng H, Wang X, Zhang C, Luo S, and Huang B**. Ketogenic diet aggravates cardiac remodeling in adult spontaneously hypertensive rats. *Nutr Metab (Lond)* 17: 91, 2020.

388. **Tao J, Chen H, Wang YJ, Qiu JX, Meng QQ, Zou RJ, Li L, Huang JG, Zhao ZK, Huang YL, Zhang HF, and Zheng JM**. Ketogenic Diet Suppressed T-Regulatory Cells and Promoted Cardiac Fibrosis via Reducing Mitochondria-Associated Membranes and Inhibiting Mitochondrial Function. *Oxid Med Cell Longev* 2021: 5512322, 2021.

389. **Guo Y, Zhang C, Shang FF, Luo M, You Y, Zhai Q, Xia Y, and Suxin L**. Ketogenic Diet Ameliorates Cardiac Dysfunction via Balancing Mitochondrial Dynamics and Inhibiting Apoptosis in Type 2 Diabetic Mice. *Aging Dis* 11: 229-240, 2020.

390. **Kruljac I, Cacic M, Cacic P, Ostojic V, Stefanovic M, Sikic A, and Vrkljan M**. Diabetic ketosis during hyperglycemic crisis is associated with decreased all-cause mortality in patients with type 2 diabetes mellitus. *Endocrine* 55: 139-143, 2017.

391. **Thai PN, Miller CV, King MT, Schaefer S, Veech RL, Chiamvimonvat N, Bers DM, and Dedkova EN**. Ketone Ester D-beta-Hydroxybutyrate-(R)-1,3 Butanediol Prevents Decline in Cardiac Function in Type 2 Diabetic Mice. *J Am Heart Assoc* 10: e020729, 2021.

392. **Wang Y, Lin HQ, Law WK, Liang WC, Zhang JF, Hu JS, Ip TM, Waye MM, and Wan DC**. Pimozide, a novel fatty acid binding protein 4 inhibitor, promotes adipogenesis of 3T3-L1 cells by activating PPARgamma. *ACS Chem Neurosci* 6: 211-218, 2015.

393. **Chandra M, Miriyala S, and Panchatcharam M**. PPARgamma and Its Role in Cardiovascular Diseases. *PPAR Res* 2017: 6404638, 2017.

394. **Clarke GD, Solis-Herrera C, Molina-Wilkins M, Martinez S, Merovci A, Cersosimo E, Chilton RJ, Iozzo P, Gastaldelli A, Abdul-Ghani M, and DeFronzo RA**. Pioglitazone Improves Left Ventricular Diastolic Function in Subjects With Diabetes. *Diabetes Care* 40: 1530-1536, 2017.

395. **van der Meer RW, Rijzewijk LJ, de Jong HW, Lamb HJ, Lubberink M, Romijn JA, Bax JJ, de Roos A, Kamp O, Paulus WJ, Heine RJ, Lammertsma AA, Smit JW, and Diamant M**. Pioglitazone improves cardiac function and alters myocardial substrate metabolism without affecting cardiac triglyceride accumulation and high-energy phosphate metabolism in patients with well-controlled type 2 diabetes mellitus. *Circulation* 119: 2069-2077, 2009.

396. **Schugar RC, Moll AR, Andre d'Avignon D, Weinheimer CJ, Kovacs A, and Crawford PA**. Cardiomyocyte-specific deficiency of ketone body metabolism promotes accelerated pathological remodeling. *Mol Metab* 3: 754-769, 2014.

397. **Drolet B, Rousseau G, Daleau P, Cardinal R, Simard C, and Turgeon J**. Pimozide (Orap) prolongs cardiac repolarization by blocking the rapid component of the delayed rectifier potassium current in native cardiac myocytes. *J Cardiovasc Pharmacol Ther* 6: 255-260, 2001.

398. **Wentz AE, d'Avignon DA, Weber ML, Cotter DG, Doherty JM, Kerns R, Nagarajan R, Reddy N, Sambandam N, and Crawford PA**. Adaptation of myocardial substrate metabolism to a ketogenic nutrient environment. *J Biol Chem* 285: 24447-24456, 2010.

399. **Pelletier A, Tardif A, Gingras MH, Chiasson JL, and Coderre L**. Chronic exposure to ketone bodies impairs glucose uptake in adult cardiomyocytes in response to insulin but not vanadate: the role of PI3-K. *Mol Cell Biochem* 296: 97-108, 2007.

400. **Tardif A, Julien N, Pelletier A, Thibault G, Srivastava AK, Chiasson JL, and Coderre L**. Chronic exposure to beta-hydroxybutyrate impairs insulin action in primary cultures of adult cardiomyocytes. *Am J Physiol Endocrinol Metab* 281: E1205-1212, 2001.

Appendix

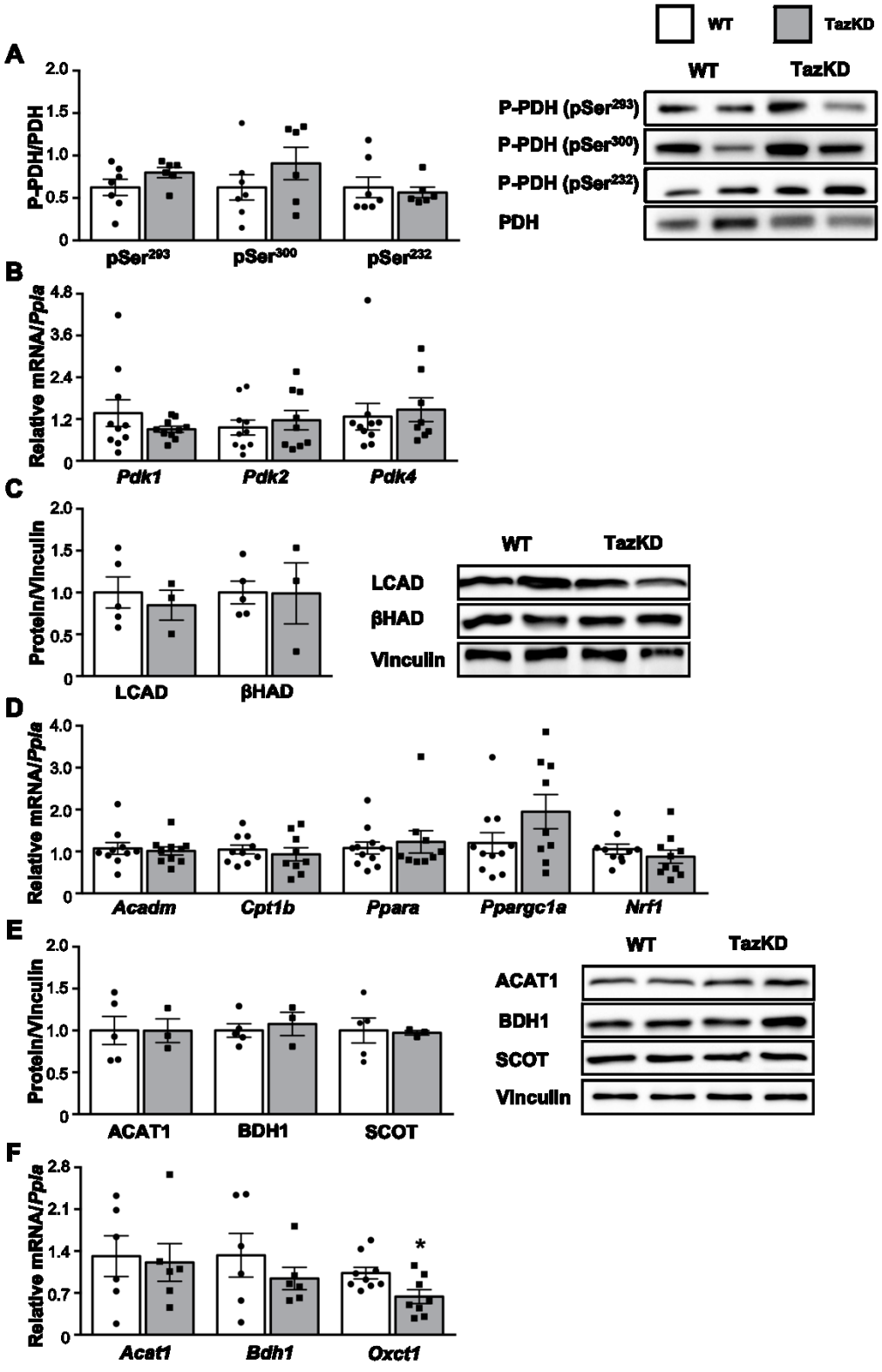
WT
TazKD
A
P-PDH/PDH
pSer293
pSer300
pSer232
P-PDH (pSer293)
P-PDH (pSer300)
P-PDH (pSer232)
PDH
B
Relative mRNA/Ppia
Pdk1
Pdk2
Pdk4
C
Protein/Vinculin
LCAD
βHAD
Vinculin
D
Relative mRNA/Ppia
Acadm
Cpt1b
Ppara
Ppargc1a
Nrf1
E
Protein/Vinculin
ACAT1
BDH1
SCOT
F
Relative mRNA/Ppia
Acat1
Bdh1
Oxct1
*

Appendix Figure 1.1. *Molecular regulation of energy metabolism in soleus muscles of male TazKD mice*. **A:** PDH phosphorylation at serine (Ser) 293, 300 and 232 in soleus extracts from WT and TazKD mice (n = 6–7). **B:** mRNA expression of genes involved in the regulation of PDH activity (PDH kinase 1 (*Pdk1*), PDH kinase 2 (*Pdk2*), and PDH kinase 4 (*Pdk4*) in soleus extracts from WT and TazKD mice (n = 8–10). **C:** Protein expression of fatty acid β-oxidation enzymes (long chain acyl CoA dehydrogenase (LCAD) and β-hydroxyacyl CoA dehydrogenase (βHAD)) in soleus extracts from WT and TazKD mice (n = 3–5). **D:** mRNA expression of genes involved in the regulation of fatty acid oxidation (medium chain acyl CoA dehydrogenase (*Acadm*), carnitine palmitoyl transferase 1 (*Cpt1b*), peroxisome proliferator-activated receptor α (*Ppara*), PPARg coactivator-1a (*Ppargc1a*) and nuclear respiratory factor 1 (*Nrf1*) in soleus extracts from WT and TazKD mice (n = 9–11). **E:** Protein expression of enzymes involved in ketone body oxidation, acetoacetyl CoA thiolase (ACAT1), β-hydroxybutyrate dehydrogenase (BDH1), and succinyl CoA:3-ketoacid CoA transferase (SCOT), in soleus extracts from TazKD and WT mice (n = 3–5). **F:** mRNA expression of *Acat1*, *Bdh1*, and *Oxct1* in soleus extracts from WT and TazKD mice (n = 6–9). Values represent mean ± SEM. Differences were determined by an unpaired two-tailed Student's t-test or a Mann-Whitney Test. *P < 0.05, significantly different from WT mice.

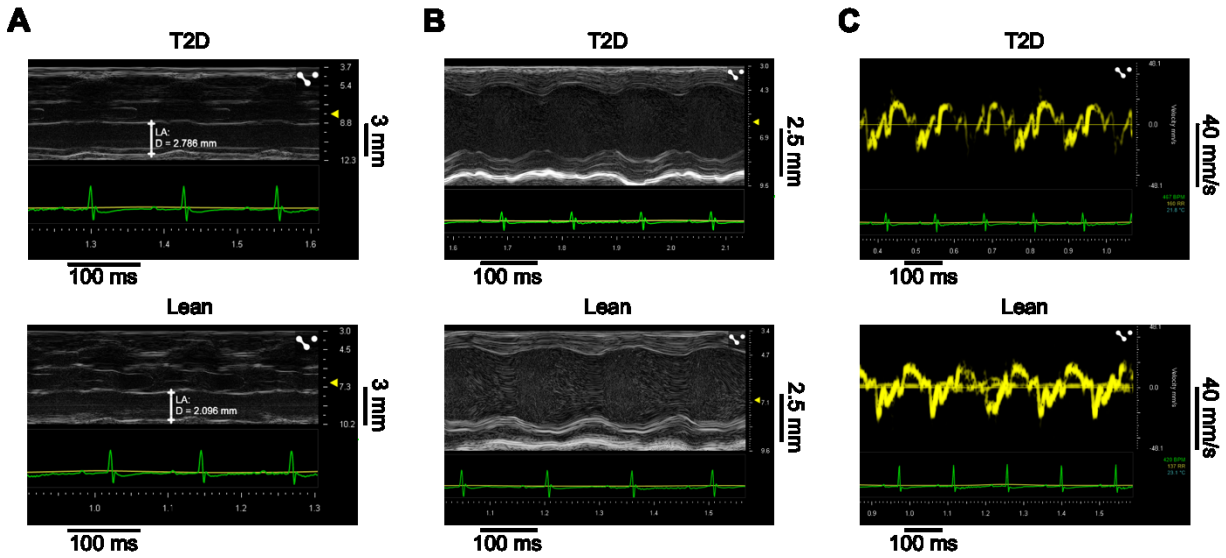

Appendix Figure 1.2. *Representative echocardiography images of T2D and lean mice at baseline.* **A:** Representative images of left atrial (LA) size acquired in the parasternal long axis view in M-mode. **B:** M-mode images of the left ventricle in the parasternal short axis view. **C:** Mitral annular velocity obtained by tissue Doppler imaging in the parasternal short axis view.